Formulation, characterisation and evaluation of peptide-loaded nanoniosomal delivery systems prepared by microfluidic technique and incorporated into oral dispersible films

Ali Abdulhaq Amer

This thesis is submitted in partial fulfilment of the

Requirements of the University of Sunderland

for the degree of Doctor of Philosophy

June-2026

Research abstract:

Abstract: Some peptides demonstrate significant biological or antibacterial therapeutic effects. However, their effectiveness is limited by poor stability, susceptibility to enzymatic degradation and restricted membrane permeability. This study evaluates niosomal drug delivery systems as nanocarrier platforms for three representative peptides: vancomycin hydrochloride, nisin and insulin. The aim of this study is to improve peptide stability, achieve controlled release, and facilitate non-invasive administration via the oral cavity.

Niosomes were synthesized through a microfluidic method by using different non-ionic surfactants, including Span 40, Span 60 and Span 65, that combined with cholesterol and co-surfactants such as Kolliphor RH40, Kolliphor ELP, and Solutol HS15. The microfluidic method produced nanosized vesicles with diameters ranging from 100 to 300 nanometers, exhibiting narrow polydispersity and high encapsulation efficiency. Dynamic light scattering (DLS) confirmed particle size and uniformity. Peptide quantification was accomplished using high-performance liquid chromatography (HPLC) and the bicinchoninic acid (BCA) assay.

The optimised niosomal formulations of vancomycin and nisin were incorporated into polyvinyl alcohol (PVA) polymer as a film former base of fast-disintegrating oral films. These films were assessed for mechanical strength, flexibility, thickness, surface pH, and disintegration time. Results indicate rapid disintegration time and consistent film performances. In addition, agar diffusion assays confirmed the release of active peptide after niosomes formulation, as evidenced by clear inhibition zones against *Bacillus subtilis*. Analytical techniques, including Fourier-transform infrared spectroscopy (FTIR), differential scanning calorimetry (DSC), thermogravimetric analysis (TGA) and scanning electron microscopy (SEM) have been employed to verify drug to excipient compatibility, thermal stability and homogeneous surface morphology.

Insulin-loaded niosomes were produced via microfluidic mixing using various Span surfactants and co-surfactants. Insulin niosomal formulation was intended for oral cavity administration in two dosage forms: microneedle films and the lyophilised buccal tablets. Optimised niosomal dispersion was freeze-dried with different lyoprotectants (mannitol, trehalose, glycine, sucrose). The most stable composition showed minimal nanoparticle size change and intact vesicle morphology using fluorescence microscope. Tablet characterization showed acceptable hardness, friability, and uniform insulin content after the tableting process. In vitro release studies using dialysis bags and permeability studies using Copley Franz cells equipped with polycarbonate membranes revealed controlled vancomycin, nisin and insulin release and enhanced drug diffusion rate over 24 hours compared to free peptides.

These results confirm that niosomal encapsulation can protect peptides from degradation and support controlled transmucosal delivery through the oral cavity.

Overall, this research demonstrates that niosomes function as stable and adaptable nanocarriers for peptide-based therapeutics. The integration of microfluidic fabrication, film casting or tablet compression technologies provides a simple and non-invasive platform to improve the stability, permeability and bioavailability of peptides.

Keywords: niosomes; peptide drug delivery; microfluidics; vancomycin; nisin; insulin; oral cavity delivery; fast-disintegrating film; microneedle film; lyophilisation; buccal tablet; controlled release; antimicrobial activity; permeability; Span surfactants.

Statement of Authorship and Contribution

This thesis is based on research conducted by the author during his PhD studies at the University of Sunderland.

The author started the main work related to conceptualisation, methodology, investigation, validation, formal analysis, data curation, experimental design, formulation development, data analysis, interpretation of results and writing the original thesis. All manuscripts included in this thesis were written by the author.

Supervisors Dr. Cheng Shu Chaw, Professor Amal Ali Elkordy and Dr. Lewis Bingle provided academic guidance and critical revision of manuscripts. Dr. Yasir Karkar provided technical support, including assistance with the TGA instrument.

Parts of this thesis are based on three peer-reviewed articles published by the author during the PhD program. The material drawn from these publications has been adapted, integrated, and expanded to form a coherent and unified thesis.

All the figures and the tables in this thesis are authorized to re-use by Ali Amer.

Statement of declaration and research activity

This thesis incorporates materials derived from the author three published as peer-reviewed articles, which were produced as part of the PhD program at University of Sunderland. The relationship between the published works and the corresponding thesis chapters is outlined below.

Chapter 1 is based on the review article:

- **Amer, A. A., Bingle, L., Elkordy, A. A., & Chaw, C. S. (2025). Overcoming Oral Cavity Barriers for Peptide Delivery Using Advanced Pharmaceutical Techniques and Nano-Formulation Platforms. *Biomedicines*, *13*(11), 2735. https://doi.org/10.3390/biomedicines13112735**

Chapter 2 is based on the methods sections of the following research articles:

- **Amer, A. A., Bingle, L., Chaw, C. S., & Elkordy, A. A. (2025). Development of Vancomycin, a Glycopeptide Antibiotic, in a Suitable Nanoform for Oral Delivery. *Molecules*, *30*(7), 1624. https://doi.org/10.3390/molecules30071624**

- **Amer, A. A., Karkar, Y., Bingle, L., Elkordy, A. A., & Chaw, C. S. (2025). Fast-Disintegrating Oral Films Containing Nisin-Loaded Niosomes. *Molecules*, *30*(18), 3715. https://doi.org/10.3390/molecules30183715**

Chapter 3 is based on the research article:

- **Amer, A. A., Bingle, L., Chaw, C. S., & Elkordy, A. A. (2025). Development of Vancomycin, a Glycopeptide Antibiotic, in a Suitable Nanoform for Oral Delivery. *Molecules*, *30*(7), 1624. https://doi.org/10.3390/molecules30071624**

Chapter 4 is based on the research article:

- **Amer, A. A., Karkar, Y., Bingle, L., Elkordy, A. A., & Chaw, C. S. (2025). Fast-Disintegrating Oral Films Containing Nisin-Loaded Niosomes. *Molecules*, *30*(18), 3715. https://doi.org/10.3390/molecules30183715**

Presentations and conferences

- **2021 – Critical Comparison of Anti-Bacterial Creams and Related Products Available in the UK [Poster Presentation], University of Sunderland**

- **2023 – Advanced Niosome Formulations for Vancomycin HCl: Comparative Study of Thin Film Hydration and Microfluidic Technology [Postgraduate Research Conference], University of Sunderland**

- **2024 – Microfluidic Synthesis of Niosome-Encapsulated Vancomycin Hydrochloride for Enhancing Antibacterial Activity [Oral and Poster Presentation, Postgraduate Research Conference], University of Sunderland**

- **2025 – Development of Vancomycin, a Glycopeptide Antibiotic, in a Suitable Nanoform for Oral Delivery [Postgraduate Research Conference], University of Sunderland**

Acknowledgment

In the name of Allah, the Most Gracious, the Most Merciful.

As stated in the Holy Qur'an: "Allah will exalt those of you who believe and those who have been given knowledge to high ranks" (**Qur'an 58:11**).

Firstly, I would like to express my honest and deepest gratitude to my supervisor, Dr Cheng Shu Chaw, for her invaluable guidance, continuous support, and encouragement throughout my PhD journey. Her insight, expertise, and constructive feedback have played a fundamental role in shaping both my research and my academic development. I am also deeply grateful to Professor Amal Ali Elkordy and Dr Lewis Bingle for their valuable suggestions, technical expertise, and unwavering support during both the experimental work and the writing of this thesis.

My sincere thanks go to the academic and technical staff for their assistance with laboratory work, instrumentation, and administrative processes. I also extend my appreciation to my colleagues and fellow researchers for their engaging discussions and collaborative spirit, which greatly enriched my experience.

As Nelson Mandela wisely said, "It always seems impossible until it's done." This quote has been a constant source of motivation throughout this journey.

I would like to express my heartfelt gratitude to my family, especially my parents and siblings, for their unwavering belief in me and for being a constant source of strength and encouragement. I am deeply thankful for their generous financial support and continuous reassurance throughout the course of my studies. Finally, my deepest appreciation goes to the person who loved me truly, for her patience, understanding, and unwavering support, which helped me remain grounded during the most demanding stages of this journey.

This thesis would not have been possible without the support, trust, and generosity of all those mentioned above.

Ali Abdulhaq Alnuemi **Sunderland, April 2025**

Novelty of the Study

This research represents the first comprehensive effort to establish a unified niosomal platform capable of encapsulating different therapeutic peptides using microfluidic technology integrated with fast-dissolving polymeric devices intended for targeting oral cavity for both local and systemic effects.

The novelty and significance of the study:

- Unique niosome nanoparticles produced by microfluidic mixed with polymer-based oral films and buccal tablets, providing a reproducible and scalable platform in formulation design.

- Three drugs (vancomycin, nisin, and insulin) were employed as models to explore how molecular size and hydrophilicity affect niosome formation, size distribution, encapsulation efficiency and other in vitro test performances by establishing a formulation concept.

- The work introduces a new localised therapeutic approach for oral infections, by demonstrating sustained antimicrobial activity and an improved peptide stability.

- The first direct comparison based on in vitro test performances between niosomal oral films and niosomal tablets for insulin delivery.

- Using niosomes tagged with a fluorescent dye to monitor the efficiency of freeze-drying process (as part of lyophilised tablet preparation) and film drying after solvent casting or oral film products.

List of abbreviations

Apparent permeability (Papp)

Bicinchoninic acid (BCA)

Bovine serum albumin (BSA)

Critical micelle concentration (CMC)

Critical packing parameter (CPP)

Croscarmellose sodium (COS)

Differential scanning calorimetry (DSC)

Differential thermogravimetric (DTG)

Dimethyl didodecyl ammonium bromide (DDAB),

Diode array detector (DAD)

Encapsulation efficiency (EE)

Ether Injection Method (EIM),

Fast-dissolving oral films (FDOFS)

Fluorescein isothiocyanate-dextrans (FITC dextrans)

Food and Drug Administration (FDA)

Fourier Transform Infrared Spectroscopy (FTIR)

Gastrointestinal tract (GIT)

High-Performance Liquid Chromatography (HPLC)

Hydrophilic-lipophilic balance (HLB)

Hydroxypropyl cellulose (HPC)

Hydroxypropyl methylcellulose (HPMC)

Isoelectric point (PI)

Large unilamellar vesicles (luvs)

Lipid-based nanomedicines (LBNMS)

Lower limit of quantification (LLOQ)

Membrane coating granules (MCGS)

Microcrystalline cellulose (MCC)

Molecular weight (M.Wt.)

Multilamellar vesicles (MLVS)

P-glycoprotein (P-gp)

Poly lactic co-glycolic acid (PLGA)

Polydispersity index (PDI)

Polydispersity index (PDI)

Polyethylene glycol (PEG)

Polyvinyl pyrrolidone (PVP)

Polyvinylpyrrolidone (PVP)

Reticuloendothelial system (RES)

Reverse Phase Evaporation (REV)

Salmon calcitonin (SCT)

Small unilamellar vesicles (SUVS)

Sodium starch glycolate (SSG)

Supercritical Carbon Dioxide ($scco_2$)

Tert-butanol (TBA)

Thermogravimetric analysis (TGA)

Thin-Film Hydration (TFH)

Transepithelial electrical resistance (TEER)

Transition temperature (Tc)

Vancomycin hydrochloride (VCM)

Table of contents

List of Tables

List of Figures

List of equations

Thesis flow

This thesis consists of 7 chapters in total.

Chapter one: starts with an introduction about peptide therapeutics and the importance of those peptides in the biological systems with a focus on the delivery methods of peptides, including nanoparticles as peptide delivery system.

Chapter two: describes the experimental design to meet the research aims and objectives. It includes all the materials, preparation approaches and testing methods of niosomes, films and /or tablets entrapped with the three peptide agents (VCM, Nisin and insulin).

Chapter three: Describes design and characterization of vancomycin hydrochloride-loaded niosomes, fabricated using microfluidic techniques for producing nanoscale vesicles with favourable properties. The study explores the effects of different excipients, including Span 60, Span 40, Kolliphor RH40, and Kolliphor ELP, on niosome size, morphology, and encapsulation efficiency.

Chapter four: Describes development and evaluatation of nisin A–loaded niosomes as a novel antimicrobial delivery system for the treatment of Gram-positive bacterial infections and integration of the optimised formulation into fast-disintegrating oral films for localised delivery within the oral cavity.

Chapter five: Describes insulin-loaded niosomes prepared using different surfactants and optimised co-surfactants incorporated into a polyvinyl alcohol matrix to form dissolving microneedle films and comparison with tablet produced by lyophilised niosomal formulations using suitable lyoprotectants in which they are compressed into tablets.

Chapter six: conclusions.

Chapter seven: References.

Chapter One: General Introduction

Parts of chapter 1 is based on the published article:
Amer *et al. Overcoming Oral Cavity Barriers for Peptide Delivery Using Advanced Pharmaceutical Techniques and Nano-Formulation Platforms*. **Biomedicines**, 2025

1. Introduction and literature review

1.1. Peptide-Based Therapeutics

Therapeutic agents with hydrophobic solubility, such as enzymes, hormones, vaccines face complications when they are administered orally. As gut conditions may affect their solubility and structural stability. The majority of these drugs are prone to hydrolysis, aggregation, or denaturation when they passage through the gut, they also suffer from instability when inappropriately stored. Colloidal systems, like nano- or microparticles, are designed to preserve, protect, encapsulate and transport macromolecules. In addition, some peptides are encapsulated in various forms that allow them to transit safely through the mouth and stomach before being released into the small intestines which is the main absorption site. However, several barriers must be overcome before such molecules can be efficiently administered orally [1]. Peptides are short polymers with less than 50 amino acids and with a molecular weight of less than 10 kDa. They have been established as a fast-expanding field in the discovery of novel therapeutics. Furthermore, peptide demonstrates unique pharmacokinetics features and provides considerable benefits as therapeutic agents, some of these agents are presented in **Table 1.1** [2].

Therapeutic peptides offer substantial pharmacological advantages. These include a reduction in drug-drug interactions, as they are digested to amino acids rather than competing for small-molecules for the same metabolic pathways. In addition, peptides demonstrated exceptional target specificity and selectivity, while decreasing off-target toxicity [3]. Despite these benefits, a number of functional and pharmacokinetic limitations restrict their overall efficacy. Peptide-based systems often have higher manufacturing costs over small-molecule drugs this is due to complex production methods and the need for specialised skills. Furthermore, peptides are quickly removed from the bloodstream and are highly vulnerable to proteolytic breakdown, resulting in short systemic exposure [4]. In addition, peptides have a lower oral bioavailability than small drug molecules due to their higher molecular weight and distinct solubility [5], [6].

Table 1-1: Clinical uses of selected Peptide Therapeutics by Routes and Molecular Weight [7].

Peptide	MW (Da)	therapeutic uses	Dosage Form
Insulin	~5800	Diabetes mellitus	Injection (subcutaneous)
GLP-1 analogues (Liraglutide, Semaglutide)	~3751 (Liraglutide)	Type 2 diabetes, obesity	Injection (subcutaneous and oral)
Oxytocin	1007	Labour induction, postpartum bleeding	Injection, IV infusion
Vasopressin	1084	Diabetes insipidus, bleeding control	Injection, nasal spray
Calcitonin	3432	Osteoporosis, hypercalcemia	Injection, nasal spray
Enfuvirtide	4492	HIV treatment (fusion inhibitor)	Injection (subcutaneous)
Leuprolide	1209	Prostate/breast cancer, endometriosis	Injection (IM, SC), implant
Desmopressin	1069	Diabetes insipidus, bleeding disorders	Nasal spray, oral
Somatostatin / Octreotide	1637 (Somatostatin) / 1019 (Octreotide)	Acromegaly, neuroendocrine tumours	Injection (IM, SC), depot injection
Exenatide	4186	Type 2 diabetes	Injection (SC), extended-release injection
Bremelanotide	1024	Hypoactive sexual desire disorder	Injection (SC)
Thymosin Alpha-1	3108	Immunomodulation (Hepatitis B, C)	Injection (SC, IM)
BPC-157	1419	Experimental: wound healing, inflammation	Experimental; injection (SC or IM)
Glucagon	3485	Severe hypoglycemia emergency treatment	Injection (IM, SC, IV)
Melanotan II	1025	Investigation: skin tanning, sexual dysfunction	Injection (SC)
Thyrotropin-releasing hormone (TRH)	362	Diagnostic for pituitary disorders; neuroregulation	Injection (IV)
Bivalirudin	2180	Anticoagulant	Injection (IV)
Goserelin	1282	Prostate cancer, breast cancer, endometriosis	Implant, injection (SC)
Follitropin alfa	~30,000	Fertility treatment (FSH analog)	Injection (SC, IM)
Vasopressin analogue (Terlipressin)	1056	Acute variceal bleeding, septic shock	Injection (IV)
Daptomycin (cyclic lipopeptide)	1620	Gram-positive bacterial infections (MRSA, VRE)	Injection (IV)
Colistin (Polymyxin E)	~1155	Multidrug-resistant Gram-negative infections	Injection (IV, IM)
Teicoplanin	~1883	Gram-positive infections, including MRSA	Injection (IV, IM)
Gramicidin	~1900	Topical infections	Topical (ointment)
Vancomycin (glycopeptide)	1449	Serious Gram-positive infections	Injection (IV), Oral (for C. diff)
Pexiganan (synthetic magainin analog)	2249	Topical diabetic foot infections (under evaluation)	Topical cream
Bacitracin	~1422	Topical antibacterial for minor skin infections	Topical ointment
Nisin	~3350	Food preservation, investigational clinical use	Topical, experimental

1.2 Routes of therapeutic peptide administration

1.2.1 Parenteral route

The most established method for peptide delivery is via the parenteral route. This route of administration has several advantages including avoiding GI enzymes and hepatic first-pass metabolism, resulting in increased systemic bioavailability of therapeutic peptides. Nonetheless, administration of peptide drug via subcutaneous and intramuscular routes are still prone to some degree of pre-systemic degradation occurring at the injection site, which is due to the presence of enzymatic activity within the interstitial space and in the lymphatic system [8].

The direct delivery of peptide actives into the systemic circulation through intravenous administration ensures 100% bioavailability. On the other hand, the systemic bioavailability of a substance following subcutaneous or intramuscular administration can vary significantly, ranging between 20% and 100%, and is governed by several factors like degradation at the injection site, absorption kinetics, and lymphatic uptake [9]. The absorption kinetics of peptides after subcutaneous or intramuscular delivery are significantly influenced by the physicochemical properties of the molecule. Following injection, peptide drugs can enter systemic circulation through both blood capillaries and lymphatic vessels (**Figure 1.1**) where their systemic exposure is dominated by peptide molecular weights. For instance, low molecular weight peptides (usually <1 kDa) are mostly absorbed by blood capillaries, while larger molecules, especially those with molecular weights higher than 16–22 kDa, predominantly face lymphatic absorption. With an increase in molecular weight, the lymphatic system emerges as the principal pathway for the absorption of peptide therapies. Given that the majority of therapeutic peptides exhibit a molecular weight less than 10 kDa, it is anticipated that both the lymphatic system and blood arteries facilitate their absorption[10], [11]. Typically, only a minor fraction of the dosage is absorbed through the lymphatic system by convective transport processes.

The majority of peptides are administered parenterally due to their vulnerability to enzyme breakdown and limited membrane permeability in the gastrointestinal tract. Parenteral administration is unpleasant and frequently uncomfortable. This is one of the fundamental pharmacokinetic limits of parenteral peptides. However, other examples, such oral semaglutide and intranasal desmopressin Table 1.1, illustrate the increasing possibility of alternative delivery methods via the oral route to enhance patient adherence. Consequently, several attempts were undertaken to identify alternative and non-invasive techniques for the administration of these peptides, involving oral, buccal, pulmonary, intranasal, and transdermal routes [2].

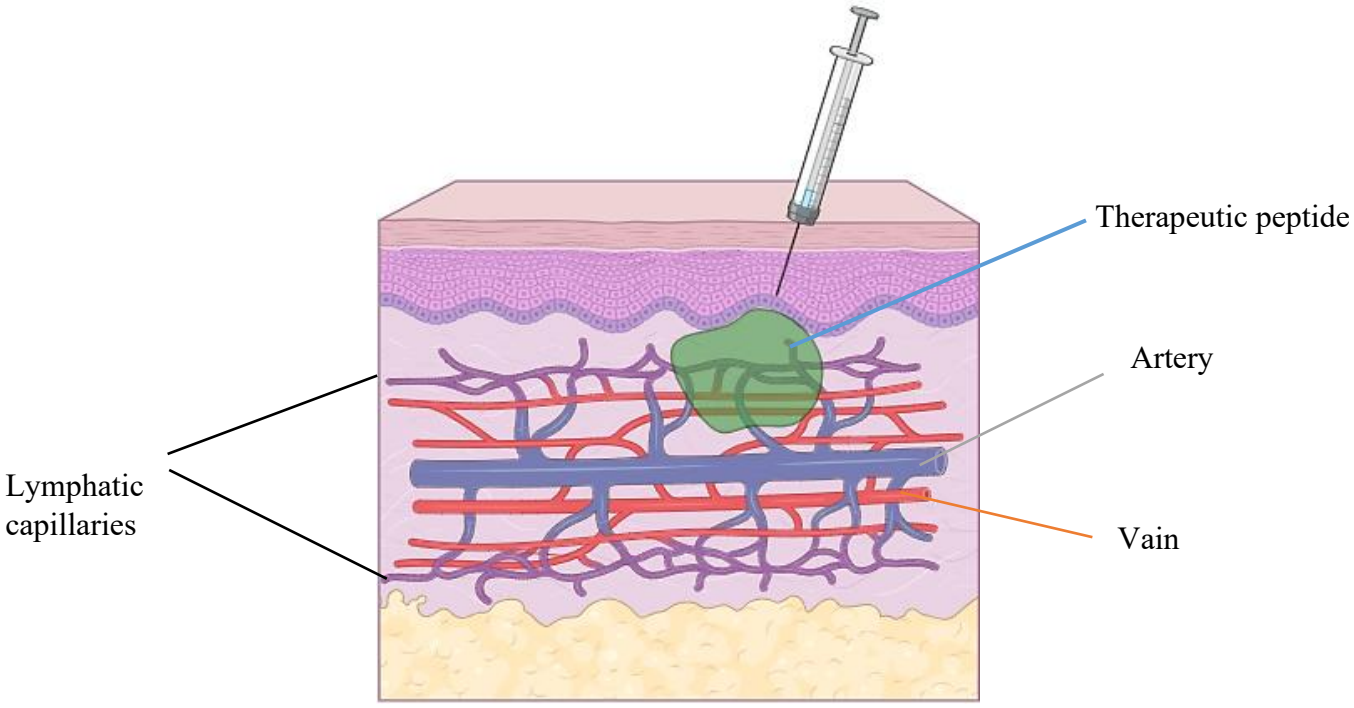

Figure 1.1: Subcutaneous administration route. figure adapted from [7].

1.2.2 Oral Administration

Orally peptides face a number of challenges before entering the systemic circulation. Physicochemical parameters such as molecule size, surface charge, and density, as well as physiological obstacles, limit uptake in the gut [12]. **Figure 1.2** represents factors and barriers that influence oral administration of peptides. The pH of the gastrointestinal tract is varied, ranging from the acidic environment of the stomach (pH 1.5 to 3.5 in fasting adults and 3 to 5 at fed state) to more neutral in the intestines (pH 5.5 to 7) [13] [14]. The stability of orally administered peptides can be substantially impacted by rapid changs in pH within the gut lumen. Peptides undergo a significant transformation as they transition from the stomach to the proximal part of small intestine (duodenum), where the pH level transitions from the highly acidic environment to a nearly neutral state. Gastric juice, which is constituted of hydrochloric acid and other components, contributes to this acidic pH. The surface charge of peptides is closely correlated with their isoelectric points, at which point they have no net charge. Changes in gastrointestinal pH can alter the ionisation state of peptide functional groups and surface-exposed amino acid residues. As a result, the net surface charge of the peptide may change depending on the surrounding pH and its isoelectric point. When the pH is close to the peptide's isoelectric point, the peptide has little or no net charge, which can reduce solubility and promote aggregation. In contrast, highly charged peptides may remain more soluble in aqueous environments but generally show poor passive diffusion across the lipophilic epithelial membrane[15]. Therefore, pH-dependent changes in peptide charge can influence solubility, aggregation behaviour, mucus interactions and epithelial permeability, contributing to poor and variable oral absorption. Peptides' absorption efficiency and membrane permeability are ultimately influenced by these variations in surface charge and density while they cross the intestine [12].

A loss of peptide functionality can be induced by pH-associated chemical reactions, including oxidation, hydrolysis, or deamidation. High acidity of the stomach is responsible for the degradation of peptide drugs into small fragments and amino acids. For instance, deamidation of peptides happens at both low and near-neutral pH levels via separate degradation mechanisms, resulting in the transformation of the side-chain amides of glutamine and asparagine residues to

glutamic and aspartic acids, respectively [14]. Amino acids such as histidine, asparagine, tryptophan, cysteine, tyrosine, and methionine, present in insulin, are susceptible to hydrolysis and oxidation in solutions. These events may particularly occur at the asparagine residue and are associated with the cleavage of peptide bonds, ultimately resulting in reduced biological activity [16], [17], [18].

Peptides are subjected to enzymatic breakdown by proteases and peptidases that are released into the gut lumen, associated with the brush-border membrane and present inside the cytosol [19], [20]. For example, pepsin is an enzyme that has been observed to exhibit extensive substrate selectivity against peptides or proteins, and it exhibits an increase in activity at a low pH in the stomach [21]. Pepsin bioactivity declines upon entering the duodenum, which maintains a higher pH value. The duodenum, jejunum, and ileum are different anatomical sections of the small intestine, primarily recognised as the main site for the absorption of nutrients and drugs. The small intestine exhibits greater enzymatic activity compared to the other sections of the GI tract [22], [23].

Pancreatic juice and its components found in the duodenum present challenges for delivery of peptide drugs. Among these are endopeptidases like trypsin and chymotrypsin, which are substrate specific and they are responsible for cleaving peptide bonds inside the peptide chain, and exopeptidases like carboxypeptidase A and B, which are responsible for cleaving amino acid residues from the ends of the peptide sequence [24]. Pancreatic juice is mild alkaline, which can activate other intestinal enzymes by increasing the pH of the duodenum. The brush border covering the surface of intestinal epithelial cells are made up of densely packed cellular extrusions known as microvilli [25]. Enzymes like peptidases and amylases are present in the brush border membrane that can degrade molecules including proteins and peptides, as well as starch and sucrose [26], [27].

The peptide therapeutics are faced by cellular barriers as they progress through the gastrointestinal tract throughout oral administration. The primary location for drug absorption is the small intestine. Peptides must tolerate the biochemical stresses and harsh environment of the stomach,

as well as the brush border and jejunum, The brush border refers to the dense layer of microvilli on the apical surface of enterocytes in the small intestine. It increases the absorptive surface area and contains membrane-bound enzymes, including brush-border peptidases, which can further hydrolyse peptides into smaller peptides or amino acids before absorption. [28], [29]. The epithelial lining is a multifaceted structure that comprises a variety of components, such as the intestinal microvilli, finger-like projections, intestinal microvilli, and tight junctions, in addition to a large sulphated mucopolysaccharide layer comprises glycocalyx, mucin. Peptides are rigorously restricted from absorption by these elements due to their physicochemical barrier [30], [31]. Diffusion across gastrointestinal membranes is reduced, particularly for hydrophilic molecules with a molecular weight exceeding 700 Da [32], [33]. Hence, peptide drugs that overcome these barriers are ultimately metabolised in the liver prior to entering the systemic circulation. The result is a low and unpredictable oral bioavailability for orally administered peptide drugs where current data has indicated that only 1–2% of therapeutic peptide achieve systemic circulation via the traditional oral route [34],[20], [35].

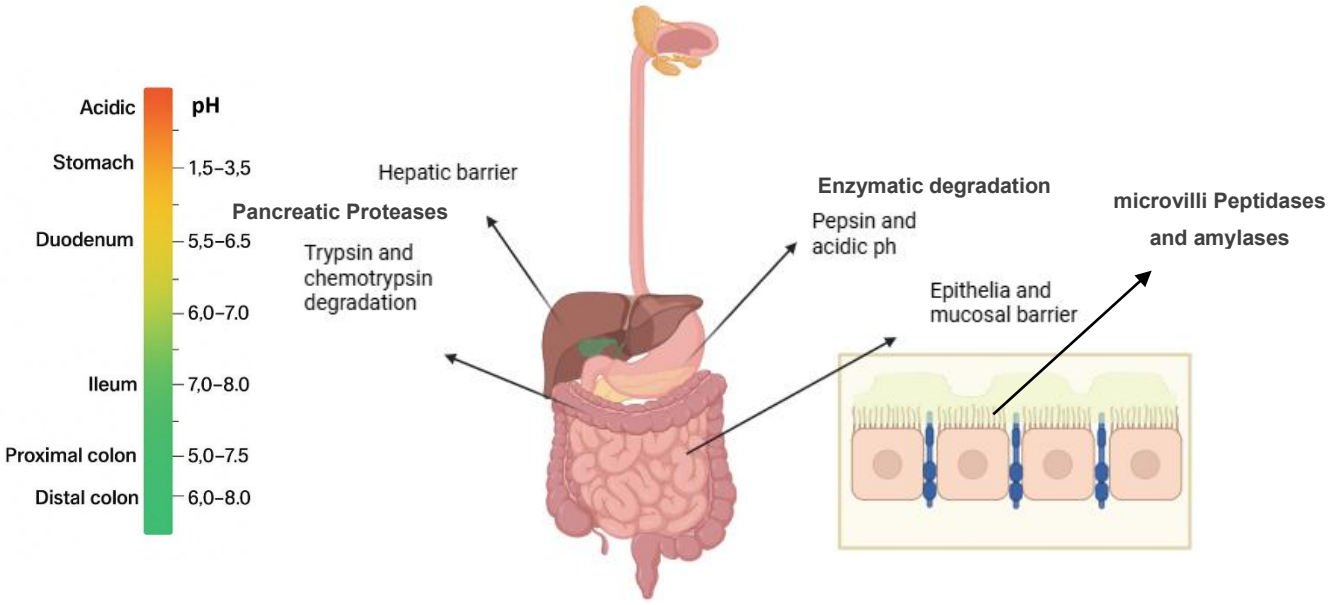

Figure 1.2: Anatomical structure of gut: Physiological and chemical hurdles for peptide drug delivery. Figure adapted from [7] .

1.2.3 Administration of Peptides through the Oral Cavity

The buccal and sublingual pathways are alternative non-invasive delivery routes that have attracted attention for both oral and systemic drug administration, for macromolecules with poor oral bioavailability. **(Figure 1.3 left)** illustrates the anatomy of the buccal mucosa and oral cavity. In the mouth, the oral mucosa is essential for drug absorption, as its structure and properties at specific sites affect the drug uptake and effectiveness of drug substances. It occupies an area of approximately 170 cm^2 [36]. The oral mucosa is made up of two primary layers: the lamina propria that supplies blood vessels and provides structural support and the outer stratified squamous epithelium, which protests and shields the underlying tissues **(Figure 1.3 Right and middle)**. In regions including the hard palate and gums, the epithelium is keratinised and organised into four layers: basal, prickle, granular, and keratinised that offers durability and mechanical strength, and it significantly lacks permeability making these regions less suited for absorption of actives [37].

Approximately 25% of the mucosal surface is comprised of these regions. However, non-keratinized regions, such as the buccal mucosa, with underlying loose connective tissues and offer a larger surface area, they are better sites for drug absorption.

Due to its dense vascularization and high permeability, the buccal mucosa is a critical site for drug uptake, facilitated by rapid molecular diffusion and higher drug absorption into the systemic circulation [38][39]. The structure of the epithelium, including its thickness and permeability, governs absorption of orally administered drugs by buccal route. The buccal epithelium, which lines the inner cheekbones, has a thickness of approximately 500–600 μm and provides a substantial absorptive surface. In addition, the sublingual epithelium, which is found on the floor of the mouth, is significantly thinner (100–200 μm) with smaller surface area. Despite the limitation, the sublingual region is distinguished by its exceptional permeability, which makes it a beneficial method for systemic drug administration [40], [41], [42].

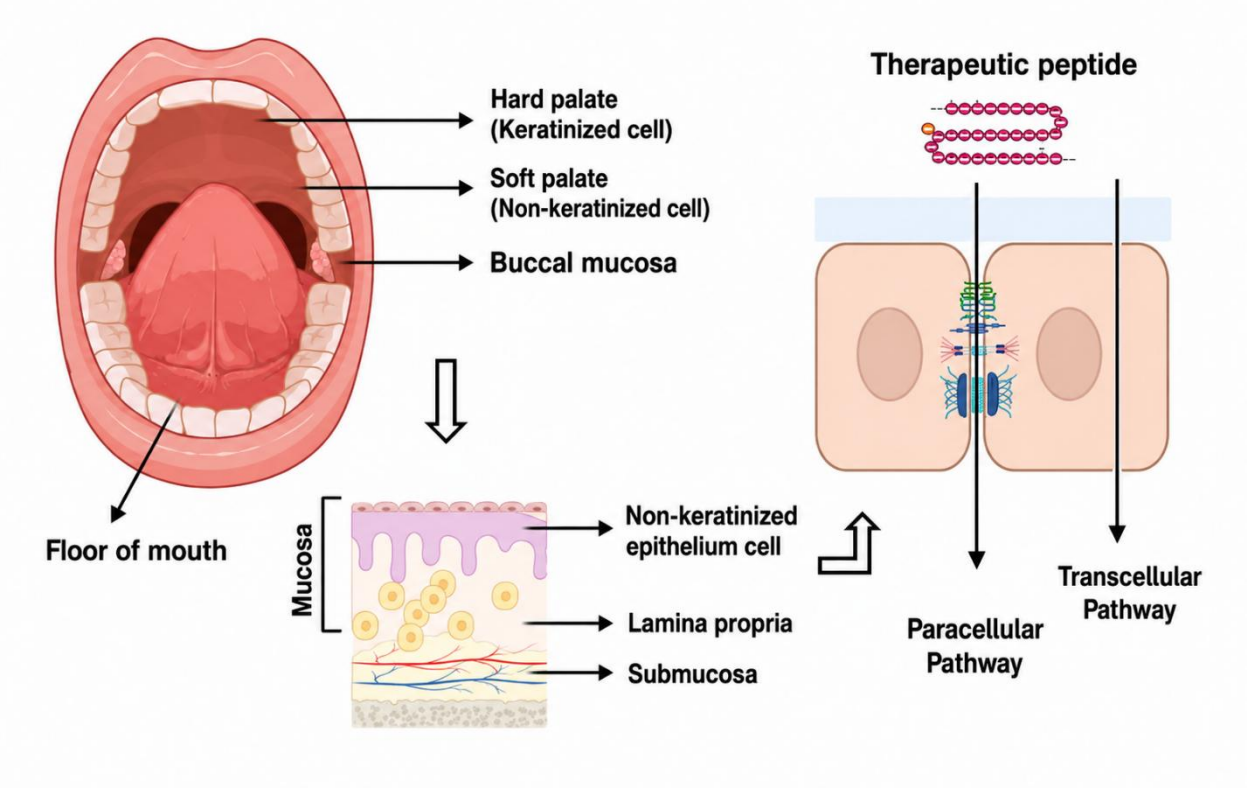

Figure 1.3: Anatomy of Oral cavity (left) and structure of oral mucosa membrane (middle). Different Transport mechanism for peptide molecules (right). Figure adapted from [7] .

The permeability of the mucosa to medications is influenced by the specific lipids produced by membrane coating granules (MCGs) located in the superficial epithelial cells. MCGs produce non-polar lipids in keratinised regions, which improve the barrier function and restrict drug penetration. In contrast, the non-keratinised regions, such as the buccal mucosa, contain MCGs that generate polar lipids, which helps more selective permeability and with a greater potential for drug absorption. These biochemical and structural properties give the buccal mucosa an optimal location for the delivery of localised or systemic peptides, thereby enabling the direct absorption of drugs such as antihistamines, analgesics, and hormone therapies into the bloodstream [43]. The two main routes of drug administration to the oral cavities are through the buccal and the sublingual mucosa. These highly vascularised regions, which cover approximately 60% of the oral mucosa, are considered the best sites for systemic absorption. Additionally, they are frequently employed

to address localised oral conditions, including periodontal disease, ulceration, and fungal infections [44], [45].

Saliva is a biological fluid present in the mouth cavity. It is secreted by the submandibular, parotid, sublingual glands, as well as by small submucosal glands. Saliva is continuously created, distributed and removes from the mouth for maintaining oral health. Its notable characteristics include proteins exhibiting various antibacterial properties, as well as the presence of electrolytes and chemical substances that regulate pH levels [46]. The quantity of peptide molecules present at the absorption site is significantly influenced by the salivary turnover. The rapid turnover of saliva limits the residence time of peptides in the oral cavity, hence restricting absorption. Moreover, the pH and composition of saliva influence the stability and solubility of therapeutic peptides. The pH of saliva is mildly acidic however, in pathological conditions such as gastro-oesophageal reflux disease and dental caries, the fluid becomes increasingly acidic, resulting in a decreased pH [47], [48]. The flow rate of saliva, which fluctuates daily and changes with food intake, influences its pH and composition. Elevated salivary secretion dilutes the drug, therefore potentially affecting its drug uptake or absorption and therapeutic efficacy [49].

Mucus is secreted by the salivary glands, contributing to the oral fluids that adhere to the epithelial cells. The mucus layer predominantly consists of water, enzymes, electrolytes, and mucins [50]. Mucins are glycoproteins, their molecular weights range between 0.5 and 50 kDa. Collectively, these substances form a 3-dimensional interconnecting network that lubricates the oral mucosa, facilitates cell migration among adjacent cells and protects the underlying tissue [51], [52]. Mucins are extensively glycosylated, and their terminal sialic acids are ionised at physiological pH to give a net negative charge for the mucus network. The electrostatic setting can either delay or enhance peptide absorption, depending on size, charge, hydrophobicity of peptide molecules, and their surface coating [53].

Approximately 15% of the oral mucosa's surface is occupied by the tongue which is a critical organ in the mouth. The tongue is composed of skeletal muscle and a mucous membrane [54]. The

extrinsic muscles of the tongue facilitate its movement. While masticating, the tongue is essential for the manipulation of food and ingesting [55].

To overcome obstacles and maximise the benefits of this route of administration, It is important to gain a comprehensive understanding of the anatomy and physiology of the oral cavity. Understanding the formulation and manufacturing techniques is necessary for the design of a drug delivery system targeting oral cavity. The simplicity of buccal dosage forms, that offer flexible design platforms, contributes to patient acceptability and compliance. In addition, buccal drug delivery facilitates the direct absorption of medications into the bloodstream, thereby bypassing hepatic first-pass effect and challenging enzymatic and acidic conditions of the GI tract **(Table 1.2)**, that have the potential to damage peptides[56].

Table1-2: Physiology and enzymatic features, cons and pros of the intestinal tract versus oral cavity [7].

Features	Intestinal Tract	Oral cavity
Epithelium cell type	Single-layer columnar epithelium with mucus layer (non-keratinised)	Stratified squamous epithelium (keratinised or non-keratinised)
Epithelial Thickness	Thin (20–30 μm) [57]	Thicker (100–200 μm) for non-keratinised epithelium
Surface Area	Very large (due to villi and microvilli)	Limited surface area
Mucus Layer	Variable Thickness and the thinnest in the small intestine	Thinner mucus layer [58]
Enzymatic Barriers	High activity of digestive enzymes (proteases, peptidases) in lumen and the brush border	Proteolytic enzymes are present but less extensive than GIT lumen
pH Environment	Variable, acidic (stomach pH 1–3), neutral to basic in intestines	Neutral pH (6.5–7)
First-Pass Metabolism	Significant hepatic first-pass metabolism	Bypasses hepatic first-pass metabolism
Transit Time	Rapid and variable; exposure is limited by gastric emptying and intestinal transit	Short residence time and increase duration of stay with special aids
Absorption Route	Transcellular, paracellular and endocytic	Transcellular, paracellular and some endocytic [59]
Salivary Washout	Not applicable	Present, reduces drug residence time
Bioavailability of peptides	low	low
Accessibility and Control	Anatomically deep within the body, limiting ease of access and direct control over administration conditions	Easily accessible and visible, allowing for precise administration and better control of the local environment
Advantages	Large surface area and non- invasive	Potential for rapid onset of drug action and less metabolism
Disadvantages	Harsh enzymatic and acidic environment, first-pass metabolism	Small surface area and presence of salivary clearance

1.2.3.1 Mechanisms of Peptide uptake via Oral Mucosa

There are 2 primary pathways through which peptides are absorbed through the oral mucosa: transcellular (across epithelial cells) and paracellular (between cells) **(Figure 1.3 right)**. Nevertheless, the permeability and absorption of peptides are significantly hindered by their physicochemical characteristics, which include enzymatic instability, polarity, and a high molecular weight [60]. Lipophilic and/or low molecular weight molecules are more likely to navigate through the transcellular route. as they partition into the lipid bilayer of the epithelial

membrane. Consequently, the majority of peptides demonstrate inadequate uptake via this pathway [40], [62]. Mechanisms like endocytosis or transcytosis may allow for very limited peptide transport due to their low capacity [63]. Similarly, paracellular transport across the oral mucosa is highly restricted by intercellular junctions, which limit the passage of large and hydrophilic molecules such as peptides. Oral epithelial cells have been reported to express several nutrient-related transporters, including glucose transporters such as SGLT1, GLUT1, GLUT2 and GLUT3, as well as amino acid transporters such as LAT1 and LAT2. However, their abundance in healthy oral mucosa appears to be variable and less well characterised than in the gastrointestinal tract. For example, glucose transporter expression has been detected in human oral mucosal epithelial cells, Whereas LAT1 expression has been reported in normal oral mucosa but is more strongly associated with increased metabolic demand in oral premalignant and malignant tissues. Therefore, although these transporters may provide potential targets for future oral-mucosal drug delivery strategies, their direct role in transporting therapeutic peptides across the buccal or sublingual mucosa remains largely unproven [63- 65].

1.3. The Challenge of Peptide Absorption and Transport via Oral Mucosa

Molecules with molecular weights greater than 500 Da often have poor membrane permeability, this limitation is related to most peptides that are typically greater than 1,000 Da. Peptides have a strong hydrophilicity that limits membrane partitioning, in which the ionisable side chains interact poorly with the lipidic mucosal surface, rendering passive diffusion ineffective. Moreover, the systemic bioavailability of peptides is reduced by the presence of aminopeptidases and esterases in the saliva before being absorbed through the epithelial barrier [66]. There was less expression of P-glycoprotein (P-gp) efflux pumps in buccal tissue in comparison to the intestinal tissue, which is important as P-gp actively transports numerous substrates back into the lumen. Therefore, buccal mucosa is a relatively favourable location for enhancing peptide absorption, despite some limitations like large molecular size, high polarity, and being prone to enzymatic degradation, as a result of the reduced efflux activity [67].

Additionally, peptides may undergo degradation in the oral cavity as a result of the pH changing in saliva, unless they are accompanied by advanced formulations, including nano delivery platforms such as vesicular forms and polymeric nanoparticles [68]. Moreover, the buccal route is not appropriate for the administration of all medications. Medications that are characterised by an intensely tastes, e.g. bitter or sour, unpleasant or bad odour, or instability at salivary pH, as well as those that trigger local irritation or allergic reactions in the oral cavity, are generally not suitable for buccal delivery. However, due to saliva secretion and renewal effect, the peptide's concentration on the mucosal surface will be decreased. Furthermore, the drug may be physically removed from the absorption site by spontaneous swallowing of saliva, or during food and/or liquid consumption, that further reduces absorption efficiency. The combination of these factors may lead to low therapeutic plasma concentrations and limited bioavailability [69].

Some evidence has shown that the conventional buccal or sublingual route delivers only approximately 1–2% of a peptide dose to the systemic circulation, as evidenced by insulin studies [34], [70]. This highlights the significant obstacles that exist for effective delivery of peptides through the oral mucosa. Effectively addressing these limitations is essential for the success of an innovative buccal delivery system for peptide drugs.

1.3.1. Molecular Weight of peptide drugs and Permeability via buccal route

The main factors influencing diffusivity of drugs through the buccal epithelium are molecular weight and size. The mucosa is easily penetrated by small molecules of molecular weights 75–100 Da. The majority of therapeutic peptides are poorly absorbed through this route without the use of additives, since permeability declines as molecular size increases. Multiple studies have been working on the effect of molecular weight on permeability **(Table 1.3)** Neutral polysaccharides such as fluorescein isothiocyanate-dextrans (FITC dextrans) have been used as model compounds to study the mucosa permeability of peptides and proteins. They demonstrate decreased permeability as their molecular weight increases, especially those above 10 kDa, according to research by Hoogstraate et al [71]**.** Furthermore, Fantini et al. (2022) reported that FITC-dextrans ≥70 kDa had less passive penetration in a buccal model using porcine esophageal mucosa tissue.

Nevertheless, co-administration of caprylic acid or sodium taurocholate greatly enhanced permeability, allowing high-MW dextrans to be transmucosally delivered [72]. Similarly, Keum et al. showed that the model peptide drug salmon calcitonin (MWt 3.4 kDa) had limited passive permeability. However, when a cell-penetrating peptide (CPP) was added, salmon calcitonin buccal absorption increased by 5.5 folds in TR146 cell layers and an exceptional increment of ~93.7times in an ex vivo porcine buccal mucosa model, demonstrating the impact of using biochemical permeation enhancers [73]. Berka et al. examined the passive diffusivity of bovine serum albumin (BSA) and various FITC-dextrans (different MW) grades across the sublingual mucosa of porcine. They discovered that dextrans' permeability dropped as molecular weight of compounds increased, and the compounds exhibited low transport above 10 kDa. However, peptides with similar molecular weight to dextrans such as BSA (~66 kDa) showed superior permeability, this is because of variations in structure and charges that influence their interaction with mucosal barrier [74]. Also, improving diffusion and absorption by applying compounds such as nanofiber mats greatly increased mucosal permeability by boosting local drug concentration and establishing close contact with the mucosa. The study has demonstrated how nanofiber-based delivery methods can help peptides and proteins to pass the sublingual mucosal barrier [72]. According to a review by Veuillez et al, smaller peptides like oxytocin (1007 Da) and protirelin (362 Da) can effectively penetrate buccal tissues, while larger ones, such as calcitonin (3500 Da) and buserelin (1239 Da) need permeability enhancers to more efficient transport [75]**.**

Table 1-3: Permeability data of various macromolecules across different oral mucosa models [7].

Route / Model	Compound and MW	Permeability Enhancer	Permeability / Outcome	Reference
Buccal (in vivo, pig)	FD-4 (4 kDa)	without enhancement	Bioavailability 1.8 %	Hoogstraate et al., 1996
Buccal (in vivo, pig)	FD-4 (4 kDa)	10 mM sodium glycodeoxycholate (GDC)	Bioavailability increased to 12.7 %	[71]
Sublingual (porcine)	FD70 dextran (~70 kDa)	without enhancement	Papp 2×10^{-10} cm/s extremely low permeability	Berka et al., 2020
Sublingual (porcine)	FITC-BSA (66 kDa) As nanofiber mats	without enhancement	Papp1 $\times 10^{-7}$ cm/s 1,000× faster than FD70 dextran (~70 kDa)	[74]
Esophageal porcine mucosa (a buccal model)	FITC-dextrans (4–70 kDa)	without enhancement	P_app $\leq 10^{-7}$ cm/s for >40 kDa FD-70 and FD-150 did not cross the membrane in detectable amounts	Fantini et al., 2022 [72]
Esophageal porcine mucosa (abuccal model)	FITC-dextrans + enhancer	+ Caprylic acid/ taurocholate	P_app significantly increased, enabling >10 kDa transport	
Buccal (TR146 cells)	Salmon calcitonin (3.4 kDa)	+ 12.2 μM Penetratin (CPP)	5.5× increase in permeability over passive	Keum et al., 2020
Buccal (porcine tissue)	Salmon calcitonin (3.4 kDa)	+ 12.2 μM Penetratin (CPP)	93.7× increase in permeability over passive	[73]

1.3.2. Conformation of peptides

Peptide therapeutics differ fundamentally from conventional small molecule drugs owing to their complex three-dimensional structures and conformational flexibility. Their structural configuration in solutions is sensitive to environmental conditions such as molecular size, ionic strength, and pH. This conformational variability directly influences their biological activity, stability and membrane permeability.

An in-silico investigation examining the mucosa diffusivity of several conformationally flexible cyclic peptides. The study has demonstrated that transmembrane transport of these molecules is governed by dynamic peptide to lipid interactions. In this case, specific amino acid residues interact with the lipid polar headgroups and acyl chains of lipid bilayers, facilitating partial insertion of the peptide into the membrane [76]. Upon insertion, the peptide may undergo a conformational rearrangement into a more compact “closed” structure. In this state, polar and

charged moieties are shielded from the hydrophobic membrane, while residues rich in hydrocarbon orient towards the lipid tails. This adaptive restructuring reduces the energetic disadvantage associated with membrane partitioning and enables the peptide to cross the mucosa membrane. These findings underline the critical role of conformational flexibility and structural adaptability in overcoming lipophilic and steric barriers presented by biological membranes. Since conformational changes can greatly affect membrane permeability, it is imperative to maintain the native shape throughout the formulation and manufacturing processes [77]. On the other hand, altering the structure of peptides or conjugating them with polyethylene glycol (PEG) or dextran enhances their mucosal permeability while simultaneously reducing their immunogenicity and shielding them from enzymatic degradation [78], [79], [80].

1.3.3. Other Physicochemical properties

Peptides are amphiphilic molecules whose ionisation states and solubility are strongly influenced by environmental pH. Their aqueous solubility typically reaches a minimum at the isoelectric point, where the molecule carries net zero charge and intermolecular aggregation is favoured. Owing to their generally high polarity and low octanol–water partition coefficients, most peptides exhibit limited passive diffusion across the lipid membranes. Consequently, membrane permeation remains one of the principal barriers to effective mucosal peptide delivery.

One established strategy to enhance peptide permeability involves lipophilic prodrug or charge-masking approach. By modifying hydrophilic peptides with lipid moieties, polarity can be reduced and membrane partitioning improved. For instance, lipid derivatives of cyclic N-methylated hexapeptides containing the Arg-Gly-Asp (RGD) motif demonstrated enhanced transcellular transport across Caco-2 monolayers, indicating improved mucosal permeability following lipophilic modification [80]. This modification approach can be employed to modify the permeability of peptides that is polar in nature across buccal mucosae. Hydrophilic substances are predominantly transported across mucosal barriers by paracellular route, while lipophilic medications are absorbed through the transcellular route [81], [82]. Passive diffusion of polar peptides across lipid membranes is restricted by their low octanol-water partition coefficients,

which are commonly characterised by their high hydrophilicity. However, recent research has demonstrated that buccal absorption and drug bioavailability can be improved by the addition of fatty acid chains or other lipophilic moieties to peptide structure, in non-linear manner. Zhang and Bulaj (2012) explored the utilization of lipidation to improve the performance of peptide drugs, emphasising that fatty acids, including lauric (C12), myristic (C14), palmitic (C16), as well as stearic acid (C18), are frequently conjugated lipid moieties. They examined lipidated analogues with pertinent peptides, such as insulin and glucagon-like peptide-1 (GLP-1), in which the attachment of fatty acids has enhanced metabolic stability, extended the half-life and promoted mucosa permeability of peptide agents. It was emphasised in the study that the pharmacokinetic and pharmacodynamic profiles are significantly influenced by the fatty acid chain length and the site of lipid attachment in these peptide agents [83].

Intermolecular hydrogen bonding of amino acid residues of a peptide sequence with water molecules can generate a hydration shell that diminishes membrane partitioning ability by making peptide agent more polar and lowering the octanol–water partition coefficient [84]. Nevertheless, recent research has demonstrated that certain cyclic peptides with robust intramolecular H bonds, which are generated during conformational folding process, can cover polar groups efficiently to reduce their exposed polarity, and hence enhance passive transport of these molecules [85]. Furthermore, a study has shown that thioamide substitutions (>C=O to >C=S) in some macrocyclic peptides can lessen desolvation energy, improve passive diffusion rate and metabolic stability in vivo by diminishing intermolecular hydration [86]. Further the evidence confirming intramolecular H bonding effect on peptide permeability has been reported [87]. The efficient method that Merz et al. (2023) developed was used to construct thioether-cyclized peptides aiming at better target binding and passive membrane permeability by using PAMPA assays. They screened a library of 8,448 N-acylated cyclic peptides and have identified candidates with favourable properties. The investigation revealed that certain peptides exhibited strong affinity for thrombin (in nanomolar concentration) and successfully achieved oral bioavailability in rats of up to 18%. Passive diffusion of cyclic peptide across epithelial membrane was again enhanced by modulating intramolecular H bonding and lipophilicity, which was the crucial factor in these discoveries. Summing, one critical method for enhancing performance of peptide agents is to

increase overall lipophilicity, lessen hydrogen bonding with water molecules, and lower effective hydrodynamic radius [88].

A recent study has also underscored the importance of peptide self-association and/or aggregation, which can affect absorption and stability of peptides. For instance, researchers have demonstrated that using non-ionic surfactants, including Pluronic F-68 and F-127, may decrease the aggregation tendency of insulin molecules while improving its solubility, [89] Furthermore, the protracted contact with the mucosal tissue can result in local irritation or toxicity in buccal formulations, such as microneedle-based devices or patches [61].

1.3.4. Electrostatic Charges of Peptide

The charge type and its distribution of a peptide play a pivotal role in its interaction with the mucus layer and epithelial barriers of the oral mucosa. Mucus, which lies epithelia, is composed primarily of negatively charged mucin molecules, which influence electrostatic interactions, residence time, and diffusion behaviour of charged molecules. Peptides that exist in zwitterionic forms, bearing both positive and negative charges and net zero charges, are often presented with reduced membrane penetration despite having favorable partition coefficients. This is because balanced charge distribution can limit interaction with molecules of lipid bilayers and epithelial membranes, thereby hindering its translocation. Glutathione (307 Da), a small tripeptide, has illustrated this limitation. Despite its low molecular weight, it demonstrates extremely poor passive membrane permeability due to its hydrophilic and zwitterionic characters.

Fluorescence spectroscopy and NMR-based studies have confirmed that glutathione does not passively penetrate lipid bilayers, as its charge distribution and hydration shell prevent efficient membrane partitioning [90], [91]**.** Nevertheless, certain non-classical zwitterions, which are engineered to establish intramolecular hydrogen bonds and internal charge offsets, can preserve high permeability and lipophilicity as described in earlier sections. This suggests that there are opportunities to enhance peptide transport across the buccal barrier using this approach that has

been Successfully demonstrated with non-classical zwitterions of small molecules, such as piroxicam where the design includes creating weak but matched pK_a values that are achieved through intramolecular stabilisation [92]**.** Moreover, peptides coated with zwitterionic nanoparticles have demonstrated a 4.5-fold increase in epithelial uptake in a cell culture model with an effective delivery of insulin to oral cavity in an in-situ rat model [93].

Furthermore, the mucosa transport efficiency could not be accurately estimated directly by the peptide net charge. Nevertheless, the mucosal transport of cationic peptides is influenced by the positions of these charged species and the hydrophobic residues within the peptide structure [94]. Peptide ionisation and charge density are affected by pH adjustments in the formulation. [94][95] Recent methods include ion-pairing technique, which involves the pairing of peptides, such as insulin, with bile salts or amino acids, to create neutral complexes that have significantly improved mucosal penetration. In a single study, the ion-paired approach utilizing sodium glycodeoxycholate had resulted in a 3–50-fold increase in intestinal insulin permeability [95]. Paracellular pathways are commonly excluded in mucosa uptake of peptides, however, this pathway has facilitated the uptake of certain positively charged peptides, including thyrotropin-releasing hormone [96].

1.3.5. Strategies for Improving Peptide Stability and Permeation through the Oral Cavity

Various techniques have been explored to address the issues associated with the oral absorption of peptides (**Figure 1.4**). They include new formulation strategies, structural modification by chemical coupling of peptide agents with hydrophobic ligands, entrapment in nanoparticles that demonstrate specific affinities, changes of the amino acid backbone, and the use of specific additives such as enzyme inhibitors, permeability enhancers, and/or selective mucoadhesive polymers [97].

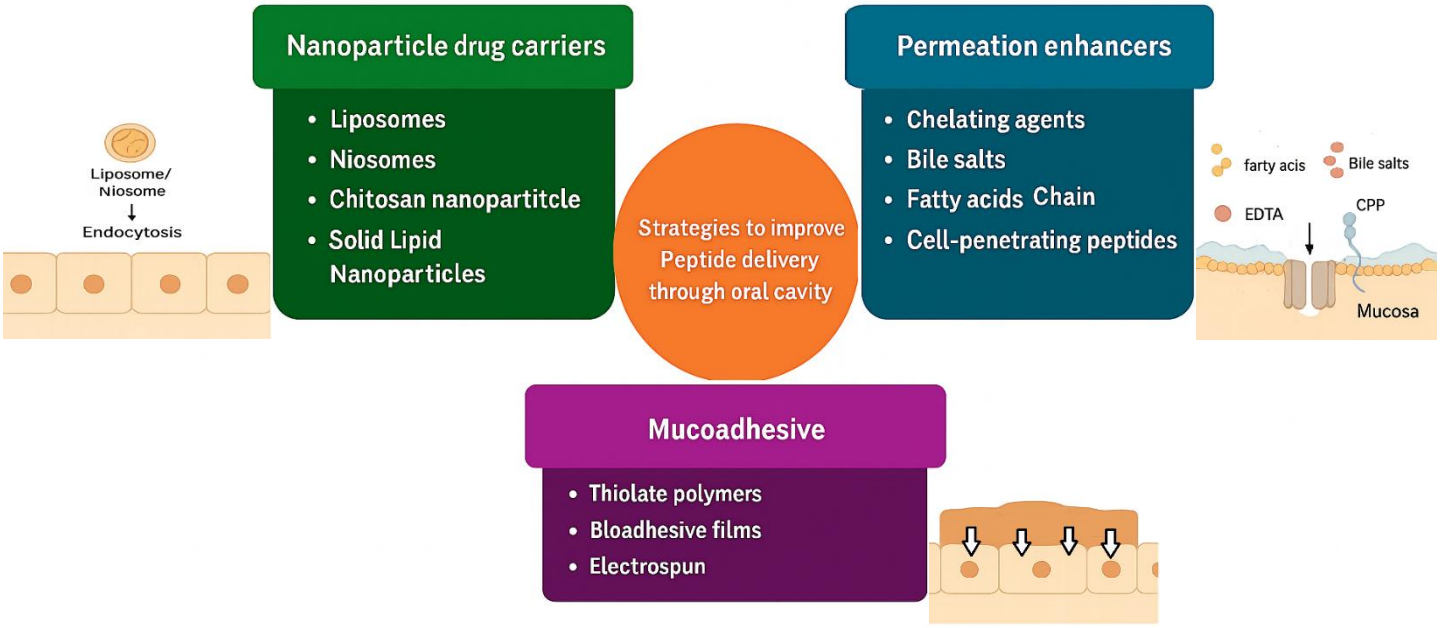

Figure 1.4: Schematic diagram illustrating different approaches to improve peptide delivery into the oral cavity. Figure adapted from [7] .

1.4. Formulation Strategies

A. Permeation enhancers have a vital role in enhancing the bioavailability of peptides delivered through the oral mucosa. They overcome the barrier aspects of the buccal epithelium. These enhancers primarily react by temporarily weakening the tight connections of the epithelial cells to boost paracellular transport. They also interact with molecules of lipid bilayers to enable better transcellular drug passage. In the context of natural enhancers like α-bisabolol (a terpene) have garnered significant attention due to its capacity to interact with lipid found in the cell membrane. This interaction resulted in an increase in drug permeability without damaging tissue integrity. This was established by in vitro investigations conducted on porcine mucosa utilizing a series of small drug molecules [98]. Chelators such as EDTA and EGTA bind to calcium ions that

preserve tight junction integrity, thus enhance paracellular permeability [99]. Bile salts, such as sodium salt forms of taurocholate and deoxycholate, act as surfactants, reducing epithelial barrier resistant and facilitating transcellular and paracellular permeability of molecules [79]. Research indicates that Na taurocholate enhances the transit of fluorescent dextrans (70-150 kDa), in porcine buccal mucosal tissues confirming its efficacy as a permeation enhancer [72]. Medium-chain fatty acids, particularly sodium caprate, fluidises lipid membrane and regulates tight junction proteins, such as claudin-5, while improving peptide absorption and preserving mucosal integrity [100]. Zwitterionic small molecules, such as SNAC (sodium N-[8-(2-hydroxybenzoyl)amino]caprylate), enhance peptide solubility and permeability, serving as crucial constituents of commercially available oral peptide pharmaceuticals, like Rybelsus [100].

Moreover, cell-penetrating peptides (CPPs), including Penetramax (a penetratin analogue), enhance cellular absorption by promoting endocytosis and changing tight junction dynamics, and Studies have demonstrated their capacity to reversibly open epithelial barriers in a controlled approach [101]. [102]. Xiao et al. created a PEGylated low-molecular-weight protamine (LMWP) insulin for the purpose of enhancing mucosal penetration and product stability. For both vitro and ex vivo studies, they have indicated that insulin molecules migrated across buccal mucosa models better, while in vivo experiments (rabbit model) have revealed a bioavailability of 26.9% after buccal administration of the conjugated form of insulin, which is considerably higher than that of free insulin[103]. The improved absorption has been attributed to CPP-mediated enhancement of transcellular transport and increased mucoadhesion that has been defined as the reversible adhesion of a dosage form to mucus or epithelial surfaces via several types of non-covalent bond interactions, or covalent disulfide interactions within the oral cavity. This interaction extends the residence time and lowers salivary wash-off without causing buccal irritation. These permeation enhancers collectively provide many effective ways to enhance buccal peptide transport, with continuing research aiming at improving safety and efficacy profiles for clinical applications.

.B. Enzyme inhibitors may avoid the rapid degradation caused by proteolytic enzymes, such as serine proteases, metalloproteinases. In order to overcome this obstacle, buccal delivery systems have been created to protect peptides. For example, by co-formulation with insulin in thiolated chitosan xerogels with aprotinin, a serine protease inhibitor has resulted in a 70% reduction in enzymatic degradation; a 1.7-fold enhancement in insulin permeability in human EpiOral™ model and higher absorption via an ex vivo sheep buccal mucosa [104]. Another method is the utilisation of chitosan–EDTA conjugates that chelate zinc ions in metalloproteases. Walker et al. (2002) conducted a study on the activity of peptidase in porcine buccal mucosa. The researchers discovered that aminopeptidase N is the key enzyme responsible for the degradation of Leu-enkephalin [only 18 ± 9% peptide survived after 2 h at 37 °C]. Degradation of such peptides was substantially reduced by enzyme inhibitors, such as amastatin, Na deoxycholate and EDTA. Furthermore, Na deoxycholate disrupts the mucosal barrier to facilitate peptide permeation. According to these results, the buccal delivery of peptides can be significantly enhanced by combining enzyme inhibitors with permeability enhancers [66]. Thiolated polymers (thiomers) have become increasingly popular due to their multifunctional properties. They not only enhance mucoadhesion and extend the mucosa residence time, but they also inhibit enzyme activity by acting as chelating metal cofactors. This has resulted in an improved bioavailability of salmon calcitonin and insulin [104]. The results of this study indicate that enzyme inhibiting property, when integrated into multifunctional or polymer-based systems, are a promising approach to safeguarding peptides at the buccal absorption site and overcoming one of the primary obstacles to transmucosal peptide drug delivery.

C. Mucoadhesive drug delivery systems. They have emerged as a critical approach to improving the bioavailability and prolonging residence times of peptides that are administered through the oral mucosa, especially to the buccal region. This type of delivery system is engineered to stick to the mucosal surface, thereby preventing salivary flow and establishing a sustained-release environment for peptide agents. Commonly used thiomers are thiolated chitosan, thiolated pectin, and thiolated hyaluronic acid as mucoadhesive agents. These polymers have the ability to form covalent disulphide bonds with cysteine-rich mucin molecules found in the mucus layer [105]. Recent research has shown that S-protected thiolated β-cyclodextrin derivatives possess

stronger mucoadhesion in comparison to native CD. This is achieved by higher product viscosity and more interpenetration of polymeric chains with the intestinal mucosal surface [106]. Additionally, pre-activated thiolated hyaluronic acid exhibited a four-fold increase in mucoadhesion when contrasted with native hyaluronic acid, thereby extending the residence times of small model drugs for potential of oral applications [107].

Another innovative approach involves bioadhesive coatings inspired by mussel shells, which employ catechol chemistry to replicate the strong but wet adhesion of marine mussels. Films produced with this niche material have exhibited adhesive forces that exceed 39 kPa, indicating that a sustained-release model of small drug molecules, which is a promising strategy for the controlled release preparation of peptides in buccal tissues [108]. Furthermore electrospun mucoadhesive membranes, which contain interwoven fibrous architecture and a high surface area, exhibit strong physical connections with the mucus and have been shown to sustain insulin activity and release for an 8-hour period [109]. In chapter 3 of this thesis niosomal formulations of vancomycin hydrochloride, a glycopeptide antibiotic, that were integrated into polyvinyl alcohol (PVA) fast-disintegrating oral films. These newly designed films exhibited antibacterial activity against *Bacillus subtilis*, rapid disintegration (~105 seconds), high drug encapsulation efficiency, and small particle sizes. This study demonstrates how the combination of nanocarriers with mucoadhesive polymers such as polyvinyl alcohol (PVA) might improve the oral delivery potential of macromolecular peptides, which normally have problems with low permeability and stability [110], [111]. Hybrid films not only adhere to the buccal mucosa they also resist enzymatic degradation, as well as provide controlled peptide release. In general, mucoadhesive strategies, which cover both natural and synthetic polymers such as PVA, are essential for the development of oral mucosal peptide delivery platforms. These platforms offer a combination of enhanced therapeutic efficacy, improved stability, and prolonged contact time.

1.5. Rationality of using Nanoparticles for Peptide Delivery

In the buccal cavity, peptide therapeutics face a variety of obstacles. The administered dose is diluted and eliminated by the continuous flow of saliva. The diffusion of large molecules is blocked by the mucus layer comprises of dense in mucin network. The movement of substances through the spaces between cells is restricted by the tight junctions between epithelial cells. Before they can reach the epithelial surface, peptides are degraded by enzymes found in saliva. Even for small peptides with appropriate properties, these factors result in limited but variable absorption across the buccal and sublingual mucosa [112] Incorporating peptide molecules into nanoparticle carriers is an approach to improve peptide delivery into the oral cavity. This approach can protect the peptides from enzymatic assaults and aids their passage through the oral epithelial barriers (**Figure 1.5**) [113], [114], [115]. The numerous techniques that are available have generated significant interest in nanocarriers [116].

Nanoparticles, which are frequently produced as submicron carriers with diameters of 300 nm or less. They are promising systems for the oral delivery of peptides. Polymeric nanoparticles have the ability to encapsulate molecules of different physicochemical properties and later release them in a controlled manner. Those carriers not only protect peptides from degradation but also extends their stays and increases their effective concentration at the absorption site. As a result, the prevalence of therapeutic peptides that are administered through the buccal mucosa can be substantially enhanced by nanoparticle systems [117], [118]. Nanoparticle carriers offer a variety of adjustable functions that are not available in conventional solutions, gels, or tablets, in addition to standard protection and controlled release. The embedded peptides are protected from salivary enzymes and dilution by vesicular and polymeric systems until they are at the epithelial surface. Polyethylene glycol or zwitterionic layers, chitosan or thiomer coatings, and other layered shells can be used to modify the surface in order to enhance mucoadhesion and prolong the residence time, or to facilitate movement through mucous when deeper access is required. The carrier can also be directed towards transcellular uptake or be internalized by endocytosis and later transcytosis by modifying composition and size, a pathway that is favoured by lipid-based particles [119].

Oromucosal models have shown that nanoparticles of approximately 200 nm penetrate the buccal epithelium more deeply and have a prolonged duration of residence within the microplicae than those of 25 to 50 nm. This trend is consistent with the interactions that have been reported in human oral epithelial cell models, such as TR146. The incorporation of these carriers into mucoadhesive systems, such as films, patches, or sprays that create thin films in the mouth, results in the retention, protection, and effective interactions with the epithelium of a amount that would otherwise be rapidly destroyed by localized enzymes [120]. In conclusion, the evidence indicates that nanoparticles are not only small containers, but also adaptable tools for oromucosal delivery and they offer flexible transport modes of molecules across the narrow epithelial barriers. All these characteristics provide a clear rationale for prioritising nanoparticle systems over traditional dosage forms for the delivery of peptides in the oral cavity [121].

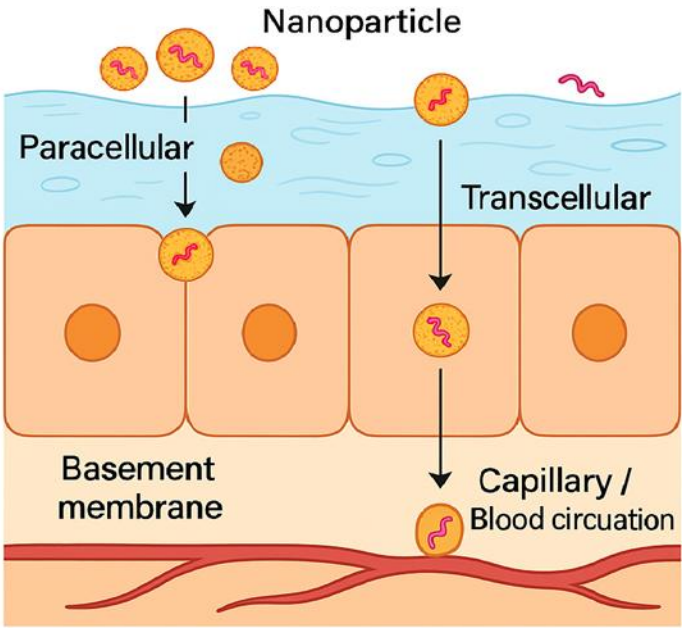

Figure 1.5: Schematic diagram showing Epithelial cell penetration using a nanocarrier system. Figure adapted from [7] .

1.6. Mechanisms and performance of oromucosal nanoparticles

1.6.1. Local microenvironments for saliva and mucus

The rapid formation of a salivary pellicle, which is a thin protein film derived from saliva, influences the behaviour of nanoparticles after getting into contact with saliva. While mucins can bridge particles, ions and electrolytes reduce the electrical double layer, and absorbed peptides form a protein corona that can alter the molecular adhesion and peptide-cell interaction [122]. In order to prevent immobilisation, brush-like densities are required, while subcritical coverage can enhance mucoadhesion. Polyethylene glycol or zwitterionic coating reduces hydrophobic and electrostatic adherence and facilitates movement of particles through mucus. To substantiate translational claims for nanocarrier systems, it is imperative to provide thorough reporting of physicochemical parameters, including grafting density, polymer conformation, and particle mobility. This can be done using multiple-particle tracking process. These measurements can be correlated with in vivo translational potential, interfacial behaviours, and nanoscale mobility by combining them with few particle tracking dyes in biological media (e.g., mucus) [123]. Designs that arrange adhesion will prevent nanoparticle slip-through and wash-off, thereby delivering carriers to the cell surface [113] [124]. Different proteases are present in Saliva, and their activities is subject to variation between individuals and overtime. The simple encapsulation of peptide is frequently insufficient. Peptide half-lives can be prolonged by local microenvironments that regulate pH or water activity, as well as barrier layers that delay enzyme access. If protease inhibitors are employed, their appropriateness for the route and any impact on pellicle formation should be demonstrated. There is a need to verify the integrity of peptides in whole saliva and, whenever possible, through applicable activity assays[125].

1.6.2. Nanoparticles Size, Surface charge and safety concerns

Evidence from route-relevant models indicates that buccal delivery is most effective when an intermediate nanoparticle size window is adopted. Yang et al. demonstrated that nanovesicles loaded with insulin, with a diameter of approximately 220 nm, induced the greatest buccal absorption and a significant glycaemic control in rabbits. Contrastingly, vesicles that were larger in size, with a diameter of approximately 400 nm, demonstrated a lower degree of bioavailability

and permeability. Combined with relevant datasets, these results suggest that nanoparticles in the 200–300 nm range offer a practicable equilibrium between the efficiency of systemic delivery, avoidance of mucus binding, and epithelial penetration for buccal applications [126]. In addition to the mean diameter, polydispersity index (PDI) and shape also govern the manner in which carriers settle within epithelial pores under shear force. Consequently, particle size before and after drying as well as rehydration should be reported, as process can transform both size and surface properties [127]. Efficacy must be analysed in conjunction with product safety. Any reported increase in permeability with enhancers or due to modification of cationic surface should be accompanied by evidence of reversibility, such as the return of protein of tight junctions (e.g. ZO-1, claudin) to cell borders by microscopy and the recovery of transepithelial electrical resistance after discharge. While TR146 culture models are beneficial for understanding the mechanism, they should be supplemented by an ex vivo buccal tissue test to enhance their reliability. Composition can increase uptake without increasing cellular stress, thereby supporting composition-guided optimisation rather than simply boosting positive charge [128]. Also, risks associated with potential cytotoxicity and limited biodegradability of inorganic and carbon-based nanoparticles should be accounted for. An example of this is carbon nanotubes and silica nanoparticles, which have the potential to accumulate in tissues or trigger unwanted inflammatory responses, these safety concerns may restrict their clinical translations [129]. Mucoadhesion effect can be improved by nanoparticles with a positive (cationic) surface charge as a result of their electrostatic interaction mucin at epithelial membranes. This interaction may enhance paracellular transport. However, membrane irritation or cytotoxicity may also result from an elevated or uniform cationic charge. Compared to uniformly high-zeta-potential systems, nanoparticles with localised or irregular positive charges on a well-hydrated surface, such as chitosan-coated PEGylated nanoparticles, can maintain adhesion and good permeability while simultaneously reducing irritation [130]. In order to target a paracellular route, a brief and reversible opening of epithelia tight junctions is necessary. Calcium chelators lower the level of extracellular calcium and loosen cadherin complexes, while medium-chain fatty acids or bile salts disrupt membrane order and temporarily organize tight junction proteins e.g. occludin, both cases aids peptide transport paracellularly. An increase in permeability should be accompanied by a decrease in transepithelial electrical resistance (TEER) and a complete recovery of transepithelial channel. Substantial evidence, therefore, indicates that

TEER recovery follows by an increase in apparent permeability. This is supported by the fact that imaging demonstrates that tight-junction proteins initially disperse and subsequently return to cell borders, followed by a washout phase that restores the baseline [131].

1.6.3. Nanoparticle cellular uptake and trafficking

Nanosystems such as liposomes, solid lipid nanoparticles and niosomes can be taken up by cells through a variety of mechanisms as discussed in earlier part actin-driven macropinocytosis is a non-selective process in which the cell membrane folds outward to incorporate surrounding fluid and particles into large vesicles within the cells. Uptake of nanoparticles in micropinocytosis is achieved without the need targeting molecules which improves intracellular trafficking and drug delivery by allowing larger or more flexible nanoparticles to enter cells efficiently. Contrastingly, the majority of transport mechanisms that were previously employed, such as paracellular diffusion or mucin penetration, occur outside of the cells, macropinocytosis creates a more active, cell-mediated route which improves the bioavailability and entry of nanoparticle-encapsulated peptides. Together, matrix lipids, the quantity and type of edge activator and the surface coating of nanoparticles determine the extent and route of uptake, as well as the equilibrium between cellular stress and transport. Intracellular trafficking in human TR146 cells is composition-dependent, which enables the development of carriers for productive transcytosis while simultaneously reducing adverse signals. CPP-conjugated liposomes enhanced the permeation of salmon calcitonin through TR146 cell model and ex vivo porcine buccal tissue, thereby illustrating CPP-assisted transcellular transport in route-relevant conditions. Other binding strategies such as conjugation with folic acid or lectins as well as employing membrane-mimicking lipid domains can facilitate peptide transport [132] [133].

1.6.4. Device Perspective

The delivery of nanoparticles as simple suspensions is uncommon, as they are susceptible to rapid spreading and are typically washed away by saliva prior to significant absorption. Mucoadhesive films, patches, or sprays that deposit thin layers over the mucosa can be used to accomplish more effective delivery. These dosage forms minimise drug loss attributed to saliva dilution or swallowing, maintain a local concentration gradient, and maintain direct and protracted contact

with the epithelium [121]. Film-forming sprays can distribute carriers uniformly and produce on site layers that enhance stability and onset [134]. The final dosage form must be characterised in saliva-mimicking media. The batch reproducibility should be documented, as processing stages such as casting and spraying can alter product properties and their performance as well as changes lipid properties and fate of peptide upon administration [121] [132].

1.7. Comparative design and human evidence

Design characteristics that are identical to buccal and sublingual models include device integration to secure mucosal residence, particle size that maximizes retention and allows for deep penetration to epithelial microarchitecture, plus transcellular engagement that balances cellular uptake. Ideal particle characteristics have illustrated by the consistent success of surface-engineered vesicles or their hybrids of ~ 200 nm in oromucosal designs, which are held firmly by a dosage form. CPP-conjugated liposomes for salmon calcitonin and deformable vesicles containing insulin are representative examples, which support the principle that vesicle performance is influenced by composition and residence time [135] [113]. Early human studies on buccal insulin sprays, although not nanoparticulate, demonstrated measurable effects and a fast onset for systemic use, but the results were inconsistent. The availability of human data for nanoparticle-enabled insulin is still restricted in comparison to animal studies. Nevertheless, strong preclinical research outcomes on nanovesicles and nanoparticle-in-film as drug transport systems have demonstrated the potential development of nanosystem-in-device strategies that utilise a longer tisuue contact [136]. An illustrative example of advanced buccal peptide delivery is the development of Midaform™ Insulin PharmFilm®, in which insulin is fabricated as glycan-coated gold nanoparticles before dispersing within a thin mucoadhesive polymeric film for trans-buccal administration. In this system, the glycan corona serves to stabilise insulin within the salivary environment, protecting it from degradation, while the gold nanoparticle core provides a uniform and robust nanoscale scaffold for peptide presentation. The mucoadhesive polymer film ensures prolonged residence time at the buccal surface under continuous salivary flow, enabling controlled insulin release of the hybrid systems directly at the mucosal interface. First-in-human clinical

studies demonstrated rapid pharmacodynamic responses alongside acceptable local tolerability, supporting the feasibility of this delivery strategy. The progress from Phase 1 evaluation to Phase 2a of such systems, has revealed its promising translational potential [137]. Reported drug exposure data was variable but acceptable and consistent with current oromucosal experiences. However, the case is a rare example of a nanoparticulate peptide being delivered via the buccal mucosa.

1.8 Nanoparticle Classes

1.8.1 Lipid-based nanoparticles

Lipid based systems are established product formats for drug delivery due to their protection properties against environmental stresses including from enzymes and versatile surface chemistry. Different types of Lipid-based vesicles exist. Conventional liposomes can encapsulate peptides of different MW, and their surfaces can be functionalised with different enhancing materials such as polyethylene glycol, zwitterionic groups, or mucoadhesive coatings. The bilayer membrane is durable and retains its flexibility under applied shear. This feature improves contact of lipid vesicles at the mucus epithelium interface and supports endocytic uptake when added within a film or a patch to control the tissue residence time for the preparation. Chitosan-coated liposomes carrying the salmon calcitonin (sCT) peptide is a representation for this system. They were reported to enhance mucoadhesion and epithelial drug uptake, with in vivo (rat model) studies showing greater bioavailability and a prolonged plasma exposure due to consistent residence time and drug protection, through the mechanisms outlined above [121]. Similarly, other lipid-based systems such as solid lipid nanoparticles exhibit good particle matrix stability to protect labile peptide against salivary proteases.

1.8.1.1 Polymeric nanoparticles

Polymeric carriers fabricated from thiolated chitosan or polyester, and layer-by-layer polyelectrolyte capsules, they provide benefits that enhance carrier systems. Poly lactic co-glycolic acid (PLGA) is a biodegradable copolymer extensively utilised in medical applications. The surface of PLGA can be modulated with chitosan or polyethene glycol so that interaction of the particles with the components of the oral mucosa is optimised, the surface modified forms also protect peptide cargo and support controlled drug release. Chitosan and thiomers demonstrate significant mucoadhesion through electrostatic and H bonding interactions, and they can temporarily open tight junctions through ionic effects and/or interaction with cysteine-rich mucins, enhancing paracellular transport of peptide agents. The surface charge must be equilibrated for translation. A slightly positive zeta potential, between approximately +5 and +20 millivolts after hydration, generally enhances adhesion and uptake without inducing irritation[138]. To achieve correct cationic density, employing blend or patchy coatings of chitosan in conjunction with PEG or zwitterionic groups, may reduce toxicity risk. Recent studies on thiolated chitosan to prepare nanoparticles provide further evidence supporting feasibility of this design with experimental outcomes utilising appropriate models such as TR146 cells and organotypic oral mucosa, for validating essential properties, i.e. Enhanced permeability and restoration of barrier function. [131], [139]. Chitosan–TPP insulin nanoparticles have demonstrated hypoglycaemic effects in animal model using diabetic rats, due to significant mucosal retention and enhanced epithelial translocation [140], [141], This was confirmed with better transepithelial transport across Caco-2 monolayers for thiolated chitosan–insulin systems[142].

1.8.2. Hybrid nanocarriers

Hybrids Lipid-polymeric nano-systems offers mucoadhesion and stability. A polymer–lipid hybrid nanoparticle (PLHN) was successfully used to encapsulate a potent therapeutic compound that has high aqueous solubility. The system was composed of a polymeric core composed of PLGA–PEG–PLGA triblock copolymers and a lipid shell comprising lecithin and cholesterol. By incorporating the drug into these polymer–lipid hybrid nanoparticles, the entrapment efficiency

was enhanced in comparison to that of conventional polymeric nanoparticles [143]. Electrospun mats can carry high Peptide loads are another e.g. They break down in a controlled way but manufacturing demands requiring reliable reproducibility of particle properties remain a challenge [144]. To sum, the delivered dose of drug in the oral cavity is determined by both residence time and particle interaction with the epithelium, rather than drug diffusion process alone, as demonstrated by studies that reflect the intended route of administration, such as in the case with deformable vesicles for insulin in animals and nanoparticle systems embedded in gels or films [145].

1.8.3. Surfactant-based nanoparticles

Niosome nanoparticles are vesicles that are made from nonionic surfactants and with suitable stabilizer, commonly cholesterol. They provide practical stability advantages over liposomes due to their reduced susceptibility to oxidative and hydrolytic degradation. They enable flexible surface modification with suitable materials, such as ligand or cell-penetrating peptide decoration, polyethene glycol, and chitosan coatings. The most effective method of delivering niosomes in buccal and sublingual delivery is to incorporate them into dosage forms that tramsform into thin films in the mouth. This is because liquid preparations like suspensions are easily washed away by saliva and may be ingested in the stomach. It is necessary to use right composition, i.e. surfactant levels and types and control edge activator ratios. This is because the amount of edge activator and the type of surfactant greatly impact membrane rigidity and tissue tolerance of the niosomes. To ensure that effects on the oral epithelium are reversible, reports of increased permeability should always be assessed in conjunction with safety indicators, as described in earlier part of the chapter[111]. These formulation factors and their effect on buccal performance have been discussed in recent route-focused reviews [146]. According to these principles, vancomycin-loaded niosomes, which were also prepared in this research work have demonstrated enhanced stability and release potential for mucosal peptide therapy [111]. While PEG-coated niosomes with thymopentin (TP5) have demonstrated high encapsulation efficiency and the vesicles exhibited an endocytosis-mediated cellular uptake with enhanced in vitro activity [147].

1.9. Niosomes

Niosomes are a type of vesicles that can be formed in unilamellar or multilamellar format. Niosomes can entrap molecules of different solubility profiles inside their vesicles. It can form by a self-assembly mechanism that involves nano-sized nanoparticles generated by a variety of hydrophilic head groups and one or two hydrophobic alkyl groups. Niosomes share similarities in both structural composition and physical attributes with liposomes. Nevertheless, niosomes offer an additional advantage due to their biocompatible and biodegradable nature. Similar to liposomes, niosomes exhibit potential for targeted effects, reduced drug dosage, and enhanced drug solubility and bioavailability for poorly soluble or absorbed substances. Niosomes hold promise in increasing the stability and photostability of drugs [148], [149], improving the protection and loading of drugs [150], prolonging circulation, [150], and facilitating controlled and targeted drug delivery [151]. Niosomes are expected to become a preferable choice over liposomes [148], [149].

1.9.1 Components of Niosomal Structures

The foundation of niosomes needs the incorporation of cholesterol or its analogues, non-ionic surfactants, and/or other ionic amphiphiles. The hydrophilic moieties are incarcerated within the bilayer hydrophobic compartments, whereas hydrophobic drugs are encapsulated within a corresponding core or between bilayer membrane. To ensure the stability of the formulation, a precise amount of cholesterol is introduced into the niosomes, forming a critical interaction with non-ionic surfactants [152].

1.9.1.1 Non-ionic surfactant

Surfactants are amphiphilic molecules consisting of hydrophobic alkyl chains linked to hydrophilic head groups, enabling them to accumulate at interfaces and self-assemble in aqueous environments [153], [154]. Based on the nature of the hydrophilic moiety, surfactants are categorised as anionic, cationic, amphoteric, or non-ionic. Their amphiphilicity permits interaction with both polar and non-polar phases, making them essential in pharmaceutical nanocarrier design (**Figure 1.6**). Upon exceeding the critical micelle concentration (CMC), surfactant molecules spontaneously organise into supramolecular assemblies such as micelles or bilayers. The type of nanostructure formed

depends largely on molecular geometry, concentration, and thermodynamic parameters. In niosomal systems, non-ionic surfactants combine with membrane stabilisers, commonly cholesterol, to form closed bilayer vesicles capable of entrapping therapeutic agents within aqueous cores or lipid domains [154], [155]. Non-ionic surfactants are especially favoured in niosomal formulations due to their relatively low toxicity, improved biocompatibility, and chemical stability as compared to ionic counterparts. Commonly used non-ionic surfactants include polysorbates (e.g., Tween series), alkyl ethers (e.g., Brij series), alkyl esters, and sorbitan fatty acid esters (e.g., Span series). The selection of an appropriate surfactant is governed by several physicochemical parameters, including the Hydrophilic–Lipophilic Balance (HLB), Critical Packing Parameter (CPP), as well as gel–liquid crystalline transition temperature (Tc). These factors determine the tendency of the surfactant to form stable surfactant-based bilayers rather than micelles and they influence vesicle size, lamellarity, membrane rigidity, and encapsulation efficiency. Notably, surfactant characteristics directly affect the physicochemical properties of niosomes, including bilayer stability, particle size distribution, permeability, and drug release kinetics. Consequently, surfactant selection not only governs formulation stability but also significantly influences the *in vivo* performance of niosomal drug delivery systems [156].

1.9.1.2. Cholesterol

Niosomes' physicochemical characteristics are greatly impacted by cholesterol, which is an essential component of their compositions [157]. Nonionic surfactants and cholesterol are chemically interacted in drug delivery systems, such as niosomes (**Figure1.6).** The components are mixed in predetermined quantities to generate gels like or dispersions [158]. The most essential characteristics of vesicles from a therapeutic standpoint is their particle size. Regardless of the kind of surfactant, studies show that cholesterol has a considerable impact on niosome particle size. However, depending on the particular type of nonionic surfactant utilised, the amount of cholesterol in the final formulation has a profound impact on particle size. For example, Nowroozi et al. reported that surfactant type significantly affected niosome size, with Tween 60 niosomes being larger than Span 60 and Brij 72 niosomes at the same cholesterol content. They also showed that increasing cholesterol from 20% to 40% reduced the particle size of Span 60 and Brij 72

niosomes, whereas the same cholesterol increase had no considerable effect on Tween 60 niosomes [159].

1.9.1.3 Additives

The structural and physicochemical characteristics of niosomes may be modified by adding various chemicals, which improves pharmacokinetics and drug delivery effectiveness. The hydrophilic surfaces of these vesicles also have a large number of functional groups that make their properties [160], [161].

To improve stability, niosomes, which are frequently used as gene delivery vehicles, are typically prepared using nonionic surfactants. Cationic lipids are added to affect transfection efficiency and toxicity through their structural and physical properties, whereas helper lipids are added to enhance the physicochemical properties [162]. To create electrostatic association with negatively charged DNA or drugs, these cationic lipids are essential. To prevent excessive accumulation or rapid removal from circulation through the reticuloendothelial system (RES), it is crucial to maintain a balanced final charge of the nanoparticles [163]. Drug features, formulation type, and polymer properties are among the key elements that determine the selection of polymers, which are crucial in drug delivery systems. Niosomes functionalised with PEG derivatives have been shown to reduce the reticuloendothelial system's (RES) intake of nanoparticles. Additionally, researchers created PEO-b-PCL-grafted niosomes, and their findings showed that PEO-b-PCL significantly affected the niosomes size and shape [164], [165], [166]. Co-surfactants are essential to improve the characteristics and functionality of niosome formulations. By decreasing surface tension and inhibiting vesicle fusion or aggregation, co-surfactants, including, various grades of Span and Tween 20, and Cremophor RH 40, help maintain the stability of niosomes. They also increased the fluidity of the bilayer, which resulted in more consistent and smaller vesicle sizes. Furthermore, by altering the structure of the bilayer, co-surfactants enhance the encapsulation effectiveness of active chemicals, making them better suited for holding medications. This alteration in the bilayer also affects the release profile of the encapsulated drugs, frequently leading to more regulated and prolonged release of actives. The permeability of niosomes is further enhanced by the flexibility provided by co-surfactants, which can also affect the effectiveness of drug transport. These

properties make co-surfactants such as Cremophor RH40 an essential additive in the optimisation of niosomal formulations and this stabiliser has been selected in current research work [111].

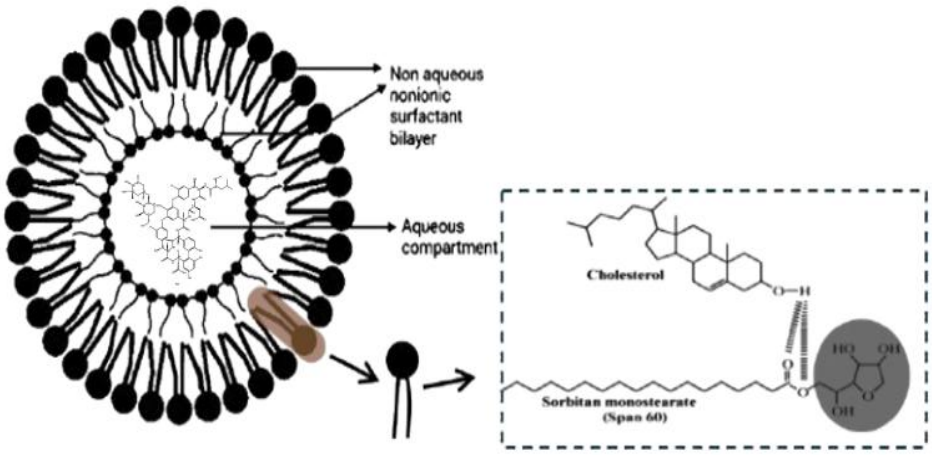

Figure 1.6: Niosomal bilayer membrane structure comprises Span 60 with cholesterol. figure adapted from[111] .

1.9.2 Lamellarity of niosomes

Niosomes are structurally classified into 3 sub- types: small unilamellar vesicles (SUVs), large unilamellar vesicles (LUVs), and multilamellar vesicles (MLVs), each differing in lamellarity, size, and encapsulation behaviour. SUVs (10–100 nm) are typically generated from MLVs using several size-reduction tools such as sonication, extrusion, microfluidisation, or homogenisation; however, their high curvature makes them thermodynamically less stable and prone to fusion, and their limited internal aqueous volume restricts hydrophilic drug loading [167],[168]. In contrast, LUVs consist of a single bilayer enclosing a relatively large aqueous core, providing a higher aqueous-to-lipid ratio and an improved encapsulation efficiency for hydrophilic compounds; they are commonly prepared by reverse-phase evaporation or ether injection methods [169]. MLVs are niosomes with multiple layers, typically larger than 50 nm. Lastly, multivesicular vesicles (MVVs)

are prepared using an outer vesicle typically over 1000 nm containing smaller vesicles. MLVs are prepared by conventional handshaking method and using transmembrane pH gradient for drug uptake [170], [171].

1.9.3 Niosome Formulation Specifications

Three crucial physicochemical parameters controlling the formation of niosomes as described in earlier part are Tc, HLB, and CPP values. For optimal vesicle stability, shape, and performance, these factors are crucial in selecting the right non-ionic surfactants blends.

1.9.3.1 HLB Parameter:

The physicochemical properties of the non-ionic surfactant, particularly its hydrophilic–lipophilic balance (HLB), play an important role in determining the size, morphology, and stability of niosomal vesicles. Surfactants with longer alkyl chains generally possess lower HLB values and greater hydrophobicity, which can promote tighter bilayer packing and influence vesicle size. In general, surfactants with very high HLB values, particularly between 14 and 17, are considered less suitable for niosome formation because their high hydrophilicity may reduce their ability to form stable bilayer vesicles [172]. Conversely, surfactants with lower HLB values are more favourable for bilayer formation. [173], [174].

1.9.3.2 Critical packaging parameters (CPP):

The molecular self-assembly and structural organisation of amphiphilic compounds, including non-ionic surfactants, into niosomal vesicles are predicted using the (CPP), a basic physicochemical descriptor **(Figure 1.7)**. The resulting vesicle morphology is spherical micelles, bilayer vesicles, or inverted micelles, as predicted and measured by the geometric relationship between a surfactant molecule's hydrophilic and hydrophobic moieties.

Critical packaging parameters

$$\boldsymbol{CPP} = \frac{v}{a_0 \cdot ic} \quad \text{(Equation 1)}$$

If the CPP value is <0.5, it suggests the formation of spherical vesicles; CPP value ranges 0.5 -1, indicates the formation of bilayer vesicles, and in the case of CPP value >1, this suggests the formation of inverted micelles [172], [173]

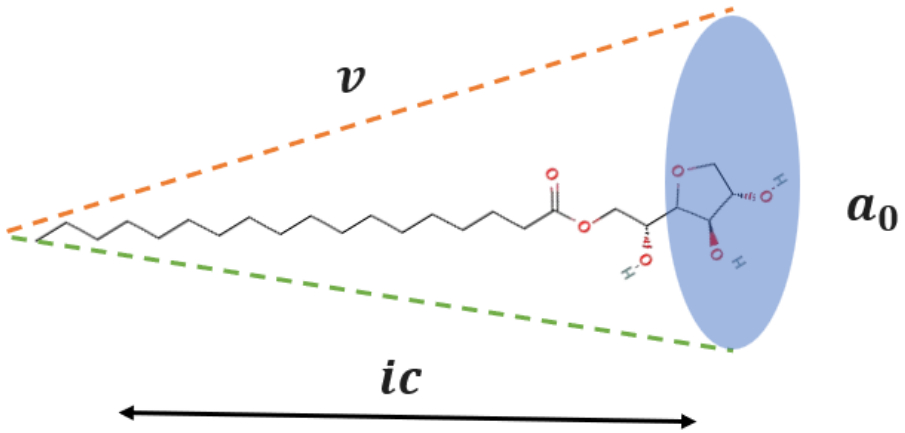

Figure 1.7: Surfactant structure (Span 60) and CPP. v is the volume of the hydrophobic group, ic is the length of the hydrophobic chain, a0 is the area of the hydrophilic head. CPP also helps in predicting the structure of niosomes as per the predetermined values.

1.9.3.3 Gel Liquid Transition Temperature

The transition temperature (Tc) is the lowest temperature at which a surfactant changes from an ordered gel phase to a disordered liquid crystalline state. This parameter has a considerable influence on drug entrapment efficiency and vesicle formation. Tc is determined by molecular characteristics such as chain length, saturation level, ionic charge, and head group type [172]. To promote homogenous vesicle formation and prevent aggregation or clumping, one must hydrate the surfactant mixture above Tc [175].

1.10. Niosomes preparation methods

To create niosomes, a surfactant-cholesterol mixture is typically hydrated at high temperatures. Size reduction procedures may then be performed to produce a colloidal dispersion. Niosome

preparation has been accomplished using a number of established methods, each with unique benefits. In the following part, these methods will be summarised [176],[177].

1.10.1 Thin-Film hydration method

The thin-film hydration (TFH) approach, also known as the hand-shaking method, remains the most widely used technique for producing multilamellar vesicles (MLVs). In this technique, Surfactant/cholesterol blend are dissolved in an organic solvent, such as chloroform, and then evaporated under decreased pressure. The resultant lipid film is subsequently hydrated with an aqueous solution containing drug at a temperature above the surfactants Tc value. Although this method is frequently employed due to its simplicity and reliability, it usually creates vesicles with a broad size dispersion unless followed by a size reduction step [178].

1.10.2 Ether injection method

The Ether Injection Method (EIM) is an extensively used approach for creating niosomal formulations. Using this procedure, diethyl ether is used to dissolve surfactants, which are frequently mixed with stabilising agents. The resulting mixture is progressively injected into the drug solution (an aqueous phase) at a temperature higher than the boiling point of the organic solvent, using a fine-gauge needle. As the ether evaporates, single-layered vesicles form spontaneously due to thermodynamic self-assembly. This technology has been effectively used to encapsulate a variety of medicinal compounds and generate stable niosomal systems [179].

1.10.3. Reverse phase evaporation method

Large unilamellar vesicles (LUVs) are frequently prepared using the reverse-phase evaporation (REV) process. This process involves first dissolving niosomal ingredients, such as surfactants and other additives, in an organic phase. The drug-containing aqueous phase is then added, and a water-in-oil emulsion is created by sonication. A rotating vacuum evaporator is used to gradually evaporate off unwanted organic solvent from this emulsion at 40–60 °C, which encourages the production of vesicles during the hydration phase [180].

1.10.4. Microfluidization method

The microfluidization method is an advanced technique used to create small, unilamellar vesicles (SUVs) with narrow and well-defined sizes. This technology operates on the submerged jet principle. The apparatus forces two fluid streams through microchannels at extremely high speeds within an interaction chamber. Their contact at a shared surface produces strong shear forces and turbulent mixing, which aids in the efficient production of vesicles [111]. By enabling controlled manipulation of fluid behaviours at the microscale, microfluidic platforms promote rapid mixing as well as efficient drug encapsulation. Typically, an aqueous phase containing the actives and an organic phase containing dissolved non-ionic surfactants are brought together within microchannels (**Figure 3.15 A**), leading to the formation of nanovesicles with uniform size and morphology. Compared with traditional preparation techniques, microfluidics offers superior control over particle characteristics, narrow size distributions, high product consistency, and the potential for scalable production, making it highly relevant for pharmaceutical applications [181].

1.10.5. Transmembrane pH gradient

The transmembrane pH gradient method requires dissolving equal parts cholesterol and surfactant in an organic solvent, often chloroform. The organic phase is later evaporated under vacuum to form a thin lipid coating on the inside surface of a round-bottomed flask. This lipid film is then rehydrated with a vortex mixer containing a citric acid solution or similar acidic buffers. The ensuing dispersion undergoes a freeze-thaw cycle to enhance bilayer integrity and vesicle homogeneity. Following that, an aqueous drug solution is introduced and extensively mixed using a vortex, allowing the drug to be actively entrapped. This active loading takes advantage of the pH difference across the bilayer between the acidic interior phase and the basic exterior environment, making drug encapsulation more efficient [182].

1.10.6. Supercritical carbon dioxide fluid

Supercritical carbon dioxide ($scCO_2$) is an eco-friendly, non-toxic, non-flammable, and cost-effective alternative to traditional organic solvents for preparing bilayer vesicular systems. Its

mild operating conditions are especially beneficial for encapsulating thermosensitive, non-polar, or slightly polar bioactive substances. Despite being utilised near its critical point, where it exhibits features of both gases and liquids, $scCO_2$ has a limited ability to dissolve highly polar compounds and high-molecular-weight lipophilic drugs. To address this limitation, ethanol is commonly used as a cosolvent to increase the solubility and encapsulation efficiency of more water-soluble and polar chemicals in vesicular systems [183].

1.11. Niosomes purification

The hydration process during niosome formation rarely results in complete drug encapsulation, even with the optimisation of drug-loading techniques. Consequently, the unentrapped medication must be removed from the formulation frequently. However, due to their potential biphasic release profile, which initially offers a burst release to initiate treatment, followed by a sustained release phase, systems containing both free and encapsulated drug fractions may provide therapeutic benefits. Unencapsulated medications have been separated using various methods [172]. Among the methods used to remove unentrapped pharmaceuticals, dialysis is regarded as a valid method for assessing entrapment efficiency (EE). However, the efficacy of this approach depends on the dialysis membrane's differential permeability and the structural integrity of the niosomal bilayer. To avoid accidental diffusion of the encapsulated medication, which could mislead the EE measurement, the dialysis regimen must be optimised. Understanding the interactions between free and encapsulated drugs during dialysis is crucial for correct assessment [184].

1.11.1 Gel filtration chromatography

This separation technique is also known as size-exclusion chromatography. It is commonly used for separating molecules based on their sizes, without causing structural changes or requiring chemical interactions. In niosomal preparation, it is often used to calculate encapsulation efficiency (EE) by separating between encapsulated and free drugs. The niosomal formulation is passed through a gel-packed column (made of Sephadex G-50), which is a cross-linked dextran gel filtration chromatography medium designed for separating soluble moieties, where larger vesicles elute first because they are unable to penetrate the small pores of the gel matrix. At the

same time, smaller, unencapsulated molecules remain in the column for a longer time. Quantitative measurement of the eluted fractions allows for precise estimation of EE. This method is beneficial for retaining vesicle integrity and enabling consistent separation, making it the recommended methodology for testing vesicle-based delivery systems [185].

1.11.2 Centrifugation

Centrifugation is a key separation technique used in niosomal drug delivery systems to isolate encapsulated vesicles from unentrapped, free drug molecules. This technique impacts the physical differences between niosomes and dissolved drug components, including particle size, shape, and density. The larger and denser niosomal vesicles settle to form a pellet at the bottom of the centrifuge tube, while the smaller, unbound drug molecules remain in the supernatant. This allows for more effective separation, which is critical for accurately determining encapsulation efficiency and maintaining formulation purity [186].

1.12. Physical properties of nanoparticles

A variety of physicochemical and biochemical properties have a prominent impact on the therapeutic efficacy and biological behaviour of lipid-based nanomedicines. These include particle size and distribution, particle concentration, structure, surface chemistry, and drug encapsulation efficiency. Regulatory agencies such as the FDA have issued technical instructions requiring comprehensive characterisation and records of these characteristics to ensure quality, consistency and safety of nanomedicine formulations [187].

1.12.1 Particle size

The physicochemical characteristics of nanoparticles loaded with drug, such as particle size and size distribution, play a crucial role in determining the drug's pharmacokinetic profile and biological interactions within the body. These characteristics have an impact on various functions, including hepatic absorption, renal clearance, preferential accumulation in disease regions, tissue biodistribution, and cellular internalisation efficiency [188]. Nanoparticles typically have diameters ranging from a few nanometres to sub-micrometres. The kidneys rapidly clear

nanoparticles smaller than approximately 10 nm because they can easily pass through the glomerular filtration barrier, which exhibits more consistent size selectivity across individuals [189]. As a result, nanocarriers with circulation times below this threshold often have insufficient residence times for efficient drug delivery. However, the optimal upper limit of nanoparticle size remains under debate. In cancer therapy, the increased permeability and retention (EPR) effect allows nanoparticles (<200 nm) to accumulate within tumour tissue via extravasation through leaky vasculature [190]. As a result, the majority of clinically authorised nanotherapeutics are designed to be between 10-200 nm in order to avoid rapid renal clearance while allowing for passive tumour targeting. Ongoing research is helping to refine the ideal size window for various treatment purposes. For example, lowering liposomal diameter from 200 nm to 50 nm has been shown to reduce macrophage-mediated phagocytosis, hence increasing circulation time considerably. Furthermore, liposomes between 40 and 160 nm appear to be the most effective in cellular internalisation, balancing systemic persistence with receptor-mediated endocytosis. In addition, particle size distribution is an essential measure of formulation quality and consistency in LBNMs, influencing both stability and biological performance [188].

1.12.2. Morphology

The morphology nanoparticles, including particle shape, lamellarity, and structural organisation, has a significant impact on their biological interactions and therapeutic efficacy. The form of nanoparticles is essential when assessing their pharmacokinetic behaviour and tissue distribution [191]. Lipid carriers naturally self-assemble into spherical forms, however, when active drugs are loaded into liposomes, they frequently adopt ellipsoidal shapes, which improve tumour site accumulation. Similarly, star-shaped lipid nanoparticles (LNPs) have demonstrated superior cell uptake compared to standard spherical systems, regardless of the drug content [192]. Lamellarity, which indicates the quantity of bilayers, has a direct relationship with loading capacity and therapeutic effectiveness. Unilamellar vesicles are more suited for hydrophilic drugs since of their larger internal volume, while multilamellar vesicles have a higher affinity for hydrophobic compounds due to increased bilayer availability [193]. Furthermore, increasing lamellarity has been associated with bigger drug loads and better RNA transfection efficiency in LNP

formulations [194]. The structural complexity of LBNMs, such as cavity configuration (micellar or vesicular) and membrane dynamics (fluidity and stiffness), influences their encapsulation capability and cellular affinity [195]. While extracellular vesicles (EVs) are naturally occurring and have a fixed morphology, their form and structure can be changed using methods including extrusion, sonication, and freeze-thaw cycling [196]. As a result, a thorough study of morphological aspects is required both for design optimisation and to maintain quality standards across pharmaceutical products.

1.12.3 Surface properties

Surface characteristics of nanoparticles, such as charge, coatings, and ligand alterations, have a significant impact on their pharmacological behaviour, including circulation perseverance, biocompatibility, biodistribution and cellular internalisation. A negatively charged surface is frequently used to avoid immune detection and maintain systemic circulation [191]. However, the same surface charge can inhibit cellular uptake due to electrostatic resistance from cell membranes. This restriction has been addressed by the development of charge-reversible nanocarriers, which enhance cellular contact at the target site by maintaining a negative charge during systemic transit and switching to a positive charge upon activation by site-specific triggers [197]. Surface coating using hydrophilic polymers, most commonly polyethylene glycol (PEG), is another frequently used method for stabilising nanoparticles and extending circulation times [198]. Despite its clinical success, PEGylation may reduce cellular absorption and perhaps activate immune responses [199]. To achieve optimal in vivo performance, parameters such as polymer molecular weight, chain structure, and grafting density need to be chosen carefully. Furthermore, the use of targeting ligands allows for selective delivery via ligand-receptor interactions, which improves absorption in specific cell types [200].

1.13. Summary

The delivery of therapeutic peptides through the oral cavity via buccal or sublingual administration offers important advantages over intestinal delivery, including avoidance of GI assualts and hepatic first-pass metabolism, as well as the potential for rapid local or systemic absorption. Nevertheless, this route remains challenging due to the inherent physicochemical properties of peptides, which are typically hydrophilic, relatively large, and structurally unstable. Enzymatic degradation occurs as proteases and peptidases are secreted into gut lumen There is also limited epithelial permeability and rapid salivary clearance. All these stresses experienced by peptides when they transverse the gut can significantly restrict its bioavailability. Moreover, anatomical and physiological variability across different regions of the oral cavity further complicates peptide absorption, necessitating carefully tailored formulation strategies. To overcome these barriers, several approaches have been explored, including peptide structural alteration, co-administration of enzyme inhibitors, incorporation of permeation enhancers, use of mucoadhesive polymers, and application of nanotechnology-based delivery systems. Nanocarriers engineered with optimised particle size and surface characteristics can enhance mucosal retention, protect peptides from enzymatic degradation, and help epithelial transport of peptide agents in *in vitro* and *ex vivo* models. Among the various nanoparticle designs investigated, niosomes offer distinct advantages. Compared with liposomes, they comprise non-ionic surfactants rather than phospholipids, which improves chemical stability, reduces oxidative degradation, and lowers production costs. In contrast to polymeric nanoparticles, niosomes can encapsulate both hydroephilic and lipophilic drugs within their bilayer and aqueous core without requiring complex polymer synthesis or potentially toxic crosslinking agents. Additionally, their bilayer structure can enhance membrane interaction and controlled release while maintaining favourable biocompatibility. Despite promising preclinical outcomes with various nanocarriers, including niosomal systems, clinical translation of nanoparticulate peptide formulations for buccal and sublingual administration remains limited. This gap highlights the need for more investigations into long-term stability, reproducibility, scale-up feasibility, and safety to fully realise the therapeutic potential of nanocarrier-based peptide delivery via the oral cavity.

1.14. Aim and objective

1.14.1. Aim

The key aim of this research works is to develop and evaluate a versatile niosomal-based oral cavity drug delivery platform capable of improving the stability and therapeutic efficacy of macromolecules and peptide-based drugs. The work integrates nanotechnology with advanced oral film and tablet systems to establish an adaptable formulation strategy suitable for both local and systemic delivery. Using vancomycin, nisin, and insulin as model drugs, this study aims to design, optimise, and characterise microfluidic-prepared niosomes and their incorporation into fast-dissolving oral films (FDOFs) and buccal tablets (for insulin), thereby demonstrating a drug delivery concept that bridges the oral cavity route and peptide therapeutics.

1.14.2. Objectives

To achieve this aim, the following specific objectives were pursued:

1. Prepare and optimise niosomal formulations encapsulating either vancomycin, nisin, or insulin using the microfluidic mixing method and compare their physicochemical properties, such as particle size, polydispersity index (PDI), zeta potential, and encapsulation efficiency (EE%) and identify the most suitable formulation for each drug.

2. Incorporate the optimised niosomal formulations into fast-dissolving oral films using suitable film-forming polymers, primarily polyvinyl alcohol (PVA), and, in the case of insulin, also compare performance with lyophilised and compressed buccal tablets.

3. Evaluate the mechanical and morphological properties of the formulated oral films and tablets, ensuring uniformity, flexibility, rapid disintegration and mucosal compatibility with surface pH values. In addition, assess the drug release kinetics, thermal stability, and diffusion behaviour of each system under in vitro conditions.

4. Determine the antibacterial activity of vancomycin- and nisin-loaded niosomal systems against *Bacillus subtilis* as a model Gram-positive bacterium using an agar diffusion plate method and validate their potential in managing oral infections and biofilm-associated diseases and studying its potential for systemic delivery.

5. Evaluate the most stable insulin niosomal formulation in both film and tablet dosage forms, examine release behavior, nanoparticle stability, and permeability across simulated mucosal barriers and identify the more efficient and manufacturable system suitable for buccal insulin administration.

Chapter 2 Materials and Methods

The construction of Chapter 2 is based on the following two published articles where experimental design (i.e. their materials and method sections) to meet the current research aim and objectives as described in sect. 1.14. Figures and tables from this chapter are adapted from the following published papers

Chapter 2 is based on the published articles (methods sections):

- **Amer et al. Development of Vancomycin, a Glycopeptide Antibiotic, in a Suitable Nanoform for Oral Delivery. Molecules, 2025 [111].**

- **Amer et al. Fast-Disintegrating Oral Films Containing Nisin-Loaded Niosomes. Molecules, 2025** [201]**.**

2.1. Materials

Vancomycin hydrochloride, nisin A, and human recombinant insulin were obtained from Molekula Group Ltd. (Darlington, UK). The non-ionic surfactants, including Span 40 (sorbitan monopalmitate), Span 60 (sorbitan monostearate), and Span 65 (sorbitan tristearate), together with cholesterol and polyvinyl alcohol (PVA; MW 31,000 Da), were obtained from Merck (Darmstadt, Germany).

Co-surfactants and/or solubilising agents, Kolliphor RH40 (polyoxyl 40 hydrogenated castor oil), Kolliphor ELP (polyoxyl 35 castor oil), Solutol® HS 15 (macrogol 15 hydroxystearate), and polyethene glycol 400 (PEG 400), were supplied by BASF (Stockport, UK).

Other pharmaceutical excipients included Sodium starch glycolate (SSG; GLYCOLYS, Roquette UK Ltd., London, UK), microcrystalline cellulose (MCC; Avicel, IFF Pharma Solutions, Shadsworth, UK), hydroxypropyl cellulose (HPC-SSL; Nisso Excipients, Düsseldorf, Germany), Croscarmellose Sodium (CCS; VIVASOL, JRS PHARMA, New York, NY, USA), hydroxypropyl methylcellulose (HPMC), and polyvinylpyrrolidone (PVP; MW 360 kDa) from Merck, Darmstadt, Germany.

For stabilisation during freeze-drying, glycine, trehalose anhydrous, and mannitol were used as lyoprotectant and cryoprotectant agents. Stearic acid (Merck, Darmstadt, Germany) was used to modify the vesicle charge and enhance membrane rigidity and niosomal bilayer stability.

Dialysis membranes with a molecular weight cut-off (MWCO) of 3000 Da (Medicall Ltd., Oldham, UK) and 20 kDa (Thermo Scientific, Waltham, MA, USA) were used for drug release studies. For nanoparticle permeation studies, polycarbonate membranes (pore size 0.1 μm) were obtained from Avanti Polar Lipids Inc. (Alabaster, AL, USA). Protein quantification was performed using the bicinchoninic acid (BCA) assay kit (Thermo Fisher Scientific, Waltham, MA,

USA). Rhodamine B base (Sigma-Aldrich, St. Louis, MO, USA) was selected as a fluorescent probe for visualisation and distribution analysis of fluorescently labelled niosomes.

For antimicrobial test, *Bacillus subtilis* NCTC 3610, which is a Gram-positive bacterial strain and culture media were obtained from the microbiological facility unit of University of Sunderland (UK). All chemicals and reagents used throughout the study were of pharmaceutical grades and/or analytical purity.

2.2. Methodology

2.2.1 Peptides quantification methods

2.2.1.1. Vancomycin

The calibration curve for vancomycin hydrochloride was generated by using a High-Performance Liquid Chromatography (HPLC) assay on a (LC system (Agilent series 1100Santa Clara, CA, USA) combining with a G4212A diode array detector (DAD). The HPLC system was fitted with a C18 reverse phase column (100 mm × 4.6 mm, 5 µm particle size) and a mobile phase consisting of water containing 0.1% formic acid and 20 mM ammonium formate (Mobile Phase A) and methanol containing 0.1% formic acid and 20 mM ammonium formate (Mobile Phase B). A gradient elution mode was used, beginning with 100% phase A and 0% phase B and progressing linearly to 0% phase A and 100% phase B over 5 minutes, followed by 1 minute of 100% phase B before returning to the initial conditions and re-equilibration. The drug detection was conducted at

230 nm, and the column temperature was maintained at 28 °C. The flow rate of mobile phase was set to 1.0 mL/min.

Vancomycin hydrochloride was dissolved in Trizma buffer, pH 7.4, to create a stock solution of 2000 µg/mL. Subsequently, serial dilutions were conducted to achieve the desired concentrations of 31.25, 62.5, 125, 250, 500, and 1000 µg/mL. The peak areas were recorded at a retention time of 3.154 min after a 20 µL aliquot of each calibration standard was injected. The linearity of the calibration curve was evaluated by calculating the correlation coefficient (r), as illustrated in **Figure 2.8**, and the peak areas were plotted against the corresponding concentrations. The data are presented as the mean ± standard deviation (n = 3).

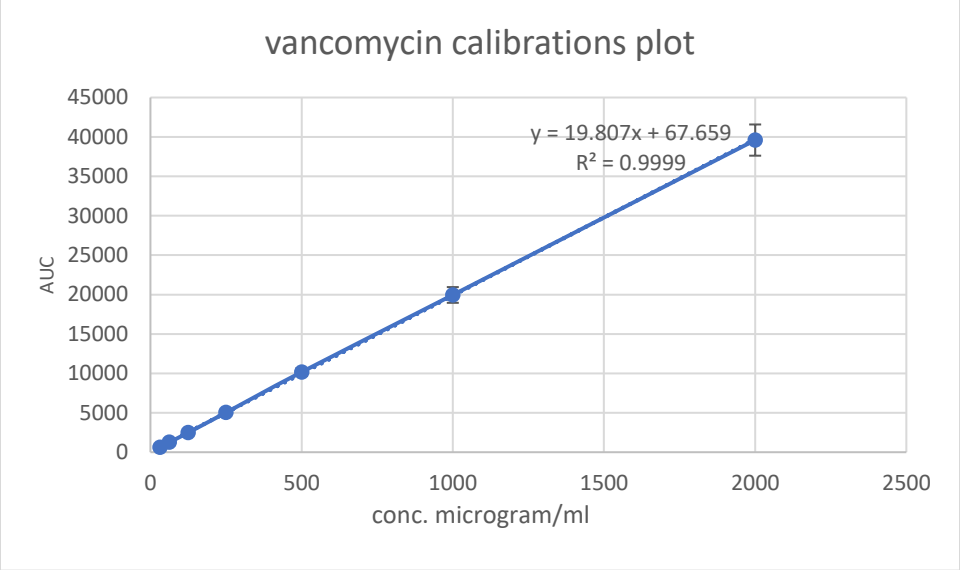

Figure 2.8: Calibration plot and equation for VCM measured using an HPLC assay. Data represent mean ± standard deviation (n = 3).

2.2.1.2. Nisin

The calibration curve for Nisin A was developed using an Agilent 1290 Infinity HPLC system in conjunction with a G4212A diode array detector (DAD) (Agilent Technologies, Inc., Santa Rosa, CA, US). The HPLC system utilised a Super C18 (100mm × 1.5 mm, 1.6 µm particle size). The mobile phases consisting of water with 0.05% trifluoroacetic acid (phase A) and acetonitrile with 0.05% trifluoroacetic acid (phase B). A gradient elution mode was employed, starting with 100% phase A and 0% phase B, and subsequently shifting linearly to 0% phase A and 100% phase B over a duration of 5 minutes. The solution was maintained at 100% B for 1 minute before reverting to the initial conditions and re-equilibrating. The flow rate was established at 0.3 mL/min, the column temperature was sustained at 28 °C, and drug detection occurred at 210 nm. Calibration standards were established by dissolving nisin A in water to create a stock solution of 50 mg/mL and subsequently performing serial dilutions to obtain the required concentrations at concentrations of 0.156, 0.3125, 0.625, 1.25, 2.5, and 5 mg/mL. A 20 µL aliquot of each standard was injected to LC system, and the peak areas were documented at a retention time of 1.8 minutes. The calibration curve was created by graphing the peak areas versus the respective concentrations, and the linearity of the curve was evaluated by determining the correlation coefficient (r), as illustrated in **Figure 2.9 A**. Determining nisin A at low concentrations via HPLC with UV detection presents challenges related to its peptide sequence which is lacking robust chromophores, such as tryptophan or tyrosine, (which contribute to substantial UV absorbance at typical detection wavelengths of peptide agent). Nisin exhibits low UV absorbance, with a lower limit of quantification (LLOQ) of 0.274 mg/mL, resulting in a poor signal-to-noise ratio and a lower sensitivity in UV-based HPLC detection technique. Due to this restriction, the quantification of minimal quantities of nisin for drug release analyses were performed utilising the bicinchoninic acid (BCA) protein assay method. The evaluation was conducted employing Thermo Scientific™ Pierce™ BCA Protein Assay Kit (Waltham, MA, US), according to the manufacturer's test tube method protocol. This assay relies on the reduction of Cu^{2+} to Cu^{+} ions (i.e. reagent B in BCA kit) by chemical groups in the Nisin under the alkaline conditions and subsequently forming a purple-coloured complex with bicinchoninic acid (found in reagent A). Serial dilutions of the sample were

created, and each was combined with the freshly prepared BCA working reagent, formulated by mixing Reagent A and Reagent B in a 50:1 ratio, according to the manufacturer's specifications. The reaction mixtures were incubated at 37 °C for 30 minutes, after which the absorbance of the sample was measured at 562 nm using a UV–Vis spectrophotometer, Drawell DU-8600R (Drawell Scientific Instrument, Chongqing, China). The sample quantification was performed through direct comparison of nisin concentrations and their absorbance values across the sample set. All calibration points for both concentration–AUC (from LC assay) and concentration–absorbance curves (BCA assay) were prepared and analysed in triplicate to guarantee reliability and reproducibility, as illustrated in **Figure 2.9 B**.

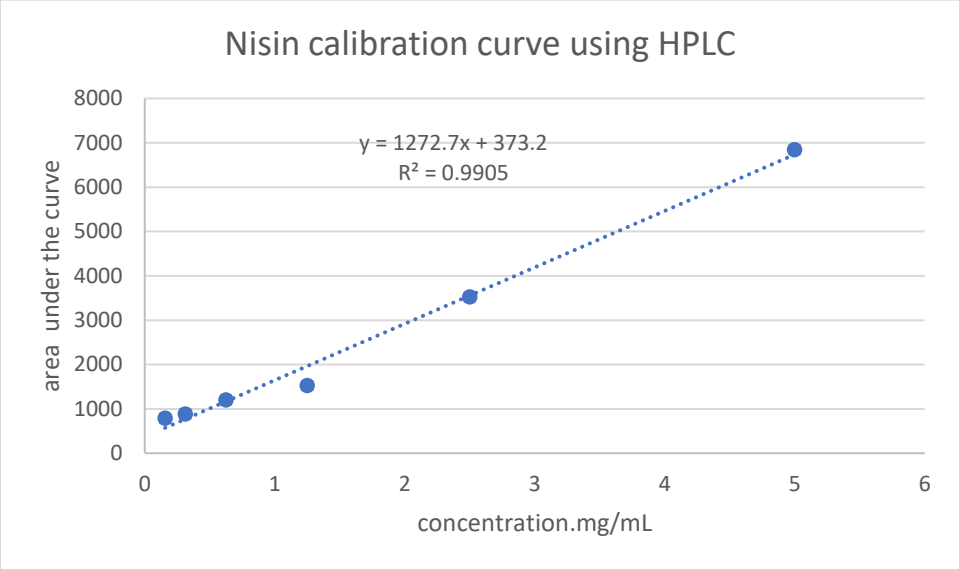

(A)

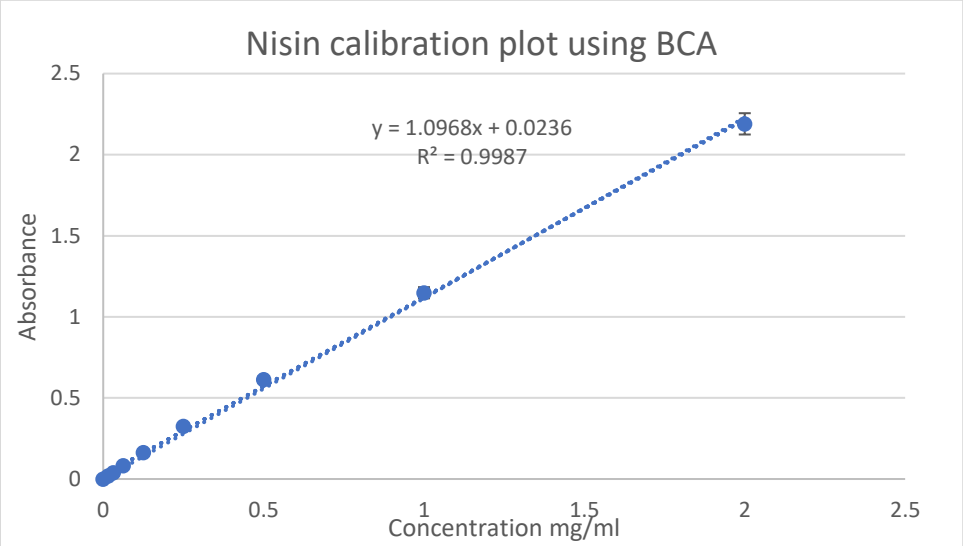

(B)

Figure 2.9: Nisin calibration plots and their equations. (A) Curve generated using HPLC analysis. (B) Curve produced using BCA protein assay.

2.2.1.3. Insulin

Quantification of insulin in all experimental analyses, including encapsulation efficiency, in vitro release, and permeability studies, was performed using the bicinchoninic acid (BCA) protein assay method as described in last section on Nisin BCA assay [202]. The analysis was performed using the same kit according to the manufacturer's test tube protocol. A series of insulin standard solutions were prepared to construct a calibration curve with concentrations of 0.0156, 0.03125, 0.0625, 0.125, 0.25, and 0.5 mg/mL. Each standard sample was mixed with freshly prepared BCA working reagent, and the absorbance of each sample was measured at 562 nm using a UV–Vis spectrophotometer (Drawell DU-8600R, Drawell Scientific Instrument, Chongqing, China) in order to create the calibration curve. All measurements were conducted in triplicate, and results were expressed as mean ± standard deviation (SD).

The calibration curve for insulin quantification using the BCA method exhibited excellent linearity over the concentration range of 0.0156–0.5 mg/mL, with a regression equation of y = 5.7561x + 0.0656 and a R^2 vlaue 0.9989 as shown in **Figure 2.10.** This validated quantification procedure was consistently applied throughout the study for determining insulin content in encapsulation efficiency assays, in vitro release profiles, and permeability evaluations.

Based on the residual standard deviation (σ) of the response and the slope (S) of the calibration line, the limit of detection (LOD) and limit of quantification (LOQ) were calculated according to the International Council for Harmonisation (ICH) Q2(R1) guidelines using the following equations [203].

limit of detection (LOD)

$$\text{LOD} = 3.3 \times \frac{\sigma}{S} \text{ (Equation 2)}$$

limit of quantification (LOQ)

$$\text{LOQ} = 10 \times \frac{\sigma}{S} \text{ (Equation 3)}$$

The calculated values were 0.023 mg/mL (LOD) and 0.069 mg/mL (LOQ), confirming the high sensitivity and reliability of the analytical method for insulin detection. These results demonstrate that the BCA assay provides precise and reproducible quantification, making it suitable for evaluating insulin content, encapsulation efficiency, and release profiles.

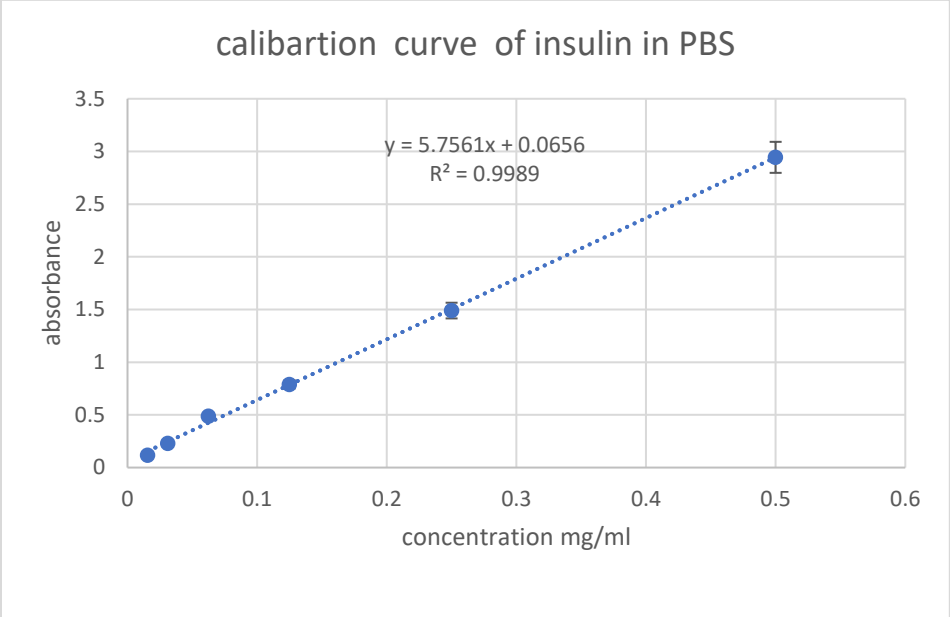

Figure 2.10: Insulin Calibration plot and its equation of obtained using the BCA protein assay [n=3].

2.3. Niosome Formulations

The microfluidic technique was employed to prepare several niosomal formulations. To assess the effects on vesicle characteristics, various molar ratios of cholesterol (Ch), Span 60 (SP60), Span 40 (SP40) or Span 65 (SP65) as main surfactant, as well as Kolliphor RH40 (RH40), Kolliphor ELP (ELP), or Solutol HS 15 (HS15) as co-surfactant were combined. The formulation compositions were initially calculated based on the thin-film hydration method, where a total lipid/surfactant mixture of 150 µmol was used. Depending on the molecular weights of the selected surfactants and cholesterol, the total mass of this 150 µmol mixture ranged from approximately 120 to 150 mg. For the microfluidic preparation method, the formulations were then scaled down to smaller total lipid/surfactant masses of 20, 40, or 60 mg, according to the specific experimental conditions, while maintaining the same molar ratios of surfactant, co-surfactant, and cholesterol as shown in **Tables 2.4, Table 2.5, and Table 2.6** for each peptide used, to enable standardised comparisons between formulations. The initial selection of cholesterol-to-surfactant molar ratios

was conducted by preliminary formulation screening, including early experiments using methylene blue as a hydrophilic model compound. These preliminary studies were mainly used to assess vesicle formation, particle size and general formulation behaviour during comparison of thin-film hydration and microfluidic preparation methods. However, as the thin-film hydration method did not produce sufficiently promising or reproducible encapsulation outcomes, these preliminary data were not included in the final thesis results. To ensure the accuracy and reproducibility of the results, each niosome formulation was prepared in duplicate (n = 2) as independent formulation batches, and each batch was analysed in triplicate (n = 3) for particle size, PDI, and encapsulation efficiency.

Table 2-4: Formulation Compositions of Vancomycin loaded niosomal formulations contain Non-ionic surfactants and cholesterol (amounts as molar ratios) Table was adapted from [111].

Formulation	Niosome Composition	Cholesterol	Span 60	Span 40	Kolliphor RH40	Kolliphor ELP
M1	Ch-SP60-RH40	35%	45%		20%	
M2	Ch-SP60-RH40	50%	40%		10%	
M3	Ch-SP40-ELP	35%		45%		20%
M4	Ch-SP60-ELP	35%	45%			20%
M5	Ch-SP40-RH40	35%		45%	20%	

Table 2-5: Formulation Compositions of Nisin loaded niosomal formulations contain Non-ionic surfactants and cholesterol (amounts as molar ratios) Table was adapted from [201].

Formulation	Niosomes Composition	Cholesterol	Span 60	Span 40	Kolliphor RH40	Kolliphor ELP
NM1	Ch-SP60- RH40	35%	45%		20%	
NM2	Ch-SP60- RH40	50%	40%		10%	
NM3	Ch-SP40-ELP	35%		45%		20%
NM4	Ch-SP60-ELP	35%	45%			20%
NM5	Ch-SP40-RH40	35%		45%	20%	

Table 2-6 : Formulation Compositions of Insulin loaded niosomal formulations contain Non-ionic surfactants and cholesterol (amounts as molar ratios).

Formulation	Niosome Composition	Cholesterol	Span 60	Span 40	Span 65	Kolliphor RH40	Kolliphor ELP	Solutol HS 15	Stearic Acid
IN1	Ch–SP60-RH40	35%	45%			20%			
IN2	Ch–SP60-RH40	50%	40%			10%			
IN3	Ch–SP40–ELP	35%		45%			20%		
IN4	Ch–SP60–ELP	35%	45%				20%		
IN5	Ch–SP40–RH40	35%		45%		20%			
IN6	Ch–SP65-RH40	35%			45%	20%			
IN7	Ch–SP65–RH40–Stearic Acid	35%			45%	15%			5%
IN8	Ch–SP65–Solu HS 15 –Stearic Acid	35%			45%			15%	5%

2.4 Microfluidic Niosome Synthesis

Peptide-loaded niosomes were fabricated by using the microfluidic technique (Precision NanoAssemblr™ Benchtop, Vancouver, BC, Canada) equipped with disposable single-use microfluidic mixing cartridges (Number: 1142-050). Several formulations were prepared, with their specific compositions shown in (**Table 2.4, Table 2.5, and Table 2.6**). The lipid and surfactant components of cholesterol (Ch), Span 40 (SP40), Span 60 (SP60), Span 65 (SP65), Kolliphor RH40 (RH40), Kolliphor ELP (ELP), Solutol HS 15 (HS15) and stearic acid, were accurately weighed using a 4 -digit balance and dissolved in ethanol to obtain an organic solution phase. The aqueous phase comprised different peptides with concentrations ranging (0.5-2 mg/mL) in Trizma buffer, pH 7.4 for vancomycin, 2mg/mL nisin in distilled water, and 1mg/mL of insulin in phosphate buffer (pH 7.4) that maintains peptide stability and solubility during vesicle

formation. One syringe was filled with the organic phase containing the dissolved lipidic components, while a second syringe was filled with the aqueous peptide solution. Both syringes were attached to the microfluidic cartridge, which was positioned within a heating block and maintained at 60 °C to promote lipid hydration and ensure vesicle self-assembly. This temperature was selected because it is slightly above the phase-transition temperature (**Tc**) of Span 60, which is reported to be approximately **53 °C**. Heating above the Tc increases surfactant chain mobility, allowing the non-ionic surfactants and cholesterol to exist in a more fluid state during mixing. This promotes better lipid hydration, bilayer packing, and vesicle self-assembly during microfluidic preparation [204]. The two phases were injected simultaneously through separate inlets into the microfluidic reaction chamber, where both phases were combined under controlled laminar flow, leading to the spontaneous formation of niosomes entrapping the peptide molecules within the core of niosmes and surrounded by the surfactant–cholesterol bilayers. The system was set to a total flow rate (TFR) of 12 mL/min and operated at aqueous-to-organic phase ratios of either 3:2 or 3:1, depending on the niosomal formulations used. The freshly prepared peptide-loaded niosomal dispersions were collected immediately after synthesis and kept at 4 °C for 10 min before characterisation. This short cooling step was used to promote bilayer solidification, as 4 °C is substantially below the Tc of the selected non-ionic surfactants, thereby helping to stabilise the vesicular structure prior to analysis.

2.5. Niosome properties

Niosomal formulations were characterised to evaluate their particle size, size distribution, surface charge, shape or morphology, and drug encapsulation efficiency (EE%). The vesicle size and polydispersity index (PDI) were measured using a Zetasizer Nano ZS (Malvern Instruments Ltd., Malvern, UK). Each formulation was diluted 50-fold to minimise multiple scattering effects during analysis. Measurements were performed at 25 ˚C and the obtained mean size and PDI values provided information about vesicle uniformity and dispersion stability.

For insulin-loaded niosomes, the zeta potential was also determined using the same instrument to assess the surface charge and electrostatic stability of the vesicles at phosphate buffer pH 7.2, absolute zeta potential value indicates strong repulsive forces between particles, minimising aggregation during storage.

Morphological examination of niosomes was performed to observe their shape and surface characteristics. Vancomycin-loaded niosomes were examined using light microscopy (Bioblue Eurmax, Rotterdam, The Netherlands). In contrast, nisin-loaded niosomes were visualised using a scanning electron microscope (HITACHI S-3000N, Tokyo, Japan) after spreading the sample on a metal stub, vacuum drying, and coating with iridium. Insulin-loaded niosomes were examined using a GX Microscopes ultraBIO-5 fluorescence microscope (GX Microscopes, Cambridge, UK). In this case, Rhodamine B base dye (1% w/w) was incorporated into the organic phase during preparation to label the vesicles fluorescently. The samples were viewed under green excitation ($\lambda \approx 490$ nm) and orange-red emission ($\lambda \approx 525–650$ nm) filters, enabling clear visualisation of vesicle morphology. The fluorescent suspensions were purified using Sephadex G-50 gel filtration to remove unentrapped dye prior to imaging to enhance image clarity.

The encapsulation efficiency (EE%) of the formulations was determined by separating unencapsulated peptide through centrifugation at 15,000 rpm for 60 minutes at 2–4 °C using a refrigerated microcentrifuge (Hettich MIKRO 200R, Kirchlengern, Germany). A clear supernatant was collected and analysed for free drug content, while the pellet contained the encapsulated fraction. For vancomycin and nisin niosomes, quantification of the free drug in the supernatant was performed using HPLC assay as described in section 2.2.1 In the case of insulin-loaded niosomes, the bicinchoninic acid (BCA) protein assay was used to quantify the insulin concentration at 562 nm as described in section 2.2.1.3. The drug encapsulation efficiency was then calculated using Equation (4) in which the known total peptide concentration was subtracted from the supernatant free drug, the concentrations that measured using calibration curve equations $y=19.807x+67.659$. The pellet fraction containing the entrapped peptide was reconstituted with

isopropanol and tert-butanol to disrupt the vesicles and release the drug, confirming that the sum of peptide recovered from both the supernatant and pellet matched the total initially loaded.

Encapsulation Efficiency (EE%)

$$EE\% = ((\text{Total drug} - \text{Free drug})/\text{Total drug}) \times 100 \quad \text{(Equation 4)}$$

2.6. Antimicrobial activity

The antibacterial efficacy of peptide-loaded niosomal formulations (vancomycin and nisin) was evaluated using an agar diffusion (disc diffusion) method against the Gram-positive bacterium *Bacillus subtilis* [205]. The bacterial culture was initially grown in nutrient broth by incubating overnight at 37°C to reach the stationary phase. The bacterial suspension was then transferred to a sterile saline solution and thoroughly mixed with a vortex mixer. The suspension's turbidity was then calibrated to a density of 0.5 McFarland units utilising a densitometer, bio-DEN-1 (Grant, Swindon, UK). The nutrient agar plate's surface was uniformly inoculated with *Bacillus subtilis* culture using a sterile cotton swab achieving even bacterial distribution. For each tested peptide preparation, the niosomal formulations were centrifuged to remove unentrapped drug and washed twice with buffer (Trizma buffer pH 7.4 for vancomycin, and water for nisin) to eliminate residual free drug. The resulting pellets were redispersed, and aliquots (5–20 µL) for vancomycin niosoms and 20uL for nisin niosomes were applied onto sterile paper discs (6 mm in diameter). Control samples included free drug solutions (vancomycin hydrochloride 1 mg/mL; nisin 2 mg/mL) and blank niosomes containing an equivalent surfactant concentration (20 mg/mL). Each paper disc was soaked of the respective sample suspension or control solution and placed on the surface of the agar plates. The plates were kept at room temperature for 15–20 minutes to allow initial drug diffusion into the agar medium, followed by incubation at 37 °C for 24 hours to permit bacterial growth and zone formation. After incubation, the diameters of the inhibition zones (clear regions lacking bacterial growth) surrounding each disc were measured in millimetres using a ruler. Antibacterial activity was expressed as the mean diameter of the inhibition zones, providing a

semi-quantitative measure of peptide antibacterial efficacy. For vancomycin-loaded niosomes, the three most successful formulations were selected for antibacterial testing, with each formulation tested on two independent agar plates. For nisin-loaded niosomes, the optimised formulation was selected and also tested on two independent agar plates. Free peptide solutions and blank niosomes were included as controls to compare antibacterial activity and confirm that the observed inhibition was due to peptide release rather than the vesicle components. Larger inhibition zones were interpreted as indicating stronger antibacterial activity under the conditions of this assay.

2.7. In Vitro Release and Permeability Study

2.7.1 Vancomycin release assay

An in vitro release analysis of vancomycin-loaded niosomes was performed utilising the dialysis bag method to compare the three different formulations (M1, M2, M3). These niosomes were prepared with a flow rate ratio of 3:2, at a drug loading of 1 mg/mL and at surfactant concentration of 20 mg/mL, A 1 mg/mL free-drug solution was selected as a control. Each formulation was placed in a dialysis bag (mw cut-off of 3 kDa). As vancomycin has a molecular weight of approximately 1449 Da**,** released drug molecules were able to diffuse through dialysis membrane, while the larger niosomal vesicles were retained within the dialysis bag. The dialysis bags were afterwards immersed in 50 mL of Trizma buffer (pH 7.4) (a medium that represents the oral environment), with continuous agitation provided by magnetic hotplate stirrers (Fisher Scientific, Leicestershire, UK) at 37 °C and 50 revolutions per minute. At 0, 0.5, 1, 2, 3, 5, 6, 12, and 24 hours, 1 mL samples were collected. Following each sampling, the vessel was replenished with 1 mL of fresh Trizma buffer to maintain a consistent volume. The collected samples were analysed for VCM levels using the HPLC method in order to quantify amount of the drug released at each time interval. The cumulative percentage of vancomycin released was calculated by comparing the cumulative amount of drug released into the receptor medium with the initial amount of vancomycin placed inside the dialysis bag. The initial formulation concentration was 1 mg/mL; therefore, the total initial amount of vancomycin was determined based on the volume of formulation added to the dialysis bag. For example, if 1 mL of formulation was used, the initial

amount of vancomycin was 1 mg. At each time point, the vancomycin concentration in the collected release sample was calculated from the HPLC calibration curve y=19.807x+67.659. This concentration was then used to determine the amount of vancomycin present in the receptor medium. Because 1 mL of release medium was removed at each sampling point and replaced with 1 mL of fresh Trizma buffer, the cumulative release calculation was corrected to account for the drug removed in previous samples. The corrected cumulative amount released was then divided by the initial amount of vancomycin added to the dialysis bag and multiplied by 100 to obtain the cumulative percentage release over 24 h. each collected sample was analysed in triplicate by HPLC. This study elucidated the sustained release properties of niosomal formulations and facilitated the identification of the formulation with the best release behaviour.

2.7.2. Nisin Release Study.

The same method, i.e. dialysis bag diffusion technique, was employed to evaluate the in vitro release of nisin from niosomal formulations and oral films (refer sect. no2.9 for production of film). The study used Thermo Fisher Slide-A-Lyzer dialysis cassettes (Waltham, MA, US) with a MWCO of 20,000 Da. Each dialysis cassette was filled with a 3 mL of nisin-loaded niosomal formulations, which contained 6 mg of nisin, and then submerged in 40 mL of distilled water (pH ~6.5) as the dissolution medium. In an orbital shaker, the equipment was maintained at 37 ± 0.5 °C with constant motion at 50 revolutions per minute to replicate physiological conditions. Two milliliters' aliquots were collected, and the vessels were replaced with an equal volume of fresh distilled water to maintain sink condition at set times (0, 0.5, 1, 2, 4, 6, 10, 20, 30 and 40 hours). Subsequently, bicinchoninic acid (BCA) reagent was added to each sample that was collected to facilitate protein quantification (refer section 2.2.1.2 for nisin quantification by BCA assay). The cumulative quantity of drug released from each specimen was calculated from a calibration curve that had been previously established to determine drug concentrations. Corrections were employed at each time interval for the dilution effect resulting from media replacement to derive the final drug concentration of each specimen.

2.7.3. Insulin Release Study.

The in vitro release profiles of insulin from different formulations, including the niosome , niosomal insulin film **(Figure 2.12)**, niosomal insulin tablet, and pure insulin solution (control), were evaluated using same dialysis method as described above by filling the specimen in the dialysis cassette (MWCO 20 kDa, Thermo Scientific, Waltham, MA, USA) under controlled sink conditions. Each sample containing the equivalent of 3 mg of insulin was loaded into the dialysis cassette and the dialysis unit was immersed in 40 mL of phosphate buffer (pH 7.4) maintained at 37 ± 0.5 °C with continuous stirring at 50 rpm on a magnetic stirrer.

Aliquots of 1 mL were fixed at intervals (0.5, 1, 2, 4, 6, 8, 12, and 24 hours), and an equal volume of fresh pre-warmed buffer was added to maintain constant volume and sink conditions. The insulin content in each withdrawn sample was quantified using the bicinchoninic acid (BCA) protein assay described earlier on (refer section 2.2.1.3), with drug absorbance measured at 562 nm. The cumulative percentage of insulin released was calculated and plotted as a function of time to compare the release behaviors of the different formulations over 24 hours. (n=3)

2.7.4. Insulin permeability study

The in vitro permeability test was performed using a Copley Franz diffusion cell apparatus (Copley Scientific Ltd., Nottingham, UK) fitted with a synthetic polycarbonate membrane (pore size 0.1 µm, Avanti Polar Lipids Inc., Alabaster, AL, USA) to evaluate insulin diffusion through a biological barrier analogue. The membrane was pre-soaked in phosphate buffer (pH 7.4) for 30 minutes before use to ensure hydration and equilibration. The donor compartment was filled with each formulation (film, tablet, insulin niosomes) equivalent to 2 mg of insulin, while the receptor compartment was filled with 11 mL of phosphate buffer (pH 7.4) maintained at 37 ± 0.5 °C and continuously stirred at 200 rpm to ensure uniform distribution. Samples of 1 mL were collected

from the receptor compartment at fixed intervals (0.5, 1, 2, 4, 6, 8, 12 and 24 hours) and replaced immediately with equal volume of fresh buffer. The insulin concentration in each sample was determined using the BCA assay (see section 2.2.1.3), and the cumulative amount of insulin permeated per unit area (A=2.83 cm^2) was plotted against time. Calculated insulin concentration was presented in $\mu g/cm^2$. All experiments were conducted in duplicate, and data were expressed as mean ± standard deviation (SD). The combined release and permeability results provided a comparative insight into the release kinetics and membrane diffusion behavior of the insulin formulations, highlighting the potential of the niosomal systems (suspension, film, and tablet) to achieve controlled release profiles and enhanced drug permeability.

2.8. Nisin Kinetic Modeling

The in vitro nisin release data were fitted to zero-order, first-order, Higuchi, Hopfenberg and Korsmeyer–Peppas kinetic models using Microsoft Excel. Model fitting was performed by minimising the residual sum of squares (RSS) between the experimental and predicted release values. The following equations were used [206]:

Zero order model:

$$Q_t = Q_0 + K_0 t \quad \textbf{(Equation 5)}$$

First order model:

$$\log Q_t = \log Q_0 - \frac{K_1 t}{2.303} \quad \textbf{(Equation 6)}$$

Higuchi model:

$$Q_t = K_H t^{1/2} \quad \textbf{(Equation 7)}$$

Hopfenberg model:

$$\frac{M_t}{M_\infty} = 1 - (1 - K_H t)^n \quad \textbf{(Equation 8)}$$

Korsmeyer–Peppas model:

$$\frac{M_t}{M_\infty} = K_{KP} t^n \quad \textbf{(Equation 9)}$$

The Akaike information criterion (AIC):

$$AIC = n \ln\left(\frac{RSS}{n}\right) + 2k \quad \textbf{(Equation 10)}$$

where Q_t is the cumulative amount of nisin released at time t, Q_0 is the initial amount of drug, M_t/M_∞ is the fraction of drug released at time t, K_0, K_1, K_H, and K_{KP} are release constants, and n is the release exponent. For the Korsmeyer–Peppas model, the initial release data were used to estimate the release exponent and gather the possible release mechanism.

The coefficient of determination (R^2)was calculated to assess the correlation between the experimental and predicted values. was also calculated using:

where n is the number of data points, RSS is the residual sum of squares, and k number of estimated parameters in the model. The best-fitting model was selected based on the highest $R^2$and the lowest AIC value.

2.9. Oral film Preparation Optimisation, and Characterisation Methods.

In order to create a stable and effective drug delivery system, several fast-disintegrating oral films were manufactured by solvent casting technique, as shown in **Figure 2.11**. Initially, various types of film-forming polymers, including polyvinyl alcohol, polyvinyl pyrrolidone, hydroxypropyl methylcellulose, and hydroxypropyl cellulose, were examined individually for their ability to make homogeneous, flexible films. Each polymer (5% w/w) was dissolved in distilled water, using a magnetic stirrer (moderate heating applied when necessary to ensure complete polymer dissolution). PEG 400 was used as a plasticiser at a concentration of 1% w/w to improve the flexibility of the film and decrease its brittleness. Additionally, a sweetener and flavouring agent (1% w/w) were incorporated to enhance the organoleptic properties. The produced niosomal suspension (3.5% w/w) was then gently stirred into the polymeric solution to form a homogeneous blend. The final casting solution (10 mL) was poured onto a levelled casting surface, and a fixed volume of 2 mL was used for each film, resulting in the formation of ten individual films.

In the preliminary stage, the films produced were assessed, after analyzing the films' appearance, in terms of transparency, uniformity, as well as film's mechanical properties including flexibility and peelability, the polymer with the best structural attributes was chosen for additional formulation optimisation. The selected polymer was then combined with one of three disintegrating agents, microcrystalline cellulose, sodium starch glycolate, or croscarmellose

sodium, in the later optimisation phase. Each disintegrating agent was incorporated into distilled water at 1% w/w. The resulting film-forming solutions were cast into uniformly levelled molds, and the film was dried in a fume hood at room temperature (25 °C) and ambient laboratory humidity for 24 hours until the solvent evaporated. In order to facilitate single-dose administration, films were prepared in dimensions of area equivalent to 3 cm × 2 cm (state volume to produce this size, The dried films were preserved in sealed containers that were shielded from light and maintained at low humidity. The mean values, along with their standard deviations were calculated to verify batch-to-batch consistency for the recorded parameters related to the film properties, and the uniformity of film weight across various samples was assessed using a analytical balance. In order to confirm the uniformity of structural integrity, the film thickness was measured at four distinct locations of a given film sample using a micrometer screw gauge (Philip Harris, Accrington, UK). The film's flexibility was evaluated through a hand-folding test, which recorded the number of folds necessary for the film to appear cracking. The maximal stress that the film could withstand before breaking and the maximum strain at break were quantified using a digital force tester (Chatillon CS2+, Berwyn, PA, USA) attached to the texture analyser. Data was collected every 50 ms, and the deformation rate was 20 mm/min. The tensile strength values of the films were also determined by the same piece of equipment. The pH of the film-dissolution medium and the surface pH of the film samples were evaluated to determine their suitability for oral administration. This was accomplished by immersing the films in distilled water and measuring the pH measurement was done by both pH meter and universal pH indicator strips (Simplex Health, Philadelphia, PA, USA). Finally, the in vitro disintegration time was evaluated by immersing individual film in 10 mL of deionised water that was maintained at 37 °C and time required for complete film disintegration was recorded. All the tests were done in triplicate. Non-niosomal films were prepared using the same polymeric composition and solvent-casting procedure but without the incorporation of the niosomal suspension and served as control formulations for comparative evaluation.

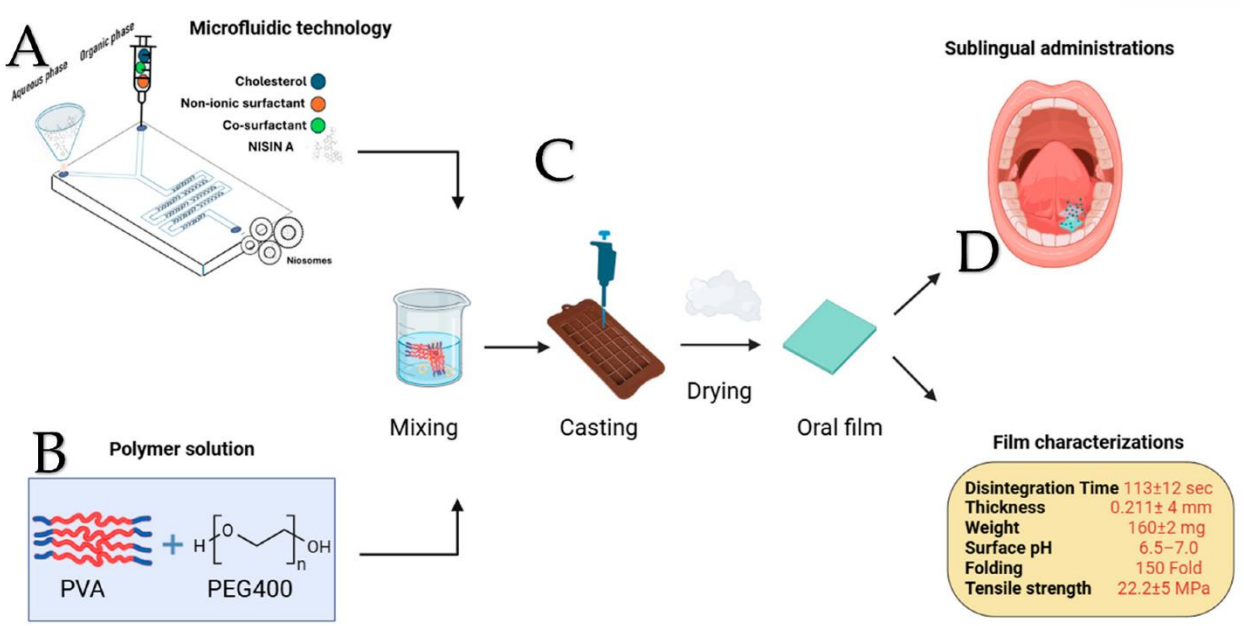

Figure 2.11: Procedure to fabricate nisin-loaded niosomal oral films by microfluidic mode. (A) MF platform to generate nisomes; (B) Preparing polymer solution containing PVA and PEG 400, (c) casting film in mold followed by a air drying process, (D) Testing oral film for sublingual administration based on in vitro methods.

2.10. Fourier Transform Infrared Spectroscopy (FTIR)

The FTIR analysis was conducted to determine the compatibility between the excipients utilised in the film and Nisin. Spectra were collected with an Agilent Cary 630 FTIR spectrometer (Agilent Technologies, Inc., Santa Rosa, CA, USA) that was equipped with a deuterated triglycine sulphate (DTGS) detector and set to % transmittance mode. A small quantity of the samples placed onto the sample holder. The SqrTriangle apodization function was employed to scan each sample over a wavenumber between 700 and 4000 cm^{-1}. A total of 32 scans were collected for each specimen, with a spectral resolution set to 2 cm^{-1}. In order to evaluate any potential wavenumber shifts,

disappearances, or emergence of new peaks that may suggest interactions between the drug and excipients, key peaks related to chemical functional groups of relevant compounds were identified and comparison was made between the spectra of pure nisin and the film preparations.

2.11. Thermal Analysis

2.11.1. Thermogravimetric Analysis (TGA/DTG)

Thermal properties and moisture content of the film formulations were assessed through thermogravimetric analysis (TGA). A platinum crucible filled with 5–10 mg of each sample (nisin-only film and nisin-loaded niosomal film) was prepared for analysis using a METTLER Thermal Analyser (Mettler Instrument AG, Greifensee, Zurich). The heating program was established to prevent oxidative degradation by maintaining a ramping rate of 10 °C/min under a nitrogen atmosphere (flow rate: 20–40 mL/min) from 25 °C to 600 °C. Initial recorded weight loss, which is associated with water content of sample and subsequent thermal degradation events of the film components were analysed using the resulting TGA curves. To facilitate a more comprehensive comparison of the thermal decomposition profiles among the tested samples, differential thermogravimetric (DTG) curves were generated to determine the temperatures that correspond to the highest degradation rates. Each measurement was conducted in triplicate to guarantee the consistency and reproducibility of the data.

2.11.2. Differential Scanning Calorimetry (DSC)

The thermal transitions and potential interactions between samples included pure nisin**,** nisin-loaded niosome film**,** nisin-only film**,** and PVA were investigated using differential scanning calorimetry. The analysis was carried out on an indium-calibrated TA Instruments DSC Q1000 (New Castle, DE, USA). For DSC analysis, no chemical pre-treatment was applied to the samples. The dried film samples were cut into small pieces to ensure representative sampling and good contact with the DSC pan. Each sample was accurately weighed and placed into a standard DSC pan, which was then sealed before analysis. Approximately 5–10 mg of each sample was

accurately weighed into a standard aluminium hermetic DSC pan, which was then sealed prior to analysis. An empty sealed aluminium pan was used as the reference. Samples were initially equilibrated at 25 °C and then the furnace temperature was gradually raised to 160 °C at a heating rate of 10 °C/min under a dry nitrogen purge (flow rate: 50 mL/min) to avoid any thermal degradation for the tested sample. Thermograms obtained were analyzed for occurrence of endothermic or glass transition events where midpoint method was employed to determine the glass transition temperature (Tg) of PVA matrix. Shifts in the Tg value were specifically investigated in order to evaluate the interactions between PVA and the niosomal system.

2.12. Fabrication of Microneedle Mold Using SLA 3D Printing

Microneedle molds were fabricated using a stereolithography (SLA) 3D printer (ELEGOO Mars 3, Shenzhen, China) with ELEGOO Standard Photopolymer Resin (Grey) (405 nm UV-curable, low-shrinkage formulation), as the printing material. The mold design was created using Tinkercad 2025, consisting of a 6 × 10 array of conical microneedle cavities that was distributed over a 1 cm^2 square base. Each microneedle cavity (or orifice) was designed with a height of 600 µm, a base diameter of 300 µm, and an inter-needle spacing of 800 µm, ensuring optimal structural integrity and sufficient space for casting polymeric microneedle formulations. The 3D design was exported in STL format and processed using slicing software .to generate printer-compatible layers. The printing parameters were optimised to achieve high geometric precision and smooth surface finish, using a layer thickness of 0.05 mm, a normal exposure time of 2.5 s, and a bottom exposure time of 30 s. Printing was conducted under standard ambient conditions using the default ELEGOO exposure settings to ensure accurate replication of the microneedle cavity geometry. After printing, the mold was carefully detached from the plate and rinsed thoroughly with isopropyl alcohol (IPA, 99%) to remove excess uncured resins. The mold was then post-cured under natural sunlight (UV exposure) for 30–40 minutes, allowing complete polymerisation and hardening of the resin. The resulting SLA-printed molds exhibited smooth, well-defined microneedle cavities with sharp, uniform tips suitable for the subsequent casting of PVA-based insulin-loaded niosomal formulations as shown in **Figure 2.12**.

2.13. Insulin Film Preparation and Characterisation Methods

The most optimised insulin-loaded niosomal formulation, selected based on its encapsulation efficiency, stability, and particle size distribution, was used for the preparation of oral films by the solvent casting technique. The objective of this step was to develop a flexible and stable polymeric film capable of delivering an accurate insulin dose through the oral cavity.

Polyvinyl alcohol was selected as the primary film-forming polymer for its biocompatibility, film-forming ability, and mechanical strength [201]. The optimised insulin-loaded niosomal suspension (1 mg/mL) (refer section 2.4) was mixed with a polymeric solution containing 800 mg of PVA and 100 mg of PEG 400, PEG 400 was incorporated into the film formulation as a **plasticiser** to improve film flexibility and reduce brittleness by increasing polymer-chain mobilit. that has been pre-dissolved in a 5 mL of distilled water at 50–60 °C. An equal volume (5 mL) of the insulin niosomal suspension was then gradually incorporated into the PVA/PEG solution after cooling and under gentle magnetic stirring at a 1:1 mixing ratio (v/v) to ensure uniform distribution of vesicles within the polymeric matrix. The combined mixture yielded a total batch volume of 10 mL. It was stirred continuously until a homogeneous, bubble-free film-forming solution was obtained, showing no visible phase separation or turbidity. From this mixture, 1 mL was cast per film, resulting in ten uniform film strips per batch. Each film (3 × 2 cm) contained a theoretical insulin content of 0.5 mg. The resulting film-forming solution was poured into leveled 3D-printed microneedle molds or casting molds and allowed to dry under a fume hood at room temperature (25 ± 2 °C) for 24 hours under ambient humidity to ensure gradual solvent evaporation **Figure 2.12**. The dried films were carefully removed and stored in airtight containers protected from moisture and light until further analysis. The content uniformity of insulin in the films was evaluated by dissolving individual film strips (n = 3) in phosphate buffer (pH 7.4), followed by quantification of insulin using the BCA assay (refer sect 2.2.1.3 for quantification method). The

results were expressed as mean ± standard deviation (SD) to confirm uniform drug distribution across the produced films.[201]

To evaluate vesicle integrity during film processing, the particle size distribution, zeta potential value, and morphology of the niosomes were determined before incorporation into the film solution and after rehydration of the dried films. Dynamic light scattering (Zetasizer Nano ZS, Malvern Instruments Ltd., UK) was used to determine particle size and surface charge, while fluorescent microscopy with Rhodamine B base dye was employed to assess vesicle shape and distribution inside the film. These analyses ensured that the film preparation process did not cause vesicle aggregation or structural deformation.

For physical and mechanical evaluations, film weight uniformity was determined using a Fisherbrand™ FAS64 Analytical Balance (Thermo Fisher Scientific, Waltham, MA, USA) with a readability of ±0.1 mg, and the results were expressed as mean ± standard deviation (SD). Film thickness was measured at 4 random positions using a micrometer screw gauge (Philip Harris, Accrington, UK) to confirm structural consistency. Flexibility of film was examined through a hand-folding endurance test, recording the number of folds required before cracking. Tensile strength and elongation at break were measured using a digital force tester (Chatillon CS2+, Berwyn, PA, USA) at a deformation rate of 20 mm/min, with data collected every 50 milliseconds. To assess mucosal compatibility, the surface pH of each film was determined by moistening the film surface with distilled water and applying universal pH indicator paper (Simplex Health, Philadelphia, PA, USA). A near-neutral pH (6.5–7.5) was considered optimal to prevent mucosal irritation. Disintegration time of films was determined by immersing individual film strips in 10 mL of deionised water maintained at 37 ± 1 °C and recording the time required for complete film disintegration.

2.14. Freeze-Drying of Insulin-Loaded Niosomes Using Various Lyoprotectants

To enhance the long-term stability and shelf-life of the optimised insulin-loaded niosomal formulation, a freeze-drying (lyophilisation) study was performed using various lyoprotectant agents as presented in **Table 2.7**. The selected formulation, prepared by the microfluidic method, was divided into equal portions, each treated with a different lyoprotectant system to evaluate its protective efficiency during freezing and drying stages. The lyoprotectants were chosen based on their well-documented cryoprotective properties and ability to form hydrogen bonds with lipid headgroups, thereby preserving vesicle structure during dehydration process [207], [208], [209], [210].

Table 2-7: Lyoprotectant Systems evaluated for Freeze-Drying of Insulin-Loaded Niosomes

Code	Cyro-/Lyoprotectant System w/v
L1	**Niosomes without additive**
L2	**Mannitol 10%**
L3	**Mannitol 2.5% + Glycine 2.5%**
L4	**Mannitol 5% + Glycine 5%**
L5	**Glycine 10%**
L6	**Trehalose anhydrous 5%**
L7	**Trehalose anhydrous 10%**
L8	**Trehalose anhydrous 2.5% + Mannitol 2.5%**

L9	**Trehalose anhydrous 15% + Sucrose 5%**

Each lyoprotectant was added to the niosomal dispersion at the indicated concentrations. The mixtures were gently vortexed for 2 minutes; they were then pre-frozen at –80 °C for 24 hours to achieve complete solidification.

The freeze-drying process was performed using a programmable bench-top lyophilizer (Christ Alpha 2-4 LDplus, Martin Christ, Germany) for 24–48 hours. The primary drying phase was conducted at a shelf temperature of –40 °C under a vacuum pressure of < 0.15 mbar for 24 hours to facilitate ice sublimation. The secondary drying phase followed, during which the temperature gradually increased to 25 °C and was maintained for 8 hours to remove bound moisture and yield a stable dry powder. After lyophilisation, the dried niosomal cakes were stored in the airtight glass vials under refrigerated conditions (4 °C) until further evaluation. For post-lyophilisation analysis, the samples were reconstituted with distilled water (state volume) and assessed for changes in their physicochemical characteristics. Particle size and polydispersity index as well as zeta potential od samples were measured using DLS technique (Zetasizer Nano ZS, Malvern Instruments Ltd., UK) at 25 °C, following appropriate dilution to ensure reliable measurements were obtained. The shape and morphology of the niosomes before and after lyophilisation were examined using a fluorescent microscope after labelling with rhodamine B dye. Images were captured and compared to evaluate vesicle integrity, aggregation or deformation resulting from the drying process.

The performance of each protectant system was determined by its ability to maintain low PDI, preserve particle size, and retain the spherical shape and dispersion stability of the niosomes. The protectant providing the best preservation of these properties, particularly minimal size variation and uniform morphology, was selected for tableting studies, see section (2.15) below.

2.15. Compression of Lyophilised Insulin-Loaded Niosomes into Tablets and Tablet Characterisations

The most optimised freeze dried niosomes loaded insulon was selected for tablet preparation.

To produce compressible powder with good flowability and compactibility, the lyophilised powder was blended with MicroceLac 100 (PharmaExcipients, Switzerland), as a filler and dry binder to improve tablet hardness, and 1% magnesium stearate (Merck) as a lubricant to minimise die-wall friction and mechanical stress on the niosomes during compression. The microcrystalline-lactose co-processed filler (MicroceLac 100) also aids in particle dispersion in aqueous media after compression.

A total batch size of 2 g of powder mixture was prepared, corresponding to 20 tablets (each weighing 100 mg). The powders were mixed manually using a geometric dilution method in a glass mortar for 5 minutes to ensure homogeneous distribution of insulin-loaded niosomes and other excipients.

A 100 mg portion of the optimised blend was accurately weighed for each tablet, corresponding to 0.5 mg of insulin per unit. Tablets were compressed using a GAMLEN Tableting Machine (Series D500, Gamlen Tableting Ltd., Nottingham, UK) equipped with 6 mm flat-faced punches. Compression was performed at a constant force of 300 kg, optimised to achieve adequate hardness and cohesion while minimising vesicle rupture or deformation. The prepared tablets were ejected smoothly, inspected for uniformity, and stored in airtight glass vials until further evaluation (**Figure 2.12).**

Tablet characterization was performed to evaluate mechanical, physical, and physicochemical properties. Tablet diameter, thickness was measured with GAMLEN electronic micrometer and hardness was determined by using a digital hardness tester (Gamlen tablet tensile analyser). Data obtained were expressed as mean ± standard deviation (SD) for 10 tablets tested. Friability was

assessed using a friabilator (Erweka TAR 220, Germany) operated at 25 rpm for 4 minutes, and the weight loss (as %) was calculated for adequate mechanical robustness. Weight uniformity was determined by weighing ten tablets on an analytical balance, while content uniformity was evaluated by dissolving individual tablets in Tert-butanol (TBA) and quantifying insulin content using BCA protein assay. The measured insulin content was compared to the theoretical value (0.5 mg/tablet) and results were reported as mean ± SD to confirm the dose. Disintegration time was determined by immersing tablets in 10 mL of distilled water maintained at 37 ± 1 °C, and the time to give complete disintegration was recorded visually. Surface pH was measured by moistening the tablet surface with a drop of distilled water and applying universal pH indicator paper, ensuring a near-neutral pH to minimise mucosal irritation. After dispersion of the tablet in distilled water, the particle size, zeta potential, and morphology of the reconstituted vesicles were analysed using DLS technique (Zetasizer Nano ZS, Malvern Instruments Ltd., UK) and fluorescent microscopy (Leica DM6 B, Wetzlar, Germany), respectively. These tests confirmed that vesicle integrity and charge were preserved after compression.

2.16. Statistical analysis

Statistical analysis was performed to evaluate the influence of formulation composition and phase ratio on the measured physicochemical parameters. All experiments were conducted in triplicate ($n = 3$), and data are presented as mean ± standard deviation (SD). Statistical analyses were carried out using IBM SPSS Statistics (version 29.0.1) and Microsoft Excel (Microsoft Corporation, USA). Normality of data distribution was assessed using the Shapiro–Wilk test, while homogeneity of variances was evaluated using Levene's test. Where the assumptions for parametric analysis were satisfied ($p > 0.05$), one-way analysis of variance (ANOVA) was applied to determine statistically significant differences between groups. Effect sizes were expressed as eta squared (η^2) to estimate the magnitude of observed effects. A p-value < 0.05 was considered statistically significant.

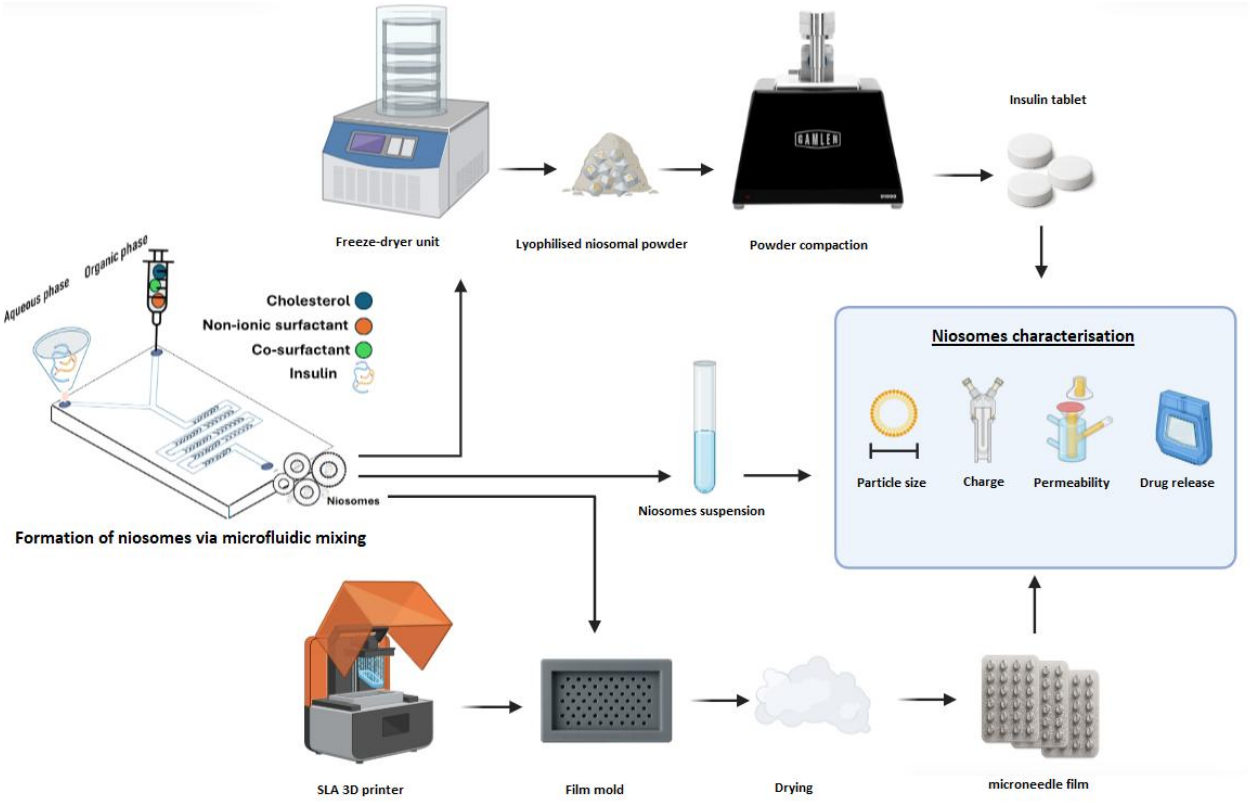

Figure 2.12: Schematic illustration of the preparation and characterisation of insulin-loaded niosomal formulations and their conversion into solid oral dosage forms

Chapter 3: Development and Characterization of Vancomycin Niosomes: A Comparative Evaluation of Microfluidic Techniques, Drug Release, and Antimicrobial Activity

The content in Chapter 3 is based on the application of VCM as a model peptide under evaluation where the methodology has been described in chapter 2 to fulfil the research aim and objectives. The experimental outcomes presented in this chapter are based on the accepted and published peer-reviewed paper as listed. some of its contents (tables and figures) are adapted from same:

Amer et al. Development of Vancomycin, a Glycopeptide Antibiotic, in a Suitable Nanoform for Oral Delivery. Molecules, 2025.

3.1. Overview

Improvements in drug permeability and absorption are among the most significant challenges in the pharmaceutical industry [211]. Antibiotic based nanoparticles have shown to exhibit extraordinary antibacterial efficacy and enhanced tissue penetration [212] Vancomycin (VCM) is a glycopeptide antibiotic that is widely recognised (**Figure 3.13**) and is employed to treat Gram-positive bacterial infections [213]. including resistant bacteria strains, such as methicillin-resistant *Staphylococcus aureus* (MRSA) [214]. In additions to those who are hypersensitive to beta-lactam antibiotics [215]. For systemic infections, VCM must be administered intravenously as the drug molecules cannot travel through the intestinal wall. This peptide antibiotic is frequently employed to address intricate or severe infections, including meningitis, endocarditis, and bone and joint infections [216]. VCM acts by inhibiting the synthesis pathway of cell walls of Gram-positive bacteria and it is ineffective against Gram-negative bacteria. Through its high affinity binding to the D-Ala-D-Ala terminus of the pentapeptide moieties of cell wall, see **Figure 3.14**, it prevents the process of transglycosylation and the subsequent cross-linking of the peptidoglycan chains, thereby inhibiting the development of bacterial cell walls [217]. VCM is a large hydrophilic molecule (1485.74 g/mol) under BSC 3 that exhibits restricted gastrointestinal permeability and absorption. It is mostly used orally to give local action to target *Clostridium difficile* colitis in the large intestines [218]. Currently, the use of VCM for systemic infections is restricted by the limitations of oral administration. However, the development of VCM formulations based on nanoparticles offers a promising solution. Despite the fact that oral administration is frequently the preferable method due to its simplicity and increased patient compliance, the absorption profile of VCM severely restricts this approach [219].

In antimicrobial therapy, niosomes have emerged as promising carriers for antibiotic delivery [220]. Niosomes are vesicular systems (**Figure 3.15 B**). As a result of the bilayer arrangement, niosomes can accommodate hydrophilic peptide drugs within the core and between bilayer membranes, offering considerable flexibility for drug delivery application [221]. The vesicle size and the number of bilayer membranes in niosomes, are governed by the critical material and process attributes such as surfactant chemistry and concentration, preparation method, molecular weight of the encapsulated compound and many other factors as mentioned earlier in chapter 1 section 1.12. Through appropriate control of these parameters, employment of MF based fabrication process and varying flow rate ratio as well as selective surfactant- cholesterol compositions, niosomal systems loaded with VCM can be optimised.

Encapsulation of VCM, a peptide antibiotic within niosomal vesicles can enhance its stability, facilitate penetration into bacterial cells, and provide sustained drug release, thereby improving therapeutic outcomes and reducing the risk of resistance development (**Figure 3.15 C**)[222].They provide a strategy to overcome physiological barriers by improving mucosal penetration, protecting drugs from enzymatic degradation, and limiting drug dilution by saliva, thereby enhancing the efficiency of buccal drug delivery. Furthermore, mucoadhesive properties can extend residence time at the application site and increase contact between the drug and the mucosal surface [223].

In summary, VCM based niosomes will be fabricated and their physico-chemical properties will be evaluated according to experimental design and methodology as described in chapter 2. The successful VCM based niosomes will also be dispersed in oral film formulations by solvent casting and their feasibility as a novel oral delivery platform for target drug candidates to achieve either localised or systemic action in the oral cavity will be examined in this chapter.

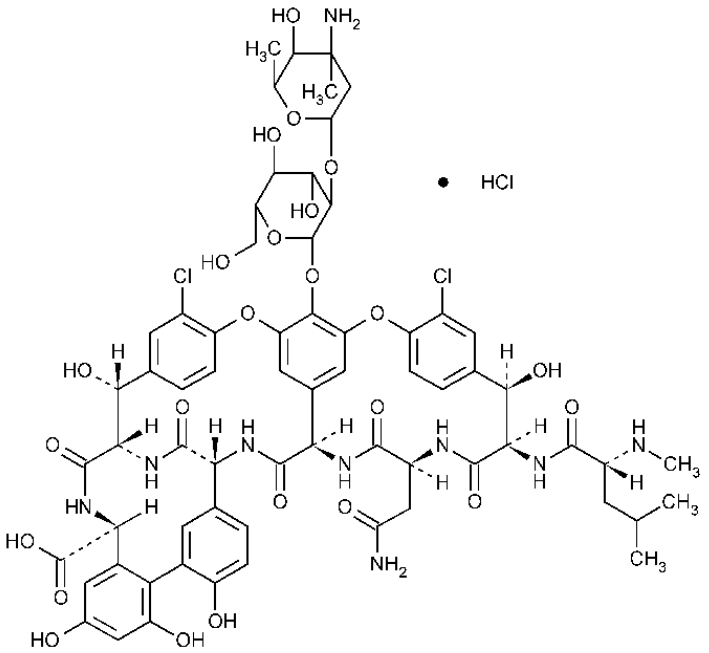

Figure 3.13: Vancomycin hydrochloride structure (Drawn by ChemDraw [111])).

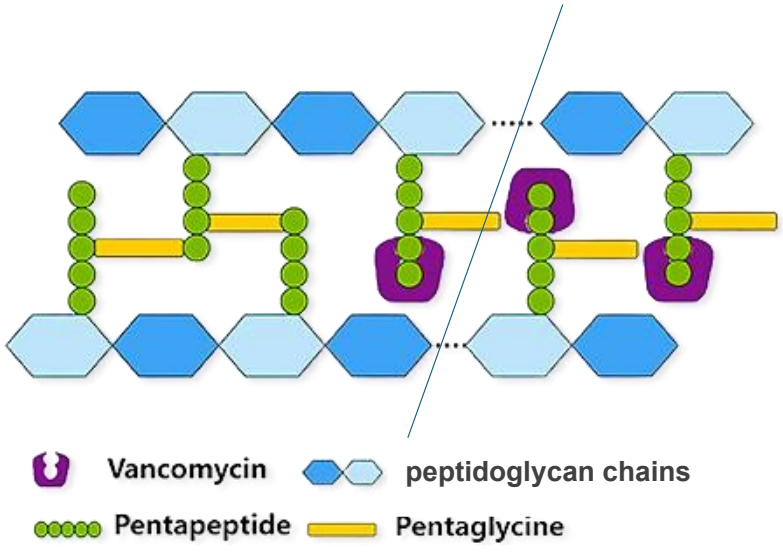

Figure 3.14: Diagram showing mechanism of VCM molecules binding to D-Ala-D-Ala terminus of the pentapeptide to inhibit transglycosylation and cross-linking of peptidoglycan chains [111].

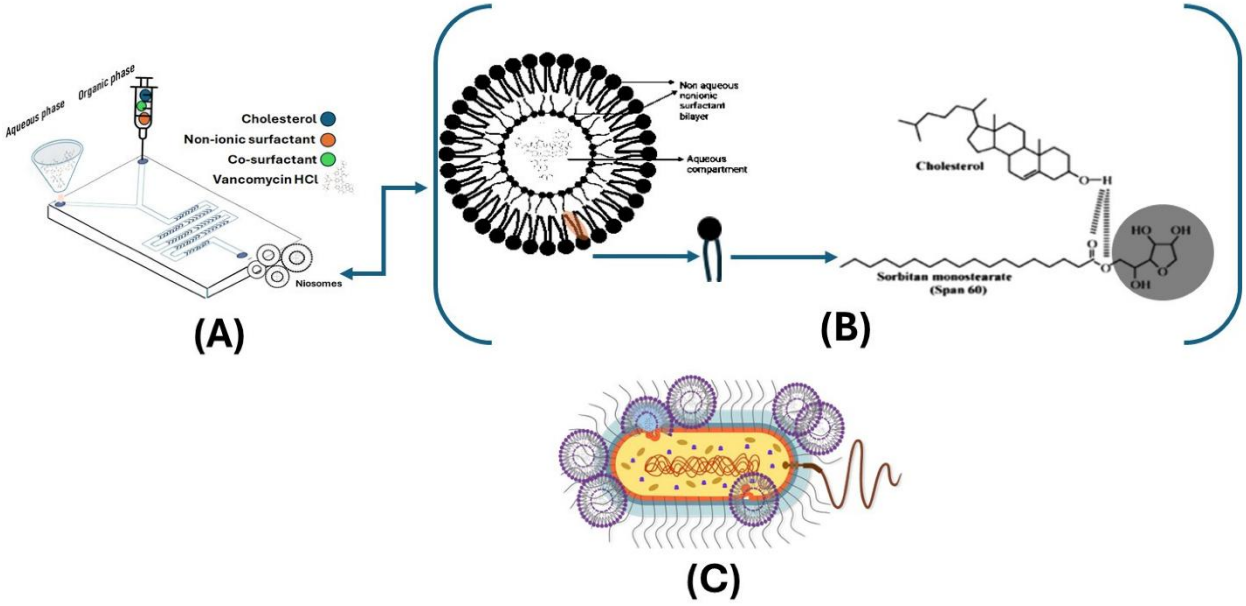

Figure 3.15: Application of Microfluidic platform to produce niosome, (B) srtuctural feastures of niosome consisting of bilayer membrane and aq. core made of non-ionic surfactant and cholesterol and (C) Scheme showing antimicrobial action of VCM-loaded niosomes on bacteria (C)) [111].

3.2. Aim and objectives

The primary aim of this research is to design and produce vancomycin hydrochloride-loaded niosomes by a bench top microfluidic device, in order to assess the suitability of this approach for producing nanoscale vesicles with favourable properties. The study explores the effects of blending various excipients, including Span 60 or Span 40 with low HLB values and cholesterol as main membrane formers, Kolliphor RH40 or Kolliphor ELP with high HLB values as stabiliser, on niosome size, morphology, and drug encapsulation efficiency.

Various combinations of non-ionic surfactants and cholesterol molar ratios are investigated to identify optimal formulation conditions. In parallel, the influence of formulation and process

parameters, i.e. drug loading, surfactant concentrations, and flow rate ratios, is examined to better understand their roles in determining niosome characteristics. In addition to formulation development, the dissolution profiles of vancomycin from the niosomes will be established, together with an assessment of antibacterial activity against a model Gram-positive bacterial strain to demonstrate therapeutic relevance.

The second phase of this research focuses on incorporating vancomycin-loaded niosomes into fast-disintegrating oral films. The resulting niosomal films are characterised for weight uniformity, content uniformity, film thickness, film flexibility, tensile strength, and surface pH, to ensure quality and reproducibility. By optimising both the niosomal formulation and the film delivery system, a stable and effective oral niosomal platforms with enhanced therapeutic potentials is anticipated to be produced.

3.3 Results and discussion

3.3.1. The influence of Using Different Non-Ionic Surfactant Concentrations for M1 formulation.

The results obtained from the microfluidic based niosomess highlight the influence of total non-ionic surfactant concentrations and flow rate ratios on vesicle size, polydispersity index and encapsulation efficiency, while maintaining a constant vancomycin concentration of 1 mg/mL. (**Table 3.8)**. The results demonstrated that formation of larger vesicles with increasing the overall surfactant concentrations ranging from 20 mg/mL to 60 mg/mL for M1 Formula (cholesterol–Span 60–Kolliphor RH40 (3.5:4.5:2)). This effect may be attributed to the greater availability of surfactant molecules, which promotes the formation of larger vesicular structures or enhances aggregation during nanoparticle assembly. Formulations prepared at the higher organic phase proportion (3:2) produced larger vesicles than those prepared at 3:1. This agrees with previous microfluidic studies showing that the aqueous:organic flow rate ratio strongly influences vesicle size. Garcia-Manrique et al. reported that increasing the aqueous ratio reduced niosome size, mainly due to faster solvent dilution, reduced residual solvent, and lower bilayer-component

concentration during assembly[224]. Similarly, Joshi et al. showed that the aqueous solvent ratio, lipid concentration, and solvent type all affected liposome size during microfluidic manufacture. Therefore, the larger vesicles observed at 3:2 may be attributed to the higher organic solvent proportion, which could delay solvent displacement and promote greater surfactant fusion or vesicle growth before stabilization [225] .

PDI analysis has shown that employing higher surfactant concentrations 20- 40- 60 mg/mL was associated with improved size uniformity, particularly at 3:1 (aqueous-to-organic phase) ratio in which 40mg/mL 3:1 showed better PDI comparing to 20mg/mL 3:1 (aqueous-to-organic phase) ratio. In contrast, formulations prepared at the 3:2 ratio exhibited higher PDI values compared to 3:1, indicating a wider size distribution, potentially a consequence from less controlled mixing conditions in solvent-rich systems. Encapsulation efficiency trends varied with phase ratios. At the 3:1 ratio, EE% increased with surfactant concentration, consistent with the availability of additional bilayer material for drug entrapment. On the other hand, at the 3:2 ratio, maximum EE% was achieved at the lowest surfactant concentration, followed by a decline at higher concentrations, potentially due to increased formulation viscosity and vesicle aggregation impairing efficient drug loading. In summary, these findings highlight the capability of microfluidic techniques to finely adjust nanoparticle characteristics through careful optimisation of formulation parameters. Balancing surfactant concentrations and phase ratios is therefore essential for achieving stable, homogeneous niosomal systems with high encapsulation efficiency suitable for drug delivery applications [226], [227].

Table 3-8: Size distribution and %EE for M1 (cholesterol: Span 60: Kolliphor RH40 (3.5:4.5:2)) at 1 mg/mL initial VCM loading: effect of non-ionic surfactant (organic phase) concentrations. Values are represented as mean ± SD (n = 3) [111].

Total Non-Ionic Surfactant (Organic Phase) Concentration	Aqueous-to-Organic Phase Ratio	Size (nm)	PDI	EE%
20 mg/mL	3:1	58.48 ± 0.676	0.408 ± 0.002	24.89 ± 0.006
	3:2	240 ± 1.5	0.240 ± 0.013	49.09 ± 0.007
40 mg/mL	3:1	90.29 ± 0.78	0.132 ± 0.013	30.17 ± 0.045
	3:2	191.5 ± 2	0.202 ± 0.014	43.55 ± 0.082
60 mg/mL	3:1	133.6 ± 1.51	0.118 ± 0.009	50.16 ±11.04
	3:2	210.1 ± 4.35	0.215 ± 0.013	42.18 ± 0.041

3.3.2. The influence of Using Different Non-Ionic Surfactant Concentrations for M2 formulation.

The Analysis and data presented in **Tables 3.8** (related to M1 sample) and **3.9** (related to M2 sample**)** reveals marked differences between the two niosomal formulations in terms of vesicle diameters, size distribution, and encapsulation efficiency, reflecting the impact of surfactant concentration, phase ratios, and cholesterol content. The first formulation (M1), incorporating cholesterol, Span 60, and Kolliphor RH40 at a ratio of 3.5:4.5:2, yielded vesicles within the nanoscale range, with sizes increasing progressively as surfactant concentration and organic phase ratio increased. Vesicle diameters ranged from 58.48 nm at 20 mg/mL to approximately 240 nm at higher organic ratios, indicating controlled vesicle growth. A notable improvement in size uniformity was observed with increasing surfactant concentration, as reflected by a reduction in PDI from 0.408 to 0.118. Encapsulation efficiency also improved with increasing total surfactant concentrations, reaching a maximum of 50.16% at 60 mg/mL under a 3:1 aqueous-to-organic flow rate ratio, before decreasing slightly at higher organic phase ratios.

In comparison, the second formulation (M2), characterised by a higher cholesterol content (5:4:1), produced substantially larger vesicles, particularly under conditions of increased organic solvent content. At a surfactant concentration of 20 mg/mL and a 3:2 phase ratio, vesicle sizes increased

to 169 nm, indicating vesicle enlargement. PDI values varied widely across this formulation, with extremely low values observed under some conditions, suggesting highly uniform vesicles, alongside higher values indicating less consistent size distributions. Importantly, this formulation achieved superior encapsulation efficiency, exceeding 60% at the 3:2 phase ratio across multiple surfactant concentrations, likely due to the increased internal volume of the larger vesicles. Taken together, these findings have demonstrated that formulation composition plays a critical role in defining niosomes' performance. The first formulation (M1) is more suitable for applications requiring small, homogeneous vesicles, while the second formulation (M2) offers advantages in applications where higher drug loading and larger vesicle size are required [228].

Table 3-9: Size distribution and %EE for M1 (cholesterol: Span 60: Kolliphor RH40 (5:4:1) at 1 mg/mL initial VCM loading: effect of non-ionic surfactant (organic phase) concentrations. Values are represented as mean ± SD (n = 3 [111].

Total Non-Ionic Surfactant Concentration	Aqueous-to-Organic Ratio	Size (nm)	PDI	EE%
20 mg/mL	3:1	142.1 ± 2.70	0.142 ± 0.03	30.52 ± 0.014
	3:2	169 ± 17.00	0.321 ± 0.004	60.35 ± 0.0003
40 mg/mL	3:1	112.1 ± 0.85	0.179 ± 0.005	32.15 ± 0.220
	3:2	137.3 ± 0.72	0.032 ± 0.02	43.12 ± 0.078
60 mg/mL	3:1	136 ± 1.22	0.135 ± 0.01	24.44 ± 0.044
	3:2	1082 ± 40.30	0.188 ± 0.11	60.59 ± 0.016

3.3.3. The influence of using Different drug (VCM) Concentrations.

A comparative assessment of the two microfluidic formulations illustrates the influence of drug concentration (ranging from 0.5 to 2mg/mL) and ratios on niosomal properties. For the first formulation (M1 in **Table 3.10**), prepared using a cholesterol–Span 60–Kolliphor RH40 ratio of 3.5:4.5:2 and a fixed surfactant concentration of 20 mg/mL, while increasing the vancomycin concentration resulted in no consistent trend in vesicle size at the 3:1 phase ratio, with diameters ranging between approximately 120 and 130 nm. In contrast, vesicles formed at the 3:2 ratio were generally larger, indicating that an increased organic phase fraction promotes vesicle enlargement.

At the highest drug concentration, particle size increased to 187.3 nm. PDI values remained relatively small under all tested conditions, reflecting a reasonably uniform size distribution, although a slight increase in PDI was observed at the 3:2 phase ratio when the drug loading reached 2 mg/mL, suggesting increased size variability. Encapsulation efficiency increased with rising drug level in use, and more specifically at the 3:2 phase ratio, where EE% reached 49.1% at 2 mg/mL, likely due to the formation of larger vesicles with greater drug-loading capacity.

In contrast, the second formulation (M2 in **Table 3.11**), composed of a cholesterol–Span 60–Kolliphor RH40 ratio of 5:4:1, exhibited different behaviours. At 3:1 phase ratio, vesicle sizes remained relatively constant across all drug concentrations, with diameters of approximately 138 nm. However, greater variability was observed at the 3:2 phase ratio, where particle sizes increased from 139.9 nm at 0.5 mg/mL to 191 nm at 1 mg/mL before decreasing down to 152.8 nm at 2 mg/mL. PDI values for this formulation were generally lower at the 3:2 phase ratio, particularly at lower drug concentrations, with values as low as 0.055 at 0.5 mg/mL, indicating a narrow size distribution and improved uniformity. Encapsulation efficiency followed a different drift, with the highest EE% recorded at the 3:2 phase ratio and the lowest drug concentration (78.03%), followed by a decline as drug concentration increased, suggesting saturation of encapsulation capacity at higher drug loads.

Overall, these findings demonstrate that the two niosome preparations have responded differently to changes in drug concentration and phase ratios. The first formulation (M1) favours increased vesicle size and higher encapsulation efficiency at elevated drug concentrations, whereas the second formulation (M2) is more effective at encapsulating at lower drug concentrations while maintaining a narrower size distribution. These results highlight the importance of optimising formulation composition and process conditions to achieve right nanoparticle characteristics for drug delivery applications.

Table 3-10 :Size distribution and %EE of M1 (chol: Span 60: Kolliphor RH40 (3.5:4.5:2). at Surfactant concentration of 20 mg/mL: effect of different VCM (aqueous phase) concentrations [111].

Drug Concentration	Aqueous-to-Organic Ratio	Size (nm)	PDI	EE%
0.5 mg/mL	3:1	130 ± 1.31	0.164 ± 0.031	26.09 ± 0.022
	3:2	188.3 ± 3.15	0.155 ± 0.017	43.85 ± 0.053
1 mg/mL	3:1	137.6 ± 1.00	0.156 ± 0.026	28.70 ± 0.412
	3:2	155.5 ± 2.10	0.151 ± 0.017	41.35 ± 0.112
2 mg/mL	3:1	120 ± 0.61	0.147 ± 0.010	34.18 ± 7.734
	3:2	187.3 ± 1.00	0.181 ± 0.014	49.10 ± 9.221

Table 3-11: Size distribution and %EE of M2 (chol: Span 60: Kolliphor RH40 (5:4:1) at Surfactant concentration of 20 mg/mL: effect of different VCM (aqueous phase) concentrations [111].

Drug Concentration	Aqueous-to-Organic Ratio	Size (nm)	PDI	EE%
0.5 mg/mL	3:1	138.2 ± 1.4	0.158 ± 0.02	36.89 ± 0.07
	3:2	139.9 ± 0.7	0.055 ± 0.01	78.03 ± 40
1 mg/mL	3:1	132 ± 1.4	0.181 ± 0.01	35.78 ± 0.4
	3:2	191 ± 19.8	0.338 ± 0.08	45.03 ± 0.04
2 mg/mL	3:1	139 ± 1.2	0.112 ± 0.01	21.48 ± 0.04
	3:2	152.8 ± 2.5	0.090 ± 0.01	43.16 ± 27.5

3.3.4. The influence of Different Non-Ionic Surfactants and Co-Surfactants blend

The results presented in **Table 3.12** demonstrate the influence of different non-ionic surfactants and co-surfactants on vesicle characteristics, while maintaining a constant vancomycin concentration of 1 mg/mL and a fixed total surfactant concentration of 20 mg/mL. Three niosomal compositions were evaluated at a cholesterol-to-surfactant ratio of 3.5:4.5:2, specifically

cholesterol–Span **40**–Kolliphor ELP (Ch-SP40-ELP), cholesterol–Span **60**–Kolliphor ELP (Ch-SP60-ELP), and cholesterol–Span 40–Kolliphor RH40 (Ch-SP40-RH40).

For M3 [Ch-SP40-ELP] formulation, vesicle size increased from 188.3 nm at phase ratio of 3:1 to 367.1 nm at a ratio of 3:2, indicating that an increased organic solvent fraction promotes vesicle size. This increase in vesicle size was accompanied by a slight rise in PDI values from 0.170 to 0.238, which suggests a broader size distribution was obtained for sample produced at higher organic ratio. Encapsulation efficiency increased markedly from 26.02% to 41.41%, consistent with the formation of larger vesicles, which typically hold greater internal capacity for drug entrapment.

The M4 (Ch-SP60-ELP) formulation produced substantially larger vesicles when compared to the M3 (Ch-SP40-ELP) system, with particle sizes of 420 nm at the 3:1 phase ratio and a pronounced increase to 2159 nm at the 3:2 phase ratio. This substantial enlargement was associated with a very high PDI value of 0.941 for sample produced at the 3:2 phase ratio, indicating a highly heterogeneous size distribution and tentative the vesicle aggregation or unstable particle formation. Encapsulation efficiency increased from 41.17% to 64% with increasing organic phase content, indicating enhanced drug loading capacity, though at the expense of size uniformity and formulation stability.

In contrast, the M5 (Ch-SP40-RH40) formulation generated the smallest and most uniform vesicles among the three tested systems, with particle sizes of ~170nm at the 3:1 phase ratio and ~358nm at the 3:2 phase ratio. Correspondingly low PDI values were observed (0.128 and 0.165, respectively), indicating narrow size distributions and controlled nanoparticle formation. Encapsulation efficiency increased moderately from 25% to 43% with increasing organic phase content, reflecting a balance between vesicle size and drug-loading capacity.

Overall, these findings demonstrate that the selection of non-ionic surfactants and co-surfactants has a pronounced effect on niosomal properties. Formulations containing Span 60 and Kolliphor

ELP produced larger, less uniform vesicles with higher encapsulation efficiencies, whereas systems incorporating Span 40 with either stabiliser (Kolliphor ELP or RH40) yielded smaller and more homogeneously distributed particles with a moderate encapsulation efficiency. These observations are consistent with previous reported findings highlighting the influence of co-surfactant type on vesicle size and encapsulation efficiency, particularly the tendency for Kolliphor ELP to promote larger vesicles and higher drug loading [33]. Previous studies investigating nanoparticle transport across sublingual and buccal mucosa have largely focused on particle sizes ranging 100-300 nm[229], [230]. Experiments using porcine buccal mucosa tissues as model have demonstrated that neutral polystyrene nanoparticles with diameters of 25, 50, and 200 nm were capable of penetrating the tissues, with the largest particles exhibiting the deepest and most efficient penetration [231]. Hence, MF approach in this work has illustrate its capability of forming niosomes loaded with VCM within this size range with relatively high amount of drugs.

Table 3-12: Different types of non-ionic surfactant (organic phase) components for Formula M3, M4, and M5 at a ratio of 3.5:4.5:2, 1 mg/mL drug loading, and 20 mg/mL surfactant concentration [111].

Non-Ionic Surfactant Composition	Aqueous-to-Organic Ratio	Size (nm)	PDI	EE%
M3 Ch-SP40-ELP	3:1	188.3 ± 3.33	0.170 ± 0.01	26.01 ± 0.20
	3:2	367.1 ± 3.06	0.238 ± 0.02	41.41 ± 0.01
M4 Ch-SP60-ELP	3:1	420 ± 4.86	0.292 ± 0.04	41.17 ± 0.12
	3:2	2159 ± 322.20	0.941 ± 0.10	63.99 ± 0.01
M5 Ch-SP40-RH40	3:1	170.4 ± 1.40	0.128 ± 0.02	25.44 ± 0.08
	3:2	358.1 ± 4.65	0.165 ± 0.01	42.51 ± 0.07

3.4. In vitro Release Profile of niosome from Bag Dialysis

Dissolution studies were conducted using niosomal formulations that demonstrated optimal particle size, morphology, PDI, and encapsulation efficiency. Three vancomycin-loaded niosomal formulations (M1, M2, and M3), each containing 1 mg/mL vancomycin and 20 mg/mL total surfactant, were evaluated alongside a vancomycin solution (1 mg/mL) as a control. Drug release was monitored over 24 h (**Figure 3.16**). All niosomal formulations exhibited similar release

profiles, with cumulative drug release ranging between 40% and 60% over the experimental period. Sustained release behaviour was observed across all formulations, supporting their suitability for oral delivery of vancomycin. At an FRR of 3:2, cumulative drug release reached 54%, 61%, and 57% for M1, M2, and M3, respectively. Although the experiment was limited to 24 h, extended studies could be performed in future work to assess long-term release behaviour prior to in vivo studies. The observed release values are consistent with expectations for niosomal systems, where complete drug release within 24 h is uncommon due to bilayer-mediated retention. An initial burst release was observed for all formulations, driven by the high concentration gradient across the dialysis membrane and the diffusion of surface-associated drug. As the gradient decreased over time, the release rate slowed down. Drug release from niosomes is governed primarily by passive diffusion pathway through the vesicular bilayer and dialysis membrane, following Fickian diffusion kinetics rather than matrix erosion or degradation. The free-drug release profile demonstrated slower initial release within the first 3 h, followed by complete drug release within approximately 12 h.

This behaviour reflects the use of a dialysis membrane for both free and encapsulated drug studies to ensure methodological consistency, as conventional dissolution testing is unsuitable for niosomal formulations. Formulation M2 exhibited the highest cumulative drug release and the greatest encapsulation efficiency at an FRR of 3:2. This finding supports the association between higher entrapment efficiency and sustained drug release, as previously reported for gliclazide-loaded niosomes [232]. Consequently, formulation M2 appears to be the most promising candidate for controlled vancomycin delivery.

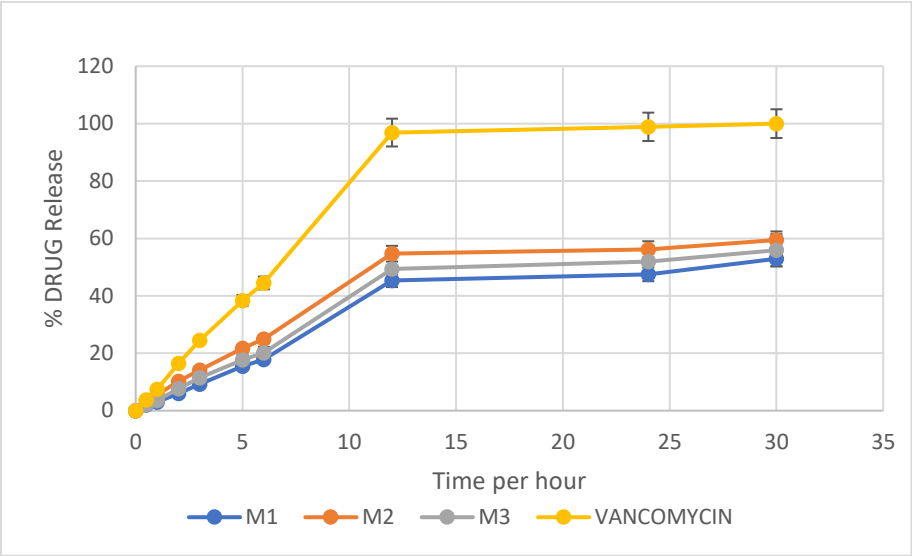

Figure 3.16: Release profiles of different VCM loaded niosomes. Data represent mean ± standard deviation (n = 3) [111].

3.5. Antimicrobial Test

Nanoparticle-based drug delivery systems have gained attention due to their ability to improve therapeutic outcomes in the treatment of intracellular infections caused by bacterial, viral, fungal, and parasitic pathogens [233]. In the present work, the antibacterial performance of niosomal formulations was investigated against *Bacillus subtilis* by employing the agar diffusion technique. Empty niosomes exhibited modest antibacterial activity, producing small inhibition zone [8–11 mm]. In comparison, vancomycin-loaded niosomes showed markedly enhanced activity, with inhibition zones measuring 19–25 mm, comparable to those obtained with free vancomycin (**Figure 3.17**). No antibacterial activity was observed against the Gram-negative strain *Escherichia coli*. These findings demonstrate that the niosomal carriers effectively encapsulated vancomycin and enabled its release in a biologically active form. The growing interest in nanoencapsulation strategies is driven by their capacity to provide sustained and targeted drug release, improve drug

stability, and reduce adverse effects. The choice of nanoencapsulation method is strongly influenced by the physicochemical characteristics of the drug, particularly its solubility, as the aqueous phase plays a key role in nanoparticle formation. Targeted antibiotic delivery using niosomes allows for increased drug accumulation at the infection site, thereby enhancing bacterial killing efficiency [234]. The adaptability of niosomes as drug delivery systems underline their promise for improving antimicrobial therapies. The incorporation of antibiotics into nanoparticulate carriers can further enhance treatment efficacy by increasing local drug concentration and strengthening antibiotic–bacteria interactions, ultimately improving therapeutic outcomes [235].

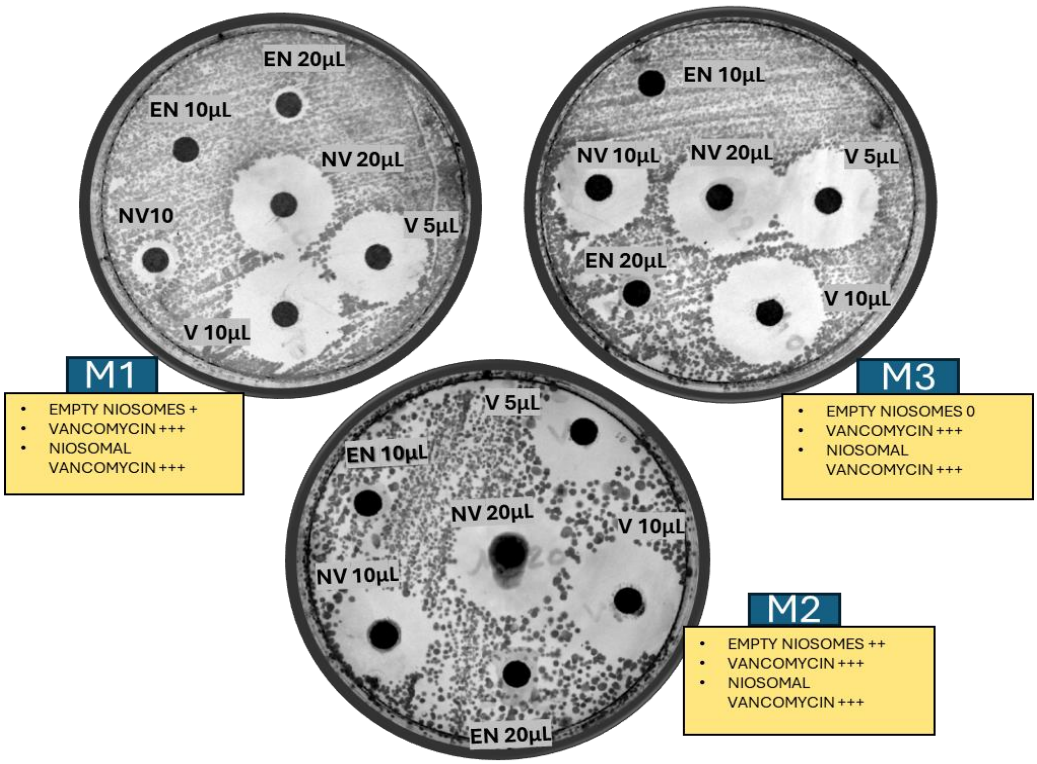

Figure 3.17: Antimicrobial action of of vcm-loaded niosomes against *Bacillus subtilis* by Agar diffusion test. EN, NV, and V refer to empty niosomes, VCM loaded niosome, and vcm alone, respectively.Symbols represent inhibition levels: +++ (strong, large zone), ++ (moderate, medium zone), +(weak, small zone), and 0 (no inhibition) [111].

3.6. In vitro performances of Vancomycin Niosome Fast-Disintegrating Oral Films (FDOFs)

The vancomycin-loaded niosome fast-disintegrating oral films (FDOFs) were assessed for their physicochemical quality, mechanical integrity, and suitability for oral administration. Film weight uniformity was evaluated across the produced batch using an analytical balance, yielding an average weight of 160 mg ± 2 mg with minimal variation, indicating good batch to batch consistency. The film thickness was measured at four different locations using a micrometer calliper and showed a mean thickness of 0.2 mm ± 0.0033 mm. This narrow variation reflects uniform film formation and controlled drying, which are critical for reproducible drug dosing. Mechanical flexibility was assessed through folding endurance testing, where all films withstood more than 100 folds without visible cracking, demonstrating adequate flexibility and resistance to mechanical damage during handling and administration. Tensile strength analysis, performed using a texture analyser, revealed a breaking stress of 9.63 MPa. This value indicates a moderate-to-high mechanical strength, confirming that the films possess sufficient robustness to withstand packaging, transport, and routine handling without compromising structural integrity. Surface pH measurements, conducted by immersing the films in water followed by pH strip analysis, showed a near-neutral pH of 6.83 ± 0.4, suggesting good compatibility with the mouth's environment and a low risk of mucosal irritation. Disintegration behaviour was assessed by immersing the films in 10 mL of deionised water. The films exhibited a rapid disintegration time of 105 s ± 12 s, indicating efficient film breakdown and prompt drug availability. Collectively, these findings demonstrate that the vancomycin-loaded niosome dispersed in FDOFs possess satisfactory uniformity, acceptable mechanical strength, good flexibility, and rapid disintegration characteristics, supporting their suitability for oral drug delivery and potential patient acceptability.

3.7. Executive summary

The study successfully developed and characterised vancomycin-loaded niosomes and fast-disintegrating oral films embedding the nano-sized niosomes, demonstrating notable progress in the design of advanced oral drug delivery systems. The application of microfluidic technology enabled precise modulation of nanoparticle characteristics, with formulation parameters such as surfactant concentration, aqueous-to-organic phase ratio and surfactant composition having extensive influence on vesicle size, polydispersity index, and encapsulation efficiency.

Formulations containing higher surfactant concentrations and, Span 40 with Kolliphor RH40, produced smaller and more homogeneous vesicles with moderate encapsulation efficiencies. In contrast, formulations incorporating Span 60 and Kolliphor ELP generated larger vesicles with enhanced encapsulation capacity but increased size heterogeneity. These niosomes exhibited sustained drug release behaviour, with approximately 40–60% of the encapsulated drug released over a 24 h period. Furthermore, they demonstrated effective antibacterial activity against *Bacillus subtilis*, producing inhibition zones comparable to that of the the control, which is vancomycin solution.

The incorporation of vancomycin-loaded niosomes into fast-disintegrating oral films has resulted in dosage forms with favourable mechanical and performance characteristics. The FDOFs displayed high folding endurance, suitable tensile strength, and rapid disintegration (105 s), indicating good durability, handling properties, and potential for improved patient compliance.

Overall, the developed vancomycin-loaded niosome FDOFs represent a promising strategy for oral drug delivery, offering controlled drug release, improved formulation stability, and effective antimicrobial performance. This is beneficial for VCM, a BCS 3 drug with poor permeability. Therefore, the beneficial effects of MF based systems and the incorporation of this niche nanoplatform into oral films to delivery peptide drug in a non- invasive manner will be further

investigated using another model BCS 3 peptide, i.e. insulin (see chapter 5) as well as nisin, which is peptide of moderate molecular weight (see chapter 4).

Chapter 4: Fast-Disintegrating Oral Films comprising microfluidic based Nisin-Loaded Niosomes: production and product performances by in vitro assessments

Chapter 4 discussed outcomes of nisin based nano-systems and nano-platform base oral films is founded on the accepted and published article described below. Figures and tables used in this chapter were adapted from the same article.

Amer et al. Fast-Disintegrating Oral Films Containing Nisin-Loaded Niosomes. Molecules, 2025 [201].

4.1. Overview

Nisin A is a naturally derived antimicrobial peptide belonging to the class of bacteriocins and lantibiotics, produced by *Lactococcus lactis*. It has a molecular weight of approximately 3.5 kDa and an isoelectric point (pI) of around 8.8 thereby nisin molecule contains a net positive charge at near neutral pH of the oral cavity. The presence of surface charge species on nisin molecules facilitate strong electrostatic interactions with negatively charged components of bacterial membranes [236], [237]. The solubility of nisin A is strongly pH dependent, with reported values of approximately 57 mg/mL at pH 2, decreasing to about 1.5 mg/mL at pH 6 and further to approximately 0.25 mg/mL at pH 8.5. Similarly, its chemical stability diminishes under neutral and alkaline conditions. While nisin exhibits high stability when subject to acidic condition, it remains susceptible to enzymatic degradation and oxidative processes unless adequately protected through encapsulation or matrix embedding [238]. Nisin is well recognised for its potent antibacterial activity against Gram-positive bacteria, including clinically and industrially relevant pathogens such as *Listeria monocytogenes* and *Staphylococcus aureus* [252]. Several variants of nisin exist. Nisin Z represents the closest natural variant of nisin A, differing by only one amino acid residue on their structures, where histidine is replaced by asparagine as shown in **Figure 4.18** [239]. This structural variation results in differences in physicochemical behaviours, with nisin Z generally demonstrating improved solubility at near-neutral pH [239]. Despite this difference, both variants share a common antibacterial mechanism of action, involving interfering bacterial cell wall synthesis by binding to lipid II the main precursor molecule ultimately leading to bacterial cell death [240]. The molecular structure of nisin contains several unusual amino acids, including lanthionine and β-methyllanthionine, which arise from post-translational modifications, and contribute to structural stability with resistance to heat and under acidic conditions [241]. Due to its favourable safety profile and antimicrobial efficacy, nisin is used as a natural food preservative [242]. Beyond food applications, nisin has gained increasing attention in pharmaceutical research for its potential role in treating infections caused by antibiotic-resistant bacteria, including methicillin-resistant *Staphylococcus aureus* and *Clostridium difficile* [243]. However, its clinical

application remains limited by rapid enzymatic degradation and a short biological half-life [244]. To address these challenges, advanced drug delivery strategies, including encapsulation within niosomes, are being actively investigated to improve nisin's stability, bioavailability, and controlled release profiles, and potentially making nisin a promising candidate for various pharmaceutical applications [245].

Fast-disintegrating oral films (FDOFs) represent an innovative and patient-friendly drug delivery approach to delivery Nisin and other peptide agents. They are designed to disintegrate or dissolve rapidly in the mouth without the need for water, offering advantages for those patients who cannot swallow medications (e.g. large tablet) or those requiring rapid therapeutic action. Incorporation of nisin-loaded niosomes into these films could strengthen its antibiofilm activity through niosomal encapsulation as well as exerting rapid and yet localised nisin action at oral mucosal surfaces. This approach is particularly advantageous for the management of oral infection diseases [246]. including persistent biofilm-associated infections reported in certain patients who wear orthodontic or dental prosthetic device [247]. or as an adjunct to conventional periodontal therapy to reduce microbial burden and/or inflammation within periodontal pockets to plaque control and maintain gingival health [248], [249]. Furthermore, nisin-based oral films offer a practical alternative to conventional mouthwashes, providing prolonged antimicrobial activity in situations where rinsing is inconvenient or impractical.

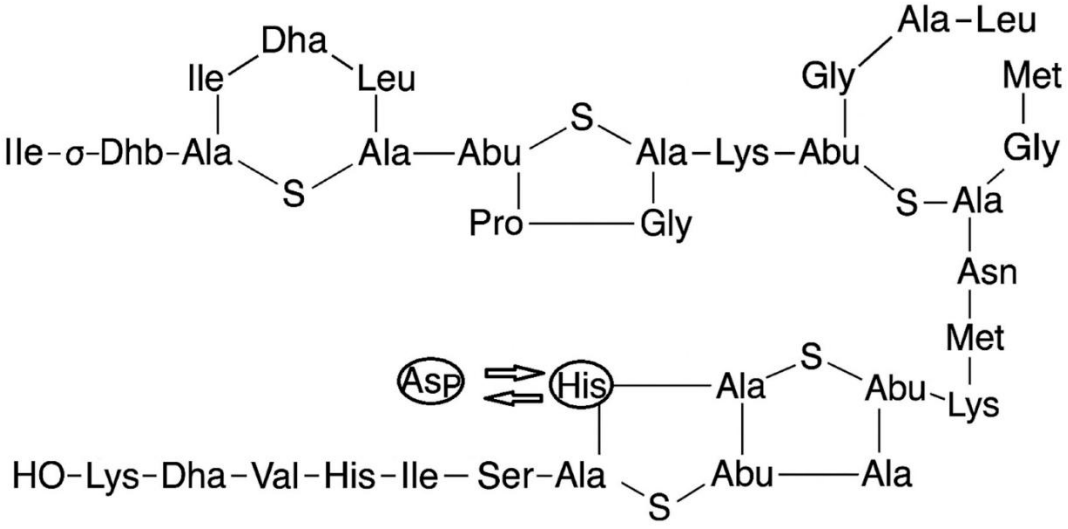

Figure 4.18: Chemical structures of Nisin A and nisin Z structures, where Histidine residue in nisin A is replaced by asparagine residue in nisin Z on the 27th position. figure adopted from [201].

In chapter 3, advantages of microfluidic technology for the fabrication of niosomes s with narrow size distributions, high reproducibility, and controlled physicochemical properties, which is consistent with existing literature [250] has been shown with VCM, a model peptide drug. Likewise, oral film dosage forms have been exploited by their benefits [251]. In addition, the development of oral film system incorporated with niosomes loaded VCM and its feasibility have been shown. However, there is still a knowledge gap on optimal process conditions and properties of products formed by integrating both MF niosomes loaded with peptide drugs and FDOF approaches., In this chapter, nisin will be used as a model peptide that bears limited oral permeability. The impact of film incorporation for nisin based niosomes produced by MF approach on drug release kinetics will be explored in detail. In addition, assessments will be made for niosomes loaded with nisin to support the development and application of MF approach in entrapment of macromolecules.

4.2. Aim and Objectives

The main aim of this chapter is to develop and evaluate a nisin A nanoplatform presented as oral films for the treatment of Gram-positive bacterial infections. Emphasis is placed on assessing the suitability of microfluidic technology for the fabrication of nisin- entrapped niosomes, with the long-term objective of integrating the optimised formulation into fast-disintegrating oral films for localised delivery within the oral cavity.

To achieve this aim, several objectives were defined. Initially, niosomes encapsulating nisin A will be prepared microfluidic technology by varying formulation compositions and phase ratios (see chap 2 sect.2.3, table 2-5) The resulting vesicles will be comprehensively characterised in terms of key physicochemical parameters, in order to identify the most suitable formulation for antimicrobial drug delivery. Comparison will also include stability studies and in vitro antimicrobial activity testing against *Bacillus subtilis* using agar plate diffusion technique as described in chapter 2.

Following optimisation, the most promising niosomal formulation will be incorporated into FDOF. The film development process will involve the investigation of different polymeric conditions and super-disintegrating agents. Film properties will be tested, including disintegration test with water as medium, release studies in relevant buffer system in addition to quantifying physical and mechanical properties of the developed films. Moreover, FTIR and thermal analysis (by TGA and DSC) were conducted to study interactive effects as well as compatibility of drug, niosomal and film components.

4.3. Results and Discussion

4.3.1 Niosomes preparation

The compositions of five nisin-loaded niosomal systems prepared using microfluidic mixing were described in chapter 2 (sect.2.3, table 2-5). Two phase ratios (3:1 and 3:2) were investigated to clarify the influence of formulation variables and processing conditions on vesicle size and its distribution, and drug entrapment efficiency and the results were shown (**Table 4.13**). All formulations consisted of cholesterol in combination with different non-ionic blends, including Span 40 or Span 60 as main surfactant, Kolliphor RH40 or Kolliphor ELP as stabiliser, enabling a systematic comparison of surfactant chemistry within a controlled microfluidic environment.

The data indicated that both surfactant compositions and phase ratios contribute to variations in niosomal characteristics, although their effects differ depending on the measured parameters. This observation highlights the multifactorial nature of microfluidic niosome formation, where compositional and process-related factors interact to determine final vesicle properties.

When considering vesicle size, notable differences were observed between formulations and between phase ratios. NM5 (Ch-SP40-RH40) prepared at a 3:1 phase ratio yielded the smallest vesicles among all systems (109.1 ± 1.19 nm). However, increasing the organic phase proportion to a 3:2 ratio resulted in a pronounced increase in hydrodynamic size (354.2 ± 3.07 nm), indicating that higher organic content can promote vesicle size under microfluidic process conditions. Despite this increase in size, the same formulation exhibited improved size uniformity and enhanced encapsulation efficiency, suggesting a trade-off between vesicle dimensions and functional performance.

A more favourable balance between vesicle size, homogeneity, and drug loading was achieved with formulations incorporating Span 60 as the primary surfactant. In particular, NM2 (Ch-SP60-RH40) prepared at a 3:2 phase ratio had the highest encapsulation efficiency (58%) while maintaining a relatively small mean diameter (165.3 ± 0.17 nm) and an exceptionally low PDI

(0.044 ± 0.020). The narrow size distribution observed for this formulation reflects the formation of a highly uniform vesicle population and is desirable for drug delivery performance.

In contrast, formulations containing Kolliphor ELP as a co-surfactant (NM3 and NM4) generally produced larger vesicles and broader size distributions. This suggests that ELP may interfere with bilayer packing during vesicle self-assembly, leading to reduced control over vesicle size. Nevertheless, when combined with Span 60, ELP still facilitated relatively high drug encapsulation, as demonstrated by NM4 at the 3:2 phase ratio, which achieved an encapsulation efficiency of 47%. This finding indicates that ELP can contribute positively to drug loading, even if its impact on size uniformity is less favourable. The superior performance of Span 60–based systems can be attributed to its long alkyl chain and high phase transition temperature, which promote the formation of rigid and stable bilayers. The inclusion of Kolliphor RH40, a PEGylated surfactant, further enhances vesicle stability by increasing surface hydration and steric repulsion, thereby reducing aggregation and facilitating improved nisin entrapment.

This interpretation is supported by comparison with niosomes loaded with VCM in the previous chapter. The NM2 formulation (with nisin) closely resembles the M2 system (with VCM) reported by Amer et al. for vancomycin-loaded niosomes prepared via microfluidic mixing [111]. Under comparable preparation conditions, the vancomycin-loaded M2 formulation produced vesicles with a mean particle size of 169 ± 17 nm**,** a PDI of 0.32, and an encapsulation efficiency of 60.35%**.** Similarly, the nisin-loaded NM2 formulation**,** which used the same formulation type and surfactant ratio, produced vesicles with a mean particle size of 165.3 ± 0.173 nm**,** a PDI of 0.044 ± 0.020, and an encapsulation efficiency of 58.32 ± 0.4%. These findings suggest that this formulation composition was suitable for encapsulating different peptide molecules while maintaining nanoscale vesicle size and high entrapment efficiency,. The consistency between these findings suggests that the Span 60/cholesterol/RH40 (5:4:1) combination at a 3:2 phase ratio represents a robust and reproducible formulation platform, capable of accommodating different antimicrobial peptides without compromising nanoscale size or encapsulation performance.

Beyond qualitative comparison, statistical analysis was undertaken to quantitatively assess the effects of formulation composition and phase ratio on the measured parameters. All niosome formulations were prepared as three independent batches (n = 3), with results expressed as mean ± standard deviation. Prior to parametric testing, the assumptions of normality and homogeneity of variance were verified using the Shapiro Wilk and Levene's tests, respectively ($p > 0.05$). One-way ANOVA revealed no statistically significant differences in vesicle size ($p = 0.746$, $\eta^2 = 0.076$) or encapsulation efficiency ($p = 0.736$, $\eta^2 = 0.071$) across the different surfactant systems whereas η^2 (eta squared) represents the effect size. In contrast, a significant effect was observed for the polydispersity index ($p = 0.021$, $\eta^2 = 0.413$), indicating that surfactant and co-surfactant selection plays a critical role in controlling vesicle size uniformity.

A separate analysis of the effect of phase ratio further clarified the role of processing conditions. While no significant differences were detected for vesicle size ($p = 0.714$, $\eta^2 = 0.005$) or PDI ($p = 0.176$, $\eta^2 = 0.075$), increasing the organic phase proportion to a 3:2 ratio resulted in a statistically significant enhancement in encapsulation efficiency ($p = 0.0136$, $\eta^2 = 0.231$). This improvement is likely attributable to more efficient self-assembly and drug incorporation during microfluidic mixing when a higher organic phase content is employed.

Table 4-13: Size distribution and encapsulation efficiency of niosomes loaded with nisin prepared by microfluidic process [201] .

Formulation	Niosome Composition	Aqueous to Organic Phase Ratio	Size (nm)	PDI	EE%
NM1	Ch-SP60- RH40	3:1	140.9 ± 1.65	0.227 ± 0.005	23.41 ± 0.53
		3:2	203.3 ± 1.29	0.198 ± 0.024	36.90 ± 0.34
NM2	Ch-SP60- RH40	3:1	145.1 ± 1.19	0.145 ± 0.009	25.74 ± 0.31
		3:2	165.3 ± 0.17	0.044 ± 0.020	58.32 ± 0.42
NM3	Ch-SP40-ELP	3:1	219 ± 1.49	0.269 ± 0.014	21.78 ± 0.51
		3:2	236.1 ± 3.44	0.316 ± 0.019	40.47 ± 0.70
NM4	Ch-SP60-ELP	3:1	260.9 ± 2.71	0.313 ± 0.063	40.21 ± 0.33
		3:2	230.1 ± 14.29	0.358 ± 0.010	47.43 ± 0.23
NM5	Ch-SP40-RH40	3:1	109.1 ± 1.19	0.231 ± 0.013	25.87 ± 0.21
		3:2	354.2 ± 3.07	0.149 ± 0.035	36.57 ± 0.22

4.3.2 Antimicrobial Activity

The antimicrobial performance of the optimised nisin-loaded niosomal formulation NM2 (phase ratio 3:2) was assessed using an agar diffusion assay. The result was compared to free nisin (2 mg/mL) and other appropriate control groups, including empty niosomes of identical composition (**Figure 4.19**). The agar diffusion method is widely employed as a semi-quantitative screening tool to confirm antimicrobial activity and, in the case of nanocarrier-based systems, to verify that the encapsulated agent retains its biological function.

The assay outcome has demonstrated that both free and encapsulated nisin remained biologically active against the tested Gram-positive strain. However, differences in inhibition zone diameter were observed, reflecting the distinct diffusion and release behaviours of the two systems. Application of nisin solution produced a larger inhibition zone (19 mm) when compared with the NM2 (phase ratio 3:2) (16 mm), an outcome that can be rationalised by considering both drug availability and release kinetics.

Firstly, the encapsulation efficiency of this NM2 formulation was 58%, indicating that only ~1.16 mg/mL of nisin was immediately available for diffusion into the agar matrix. This reduced freely diffusible drug fraction inherently limits the extent of zone formation when compared with an equivalent concentration of unencapsulated drug in nisin solution. Secondly, nisin encapsulated within niosomal vesicles is released in a controlled and sustained manner, which slows diffusion rate of nisin through the semi-solid agar medium (refer sect 4.3.9 for dissolution result) as opposed to e rapid and unrestricted diffusion of free peptide in solution form. Consequently, the smaller inhibition zone recorded for the niosomal formulation does not reflect diminished antimicrobial efficacy, but rather it has shown a modified release profile consistent with controlled drug delivery behaviour.

This characteristic is particularly relevant when interpreting agar diffusion data for nanoparticle-based systems, as the assay inherently favours rapidly diffusing agents. While free nisin (as solution) disperses quickly and uniformly, it is known to be susceptible to degradation by enzymes in complex environments such as the oral cavity [252]. It is anticipated that encapsulation of peptide agents within niosomes provides a protective barrier that can shield them from premature degradation, thereby enhancing stability and prolonging local therapeutic presence at the target site.

Comparison was also made with previously niosomal antibiotic systems loaded with VCM (see chapter 3m sect no. 3.5). Vancomycin-loaded niosomes prepared using the same formulation composition and microfluidic process (M2, phase ratio 3:2) produced inhibition zones ranging from 19 to 25 mm against *Bacillus subtilis*[111]. The larger zones observed are likely attributable to the higher intrinsic potency of vancomycin. VCM typically exhibits lower minimum inhibitory concentrations (MICs) than nisin. For instance, vancomycin MIC values against *Staphylococcus aureus* generally range between 0.5 and 2 µg/8mL, whereas reported MICs for nisin often lie 8 to 32 µg/mL, depending on the bacterial strains and experimental conditions for testing [253], [254]. These intrinsic differences in antimicrobial potency must therefore be considered when comparing zone sizes across different drug-loaded systems.

Importantly, no inhibition zones were detected around wells containing empty niosomes, confirming that the vesicular components and excipients do not possess inherent antimicrobial activity. The findings verify that the observed antibacterial effect is exerted solely by nisin molecules. The absence of antimicrobial activity from individual formulation constituents, including Span 60, RH40, Span 40, ELP, and cholesterol was demonstrated on the control agar plates **(Figure 4.19)**. Although these components are essential for the formation and stabilisation of the vesicular architecture, they do not contribute independently to bacterial growth inhibition under the tested conditions.

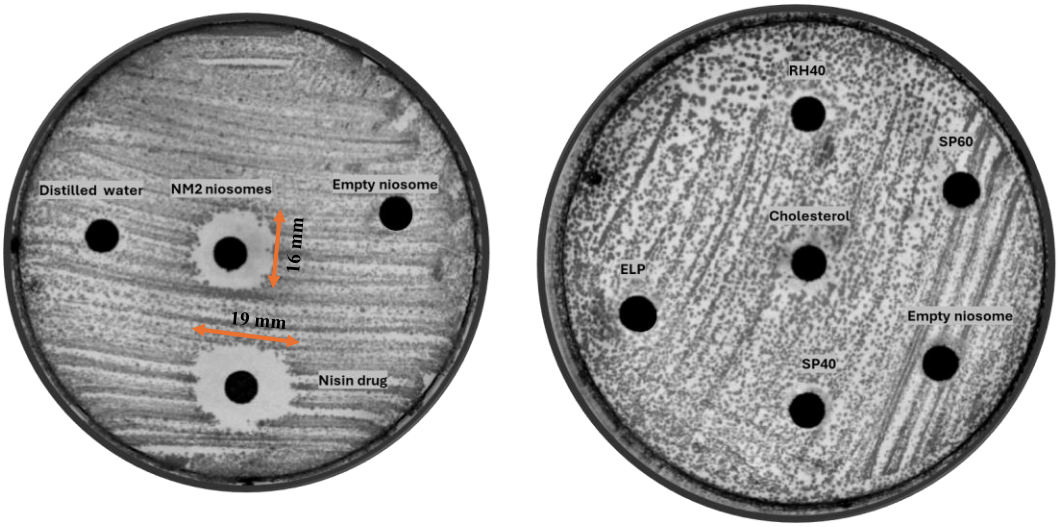

Figure 4.19: Antimicrobial activity of the optimized NM2 formulation and its components using Agar plate method. Plate on left had side showing inhibition zones for NM2 (16 mm) and free nisin (19 mm); plate on the right-hand side confirms the absence of antimicrobial activity from individual excipients (Span 60, RH40, Span 40, ELP, cholesterol) and blank vesicles. n = 2. figure adopted from [201].

4.3.3. Film Characterization

The initial screening of film-forming polymers (**Table 4.14**) revealed marked differences in film integrity, mechanical behaviour, and handling performance, highlighting the critical role of polymer selection in fast-dissolving oral film development. Among the polymers evaluated, polyvinyl alcohol (PVA) emerged as the most suitable candidate. PVA-based films were transparent, slightly sticky, and highly flexible, with excellent peelability from the casting surface. These favourable attributes are consistent with the semi-crystalline structure of PVA and its strong intermolecular hydrogen bonding capacity, which collectively show mechanical robustness while maintaining sufficient flexibility for rapid-disintegration dosage forms [255]. In contrast, hydroxypropyl methylcellulose (HPMC), although capable of forming clear and smooth films, but

it exhibited poor flexibility and brittleness. This behaviour is likely associated with HPMC's relatively high glass transition temperature (Tg 160–180 °C), which promotes the formation of rigid polymer matrices upon solvent evaporation [256]. Furthermore, HPMC films adhered strongly to the casting substrate, complicating removal and limiting their practical utility for oral film fabrication. Polyvinylpyrrolidone (PVP) demonstrated moderate film-forming ability and acceptable peelability however, brittleness and shrinkage were observed following drying. This shrinkage can be attributed to PVP's hygroscopic nature, where the water uptake during casting followed by rapid moisture loss during drying induces internal stresses and microfractures within the film matrix [257]. Similarly, hydroxypropyl cellulose (HPC) films showed excessive stickiness, poor peelability, and limited flexibility. The high moisture retention capacity of HPC likely hindered complete film setting under standard drying conditions, resulting in unacceptable mechanical properties [258]. Based on these comparative observations, PVA was selected as the polymer of choice for subsequent film formulation development that incorporated disintegrants and noisome-loaded suspensions. Its superior film uniformity, good mechanical strength, and ease of handling make it particularly suitable for fast-dissolving oral film applications aimed at ensuring dose accuracy and patient compliance.

Table 4-14: Effect of polymer types on Film-forming ability, mechanical properties, and visual characteristics for oral film formulation, (N= 3), [201].

Polymer	Film-Forming Ability	Visual Appearance	Flexibility	Peelability	Brittleness	Selected for Further Optimization	Film Shape and Surface Uniformity
HPMC	Poor	Clear, smooth	Low	Poor	High	No	
PVA	Excellent	Transparent, slightly tacky	High	Good	Slight	Yes	
PVP	Moderate	Brittle, shrinks on drying	Low	Good	High	No	
HPC	Poor	Sticky on drying	Low	Poor	None	No	

Following polymer selection, the influence of disintegrant type (≤1% w/w) on the physicomechanical properties and disintegration behaviour of the films was evaluated (**Table 4.15**). Among the tested formulations, F2 containing sodium starch glycolate (SSG, 1%) exhibited the most rapid disintegration time (27 ± 6 s), significantly out-performing films containing microcrystalline cellulose (MCC; 59 ± 4 s), croscarmellose sodium (COS; 104 ± 2 s), and the control film without disintegrant (113 ± 12 s). The superior disintegration property of SSG is attributed to its rapid swelling and wicking mechanisms, which accelerate water penetration and promote rapid matrix rupture upon hydration. SSG is widely reported as an effective superdisintegrant at concentrations around 1% w/w in fast-dissolving formulations [259]. Film thickness remained consistent across all film formulations (~0.211 mm), suggesting that

disintegrant incorporation did not adversely affect casting uniformity. Weight variation was within acceptable limits for uniform dosage forms, although MCC-containing films displayed slightly bigger mass variations (188 ± 30 mg), potentially due to the particulate nature of MCC and its influence on homogeneity and moisture retention during drying. Importantly, all films-maintained surface pH values within the physiologically acceptable range (6.5–7.0), minimising the risk of oral mucosal irritation.

Film flexibility, assessed via folding endurance, further distinguished the formulations. F2 (with SSG) demonstrated superior flexibility (77 ± 10 folds) relative to MCC (44 ± 6 folds) and COS (20 ± 8 folds), while the control film without disintegrant exhibited the highest folding endurance (150 folds). This observation suggests that while the absence of disintegrant enhances mechanical strength, it compromises film disintegration time. Collectively, these findings highlight SSG-containing PVA films as the most favourable film with properties that balance between rapid disintegration profile and acceptable mechanical strength, supporting their selection for further development.

All formulations were tested in triplicate ($n = 3$), and results are reported as mean ± SD. Prior to analysis, normality of disintegration times for each group (MCC, SSG, COS, and control) was assessed using the Shapiro–Wilk test ($W = 0.954–0.981$, $p = 0.689–0.824$), confirming normal distribution of data , W represents the test statistic that quantifies how closely the sample data conform to a normal distribution. Homogeneity of variance was verified with Levene's test ($p = 0.78$). Statistical analysis confirmed the significant influence of disintegrant type on disintegration time (one-way ANOVA, $p < 0.0001$, $\eta^2 = 0.912$), with Tukey's post-hoc analysis identifying SSG as significantly superior to all other groups. Collectively, these results support the selection of a PVA–SSG system as the most appropriate platform for fast-dissolving oral film development.

Table 4-15: Physiocochemical properties of oral fast-disintegrating films produced using different super-disintegrants [201].

Formulation Code	Disintegrant	Disintegration Time (s)	Thickness (mm)	Weight Variation (mg)	Surface pH	Folding	Surface Uniformity
F1	Microcrystalline Cellulose (MCC)	59 ± 4	0.211 ± 4	188 ± 30	6.5–7.0	44 ± 6	
F2	Sodium Starch Glycolate (SSG)	27 ± 6	0.211 ± 4	173 ± 8	6.5–7.0	77 ± 10	
F3	Croscarmellose Sodium (COS)	104 ± 2	0.201 ± 4	165 ± 20	6.5–7.0	20 ± 8	
F4	None	113±12	0.211 ± 4	160 ± 2	6.5–7.0	150	

4.3.4. Microscopic Appearance

The changes in appearance of film structure were examined under microscope after immersion in water for 5 min at 37 C˚. Clear differences were observed between the dissolved blank oral film (A) and the nisin-loaded niosomal film (B) (**Figure 4.20)**. The blank film, containing only PVA and PEG 400, dissolved to form a clear, smooth, and homogeneous solution, reflecting uniform polymer dispersion and confirming the absence of dispersed niosomes. Conversely, the niosome-loaded film displayed a uniformly distributed population of spherical vesicles upon dissolution. The preservation of vesicle morphology indicates that the niosomes successfully rehydrate from the dried film matrix without aggregation or structural collapse.

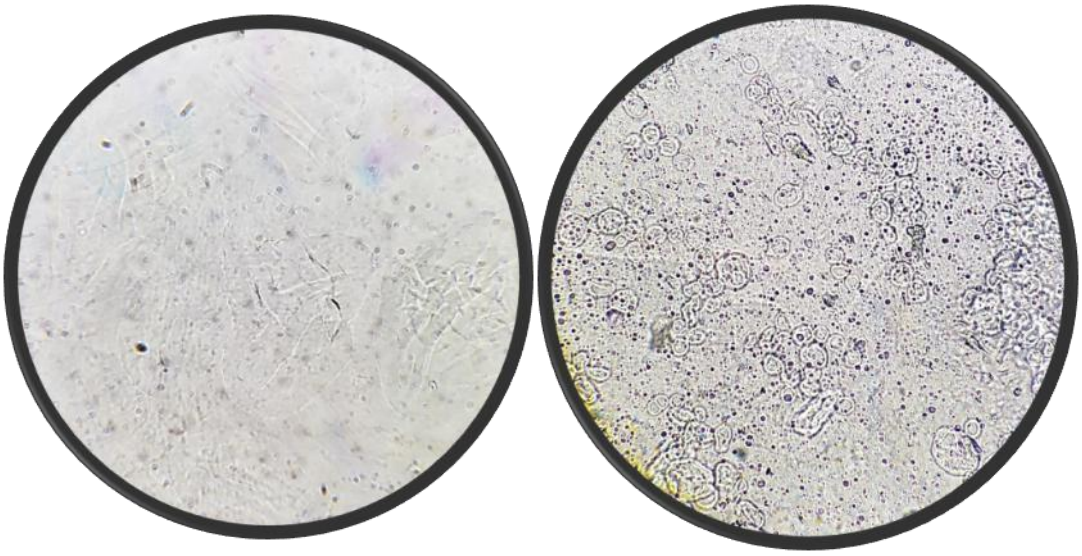

(**A**) (**B**)

Figure 4.20: Microscopic images of blank oral film (A) and nisin niosome film (B) dispersed in water. Objective Magnification: 40x, figure adopted from [201].

4.3.5. Scanning Electron Microscope

The scanning electron micrograph of the NM2 (phase ratio 3:2) niosomal formulation shown in **Figure 4.21** reveals a heterogeneous population of vesicles exhibiting spherical morphology, with slightly elongated or oval shapes. The surfaces of these vesicles appear smooth. Importantly, the micrograph does not indicate extensive aggregation or fusion among vesicles, suggesting that the formulation maintains structural integrity and colloidal stability under the conditions used for imaging.

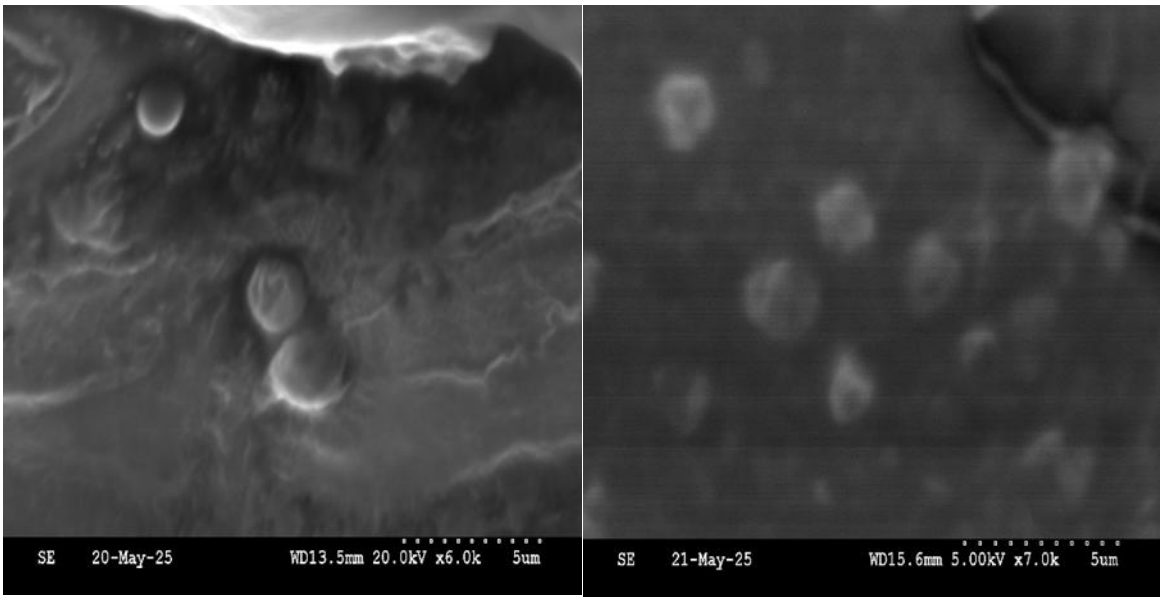

(A) **(B)**

Figure 4.21: Shape and size of NM2 niosomes illustrared with SEM micrographs at different magnification (A) X6000; (B) X7000.fig adopted from [201]**.**

4.3.6. Fourier Transform Infrared Spectroscopy (FTIR) Analysis

FTIR spectroscopy was employed to evaluate potential chemical or physical interactions between the niosomal system, the film-forming polymers, and the encapsulated nisin. This analysis was undertaken to assess formulation compatibility and to identify any evidence of molecular interactions, like hydrogen bonding or changes in functional group environments within the polymeric matrix.

Owing to the use of low level of nisin (less than 2%) in the final formulations, its characteristic absorption bands associated to nisin were not clearly distinguishable in the FTIR spectra (**Figure 4.22**). This is likely due to dilution below the detection threshold of the equipment and spectral overlaps with the dominant absorption bands of the polymeric excipients. Similar masking effects have been reported previously in polymer–peptide systems where the active compound is present at low concentrations [260], [261]. A characteristic C–H stretching vibration was observed at 2903.6 cm^{-1} in pure PVA powder, this band shifted to 2906.4 cm^{-1} in the blank film, suggesting molecular rearrangement or interaction induced during the film formation process [262], [263]. The persistence of this band shift in the nisin-loaded film indicates that the presence of nisin does not interfere with these interactions.

In addition, the C=O stretching vibration at 1729.5 cm^{-1} of PVA exhibited a shift when comparing spectrum of pure powder to that of the blank film, which can be attributed to interactions involving addition of polyethylene glycol (PEG) within the film matrix [262], [263]. Only minor changes were observed following the incorporation of nisin or nisin-loaded niosomes to PVA film, indicating that the carbonyl environment remained largely unaffected. Similarly, the band at 1087.45 cm^{-1}, corresponding to C–O stretching of PVA, shifted upon film formation but showed no further significant changes after drug or niosome incorporation. Collectively, these findings indicate that the dominant interactions occur between PVA and PEG, while nisin remains physically entrapped within the polymeric network without forming new chemical bonds, confirming formulation compatibility and chemical stability.

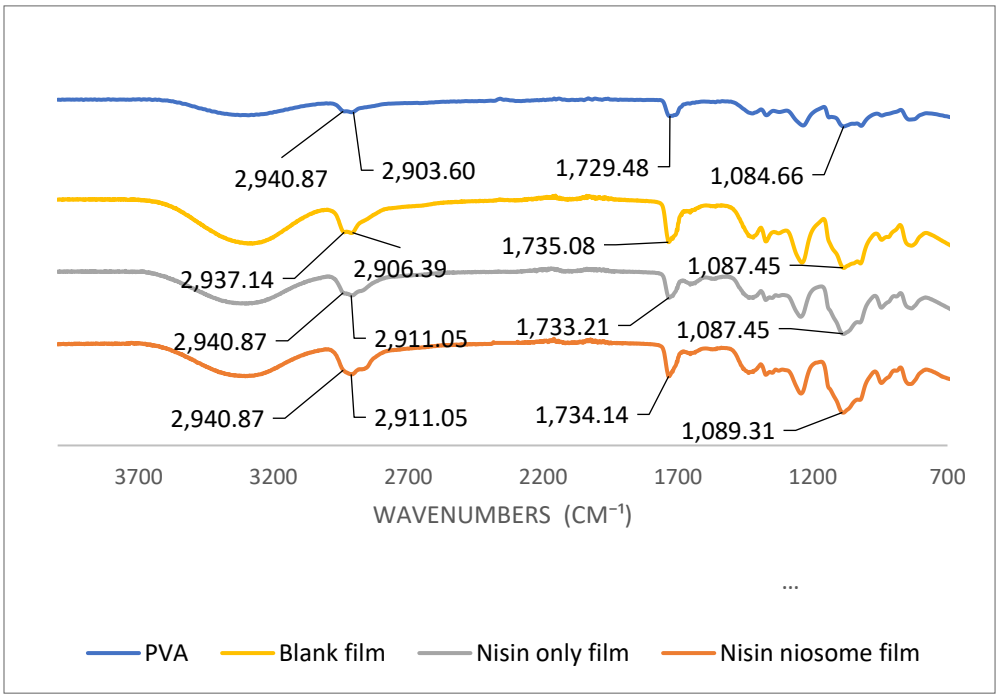

Figure 4.22: Spectra of nisin niosome film. Nisin-only film versus blank film and PVA powder by Fourier transformed infrared analysis. figure adopted from [201].

4.3.7 Thermal Analysis results

4.3.7.1. Thermogravimetric Analysis

Thermogravimetric analysis (TGA) was employed to evaluate film stability under a programmed heat regime. The method allows moisture content of the niosome-based nisin oral film formulation to be determined based on mass loss. Based on results presented **(Figure 4.23 a**), niosome-containing film showed a higher mass loss (3.7%) than the nisin-only film (2.37%), which is attributed to increased water content within the samples. This observation is consistent with the presence of an aqueous core within the niosomal vesicles, where water molecules are retained within the bilayer structure.

This interpretation is further supported by the differential thermogravimetric (DTG) **(Figure 4.23 b**), The first thermal event, corresponded to moisture evaporation, displayed both increased peak intensity and a slight shift towards a higher temperature in the niosome-loaded oral film. Such behaviour suggests that water molecules are more strongly associated with the formulation matrix, requiring higher thermal energy for release, and indicates effective water entrapment within the vesicular system.

Polyvinyl alcohol (PVA), composed of repeating vinyl alcohol units $[–CH_2–CH(OH)–]_n$, typically undergoes an initial degradation step associated with its hydroxyl groups along the polymer backbone. In the present study, this event occurred at a higher temperature in the niosome-based film (328 °C) when compared to the nisin-only film (321 °C). The right peak shift, together with the broader degradation peak observed in the DTG profile, suggests that the incorporation of niosomes contributes to enhanced thermal stabilisation of the film matrix. The wider temperature ranges reported for this thermal event may further indicate a more gradual degradation mechanism, potentially arising from greater intermolecular interactions such as hydrogen bonding between PVA chains and the niosomal components. Overall, these findings have demonstrated that the niosomal system improves the structural and thermal stability of the film, which may positively influence its mechanical performance, storage stability, and controlled drug release behaviour.

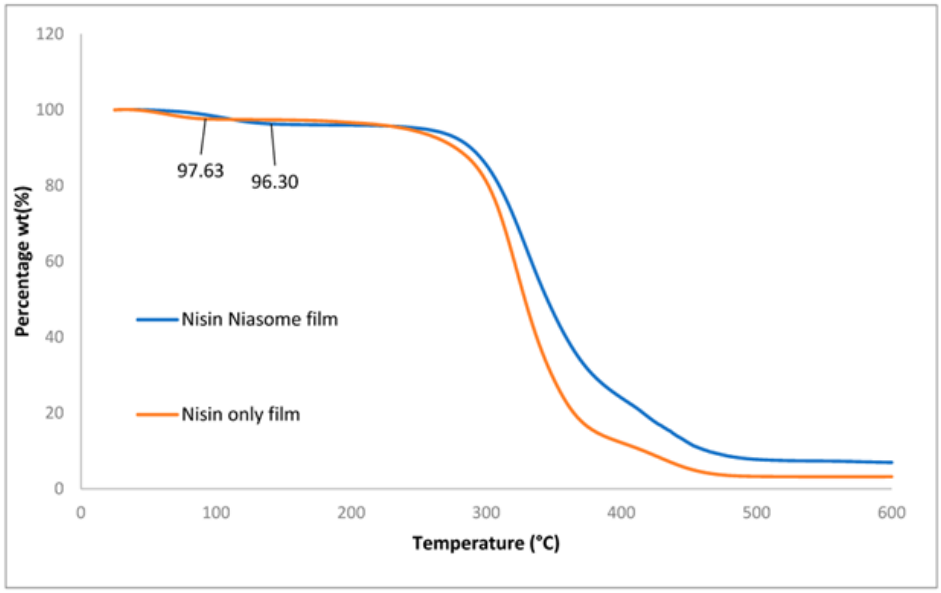

(A)

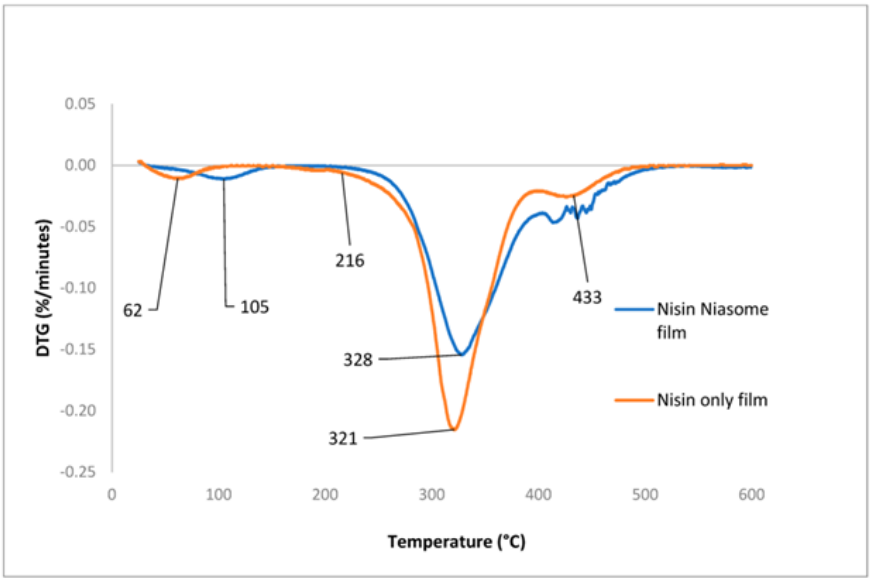

(B)

Figure 4.23: Thermal profiles based on (A) TGA analysis (A) and (B) DTGA for nisin niosome and nisin-only film. figure adopted from [201].

4.3.7.2. Differential Scanning Calorimetry

Differential scanning calorimetry (DSC) is a calorimetric technique routinely used in R&D development to examine the thermal behaviour of pharmaceutical products, in this case the film formulations, Data derived from DSC analysis also helps to detect any potential interactions between the PVA-based film matrix and the incorporated niosomal system. Pure nisin powder did not exhibit a sharp endothermic melting peak, which is consistent with its predominantly amorphous structure. The DSC thermogram of PVA powder showed a glass transition temperature (Tg) at 42.4 °C, which is lower than the Tg values commonly reported in the literature (75–85 °C) [264] This reduction is attributed to the presence of residual moisture, which acts as a plasticiser and increases the mobility of PVA polymer chains, thereby lowering the polymer Tg value as showen in (**Figure 4.23 C)** below.

In contrast, the blank PVA film exhibited a higher Tg, reflecting the partial removal of moisture during the solvent casting and drying process. A pronounced change in thermal behaviour was observed following incorporation of the niosomal formulation. Specifically, the Tg value corresponded to the PVA matrix dropped from 94.7 °C in the nisin-only film to a smaller value of 66.5 °C in the nisin-loaded niosomes based oral films. This reduction in Tg value suggests increased polymer chain mobility, likely arising from plasticising effects or molecular-level interactions between the PVA chains and the niosomal components. The findings based on DSC analysis are consistent with the outcomes of FTIR analysis, which indicated interactions within the film matrix without evidence of chemical incompatibility. The decrease in Tg from 94.7 °C in the nisin-only film to 66.5 °C in the nisin-loaded niosome film may be explained by increased PVA chain mobility caused by plasticising effects from the niosomal components and residual moisture/PEG 400. This interpretation is supported by Mohammed et al., who reported that PEG incorporation into PVA films reduced Tg from 89.2 °C to 60.6 °C, confirming the ability of PEG to plasticise PVA by increasing polymer-chain mobility [265]. Collectively, the complementary results from DSC, FTIR and TGA have supported that niosome incorporation alters the thermal properties of the film through physical interactions rather than chemical modification.

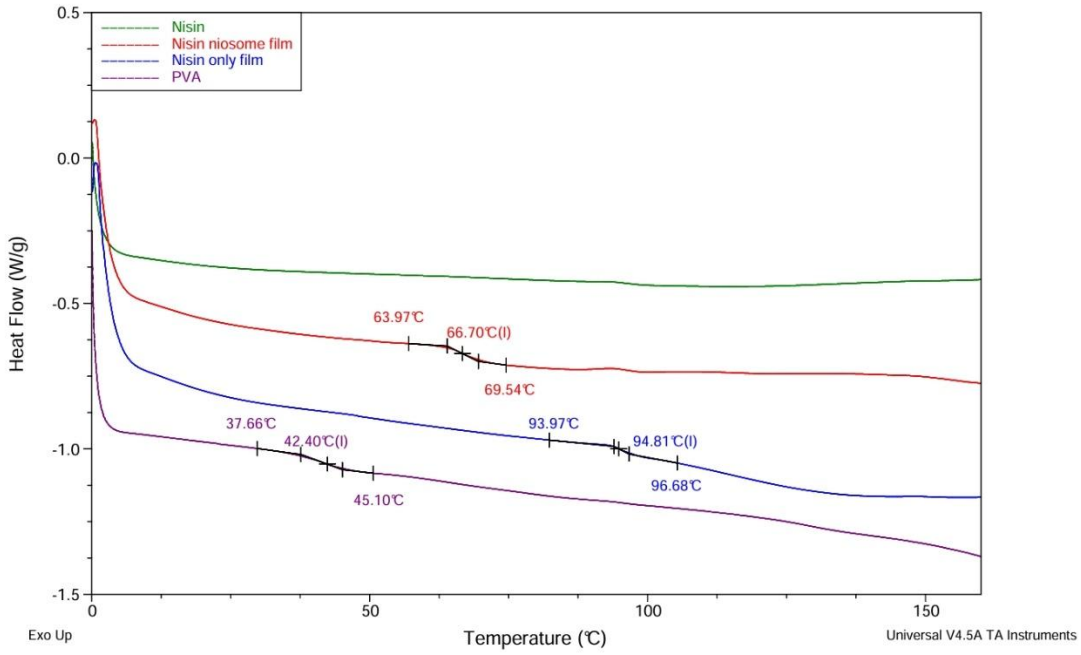

Figure 4.23 c: Differential scanning calorimetry (DSC) thermograms of pure nisin, PVA, nisin-only film, and nisin-loaded niosome film.

4.3.8. Film Tensile Strength

The results from tensile testing demonstrated clear differences in the mechanical behaviour of the nisin-only film to nisin-loaded niosome based film. This was shown as the stress-strain curves (**Figure 4.24**). The nisin-only film possessed a higher strain at break (0.3078 mm) than the niosome-containing film (0.2152 mm), indicating greater elasticity and an enhanced ability to deform before failures. In contrast, the maximum stress required to rupture the film increased from 0.7190 MPa for the nisin-only film to 0.8879 MPa following incorporation of niosomes in the film preparation. This increase in tensile strength suggests that the presence of niosomal vesicles strengthens the polymer matrix, likely through physical interactions between the PVA chains and the vesicular components.

Statistical analysis confirmed that the observed differences in both stress and strain values were significant between these films ($p = 0.0002$ for stress and $p = 0.0035$ for strain). In addition, a marked increase in Young's modulus was observed upon niosome incorporation. The nisin-only film displayed a Young's modulus of 2.437 MPa, indicative of a relatively flexible and compliant structure, while the niosome-loaded film exhibited a substantially higher modulus of 4.238 MPa, reflecting increased stiffness and resistance to deformation. Collectively, these findings highlight the effect of elasticity and mechanical strength, where niosomal incorporation enhances film robustness at the expense of extensibility. This may be advantageous for handling, packaging, and storage of fast-dissolving oral films.

The difference between the two stress–strain profiles may also be explained by the different plasticising effects of nisin-film and niosome-associated nisin within the PVA film matrix. In the nisin-only film, the peptide is more freely dispersed within the hydrated PVA–PEG 400 network and may act as a small molecular additive that disrupts intermolecular interactions between PVA chains. This can increase chain mobility and flexibility, explaining the higher strain at break observed for the nisin-only film. This behaviour is consistent with the general effect of plasticisers, which reduce intermolecular forces between polymer chains, increase mobility, and usually increase elongation while reducing stiffness or modulus [266].

In contrast, when nisin was incorporated within niosomes, the vesicular system appeared to reduce the plasticising effect of the free peptide and acted more like a dispersed reinforcing phase within the PVA matrix. The higher maximum stress and Young's modulus observed for the nisin-loaded niosome film suggest stronger resistance to deformation, possibly due to physical interactions between PVA chains and the niosomal components, including surfactants and cholesterol. Similar behaviour has been reported in PVA-based nanocomposite films, where incorporation of particulate or nanostructured components increased tensile strength and stiffness but often reduced elongation at break [267]. The DSC and tensile results indicate mixed effects. The decrease in Tg suggests that niosomal components, together with PEG 400/residual moisture, increased PVA chain mobility at the thermal-transition level. However, during tensile testing, the dispersed

niosomal vesicles appeared to act as strengthening domains within the film matrix, increasing tensile strength and Young's modulus while reducing strain at break. Therefore, niosome incorporation may have introduced local plasticising effects while also strengthening the film structure through vesicle–polymer interactions.

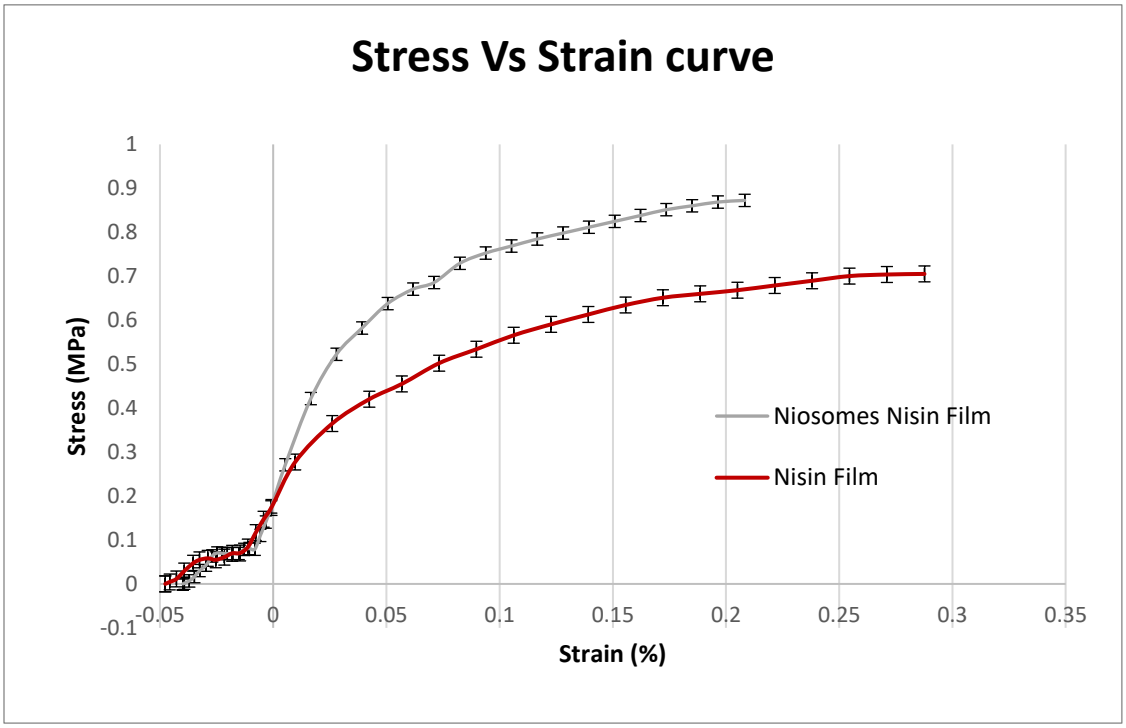

Figure 4.24: Mechanical property represented by stress vs. strain curve for tensile strength of nisin-loaded niosome film and nisin-only film (n = 3), figure adopted from [201].

4.3.9. In Vitro Release Profile

The in vitro release behaviours of nisin of different preparations were investigated for over a 40 hr period using a dialysis cassette (MWCO 20,000) (**Figure 4.25**). The formulations included two

film-based systems (nisin-only film and nisin-loaded NM2 niosome based film) and three niosomal suspensions prepared by microfluidic mixing at a 3:2 flow rate ratio, i.e. NM1 (Ch–SP60–RH40, 35:45:20), NM2 (Ch–SP60–RH40, 50:40:10), and NM4 (Ch–SP60–ELP, 35:45:20). All niosomal formulations contained a combination of encapsulated and non-encapsulated nisin.

Clear differences in overall release profiles were observed among the tested preparations, depending on formulation type and compositions. Overall, the film-based systems demonstrated faster and more extensive drug release than the niosomal suspensions. The nisin-loaded NM2 niosome film exhibited the highest cumulative release, reaching 97.03% at 40 h. This enhanced release is likely the result of a synergistic effect between the hydrophilic polymer matrix (PVA and PEG 400) and the incorporated niosomes. PEG 400, acting as both a plasticiser and solubilising agent, is known to increase matrix hydrophilicity and facilitate drug diffusion, which may have contributed to the accelerated release of both free and encapsulated nisin from the film matrix [275]. The nisin-only film showed a similarly high release (89.73% at 40 h), reflecting the diffusion of unencapsulated peptide dispersed within the polymeric network.

Both film formulations exhibited an initial burst release within the first 4–6 h (approximately 50%), followed by a sustained drug release phase. This behaviour suggests that the initial release is largely managed by weakly associated or freely dispersed nisin, while the later phase reflects diffusion-controlled release from the polymer matrix and niosomal vesicles. These findings suggest that nisin release pattern is influenced not only by encapsulation efficiency but also by complex interactions sought in nisin, surfactants, and the film-forming polymers.

The release curves of niosomal suspensions loaded with Nisin exhibit similar patterns as those entrapping VCM (**fig 3.16**). Both NM2 (with nisin) & M2 (with VCM) fabricated under same condition have demonstrated the highest cumulative release of (71% at 40 h), and 54%, respectively. This behaviour is consistent with NM2 favourable physicochemical characteristics, including the smallest vesicle size (165 nm), narrowest PDI (0.044), and biggest encapsulation efficiency (58%) (Table 4 13). Smaller and more homogeneous vesicles are expected to enable

more uniform diffusion through the dialysis membrane. NM4 showed moderate overall nisin release (68%), potentially due to its larger mean particle size (230.1 nm) and PDI (0.358), indicating a more heterogeneous vesicle population. NM1 exhibited the lowest cumulative drug release (63%), which may be attributed to its lower encapsulation efficiency (36.9%) and intermediate vesicle size (203.3 nm). The relatively faster release observed during the initial 5 h for NM1 is likely related to the presence of a higher fraction of non-encapsulated nisin.

The nisin solution, which was the control, displayed a delayed release profile, with only 2.74% released at 0.5 h and 11.35% at 4 h, followed by a sharp increase after 30 h, reaching approximately 91% at 40 h. This lag phase may be associated with diffusion resistance across the dialysis membrane and the absence of solubilising excipients such as PEG 400 or non-iourfactants.

Encapsulation within niosomes is anticipated to enhance nisin stability against enzymatic degradation and promote interaction with bacterial cell membranes, whereas free nisin in film form may be more readily washed away by saliva. Overall, incorporation of nisin into NM2-based niosomes, particularly within a film matrix, significantly improved the release profile in terms of both extent and control, highlighting the potential of niosome–polymer hybrid systems for mucosal delivery of antimicrobial peptides. Niosomes is anticipated to facilitate penetration of nisin through bacterial cell walls, thereby enhancing efficacy. In summary, the superior performance of the nisin-loaded niosome NM2-film is attributed to the combined benefits of high EE%, small vesicle size, and polymer-facilitated sustained release. These findings highlight the potential of tailored niosome-polymer hybrid systems for mucosal or controlled drug delivery of peptide therapeutics like nisin.

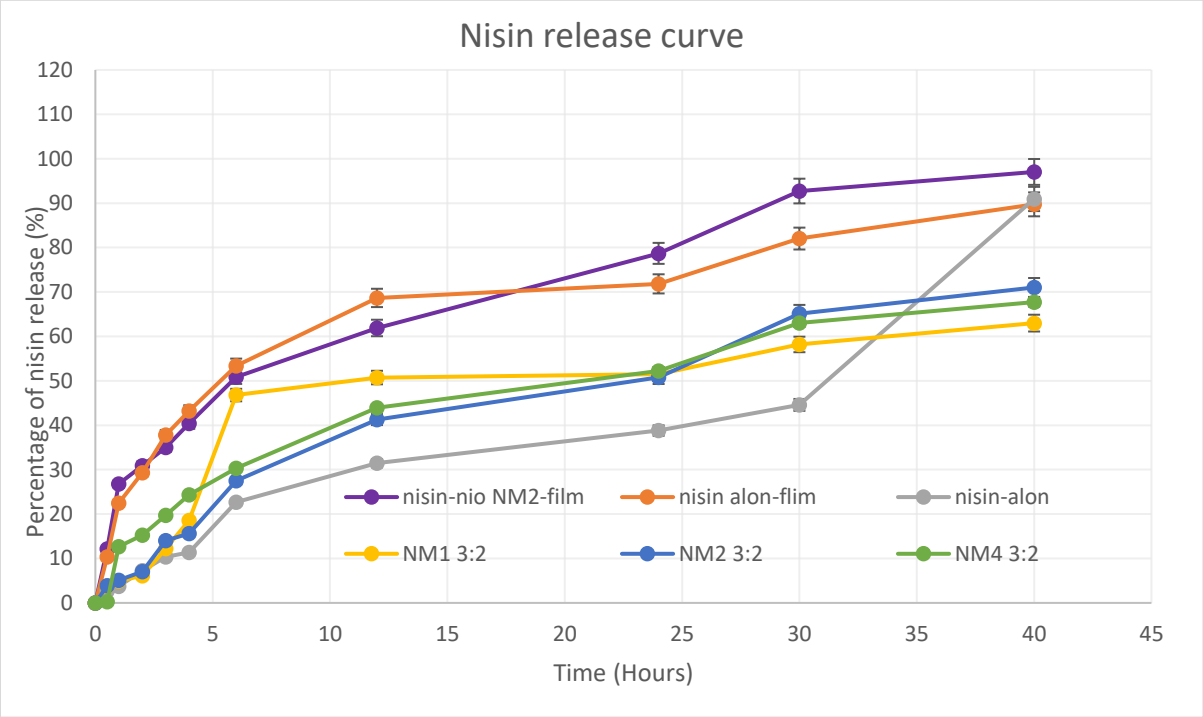

Figure 4.25: Dissolution profiles of different nisin niosomes in films, Nisin film, MF based niosome formulations and free Nisin (mean ± SD, n = 3). Note microfluidic-based niosomes NM1, NM2, and NM4 were generated with a flow rate ratio of 3:2. [201].

4.3.9.1. Kinetic Modelling of Drug Release

The release profiles of free nisin, nisin based niosomes, and nisin–niosomes in oral films were analysed using several mathematical models to describe their release kinetics (**Table 4.16**) to explain the dominant release mechanisms to each system. The zero-order model was applied to assess concentration-independent release behaviour, which is typically associated with ideal sustained-release systems where the system provides constant amount of drug release over time. The first-order kinetic model describes concentration-dependent release and is commonly observed in diffusion-controlled or immediate-release formulations. The Higuchi model was employed to evaluate diffusion-controlled release from polymeric matrices, while the Hopfenberg

model accounts for drug release driven by surface erosion of the delivery matrix. In addition, the Korsmeyer–Peppas (KS) model was used as a semi-empirical approach to describe drug release mechanism with the release exponent (n), allowing differentiation among Fickian diffusion, anomalous (non-Fickian) transport, and Case II transport [268].

To identify the most appropriate kinetic model for each formulation, two complementary statistical criteria were employed: R^2 value and the Akaike information criterion (AIC). While R^2 provides a measure of goodness of fit between experimental and predicted data, it may favour more complex models. In contrast, AIC penalizes excessive model complexity and is therefore considered more robust for comparative model selection across different datasets [269]. The combined use of both parameters enabled a more reliable and balanced assessment of the release kinetics.

For free nisin, the release profile was best described by the zero-order ($R^2 = 0.955$, AIC = 44.55) and Korsmeyer–Peppas ($R^2 = 0.952$, AIC = 45.50) models, indicating a near concentration-independent release dominated by diffusion. This behaviour is consistent with the absence of a structural matrix to regulate drug liberation. The nisin-only film followed first-order kinetics ($R^2 = 0.983$, AIC = 36.63), suggesting a concentration-dependent release mechanism governed by diffusion of nisin through the hydrated polymeric film matrix.

The release behaviour of the niosomal formulations differed from that of free nisin and film-based systems. NM1 exhibited the best fit to the first-order model ($R^2 = 0.964$, AIC = 41.10), with a KS release exponent (n = 0.48), indicating anomalous transport governed by a combination of diffusion and vesicular or matrix relaxation. Similarly, NM2 fit well to the first-order model ($R^2 = 0.992$, AIC = 26.04), and with comparable fits to the Higuchi and KS models ($R^2 = 0.991$ and 0.990, respectively). The corresponding release exponent (n = 0.61) further supports a non-Fickian release mechanism involving both diffusion and structural rearrangement of the niosomal bilayer. NM4 showed closest fit to Higuchi model ($R^2 = 0.987$, AIC = 26.75) and a release model of n = 0.48, suggesting a predominantly diffusion-controlled release mechanism. This shift in release behaviour is likely attributable to the use of a different co-surfactant (Kolliphor ELP) found in

NM4, compared with Kolliphor RH40 used in NM1 and NM2, which may alter bilayer fluidity and drug to membrane interactions.

Notably, incorporation of NM2 niosomes into the oral film matrix resulted in a marked change in release kinetics. The NM2-film formulation followed the KS model (R^2 = 0.994, AIC = 25.39) with a release exponent of n = 0.39, confirming a Fickian diffusion-controlled mechanism. This transition indicates that the polymeric film forces an additional diffusion barrier, dominating the unusual release behaviour observed in the niosomal suspension alone. Collectively, the findings demonstrate that free nisin is released primarily through rapid diffusion, niosomal formulations exhibit irregular transport involving both diffusion and structural relaxation, and niosome-loaded films provide a more controlled, diffusion-regulated release. The incorporation of niosomes into the film matrix therefore represents an effective strategy for modulating release kinetics and achieving sustained delivery of peptide therapeutics.

Table 4-16: Different Kinetic models of nisin release profiles from niosomes and film formulations. Parameters include R^2, AIC [270].

Kinetic Model		Nisin-Loaded Niosome NM2-Film	Nisin-Only Film	Nisin Only	NM1 3:2	NM2 3:2	NM4 3:2
Zero order	R2	0.954	0.905	0.955	0.857	0.968	0.946
	AIC	47.510	51.462	44.553	53.604	39.995	42.975
First order	R2	0.971	0.983	0.838	0.964	0.992	0.986
	AIC	45.253	36.636	71.497	41.106	26.045	30.475
Higuchi	R2	0.991	0.966	0.932	0.923	0.991	0.987
	AIC	42.523	47.018	64.706	45.890	33.530	26.758
Hopfenberg	R2	0.967	0.984	0.836	0.966	0.965	0.980
	AIC	49.257	47.316	71.179	42.812	45.306	35.582
Korsmeyer–Peppas model	R2	0.994	0.981	0.952	0.925	0.990	0.988
	AIC	25.389	36.128	45.498	47.826	28.966	46.130
Korsmeyer–Peppas model release exponent (*n*)		0.390	0.352	0.881	0.480	0.611	0.481

4.4 Summary

Fast-disintegrating oral films incorporating MF based nisin-loaded niosomes have been successfully developed as a potential platform for local antimicrobial therapy. This was based on outcomes of physicochemical testing that confirmed best niosomal formulation exhibited favourable size distribution with low PDI, and high nisin encapsulation efficiency, supporting its suitability for incorporation into polymeric oral film systems. In addition, Polyvinyl alcohol (PVA) and SSG have been identified as the most appropriate film-former and disintegrant for solvent cast FDOF. The nisin niosomes loaded PVA film exhibits acceptable properties including uniformity in weight and thickness to ensure formulation consistency, as well as tensile strength and Young's modulus values reflect robust film mechanical strength to secure structural integrity of embedded niosomes. FTIR and DSC analyses confirm the existence of interactions between the PVA matrix and niosomal components and compatibility without chemical modification of the system components. Additionally, TGA/DTG analysis demonstrated improved thermal stability and higher moisture retention in the niosome-loaded films, Moreover, agar diffusion assay confirmed that both free nisin and nisin-loaded niosomal films exhibited pronounced antibacterial activity against the tested bacterial strains. and the niosomal formulation offers distinct advantages in terms of controlled release and enhanced stability, which are expected to contribute to prolonged antimicrobial activity under physiological conditions.

Collectively, these results highlight nisin-loaded MF based niosomal fast-disintegrating oral films as a promising platform for targeted antimicrobial therapy in the oral cavity, with potential applications in the management of oral infections, dental biofilms and related conditions. With evidence presented currently, the next chapter will adopt the similar approach, i.e. MF based niosomes to entrap insulin, which is a model peptide drug of higher molecular weight and poor

permeability. The drug entrapped niosomal formulations will be incorporated into modified oral film and tablet for comparison.

Charter 5: Formulation and Characterisation of Oral Insulin Nanoparticles Using Niosomal Carriers in Film and Dried tablet Form.

5.1 Overview

Diabetes mellitus is a chronic metabolic disorder, which is characterised by hyperglycemia and other complications in which blood sugar level is poorly controlled. There are 2 types of DM, which is a consequence from defects in insulin secretion, insulin action, or both [271]. According to statistical data from the World Health Organisation, the global prevalence of this disease continues to rise, posing serious health and economic challenges [272]. Insulin remains the most effective therapy for patients with type 1 diabetes and for advanced cases of type 2 diabetes where oral hypoglycemic agents fail to maintain glycemic control [273], [274]. However, insulin is almost exclusively administered by the subcutaneous route, which is associated with several drawbacks, such as pain, risk of infection, lipodystrophy at injection sites, and poor patient compliance during lifelong therapy [275], [276]. In addition, subcutaneous administration does not mimic the physiological pattern of endogenous insulin secretion, leading to fluctuating blood glucose levels and potential complications such as hypoglycemia. These limitations have driven intensive research into alternative non-invasive routes for insulin delivery [274].

Among the explored routes, oral, buccal, nasal, pulmonary, and transdermal administrations have shown varying degrees of promise location for therapeutic delivery. Oral delivery, in particular, is considered the most patient-friendly and convenient [7]. Yet the oral route faces formidable physiological barriers. Insulin, being a hydrophilic peptide with a molecular weight of ~5.8 kDa, undergoes rapid degradation in the gastrointestinal tract due to unfavourable environments including acidic pH in stomach and presence of digestive enzymes such as pepsin, trypsin, and chymotrypsin [277]. Even if partially protected, its absorption through the intestinal epithelium remains extremely low because of its large molecular size and poor permeability across the lipid-rich membranes. Consequently, the bioavailability of orally administered insulin rarely exceeds 1%, making this route impractical without protective and permeation-enhancing technologies[278], [279]. Some literatures have considered insulin as class 3 according to BCS as it has high solubility but poor permeability in gut.

To overcome these challenges, insulin has been entrapped in niosomes by a benchtop microfluidic device, as it has shown to be beneficial for delivery of anti-microbial peptides, VCM and nisin of smaller molecular weights as reported in the previous chapters. One promising strategy to enhance mucosal transport of peptides is the incorporation of niosomal carriers into microneedle (MN) films designed for oral cavity applications. Microneedle technology, traditionally used for transdermal delivery, has recently been adapted to buccal drug administration [280]. MN films consist of arrays of microscopic projections, typically 200–600 μm in height, fabricated from biocompatible and water-soluble polymers. When applied to the buccal mucosa, the microneedles painlessly penetrate the superficial epithelial layer, creating transient microchannels through which the drug or nanoparticles can be deposited directly into the underlying tissue. Upon contact with saliva or mucosal fluid, the microneedles dissolve rapidly, releasing their payload without leaving any residue or causing injury. This approach combines the advantages of non-invasive delivery, enhanced permeation, and improved patient comfort.

In the present chapter, insulin-loaded niosomes prepared using different surfactants and optimised co-surfactants by MF means are incorporated into a polyvinyl alcohol (PVA) matrix to form dissolving microneedle films to control ins release. The microneedle molds are designed using 3D printing technology, which allows precise control over geometry, needle height, and array density to achieve consistent penetration depth and drug loading per unit area [281]. The use of 3D printing also enables reproducibility and easy customisation of the microneedle design for oral mucosal tissues, which are thinner and more delicate than the skin [282].

In addition, tablets were prepared as an alternative solid dosage form using dried niosomes loaded with INS. The performances of niosomes based MN platform and tablet were presented and compared in this chapter. The niosomal dispersion was freeze-dried to obtain a free-flowing powder suitable for solid dosage form development while improving the physical stability and storage life of the vesicular system. The resulting dried niosome powder was subsequently incorporated into tablets using the direct compression (DC) method due to its simplicity, minimal

processing steps, and reduced exposure of the vesicles to moisture and heat that could otherwise compromise the stability of the niosomal system.

5.2. Aim and objectives

The overall aim of this study is to develop and optimise an insulin-loaded niosomal delivery system that can be effectively incorporated into a dissolving microneedle film for oral cavity administration, thereby improving insulin stability, mucosal permeability, and patient compliance when compared to conventional subcutaneous injections. Additionally, the research seeks to prepare a lyophilised form of the niosomal formulations using suitable lyoprotectants to produce a stable powder that can later be compressed into tablets. This dual approach aims to establish a versatile and patient-friendly platform for oral cavity insulin delivery while addressing formulation stability, process scalability, and bioavailability limitations.

To accomplish this aim, insulin-loaded niosomes will first be formulated using different non-ionic surfactants from the Span series combined with appropriate co-surfactants and cholesterol. The main composition and methodology have been described in sect 2.3 of chapter 2. The selected niosomal system will then be incorporated into a polyvinyl alcohol (PVA) based microneedle film fabricated using a 3D-printed mold designed specifically for the buccal mucosa delivery. This fabrication step aims to produce a mechanically strong film capable of efficient mucosal insertion and insulin release. Both niosomal suspension and microneedle films will be characterised for physicochemical properties, including particle size distribution, zeta potential, encapsulation efficiency permeability and insulin release behaviour. The shape and distribution of the niosomes within the suspension, lyophilised powder, and oral film will be visualised by using fluorescent microscopy after tagging the vesicles with a suitable fluorescent dye to confirm their structural integrity and uniform distribution within different dosage forms.

Furthermore, evaluation will include detailed characterisation of the microneedle film in terms of thickness, mechanical strength, drug content uniformity, disintegration time and surface

morphology. Similarly, the tablet that produced by direct compression from lyophilised niosomal powder will be assessed for appearance, hardness, friability, uniformity of weight and content and disintegration time to ensure physical stability and accurate dosing. The lyophilised powder itself will be evaluated for reconstitution capacity, particle size following freeze-drying, as well as the protective effect of different lyoprotectants such as trehalose, mannitol, and sucrose on vesicle stability.

To further confirm the delivery potential of the developed system, permeation studies will be performed using a synthetic polycarbonate membrane (0.1 μm pore size) to investigate the penetration behaviour of the insulin-loaded niosomes. This will provide valuable insight into how different dosage forms, such as films, tablets, and suspensions, modulate insulin permeability by altering vesicle integrity, matrix interaction and surface characteristics.

5.3. Results and discussions

5.3.1 Size distribution and Entrapment Efficiency of Insulin-Loaded Niosomes

Niosomes loaded with INS were fabricated according to compositions described in sect. 2.3, Table 2- 6 in chapter 2 and their particle size, polydispersity index, and encapsulation efficiency are presented in **(Table 5.17)**. All formulations exhibited nanoscale vesicle sizes ranging between 102 and 398 nm, with PDI values below 0.5 except for IN4 sample (3:2), indicating acceptable size uniformity and stable dispersion. Both the surfactant type and the phase ratio significantly influenced vesicle formation and drug entrapment efficiency.

Formulations containing Span 65 (IN6–IN8) produced small and more uniform vesicles (PDI value 0.301-0.355) with comparatively higher encapsulation efficiencies (62.9–80.5%) than those prepared with Span 40 or Span 60 as main membrane component. This can be attributed to the longer alkyl chain and the higher hydrophobicity of Span 65, which contains three fatty acid

chains, promoting tighter bilayer packing and improved retention of the hydrophilic insulin molecules. The presence of cholesterol further enhanced membrane rigidity and reduced vesicle permeability, improving encapsulation stability [283].

Steric acid has been added to some formulation as charge stabilizer in INS7 and INS8. The incorporation of stearic acid in formulations IN7 and IN8 produced smaller vesicle sizes (101.8–136.1 nm) compared to other compositions (**Table 5.17),** suggesting that the additional fatty acid increased the lipid bilayer compactness through hydrophobic interactions. Furthermore, the inclusion of Solutol HS 15 in IN8 slightly increased PDI values at phase ratio 3:2, suggesting a broader size distribution likely due to HS15 having only one fatty chain, which can disturb the regular packing of the bilayer. This formulation didn't show the highest INS entrapment, possibly due to charge repulsion effect between INS and SA.

Formulations prepared at a 3:1 ratio produced smaller vesicles, while those at a 3:2 ratio showed a moderate increase in size, possibly due to slower self-assembly kinetics at higher organic solvent content [284]. In contrast, encapsulation efficiency tended to increase slightly at the 3:2 phase ratio, likely because slower solvent exchange allowed more insulin to partition within the forming vesicles. This observation is consistent with results derived from earlier chapters using either VCM or nisin as model peptide agents. Beyond the solvent ratio, several additional parameters influenced vesicle characteristics. A higher total lipid and surfactant content tends to increase the overall viscosity of the organic phase, which can slow down micro-mixing and lead to the formation of larger vesicles [111].

All experiments were conducted in triplicate ($n = 3$), and their results are presented as mean ± SD. Normality and homogeneity of variance of data were confirmed using the Shapiro–Wilk and Levenes tests ($p > 0.05$), validating the use of parametric analysis. A one-way ANOVA was performed to evaluate the effect of formulation composition (IN1–IN8) on vesicle size, PDI, and encapsulation efficiency.

Statistical analysis demonstrated significant differences ($p < 0.001$) among formulations for all evaluated parameters, including particle size ($F = 1326.95$, $p = 6.8 \times 10^{-21}$), PDI ($F = 2202.75$, $p = 1.18 \times 10^{-22}$), and EE% ($F = 660.76$, $p = 1.76 \times 10^{-18}$). The large F-values indicate the variability between formulation groups These findings confirm that changes in surfactant type and lipid composition strongly influence vesicle formation and drug entrapment efficiency. Formulations containing Span 65 (IN6–IN8) produced significantly smaller, more uniform vesicles with higher encapsulation efficiency compared to those based on Span 40 or Span 60, consistent with the effect of increased hydrophobic chain length on bilayer compactness.

Among all tested formulations, IN6 (Ch–SP65–RH40) demonstrated the most favourable combination of particle size (148 ± 2.7 nm), low PDI (0.133 ± 0.033), and high encapsulation efficiency (75.57–80.55%). These characteristics suggest a well organised bilayer structure and effective encapsulation of insulin within the vesicular core. Consequently, IN6 was selected as the optimised formulation for subsequent film formation, lyophilisation, and tablet development steps.

Table 5-17: Effect of non-ionic surfactant type, composition, and aqueous-to-organic phase ratio on the physicochemical characteristics of insulin-loaded niosomes prepared by microfluidic mixing. Particle size, polydispersity index (PDI), and encapsulation efficiency (EE%).

Formulation	Niosome Composition	Aqueous to organic phase ratio	Size (nm)	PDI	EE%
IN1	Ch–SP60–RH40	3:1	129.8±0.84	0.15±0.01	52.47
		3:2	398±7.14	0.38±0.006	56.57
IN2	Ch–SP60–RH40	3:1	130.3±1.53	0.112±0.02	54.11
		3:2	163.5±0.73	0.209±0.02	48.31
IN3	Ch–SP60–ELP	3:1	213.4±17.08	0.45±0.019	46.61
		3:2	161.9±3.38	0.226±0.01	52.65
	Ch–SP40–RH40	3:1	245.5±18.48	0.523±0.01	45.85
IN4		3:2	193.7±0.66	0.262±0.02	51.46
IN5	Ch-SP40-ELP	3:1	139±0.92	0.180±0.008	47.07
		3:2	181.1±1.81	0.241±0.03	52.11
IN6	Ch–SP65–RH40	3:1	159.5±5.22	0.355±0.11	80.55
		3:2	148±2.74	0.133±0.03	75.57
IN7	Ch–SP65–RH40–Stearic Acid	3:1	101.8±4.44	0.308±0.03	69.19
		3:2	136.1±0.67	0.164±0.01	68.93
IN8	Ch–SP65–Solu HS 15 –Stearic Acid	3:1	129±0.45	0.301±0.04	68.70
		3:2	109.7±9.53	0.337±0.02	62.97

5.3.2. Film Characterisation

The physicochemical parameters of the optimised insulin-loaded niosomal oral film are summarized in **Table 4.18** The films were transparent, flexible, and smooth, without visible cracks or air bubbles, confirming uniform polymer dispersion and stable incorporation of the niosomal suspension within the PVA matrix, see **Figure 5.23**. Films produced using microneedle molds showed a well-defined microstructured surface corresponding to the mould cavities, resulting in regularly arranged protrusions and a uniform base layer. The overall dimensions and geometry of these films were determined by the mould design, ensuring consistent size and microstructure across samples.

In contrast, conventional solvent-cast films exhibited a flat, smooth, and homogeneous surface without microstructures. Their thickness and dimensions depended mainly on the casting area and the volume of polymer solution used. Therefore, while solvent-cast films form uniform planar layers, microneedle-moulded films possess controlled micro-architectures that distinguish them structurally and functionally.

The mean film weight (111 ± 2.47 mg) and thickness (0.249 ± 0.006 mm) exhibited minimal variation, reflecting good reproducibility of the solvent-casting technique using customized MN mold. The casting and drying processes played a critical role in maintaining this uniformity. Even spreadingof the film-forming solution and slow, controlled solvent evaporation ensured homogeneous polymer deposition and prevented local differences in film density. This uniform casting behaviour directly contributed to the consistent weight uniformity across samples.

A notable relationship was observed between weight uniformity and content uniformity. Slight variations in film mass were mirrored by marginal fluctuations in insulin content, as heavier films generally contained more encapsulated insulin. This is likely due to localised accumulation of polymer niosomal dispersion in thicker regions during solvent evaporation. Despite this, the content uniformity (95.96 ± 7.9%) remained well within the acceptable pharmacopoeial range (85–115%), confirming the reproducibility of the film-forming process and homogeneous dispersion of insulin-loaded niosomes within the matrix [285], [286].

The tensile strength (2.5 ± 0.28 MPa) indicated sufficient mechanical robustness to allow handling, storage, and application without tearing. Flexibility was evaluated qualitatively using the hand-folding test, which demonstrated that the films could be bent and flexed easily without cracking or losing integrity, an essential property for maintaining adherence to the moist oral mucosa.

The surface pH (6.5 ± 0.5) was close to neutrality, indicating good compatibility with the buccal environment and minimising the risk of mucosal irritation. This is consistent with films loaded with VCM and nisin as they were fabricated using same materials.

The disintegration time (462.2 ± 27.7 s) was notably longer than in earlier formulations [201]. This extended disintegration was intentional and achieved by increasing the PVA concentration (800 mg of PVA for insulin film without adding any disintegrant and 500mg for both vancomycin and nisin) in the film. The denser polymeric network slowed hydration and dissolution, ensuring that the microneedle structures did not dissolve early before penetrating or interacting with the mucosal surface. Furthermore, the slower disintegration facilitates controlled release of insulin-loaded niosomes and reduces drug loss due to saliva washout, thereby this platform is expected to enhance the residence time of particles and bioavailability of insulin within the oral cavity.

In terms of vesicular stability, the mean niosome particle size increased from 159.5 ± 5.22 nm before casting to 204 ± 1.55 nm after casting, suggesting slight swelling or aggregation of vesicles during the film-forming process or some PVA polymers entities stuck around the niosomes vesicular. This minor change indicates that while some structural reorganisation occurred during drying, the vesicles largely retained their morphology. Similarly, the zeta potential shifted only slightly from –4.08 ± 1.1 mV before casting to –6.53 ± 1.16 mV after reconstitution. The slight increase in negative zeta potential observed after film reconstitution may be attributed to partial hydroxyl deprotonation of PVA. Under neutral to slightly basic conditions, a small fraction of PVA's –OH groups can deprotonate, generating weakly negative surface sites. When these polymer chains adsorb onto the niosomal surface, they contribute additional surface charge, resulting in a modest increase in the measured negative potential. confirming that the colloidal stability of the niosomes were preserved within the PVA matrix. The minimal variation in electrokinetic potential demonstrates that the polymer network provided a stabilising environment for the vesicles during both casting and rehydration.

Beyond stabilisation, the PVA-based polymer matrix also contributed significantly to the mucoadhesive properties of the film. The abundance of hydroxyl groups in PVA enables the formation of non- covalent bonds like hydrogen bonds and van der Waals interactions with mucin glycoproteins present on the oral mucosa [287]. These interactions are expected to enhance the film's ability to adhere to wet epithelial surfaces, prolonging its residence time in the oral cavity

and ensuring intimate contact between the loaded vesicles and the absorption site. The moderate negative zeta potential (around –6 mV) further supports mucoadhesion, as it avoids strong electrostatic repulsion with the negatively charged mucosal surface, allowing the polymer chains to anchor more effectively through nonionic interactions.

Fluorescence microscopy provided visual confirmation of niosome incorporation within the microneedle film. As shown in **Figure 5.26** (Right), the labelled vesicles appeared uniformly distributed across the surface of the film, indicating successful entrapment of niosomes within the polymeric matrix without aggregation or phase separation. This homogeneous fluorescence pattern supports the observed physicochemical uniformity and suggests the existence of vesicle–polymer interaction throughout the film structure, which has been demonstrated in chapter 4 where several analysis showed system compatibility (sect 4.3.7, FTIR and thermal analysis).

Overall, the optimised insulin-loaded niosomal film exhibited excellent mechanical integrity, flexibility, and compatible pH, along with preserved vesicular stability and controlled disintegration behaviour. These results confirm that the formulation successfully combines the structural advantages of PVA-based MN films for incorporation of niosomal vesicles, making it a promising system for oral cavity delivery of insulin.

Table 5-18: Physicochemical Characteristics of the Insulin-Loaded Niosomal Film (n = 3)

Parameter	Mean ± SD	Unit
Film weight	111 ± 2.47	mg per 3 × 2 cm film
Film thickness	0.249 ± 0.006	mm
Tensile strength	2.5± 0.28	N/mm²
Folding endurance	49.67 ± 13.47	Number of folds before crack
pH	6.5±-0.5	–
Disintegration time	462.2 ± 27.7	Seconds
Content uniformity	95.96 ± 7.9%	% of theoretical 0.5 mg dose
Niosome particle size before casting	159.5±5.22	nm
Niosome particle size after casting	204 ± 1.55	nm
Zeta potential before casting	–4.08 ± 1.1	mV
Zeta potential after film reconstitution	–6.53 ± 1.16	mV

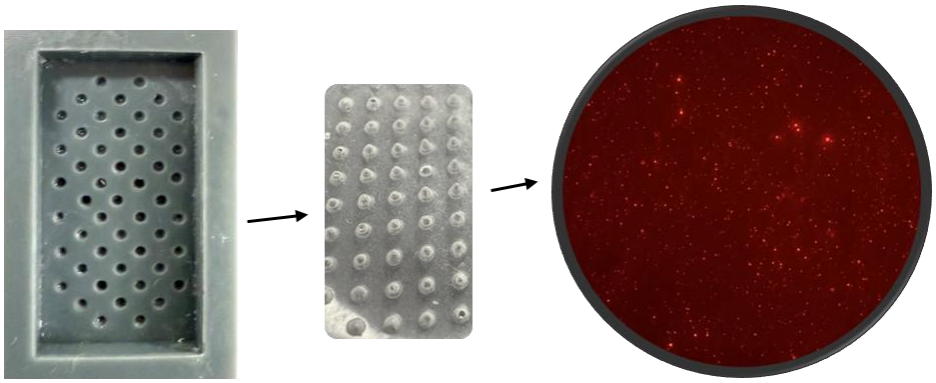

Figure 5.26: Fabrication and Visualisation of Insulin-Loaded Niosomal Microneedle Film.

(Left) 3D printed microneedle mold fabricated using a stereolithography (SLA) printer. (Middle) Casted microneedle film formed using the optimised PVA based formulation loaded with insulin-loaded niosomes. (Right) Fluorescent microscopy 40X image of Rhodamine B base–labelled niosomes confirming uniform vesicle distribution within the microneedle film matrix.

5.3.3. Evaluation of Lyophilised Insulin-Loaded Niosomal Powder

Freeze drying is a low temperature process to remove water and dry sample, it is employed to dry niosomes loaded with insulin, which is a heat sensitive ingredient. Despite employing low temperature to dry niosomes, lyophilization processes subject both insulin and niosomes to several stresses such as cold induced denaturation of products. Therefore, it is crucial to protect niosomes using suitable stabilisers at different lyophilization stages (refer to section 2.14 of chapter 2 for protection systems used in this piece of work). The influence of different lyoprotectant systems on niosomal stability (based on changes in particle size upon reconstitution with same quantity of water during lyophilisation of niosome loaded INS is summarised in **Table 5.19** and visually demonstrated by using niosomes containing RhB probe (**Figure 5.27)**. The experiments were performed using the optimised INS6 formulation (Span 65–RH40 niosomes), chosen for its high encapsulation efficiency and stability before freeze-drying. A clear correlation was observed between the type and concentration of lyoprotectants used and the extent of vesicle preservation after drying. A slight increase in particle size was already evident upon the addition of lyoprotectants before freeze-drying, which can be attributed to hydration and osmotic interactions between the sugar molecules and vesicle surfaces. The dissolved sugars increase the viscosity of the medium and promote bilayer swelling, leading to size enlargement due to lyoprotectant addition.

The niosomes prepared without any additive (L1) exhibited a dramatic increase in particle size from 163.5 ± 0.7 nm to 1799 ± 194.4 nm, indicating severe aggregation and structural collapse due to dehydration stress (Figure 5.27….4D–E). Similarly, formulations containing mannitol or glycine alone (L2–L5) offered only partial cryoprotection, with post-lyophilisation sizes exceeding 1 μm, suggesting vesicle fusion and bilayer disruption. These outcomes are consistent with reports that a low but adequate amount of lyoprotectant is required to prevent aggregation during drying as insufficient sugar content can result in weak, fragile cakes unsuitable for form stable lyophilized tablets or be use as powder for subsequent tablet production by direct compaction.

Conversely, high concentrations of sugars, such as mannitol, are beneficial for producing a bulkier, more crystalline freeze-dried solid but on the other hand it can induce osmotic stresses during the freezing phase [288]. These stresses alter bilayer curvature and increase the likelihood of vesicle deformation or size expansion. Therefore, achieving an optimal sugar concentration is critical to provide structural protection during sublimation process.

Among all tested systems, formulations containing trehalose showed superior cryoprotective ability. The 5% trehalose formulation (L6) maintained vesicle size below 640 nm, while the combined trehalose–sucrose system (L9) provided the most efficient stabilisation (**Figure 5.27. 4B–C**), with only a slight size increase from 288.3 ± 14.5 nm to 358.1 ± 4.8 nm after freeze-drying. This optimal performance is attributed to trehalose's strong hydrogen-bonding capacity and glass-forming ability which preserve bilayer structure and prevent vesicle fusion [289].

Overall, these findings highlight that while lyoprotectants are essential for vesicle preservation, their concentration must be finely tuned to avoid adverse osmotic effects. The L9 trehalose–sucrose system achieved the best particle stability, and the resulting lyophilised powder was selected for further tablet formulation due to its excellent redispersion, low polydispersity, and morphological integrity.

Table 5-19: Effect of Different Lyoprotectant Systems on Particle Size of Insulin-Loaded Niosomes Before and After Lyophilisation.

Lyoprotectant System	Code	Particle size before lyophilisation nm	Particle size after lyophilization nm
Niosomes without additive	L1	163.5±0.7	1799±194.4
Mannitol 10%	L2	346.7±4.3	1250±94.8
Mannitol 2.5% + Glycine 2.5%	L3	457±14.35	1695±225.3
Mannitol 5% + Glycine 5%	L4	240.3±23	1340±68.25
Glycine 10%	L5	218.6±43.1	2941±626.8
Trehalose anhydrous 5%	L6	294.8±22.25	639.5±78.16
Trehalose anhydrous 10%	L7	296.7±2	1367±31
Trehalose anhydrous 2.5% + Mannitol 2.5%	L8	307.4±11.14	1018±144.3
Trehalose anhydrous 15% + Sucrose 5%	L9	288.3±14.5	358.1±4.8

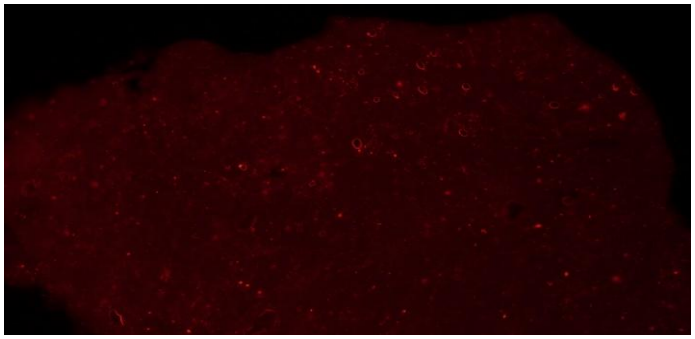

(B) Lyophilized niosomal powder with lyoprotectant system (L9)

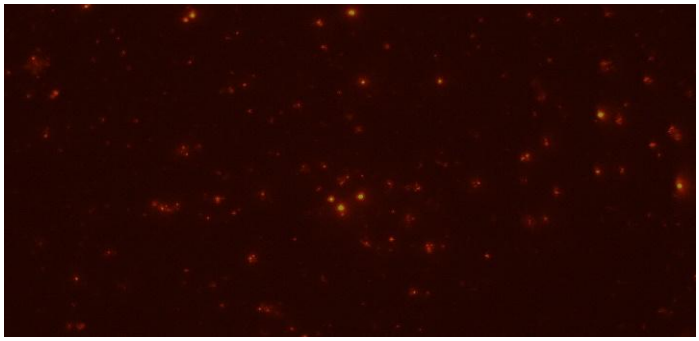

(C) Reconstituted niosomal powder with lyoprotectant (L9)

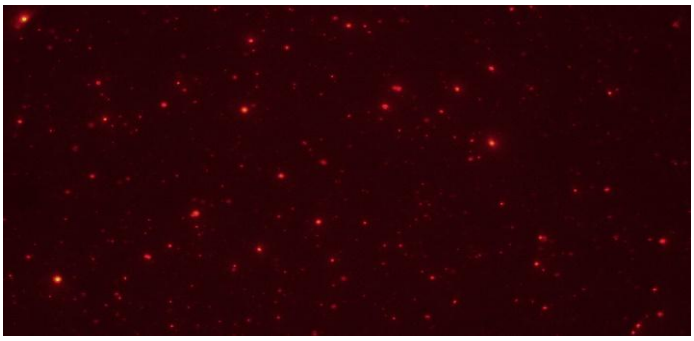

(A) Niosomal dispersion before drying

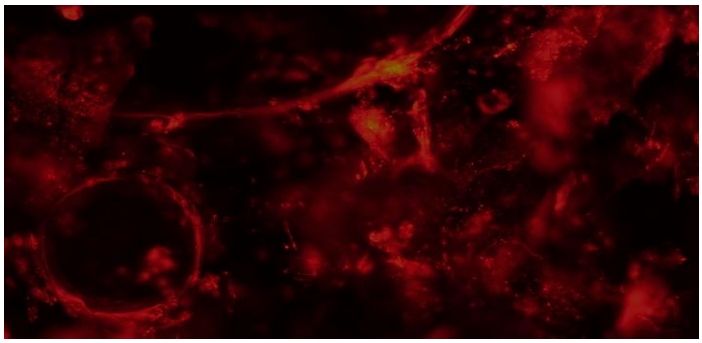

(D) Lyophilized niosomal powder without lyoprotectant (L1)

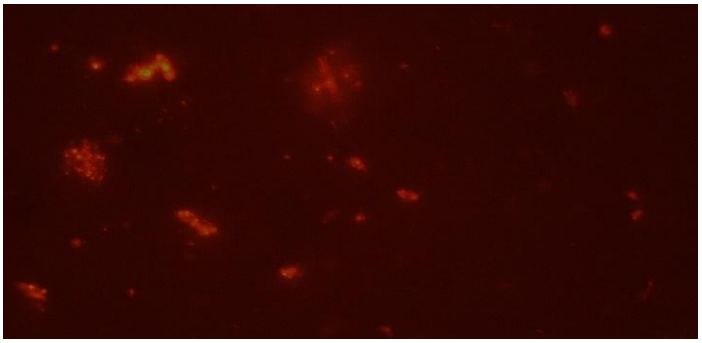

(E) Reconstituted niosomal powder without lyoprotectant (L1)

Figure 5.27: Fluorescent Microscopy Images of Insulin-Loaded Niosomal Formulations (40× Magnification). Fluorescent micrographs show the morphology and dispersion ofinsulin-loaded niosomes before and after lyophilisation, with and without lyoprotective agents (rhodamine B base labeling).

5.3.4. Tablet Characterisation

Tablets were produced by compacting L9 formulation with xxx as bulking agent (if lubricant used, also add to remind reader), the powder blend were compacted by DC process (**refer sect. 2.15, chapter 2).** The physicochemical properties of the optimised insulin-loaded niosomal tablets prepared from the L9 lyophilised formulation (trehalose 15% + sucrose 5%) are summarised in **Table 5.20**. This was the only formulation advanced to the tableting stage due to its superior stability, redispersibility, and morphological integrity after lyophilisation. The resulting tablets were uniform in shape and appearance, showing no signs of cracking, capping, or lamination following compression. The mean diameter (6.08 ± 0.04 mm) and thickness (2.80 ± 0.03 mm) exhibited minimal variation across ten units, confirming excellent reproducibility and uniform die filling. The mean tablet weight (100 ± 1.52 mg) aligned closely with the target formulation, which was expected since each tablet portion was individually weighed prior to compression

The tablet hardness (5.48 ± 0.66 kg) demonstrated sufficient mechanical strength to withstand handling and packaging, while the friability (0.41 ± 0.07%) remained well below the pharmacopeial limit of 1%, indicating that the compressed tablets were physically stable and resistant to abrasion. The disintegration time (631 ± 12 s) confirmed a moderately slow hydration profile, aligning with the intended design for controlled release of insulin within the oral cavity. This delay in disintegration helps maintain mucosal contact, reducing drug loss from saliva washout and ensuring sustained release of insulin-loaded vesicles.

The content uniformity (86.36 ± 7.83%) was within the acceptable range for experimental formulations. The slight variation between units can be attributed to the multiple processing steps the niosomes such as mixing, drying, and compression which may have caused partial segregation within the powder bed. During these stages, differences in particle size, density, or surface charge between the niosomal powder and excipients could have led to minor uneven distribution of insulin across individual tablets. Despite this, the overall variability remained within acceptable limits, confirming that the manufacturing process maintained a reasonably consistent drug distribution

throughout the batch. The surface pH (6.5) was close to neutrality, indicating compatibility with the buccal mucosa and minimising irritation risk upon application.

The niosomal particle size following sample reconstitution increased from 358.1 ± 4.8 nm before compression to 676.3 ± 19.73 nm after, indicating that vesicle aggregation and partial fusion occurred during tablet formation. The applied 300 kg = 2.9 kN compression pressure likely promoted close packing of vesicles and interfacial contact between bilayers within the lyophilised matrix. Additionally, the inclusion of MicroceLac 100 as a filler contributed to this apparent increase in size. Because MicroceLac 100 is poorly water-soluble, it tends to disperse rather than dissolve upon rehydration, forming a colloidal suspension that can physically associate with niosomal particles.

Meanwhile, the zeta potential shifted from –12 ± 1.27 mV to –21.7 ± 0.721mV after compression. This change is likely due to the electrostatic nature of the powder bed, where particle–particle contact during compression may result in charge redistribution or partial neutralisation. Overall, the tablets exhibited good mechanical strength, acceptable disintegration properties, and preserved vesicular stability, validating the robustness of the lyophilised niosomal powder and the suitability of the formulation for oral cavity delivery.

Table 5-20: Physicochemical Properties of Optimised Niosomal Tablets

Parameter	Mean ± SD	Unit	Number of Tablets
Tablet diameter	6.08 ± 0.04	mm	10
Tablet thickness	2.80 ± 0.03	mm	10
Tablet weight	100 ± 1.52	mg	10
Hardness	5.48 ± 0.66	kg	10
Friability	0.41 ± 0.07	% weight loss	20
Disintegration time	631 ± 12	seconds	6
Content uniformity	86.36 ± 7.83%	% of theoretical insulin dose	3
Surface pH	6.5	–	3
Niosome particle size (before compression)	358.1±4.8	nm	3
Niosome particle size (after compression)	676.3 ± 19.73	nm	3
Zeta potential (before compression)	–12 ± 1.27	mV	3
Zeta potential (after compression)	–21.7 ± 0.721	mV	3

5.3.5. In Vitro Release and Permeability Studies

5.3.5.1 Dissolution test

The in vitro release profiles of insulin from various formulations, including free insulin, niosomal suspension (IN6), insulin–niosomal film, and insulin–niosomal tablet (L9), were evaluated using dialysis cassettes over 24 hours (**Figure 5.28**). All niosomal formulations exhibited a biphasic release pattern, characterised by an initial burst for unencapsulated insulin followed by a slower, controlled phase. The control using free insulin reached only 35% overall release in the first 8 hours and plateauing near 36% at 24 hours. The incomplete and slow release of free insulin can be attributed to several factors. Insulin molecules freely self-associate into dimers and hexamers, forming large aggregates with limited diffusivity through the membrane that hinder effective release [290]. In addition, insulin is prone to hydrophobic and electrostatic adsorption onto container and membrane surfaces, leading to a measurable loss [291], [292] Under physiological or buffered conditions, partial peptide unfolding and further aggregation contribute to precipitation and surface adhesion, producing a pseudo-plateau in cumulative release around 30–40%. Collectively, these effects explain the restricted release behaviour of free insulin and highlight the stabilising and diffusion-modifying advantages of vesicular or polymer-based encapsulation systems.

The release profiles obtained for nisin (chapter 4 sec4.3.9.) and insulin demonstrated broadly similar behaviour when compared in their free forms. Both peptides exhibited relatively limited cumulative release over the experimental period, reaching approximately 44.6% for nisin and 35.6% for insulin. This similarity can be attributed primarily to their relatively high molecular weights and peptide nature, which limit diffusion through the dialysis membrane and aqueous medium. Nisin (3.4 kDa) and insulin (5.8 kDa) are larger molecules compared with vancomycin (1.45 kDa), resulting in slower diffusion and consequently lower release in their free forms. In contrast, vancomycin previously demonstrated in (chapter 3 sec 3.4.) a higher cumulative release which can be explained by its lower molecular weight and comparatively greater diffusivity. In contrast, the insulin niosomal suspension (IN6) demonstrated a more controlled release pattern, reaching full ins release at 24 hours.

The insulin-loaded polymeric film achieved the highest release among the solid systems, reaching ~91% within 24 hours. Its relatively faster release is attributed to the absence of vesicular encapsulation. The PVA–PEG 400 matrix forms a semi-hydrated gel layer that allows the rapid diffusion of unencapsulated insulin molecules once it is wetted. PEG 400, being hydrophilic, also improves insulin solubility at the film–medium interface, accelerating release kinetics [293]. The insulin niosomal film exhibited a slower release, reaching ~57% at 24 hours, demonstrating the dual diffusion barrier imposed by both the PVA–PEG matrix and the lipid bilayer of niosomes. The initial burst (approximately 12% within 30 min) corresponds to surface-associated or loosely bound insulin, while the subsequent control phase occurs from the gradual diffusion of entrapped insulin through the bilayer and polymeric network. The niosomal formulation incorporated in tablet, formulated from the L9 lyophilised powder system (trehalose 15% + sucrose 5%), exhibited overall release similar to the niosomes based films, reaching approximately 61% after 24 hours. The reduced release rate can be attributed to presence of bilayer membrane and the high sugar content of the lyoprotectant matrix, which likely formed partially crystalline barrier around the niosomes during compression, thereby delaying the diffusion of entrapped insulin. In addition, the variation in content uniformity (86.36 ± 7.83%) among tablets may have introduced slight fluctuations in release behaviour, as uneven insulin distribution within the powder blend results in localised differences in drug exposure during dissolution. When subsequently compressed into tablets, these swollen vesicles were more susceptible to membrane disruption, causing a fraction of insulin to leak out of the vesicles and be released immediately as free insulin. This phenomenon justifies the early-phase burst seen in the dissolution profile.

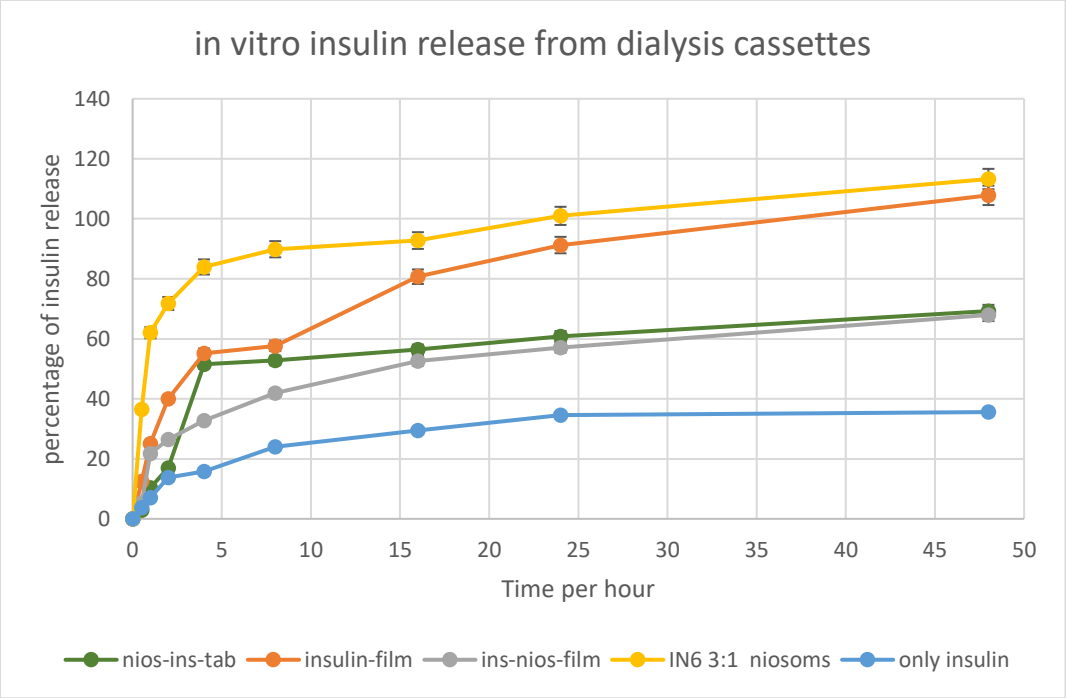

Figure 5.28: In vitro insulin release from dialysis cassettes. Data represent mean ± standard deviation (n = 3).

5.3.5.2 Permeability test

The in vitro permeability study was carried out using Franz diffusion cells fitted with 0.1 µm polycarbonate membranes to study insulin transport across a simulated mucosal barrier. The permeation profiles of samples were presented in Figure **5.29**. Unlike the dialysis system, this setup does not limit drug diffusion by its molecular weight, so both free insulin and some intact or partially fused niosomes could move through the membrane. The 0.1 µm pore size provides a simplistic mean to predict how insulin may pass across the oral mucosa.

The control comprised of free insulin solution showed the fast drug diffusion, reaching about 705 µg/cm² after 24 hours, as expected for unencapsulated molecules that can move freely through the membrane. The niosomal suspension (IN6) showed a close value (≈690 µg/cm² of overall permeated amount), meaning that the small vesicles (~150 nm) could interact with or partly pass

through the pores. This agrees with the idea that the Franz cell setup measures both free insulin and vesicle-associated insulin, unlike the dialysis study where the membrane blocks nanoparticles or peptide aggregates. Among the solid systems, the insulin loaded film (unentrapped format) gave the highest amount of peptide permeation at 24 hr (778 μg/cm²), followed closely by the INS niosomal film (711 μg/cm²). The film formulations improved diffusion because the PVA–PEG 400 matrix is hydrophilic and flexible, allowing better membrane wetting and faster polymer hydration. PEG 400 also acts as a permeation enhancer, softening the film and helping insulin and niosomes move across the membrane. The slightly lower permeability of the niosomal insulin film compared with the plain insulin film shows that encapsulation slows peptide diffusion a bit but also provides more controlled transport. The niosomal tablet (L9) showed the lowest extent of permeated insulin at 24 hr (592 μg/cm²). This result fits with its compact structure, slower water uptake, and limited vesicle movement. The trehalose–sucrose lyoprotectant system in this tablet may have formed a crystalline matrix that restricted hydration and delayed insulin release. Also, swelling of the lyophilized powder and possible leakage of insulin during rehydration could explain the small burst observed at the start. The permeation profiles suggest two main phases of insulin transport. The initial rapid increase observed during the early time points was likely associated with free or surface-associated insulin, which was immediately available for diffusion across the polycarbonate membrane. This was particularly evident for the free insulin solution and the insulin-only film, which showed faster early permeation due to the absence of a vesicular barrier. In contrast, the slower increase observed at later time points indicates more controlled insulin transport, which may be attributed to insulin retained within the niosomal vesicles and/or restricted within the film or tablet matrix.

Overall, the results show that the structure and hydration rate of each formulation strongly affects how insulin molecules were transported over the artificial membrane. The films allowed a faster and higher insulin passage, suitable for quick absorption, while the tablet gave slower, more controlled delivery that may prolong the drug's contact in the oral cavity. The niosomal suspension (IN6) showed balanced results, proving that niosomes can protect insulin and still support controlled diffusion.

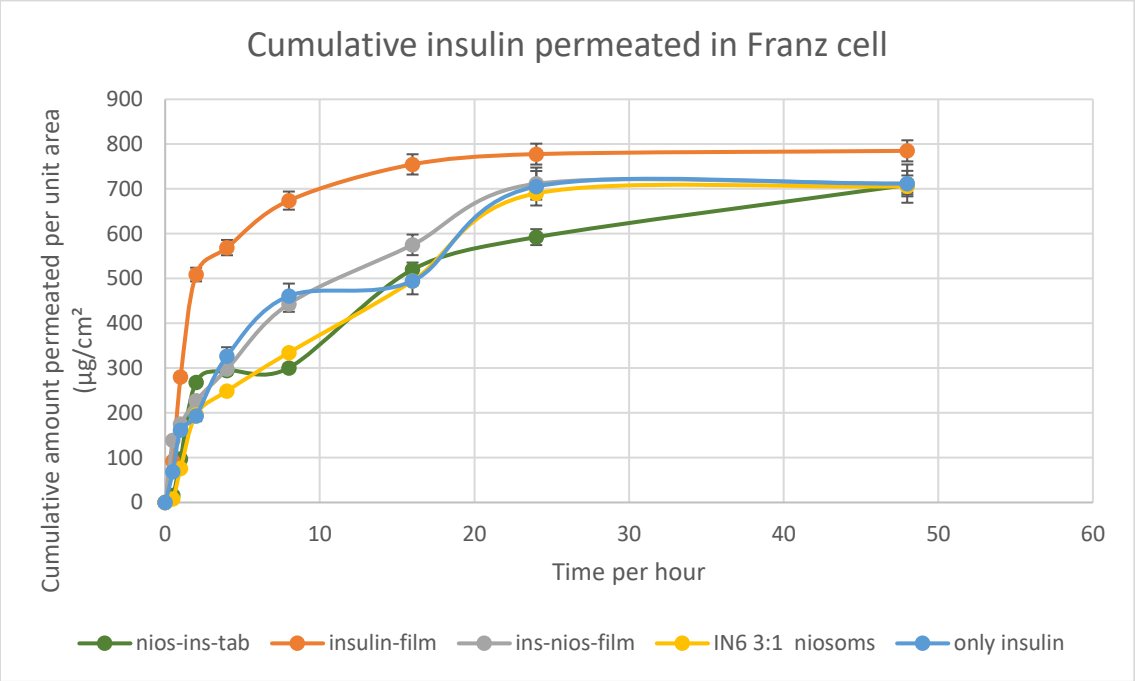

Figure 5.29: Cumulative insulin permeated in the Franz cell. Data represent mean ± standard deviation (n = 3).

5.4. Summary and future work

INS niosomes (by MF mode) and INS niosome-based oral solid dosage forms (table and customized design NN film) have been fabricated and charaterised by using several in vitro assessment tools. Between the two optimized solid formulations, the niosomal oral film demonstrated several physicochemical advantages over the niosomal tablet, making it a more efficient and versatile platform for oral cavity delivery. The film exhibited microneedle-shaped architecture, which may enhance mechanical contact with the mucosal surface, improving adhesion and facilitating localized diffusion of insulin-loaded vesicles. Its softer and more flexible structure allowed comfortable placement in the oral cavity, adapting easily to mucosal lines and is assumed not to cause irritation or damage. In terms of nanoparticle stability, the niosomes within the film preserved its nonosize and with minimal higher zeta potential. This stability arises from the solvent-casting process, which avoids mechanical deformation, charge redistribution, and better content uniformity that occur during tablet compression. The film also achieved notable release and acceptable permeability profiles, delivering insulin faster and in greater amounts due to the presence of PEG 400, which enhanced hydration, vesicle mobility, and drug diffusion and avoiding insulin aggregation. From a manufacturing standpoint, the film required fewer preparation steps, less equipment and fewer excipients compared with the tablet. Collectively, these attributes make the niosomal oral film a simpler, more stable, and more effective delivery system, offering a favorable balance between formulation efficiency, vesicle integrity and therapeutic performance for buccal insulin administration. Additional future characterisation could include ex vivo mucoadhesion and residence-time testing to confirm how long the insulin-loaded film remains attached to the buccal mucosa under simulated saliva flow. Swelling and hydration studies would also be useful to better understand water uptake, polymer relaxation and vesicle mobility within the PVA/PEG 400 matrix.

Chapter 6: Conclusions

In this study, it has been demonstrated that the oral cavity, despite its enzymatic activity and dynamic environment, represents a viable site as well as highly promising route for the delivery of macromolecules and peptide-based therapeutics. This research aimed to develop and optimize a niosomal-based peptides delivery platform capable of enhancing drug stability, prolonging mucosal residence and improving therapeutic performance. Through a serial investigation of vancomycin, nisin, and insulin as model molecules, this work established how precise niosome engineering using MF approach and niosome integration into solid oral systems (fast-dissolving oral films) and (tablets) can transform unstable drugs into effective and patient-compliant dosage forms.

The introductory chapter defined the scientific rational and translational significance of this approach. Traditional oral formulations are severely limited by enzymatic degradation, poor permeability, and hepatic first-pass metabolism, whereas parenteral delivery remains invasive and poorly accepted by patients requiring chronic therapy. The buccal and sublingual mucosa provide an attractive alternative, offering direct access to systemic circulation while avoiding hepatic metabolism and enabling rapid onset of action. Yet peptide drug delivery via these routes is facing several formulation challenges such as limited permeability, rapid salivary clearance, and enzymatic degradation. Within this thesis, niosomes, which are representative of non-ionic surfactant-based vesicles, have emerged as an adaptable solution, capable of encapsulating both hydrophilic and lipophilic drugs as well as macromolecules, shielding them from breakdown by harsh and stressful conditions, as well as modulating their release profiles. Furthermore, embedding niosomes within mucoadhesive or fast-dissolving oral devices was identified as the key strategy to ensure mucosal retention and controlled drug diffusion.

The development of fast-disintegrating oral films embedding niosomes of specifically engineered size marked a significant step forward in the design of advanced oral delivery systems. The use of microfluidic synthesis provided precise control over particle characteristics, with surfactant and drug concentration, type, and aqueous-to-organic phase ratio directly influencing particle size distribution and encapsulation efficiency when VCM, a BCS 3 drug with limited oral permeability,

was used as a model peptide. Combinations of different surfactants, such as Span 40 with Kolliphor RH40, produced smaller vesicles with narrow distribution but moderate %EE, whereas Span 60 with Kolliphor ELP yielded larger particles with a wider distribution and higher drug encapsulation. The best performed vancomycin-loaded niosomes achieved controlled release of 40–60% over 24 hours and the vesicles demonstrated antimicrobial efficacy against *Bacillus subtilis*. The FDOFs exhibited excellent mechanical strength (9.63 MPa), high folding endurance (>100 folds), and rapid disintegration (105 seconds), ensuring both durability and user comfort. Overall, the vancomycin-loaded niosomal systems improved drug stability and preserved antimicrobial activity, presenting a viable alternative to traditional administration routes, e.g. injection for systemic drug exposure and oral capsule for local drug action.

Building upon this success, fast-disintegrating oral films incorporating nisin-loaded niosomes were developed and optimized for potential application as a non-invasive antimicrobial therapy to target oral cavities. Niosomes were prepared, producing nanoscale vesicles with high uniformity and efficient entrapment of nisin. Polyvinyl alcohol has been proved to be the most appropriate film former. Incorporating sodium starch glycolate at 1%w/w as the disintegrant yielded the most rapid disintegration (27 ± 6 seconds) while maintaining acceptable film strength. Data from antimicrobial testing has shown that both free and niosomal nisin exhibited clear inhibition zones, confirming no adverse effects on nisin when subject to different manufacturing conditions. FTIR and DSC analyses revealed the presence of only favourable physical interactions between the PVA matrix and niosomal components, with thermal analysis (TGA/DTG) confirming enhanced thermal stability and moisture retention that is essential for film performance. The film matrix has acted as a protective scaffold, reducing nanoparticle aggregation and preserving peptide activity. These findings indicate that nisin-loaded niosomal films combine rapid disintegration and peptide stability, making them an effective and localized therapeutic platform to treat oral infection diseases.

This formulation strategy using niosome loaded FDOF has extended to aim for better system uptake therapeutic peptide by targeting oral cavities. In chapter 5, insulin-loaded niosomes were successfully prepared by MF device, the formulation was optimized and evaluated. Among several compositions tested, the formulation coded IN6 has demonstrated the most favorable physicochemical profiles, achieving small particle size, low PDI, and high encapsulation efficiency. Notably, the optimal vesicle composition for insulin entrapment differed from that of vancomycin and nisin despite suing same platform and phase ratio for particle synthesis, highlighting the necessity for drug-specific optimization. While vancomycin and nisin have shorter peptide sequences with MW less than 3.5 kDa and comparable IEP, they were best entrapped in the same niosomal formulation and process conditions. Insulin, being a larger peptide comprises of 2 polypeptide chains in it monomeric form as well as a lower IEP value, required a different surfactant–cholesterol balance to achieve high peptide encapsulation.

Two solid dosage forms incorporating insulin niosomes were prepared. i.e. customized MN film and tablet to target different sites in the oral cavity (buccal and sublingual spaces, respectively). The INS niosomal oral film demonstrated several practical and physicochemical advantages over the INS niosomal based tablet, making it a more efficient and versatile platform for oral cavity delivery. The film exhibited a microneedle-shaped microarchitecture that would enhance mechanical contact with the mucosal surface, promoting adhesion and facilitating localized diffusion of insulin-loaded vesicles. In terms of nanoparticle stability, the niosomes embedded within the film retain vesicles (~200nm) and near neutral zeta potential (~6 mV) more effectively than those dispersed within the compressed tablets. The solvent-casting process is a gentler manufacturing method that avoids the use of high temperature and mechanical stress and non-uniform compression. The film also achieved superior release and permeability profiles, delivering insulin faster and in higher amounts due to the presence of PEG 400, which enhanced hydration, vesicle mobility, avoid aggregation and promotes and peptide diffusion. The film was simpler to produce, requiring fewer steps, less equipment, and fewer excipients compared to the tablet that required dried niosomes.

Taken together, the findings from all formulations, niosomal nanocarriers, precisely engineered through microfluidic synthesis and appropriately integrated into solid oral devices, can effectively protect sensitive molecules, control their release, and enhance therapeutic outcomes.

Future work should focus on further biological and translational evaluation of the developed microfluidic niosomal platform. A Quality by Design (QbD) approach could be applied to optimise formulation and processing variables more systematically and define a robust design space for reproducible niosome and film production. In addition, fluorescently labelled niosomes should be used to study vesicle penetration, mucosal retention and cellular uptake in live oral epithelial cell models and ex vivo buccal or sublingual mucosa. These studies would help clarify whether peptide delivery is mainly driven by vesicle penetration, mucosal adhesion, cellular internalisation or controlled peptide release at the mucosal surface. Further work should also include long-term storage stability, mucosal irritation/histological assessment and, eventually, in vivo pharmacokinetic studies to confirm safety, peptide absorption and therapeutic performance.

In conclusion, this thesis successfully established a comprehensive niosomal drug delivery platform capable of overcoming the inherent limitations of peptide and macromolecule administration via the oral route, and more specifically via the oral cavity. The progression from vancomycin and nisin to insulin, with increasing MW demonstrates the flexibility of this MF based nanosystem, could be used to treat localized diseases, e.g. as antimicrobial therapy to systemic peptide delivery to treat diseases such as DM. By combining nanotechnology, and oral solid dosage form design platform, this work offers a promising approach to delivery for peptide drugs with poor permeability and stability (classified or considered as BCS3 drug) as a non-invasive therapy via oral cavity.

Charter 7: Reference list

References

[1] D. J. McClements, "Encapsulation, protection, and delivery of bioactive proteins and peptides using nanoparticle and microparticle systems: A review," *Adv. Colloid Interface Sci.*, vol. 253, no. 2017, pp. 1–22, 2018, doi: 10.1016/j.cis.2018.02.002.

[2] K. Fosgerau and T. Hoffmann, "Peptide therapeutics: current status and future directions," *Drug Discov. Today*, vol. 20, no. 1, pp. 122–128, Jan. 2015, doi: 10.1016/J.DRUDIS.2014.10.003.

[3] G. Rossino *et al.*, "Peptides as Therapeutic Agents: Challenges and Opportunities in the Green Transition Era," *Molecules 2023, Vol. 28, Page 7165*, vol. 28, no. 20, p. 7165, Oct. 2023, doi: 10.3390/MOLECULES28207165.

[4] Purva Patel, "Innovative Strategies In Peptide Therapeutics: Stability Challenges And Advanced Analytical Methods," *International Journal of Pharmaceutical Sciences*, vol. 2, pp. 97–108, 2024, doi: 10.5281/ZENODO.13629324.

[5] A. K. Sato, M. Viswanathan, R. B. Kent, and C. R. Wood, "Therapeutic peptides: technological advances driving peptides into development," *Curr. Opin. Biotechnol.*, vol. 17, no. 6, pp. 638–642, Dec. 2006, doi: 10.1016/J.COPBIO.2006.10.002.

[6] P. W. Latham, "Therapeutic peptides revisited," *Nat. Biotechnol.*, vol. 17, no. 8, pp. 755–757, Aug. 1999, doi: 10.1038/11686.

[7] A. A. Amer, L. Bingle, A. A. Elkordy, and C. S. Chaw, "Overcoming Oral Cavity Barriers for Peptide Delivery Using Advanced Pharmaceutical Techniques and Nano-Formulation Platforms," *Biomedicines 2025, Vol. 13, Page 2735*, vol. 13, no. 11, p. 2735, Nov. 2025, doi: 10.3390/biomedicines13112735.

[8] J. Bayry, D. S. Dimitrov, I. Mahmood, and M. Pettinato, "Impact of Intrinsic and Extrinsic Factors on the Pharmacokinetics of Peptides: When Is the Assessment of Certain Factors Warranted?," *Antibodies 2022, Vol. 11, Page 1*, vol. 11, no. 1, p. 1, Dec. 2021, doi: 10.3390/ANTIB11010001.

[9] J. Lin, “Pharmacokinetics of biotech drugs: peptides, proteins and monoclonal antibodies,” *Curr. Drug Metab.*, vol. 10, no. 7, pp. 661–691, Nov. 2009, doi: 10.2174/138920009789895499.

[10] L. Di, “Strategic Approaches to Optimizing Peptide ADME Properties,” *AAPS Journal*, vol. 17, no. 1, pp. 134–143, Jan. 2015, doi: 10.1208/S12248-014-9687-3,.

[11] L. Diao and B. Meibohm, “Pharmacokinetics and pharmacokinetic-pharmacodynamic correlations of therapeutic peptides,” *Clin. Pharmacokinet.*, vol. 52, no. 10, pp. 855–868, Oct. 2013, doi: 10.1007/S40262-013-0079-0.

[12] S. Mehrotra, P. B. G. Kalyan, P. G. Nayak, A. Joseph, and J. Manikkath, “Recent Progress in the Oral Delivery of Therapeutic Peptides and Proteins: Overview of Pharmaceutical Strategies to Overcome Absorption Hurdles,” *Adv. Pharm. Bull.*, vol. 14, no. 1, pp. 11–33, 2024, doi: 10.34172/APB.2024.009,.

[13] J. E. Brinck *et al.*, “Intestinal pH: a major driver of human gut microbiota composition and metabolism,” *Nat. Rev. Gastroenterol. Hepatol.*, vol. 22, no. 9, pp. 639–656, Sep. 2025, doi: 10.1038/S41575-025-01092-6;SUBJMETA.

[14] T. L. Russell *et al.*, “Upper gastrointestinal pH in seventy-nine healthy, elderly, North American men and women,” *Pharm. Res.*, vol. 10, no. 2, pp. 187–196, 1993, doi: 10.1023/A:1018970323716.

[15] K. L. Zapadka, F. J. Becher, A. L. Gomes dos Santos, and S. E. Jackson, “Factors affecting the physical stability (aggregation) of peptide therapeutics,” *Interface Focus*, vol. 7, no. 6, Dec. 2017, doi: 10.1098/RSFS.2017.0030/64178.

[16] G. Cimino *et al.*, “Fortschritte der Chemie Organischer Naturstoffe / Progress in the Chemistry of Organic Natural Products,” vol. 33, 1976, doi: 10.1007/978-3-7091-3262-3.

[17] V. G. Badelin *et al.*, “Physico-chemical properties of peptides and their solutions,” *Thermochim. Acta*, vol. 169, no. C, pp. 81–93, Nov. 1990, doi: 10.1016/0040-6031(90)80135-L.

[18] D. Jacob, M. J. Taylor, P. Tomlins, and T. Sahota, “Insulin Solution Stability and Biocompatibility with Materials Used for an Implantable Insulin Delivery Device Using

Reverse Phase HPLC Methods," *Applied Sciences 2019, Vol. 9, Page 4794*, vol. 9, no. 22, p. 4794, Nov. 2019, doi: 10.3390/APP9224794.

[19] L. Granero and A. Polache, "Absorption of Drugs after Oral Administration," *Pharmaceutical Sciences Encyclopedia*, Mar. 2010, doi: 10.1002/9780470571224.PSE039.

[20] Y. Yun, Y. W. Cho, and K. Park, "Nanoparticles for oral delivery: targeted nanoparticles with peptidic ligands for oral protein delivery," *Adv. Drug Deliv. Rev.*, vol. 65, no. 6, pp. 822–832, Jun. 2013, doi: 10.1016/J.ADDR.2012.10.007.

[21] L. A. Campos and J. Sancho, "The active site of pepsin is formed in the intermediate conformation dominant at mildly acidic pH," *FEBS Lett.*, vol. 538, no. 1–3, pp. 89–95, Mar. 2003, doi: 10.1016/S0014-5793(03)00152-2.

[22] K. S. Pang, "Modeling of intestinal drug absorption: roles of transporters and metabolic enzymes (for the Gillette Review Series)," *Drug Metab. Dispos.*, vol. 31, no. 12, pp. 1507–1519, Dec. 2003, doi: 10.1124/DMD.31.12.1507.

[23] P. Langguth *et al.*, "The challenge of proteolytic enzymes in intestinal peptide delivery," *Journal of Controlled Release*, vol. 46, no. 1–2, pp. 39–57, May 1997, doi: 10.1016/S0168-3659(96)01586-6.

[24] R. I. Mahato, A. S. Narang, L. Thoma, and D. D. Miller, "Emerging trends in oral delivery of peptide and protein drugs," *Crit. Rev. Ther. Drug Carrier Syst.*, vol. 20, no. 2–3, pp. 153–214, 2003, doi: 10.1615/CRITREVTHERDRUGCARRIERSYST.V20.I23.30.

[25] B. Mödl, K. Schmidt, D. Moser, and R. Eferl, "The intermicrovillar adhesion complex in gut barrier function and inflammation," *Open Exploration 2019 1:2*, vol. 1, no. 2, pp. 72–79, Oct. 2022, doi: 10.37349/EDD.2022.00006.

[26] H. Daniel, "Molecular and integrative physiology of intestinal peptide transport," *Annu. Rev. Physiol.*, vol. 66, pp. 361–384, 2004, doi: 10.1146/ANNUREV.PHYSIOL.66.032102.144149.

[27] R. P. Ferraris, "Dietary and developmental regulation of intestinal sugar transport," *Biochemical Journal*, vol. 360, no. 2, pp. 265–276, Dec. 2001, doi: 10.1042/BJ3600265.

[28] G. Mustata and S. M. Dinh, “Approaches to oral drug delivery for challenging molecules,” *Crit. Rev. Ther. Drug Carrier Syst.*, vol. 23, no. 2, pp. 111–135, 2006, doi: 10.1615/CRITREVTHERDRUGCARRIERSYST.V23.I2.20.

[29] M. Goldberg and I. Gomez-Orellana, “Challenges for the oral delivery of macromolecules,” *Nat. Rev. Drug Discov.*, vol. 2, no. 4, pp. 289–295, 2003, doi: 10.1038/NRD1067.

[30] P. Mukhopadhyay, R. Mishra, D. Rana, and P. P. Kundu, “Strategies for effective oral insulin delivery with modified chitosan nanoparticles: A review,” *Prog. Polym. Sci.*, vol. 37, no. 11, pp. 1457–1475, Nov. 2012, doi: 10.1016/J.PROGPOLYMSCI.2012.04.004.

[31] E. S. Khafagy, M. Morishita, Y. Onuki, and K. Takayama, “Current challenges in non-invasive insulin delivery systems: a comparative review,” *Adv. Drug Deliv. Rev.*, vol. 59, no. 15, pp. 1521–1546, Dec. 2007, doi: 10.1016/J.ADDR.2007.08.019.

[32] T. Kremsmayr, A. Aljnabi, J. B. Blanco-Canosa, H. N. T. Tran, N. B. Emidio, and M. Muttenthaler, “On the Utility of Chemical Strategies to Improve Peptide Gut Stability,” *J. Med. Chem.*, vol. 65, no. 8, pp. 6191–6206, Apr. 2022, doi: 10.1021/ACS.JMEDCHEM.2C00094/SUPPL_FILE/JM2C00094_SI_001.PDF.

[33] M. Nicze, M. Borówka, A. Dec, A. Niemiec, Ł. Bułdak, and B. Okopień, “The Current and Promising Oral Delivery Methods for Protein- and Peptide-Based Drugs,” *International Journal of Molecular Sciences 2024, Vol. 25, Page 815*, vol. 25, no. 2, p. 815, Jan. 2024, doi: 10.3390/IJMS25020815.

[34] W. Weitschies, K. H. Ong, D. Asano, H. Takakusa, and D. Nakai, “Oral Absorption of Middle-to-Large Molecules and Its Improvement, with a Focus on New Modality Drugs,” *Pharmaceutics 2024, Vol. 16, Page 47*, vol. 16, no. 1, p. 47, Dec. 2023, doi: 10.3390/PHARMACEUTICS16010047.

[35] D. J. Drucker, “Advances in oral peptide therapeutics,” *Nat. Rev. Drug Discov.*, vol. 19, no. 4, pp. 277–289, Apr. 2020, doi: 10.1038/S41573-019-0053-0,.

[36] C. A. Squier and M. J. Kremer, “Biology of oral mucosa and esophagus.,” *J. Natl. Cancer Inst. Monogr.*, vol. 2001, no. 29, pp. 7–15, Oct. 2001, doi:

10.1093/OXFORDJOURNALS.JNCIMONOGRAPHS.A003443/2/33785-3F3_F1TT.JPEG.

[37] M. Brizuela and R. Winters, “Histology, Oral Mucosa,” *StatPearls*, May 2023.

[38] M. Gavriiloglou, M. Hammad, J. M. Iliopoulos, P. Layrolle, and D. A. Apazidou, “Bioengineering the Junctional Epithelium in 3D Oral Mucosa Models,” *J. Funct. Biomater.*, vol. 15, no. 11, p. 330, Nov. 2024, doi: 10.3390/JFB15110330.

[39] A. Wanasathop, P. B. Patel, H. A. Choi, and S. K. Li, “Permeability of Buccal Mucosa,” *Pharmaceutics 2021, Vol. 13, Page 1814*, vol. 13, no. 11, p. 1814, Oct. 2021, doi: 10.3390/PHARMACEUTICS13111814.

[40] Y. Sudhakar, K. Kuotsu, and A. K. Bandyopadhyay, “Buccal bioadhesive drug delivery — A promising option for orally less efficient drugs,” *Journal of Controlled Release*, vol. 114, no. 1, pp. 15–40, Aug. 2006, doi: 10.1016/J.JCONREL.2006.04.012.

[41] Y. gong Guo and A. Pratap Singh, “Emerging strategies for enhancing buccal and sublingual administration of nutraceuticals and pharamaceuticals,” *J. Drug Deliv. Sci. Technol.*, vol. 52, pp. 440–451, Aug. 2019, doi: 10.1016/J.JDDST.2019.05.014.

[42] S. Jacob, A. B. Nair, S. H. S. Boddu, B. Gorain, N. Sreeharsha, and J. Shah, “An Updated Overview of the Emerging Role of Patch and Film-Based Buccal Delivery Systems,” *Pharmaceutics*, vol. 13, no. 8, p. 1206, Aug. 2021, doi: 10.3390/PHARMACEUTICS13081206.

[43] L. Coderch *et al.*, “Permeation Protection by Waterproofing Mucosal Membranes,” *Pharmaceutics*, vol. 15, no. 12, p. 2698, Dec. 2023, doi: 10.3390/PHARMACEUTICS15122698.

[44] Tharini L, “A review: Treatment of gingivitis by buccal patches,” vol. 5, no. 1, pp. 7–14, doi: 10.33545/26647222.2023.v5.i1a.26.

[45] V. F. P. Marc B. Brown, “Buccal and Sublingual Drug Delivery | Basicmedical Key.” Accessed: Jun. 28, 2025. [Online]. Available: https://basicmedicalkey.com/buccal-and-sublingual-drug-delivery

[46] G. H. Carpenter, “The secretion, components, and properties of saliva,” *Annu. Rev. Food Sci. Technol.*, vol. 4, no. 1, pp. 267–276, Feb. 2013, doi: 10.1146/ANNUREV-FOOD-030212-182700.

[47] E. Kubala *et al.*, “A Review of Selected Studies That Determine the Physical and Chemical Properties of Saliva in the Field of Dental Treatment,” *Biomed Res. Int.*, vol. 2018, p. 6572381, 2018, doi: 10.1155/2018/6572381.

[48] Y. He, K. Vasilev, and P. Zilm, “pH-Responsive Biomaterials for the Treatment of Dental Caries—A Focussed and Critical Review,” *Pharmaceutics 2023, Vol. 15, Page 1837*, vol. 15, no. 7, p. 1837, Jun. 2023, doi: 10.3390/PHARMACEUTICS15071837.

[49] S. Hua, “Advances in nanoparticulate drug delivery approaches for sublingual and buccal administration,” *Front. Pharmacol.*, vol. 10, p. 491535, Nov. 2019, doi: 10.3389/FPHAR.2019.01328/BIBTEX.

[50] S. P. Authimoolam and T. D. Dziubla, “Biopolymeric Mucin and Synthetic Polymer Analogs: Their Structure, Function and Role in Biomedical Applications,” *Polymers (Basel).*, vol. 8, no. 3, p. 71, 2016, doi: 10.3390/POLYM8030071.

[51] C. Walia and A. Arya, “Review on Buccal Drug Delivery System,” *© 2023 IJNRD* |, vol. 8, pp. 2456–4184, 2023.

[52] C. Chen, A. Patel, L. Demirkhanyan, and C. S. Gondi, “The Role of Mucins in Cancer and Cancer Progression: A Comprehensive Review,” *Current Issues in Molecular Biology 2025, Vol. 47, Page 406*, vol. 47, no. 6, p. 406, May 2025, doi: 10.3390/CIMB47060406.

[53] M. Boegh and H. M. Nielsen, “Mucus as a barrier to drug delivery - Understanding and mimicking the barrier properties,” *Basic Clin. Pharmacol. Toxicol.*, vol. 116, no. 3, pp. 179–186, Mar. 2015, doi: 10.1111/BCPT.12342;JOURNAL:JOURNAL:16000773;WGROUP:STRING:PUBLICATION.

[54] G. A. Chavan, A. S. Tawani, and Y. N. Gavhane, “Buccal Patches: A Promising Buccal Bioadhesive Drug Delivery System-A Review INTRODUCTION,” vol. 19, no. 4, pp. 533–572, 2020.

[55] S. Akbar and M. H. Hohman, “Anatomy, Head and Neck, Styloglossus,” *StatPearls*, Sep. 2023.

[56] S. Jacob, A. B. Nair, S. H. S. Boddu, B. Gorain, N. Sreeharsha, and J. Shah, “An Updated Overview of the Emerging Role of Patch and Film-Based Buccal Delivery Systems,” *Pharmaceutics*, vol. 13, no. 8, p. 1206, Aug. 2021, doi: 10.3390/PHARMACEUTICS13081206.

[57] A. S. Ismail and L. V. Hooper, “Epithelial cells and their neighbors. IV. Bacterial contributions to intestinal epithelial barrier integrity,” *Am. J. Physiol. Gastrointest. Liver Physiol.*, vol. 289, no. 5 52-5, Nov. 2005, doi: 10.1152/AJPGI.00203.2005/ASSET/IMAGES/LARGE/ZH30110542510002.JPEG.

[58] M. Derrien, M. W. J. van Passel, J. H. B. van de Bovenkamp, R. G. Schipper, W. M. de Vos, and J. Dekker, “Mucin-bacterial interactions in the human oral cavity and digestive tract,” *Gut Microbes*, vol. 1, no. 4, pp. 254–268, 2010, doi: 10.4161/GMIC.1.4.12778.

[59] M. J. . Rathbone, “Oral mucosal drug delivery,” p. 440, 1996.

[60] J. Renukuntla, A. D. Vadlapudi, A. Patel, S. H. S. Boddu, and A. K. Mitra, “Approaches for Enhancing Oral Bioavailability of Peptides and Proteins,” *Int. J. Pharm.*, vol. 447, no. 0, p. 75, Apr. 2013, doi: 10.1016/J.IJPHARM.2013.02.030.

[61] S. Malhotra, T. Lijnse, E. O. Cearbhaill, and D. J. Brayden, “Devices to overcome the buccal mucosal barrier to administer therapeutic peptides,” *Adv. Drug Deliv. Rev.*, vol. 220, May 2025, doi: 10.1016/j.addr.2025.115572.

[62] S. Rehmani and J. E. Dixon, “Oral delivery of anti-diabetes therapeutics using cell penetrating and transcytosing peptide strategies,” *Peptides (N.Y.).*, vol. 100, pp. 24–35, Feb. 2018, doi: 10.1016/j.peptides.2017.12.014.

[63] G. C. Lin *et al.*, “Investigations Towards Tryptophan Uptake and Transport Across an In Vitro Model of the Oral Mucosa Epithelium,” *International Journal of Tryptophan Research*, vol. 17, Jan. 2024, doi: 10.1177/11786469241266312.

[64] H. Y. Jung *et al.*, “Amino acid transport system L is differently expressed in human normal oral keratinocytes and human oral cancer cells,” *Cancer Lett.*, vol. 222, no. 2, pp. 237–245, May 2005, doi: 10.1016/j.canlet.2004.09.040.

[65] Y. Oyama, H. Yamano, A. Ohkuma, K. I. Ogawara, K. Higaki, and T. Kimura, “Carrier-mediated transport systems for glucose in mucosal cells of the human oral cavity,” *J. Pharm. Sci.*, vol. 88, no. 8, pp. 830–834, 1999, doi: 10.1021/js980298f.

[66] G. F. Walker, N. Langoth, and A. Bernkop-Schnürch, “Peptidase activity on the surface of the porcine buccal mucosa,” *Int. J. Pharm.*, vol. 233, no. 1–2, pp. 141–147, Feb. 2002, doi: 10.1016/S0378-5173(01)00934-6.

[67] X. Gao, S. Bhattacharya, W. K. Chan, B. R. Jasti, B. Upadrashta, and X. Li, “Expression of P-glycoprotein and CYP3A4 along the porcine oral-gastrointestinal tract: Implications on oral mucosal drug delivery,” *Drug Dev. Ind. Pharm.*, vol. 40, no. 5, pp. 599–603, 2014, doi: 10.3109/03639045.2014.884118,.

[68] N. V. Dubashynskaya, V. A. Petrova, and Y. A. Skorik, “Biopolymer Drug Delivery Systems for Oromucosal Application: Recent Trends in Pharmaceutical R&D,” *Int. J. Mol. Sci.*, vol. 25, no. 10, p. 5359, May 2024, doi: 10.3390/IJMS25105359.

[69] K. Senthil Kumar, S. Valarmathi, M. A. M. Siddique, T. Anil Kumar, and K. Chiranjeevi, “Mucoadhesive buccal drug delivery system - an overview,” *International Journal of Pharmacy and Technology*, vol. 4, no. 1, pp. 3951–3969, 2012.

[70] D. A. Patel, M. R. Patel, K. R. Patel, and N. M. Patel, “Buccal mucosa as a route for systemic drug delivery: A review,” *International Journal of Drug Development and Research*, vol. 4, no. 2, pp. 99–116, 2012.

[71] A. J. Hoogstraate *et al.*, “Diffusion Rates and Transport Pathways of Fluorescein Isothiocyanate (FITC)-Labeled Model Compounds Through Buccal Epithelium,” *Pharmaceutical Research: An Official Journal of the American Association of Pharmaceutical Scientists*, vol. 11, no. 1, pp. 83–89, 1994, doi: 10.1023/A:1018949828548/METRICS.

[72] A. Fantini *et al.*, “Buccal Permeation of Polysaccharide High Molecular Weight Compounds: Effect of Chemical Permeation Enhancers,” *Pharmaceutics*, vol. 15, no. 1, p. 129, Jan. 2023, doi: 10.3390/PHARMACEUTICS15010129/S1.

[73] T. Keum, G. Noh, J. E. Seo, S. Bashyal, and S. Lee, “In Vitro and Ex Vivo Evaluation of Penetratin as a Non-invasive Permeation Enhancer in the Penetration of Salmon Calcitonin through TR146 Buccal Cells and Porcine Buccal Tissues,” *Pharmaceuticals 2020, Vol. 13, Page 408*, vol. 13, no. 11, p. 408, Nov. 2020, doi: 10.3390/PH13110408.

[74] P. Berka, D. Stránská, V. Semecký, K. Berka, and P. Doležal, “In vitro testing of flash-frozen sublingual membranes for storage and reproducible permeability studies of macromolecular drugs from solution or nanofiber mats,” *Int. J. Pharm.*, vol. 572, Dec. 2019, doi: 10.1016/j.ijpharm.2019.118711.

[75] F. Veuillez, Y. N. Kalia, Y. Jacques, J. Deshusses, and P. Buri, “Factors and strategies for improving buccal absorption of peptides,” *European Journal of Pharmaceutics and Biopharmaceutics*, vol. 51, no. 2, pp. 93–109, Mar. 2001, doi: 10.1016/S0939-6411(00)00144-2.

[76] S. M. Linker *et al.*, “Lessons for Oral Bioavailability: How Conformationally Flexible Cyclic Peptides Enter and Cross Lipid Membranes,” *J. Med. Chem.*, vol. 66, no. 4, pp. 2773–2788, Feb. 2023, doi: 10.1021/ACS.JMEDCHEM.2C01837/SUPPL_FILE/JM2C01837_SI_004.MPG.

[77] T. Kremsmayr, A. Aljnabi, J. B. Blanco-Canosa, H. N. T. Tran, N. B. Emidio, and M. Muttenthaler, “On the Utility of Chemical Strategies to Improve Peptide Gut Stability,” *J. Med. Chem.*, vol. 65, no. 8, pp. 6191–6206, Apr. 2022, doi: 10.1021/ACS.JMEDCHEM.2C00094/SUPPL_FILE/JM2C00094_SI_002.CSV.

[78] R. P. Sivasankaran, K. Snell, G. Kunkel, P. G. Georgiou, E. G. Puente, and H. D. Maynard, “Polymer-mediated protein/peptide therapeutic stabilization: Current progress and future directions,” *Prog. Polym. Sci.*, vol. 156, p. 101867, Sep. 2024, doi: 10.1016/J.PROGPOLYMSCI.2024.101867.

[79] N. Dan, K. Samanta, and H. Almoazen, “An Update on Pharmaceutical Strategies for Oral Delivery of Therapeutic Peptides and Proteins in Adults and Pediatrics,” *Children 2020, Vol. 7, Page 307*, vol. 7, no. 12, p. 307, Dec. 2020, doi: 10.3390/CHILDREN7120307.

[80] A. Schumacher-Klinger *et al.*, “Enhancing Oral Bioavailability of Cyclic RGD Hexapeptides by the Lipophilic Prodrug Charge Masking Approach: Redirection of Peptide Intestinal Permeability from a Paracellular to Transcellular Pathway,” *Mol. Pharm.*, vol. 15, no. 8, pp. 3468–3477, Aug. 2018, doi: 10.1021/ACS.MOLPHARMACEUT.8B00466/ASSET/IMAGES/MEDIUM/MP-2018-00466G_0008.GIF.

[81] J. A. Nicolazzo, B. L. Reed, and B. C. Finnin, “The Effect of Various In Vitro Conditions on the Permeability Characteristics of the Buccal Mucosa,” *J. Pharm. Sci.*, vol. 92, no. 12, pp. 2399–2410, Dec. 2003, doi: 10.1002/JPS.10505.

[82] A. A. Tokmakov, A. Kurotani, and K. I. Sato, “Protein pI and Intracellular Localization,” *Front. Mol. Biosci.*, vol. 8, p. 775736, Nov. 2021, doi: 10.3389/FMOLB.2021.775736.

[83] L. Zhang and G. Bulaj, “Converting Peptides into Drug Leads by Lipidation,” *Curr. Med. Chem.*, vol. 19, no. 11, pp. 1602–1618, Mar. 2012, doi: 10.2174/092986712799945003,.

[84] P. F. Augustijns *et al.*, “Hydration changes implicated in the remarkable temperature-dependent membrane permeation of cyclosporin A,” *Biochemistry*, vol. 39, no. 25, pp. 7621–7630, Jun. 2000, doi: 10.1021/BI9929709;REQUESTEDJOURNAL:JOURNAL:BICHAW;WGROUP:STRING:ACHS.

[85] S. Liras and K. F. McClure, “Permeability of Cyclic Peptide Macrocycles and Cyclotides and Their Potential as Therapeutics,” *ACS Med. Chem. Lett.*, vol. 10, no. 7, p. 1026, Jun. 2019, doi: 10.1021/ACSMEDCHEMLETT.9B00149.

[86] P. Ghosh *et al.*, “An amide to thioamide substitution improves the permeability and bioavailability of macrocyclic peptides,” *Nat. Commun.*, vol. 14, no. 1, pp. 1–14, Dec. 2023, doi: 10.1038/S41467-023-41748-Y;TECHMETA=49,75;SUBJMETA=309,436,611,638,639,92,96;KWRD=CHEMICAL+TOOLS,PEPTIDES,PHARMACOLOGY.

[87] J. Li, K. Yanagisawa, and Y. Akiyama, “CycPeptMP: enhancing membrane permeability prediction of cyclic peptides with multi-level molecular features and data augmentation,” *Brief. Bioinform.*, vol. 25, no. 5, p. 417, Jul. 2024, doi: 10.1093/BIB/BBAE417.

[88] M. L. Merz *et al.*, “De novo development of small cyclic peptides that are orally bioavailable,” *Nature Chemical Biology 2023 20:5*, vol. 20, no. 5, pp. 624–633, Dec. 2023, doi: 10.1038/s41589-023-01496-y.

[89] N. U. Khaliq, J. Lee, S. Kim, D. Sung, and H. Kim, “Pluronic F-68 and F-127 Based Nanomedicines for Advancing Combination Cancer Therapy,” *Pharmaceutics*, vol. 15, no. 8, p. 2102, Aug. 2023, doi: 10.3390/PHARMACEUTICS15082102.

[90] A. Pratap-Singh, Y. Guo, A. Baldelli, and A. Singh, “Concept for a Unidirectional Release Mucoadhesive Buccal Tablet for Oral Delivery of Antidiabetic Peptide Drugs Such as Insulin, Glucagon-like Peptide 1 (GLP-1), and their Analogs,” *Pharmaceutics*, vol. 15, no. 9, Sep. 2023, doi: 10.3390/PHARMACEUTICS15092265.

[91] A. Garcia *et al.*, “Membrane accessibility of glutathione,” *Biochimica et Biophysica Acta (BBA) - Biomembranes*, vol. 1848, no. 10, pp. 2430–2436, Oct. 2015, doi: 10.1016/J.BBAMEM.2015.07.016.

[92] H. Möbitz, B. Dittrich, S. Rodde, and R. Strang, “Nonclassical Zwitterions as a Design Principle to Reduce Lipophilicity without Impacting Permeability,” *J. Med. Chem.*, vol. 67, no. 11, pp. 9485–9494, Jun. 2024, doi: 10.1021/ACS.JMEDCHEM.4C00596,.

[93] W. Shan *et al.*, “Enhanced Oral Delivery of Protein Drugs Using Zwitterion-Functionalized Nanoparticles to Overcome both the Diffusion and Absorption Barriers,” *ACS Appl. Mater. Interfaces*, vol. 8, no. 38, pp. 25444–25453, Sep. 2016, doi: 10.1021/ACSAMI.6B08183/SUPPL_FILE/AM6B08183_SI_001.PDF.

[94] T. Samad, J. Witten, A. J. Grodzinsky, and K. Ribbeck, “Spatial configuration of charge and hydrophobicity tune particle transport through mucus,” *Biophys. J.*, vol. 121, no. 2, pp. 277–287, Jan. 2022, doi: 10.1016/j.bpj.2021.12.018.

[95] S. Bashyal *et al.*, “Facilitated buccal insulin delivery via hydrophobic ion-pairing approach: In vitro and ex vivo evaluation,” *Int. J. Nanomedicine*, vol. 16, pp. 4677–4691, 2021, doi: 10.2147/IJN.S318092,.

[96] M. E. Dowty, K. E. Knuth, B. K. Irons, and J. R. Robinson, “Transport of Thyrotropin Releasing Hormone in Rabbit Buccal Mucosa in Vitro,” *Pharmaceutical Research: An*

Official Journal of the American Association of Pharmaceutical Scientists, vol. 9, no. 9, pp. 1113–1122, 1992, doi: 10.1023/A:1015883217858/METRICS.

[97] C. : Baral, K. C. ; Choi, K. Chandra Baral, and K. Y. Choi, "Barriers and Strategies for Oral Peptide and Protein Therapeutics Delivery: Update on Clinical Advances," *Pharmaceutics 2025, Vol. 17, Page 397*, vol. 17, no. 4, p. 397, Mar. 2025, doi: 10.3390/PHARMACEUTICS17040397.

[98] R. Oliveira Do Couto *et al.*, "Assessing α-Bisabolol as a Transmucosal Permeation Enhancer of Buccal Local Anesthetics," *Pharmaceutics 2024, Vol. 16, Page 1198*, vol. 16, no. 9, p. 1198, Sep. 2024, doi: 10.3390/PHARMACEUTICS16091198.

[99] D. A. Panou, S. F. Pedersen, M. Kristensen, and H. M. Nielsen, "Epithelium dynamics differ in time and space when exposed to the permeation enhancers penetramax and EGTA. A head-to-head mechanistic comparison," *Frontiers in Drug Delivery*, vol. 3, p. 1221628, Aug. 2023, doi: 10.3389/FDDEV.2023.1221628/BIBTEX.

[100] G. Del Vecchio *et al.*, "Sodium caprate transiently opens claudin-5-containing barriers at tight junctions of epithelial and endothelial cells," *Mol. Pharm.*, vol. 9, no. 9, pp. 2523–2533, Sep. 2012, doi: 10.1021/MP3001414,.

[101] C. Solis-Herrera, M. P. Kane, and C. Triplitt, "Current Understanding of Sodium N-(8-[2-Hydroxylbenzoyl] Amino) Caprylate (SNAC) as an Absorption Enhancer: The Oral Semaglutide Experience," *Clinical Diabetes*, vol. 42, no. 1, pp. 74–86, Jan. 2024, doi: 10.2337/CD22-0118,.

[102] J. Wu, S. Roesger, N. Jones, C. M. J. Hu, and S. D. Li, "Cell-penetrating peptides for transmucosal delivery of proteins," *Journal of Controlled Release*, vol. 366, pp. 864–878, Feb. 2024, doi: 10.1016/j.jconrel.2024.01.038.

[103] Y. Xu *et al.*, "Cell-penetrating peptide enhanced insulin buccal absorption," *Int. J. Pharm.*, vol. 584, Jun. 2020, doi: 10.1016/j.ijpharm.2020.119469.

[104] J. Boateng, J. Mitchell, H. Pawar, and I. Ayensu, "Functional Characterisation and Permeation Studies of Lyophilised Thiolated Chitosan Xerogels for Buccal Delivery of Insulin," *Protein Pept. Lett.*, vol. 21, no. 11, pp. 1163–1175, Oct. 2014, doi: 10.2174/0929866521666140805124403,.

[105] K. Mfoafo, R. Mittal, A. Eshraghi, Y. Omidi, and H. Omidian, “Thiolated polymers: An overview of mucoadhesive properties and their potential in drug delivery via mucosal tissues,” *J. Drug Deliv. Sci. Technol.*, vol. 85, p. 104596, Aug. 2023, doi: 10.1016/J.JDDST.2023.104596.

[106] G. Kali *et al.*, “Enhanced Mucoadhesion of Thiolated β-Cyclodextrin by S-Protection with 2-Mercaptoethanesulfonic Acid,” *ACS Omega*, vol. 9, no. 5, pp. 5819–5828, Feb. 2024, doi: 10.1021/ACSOMEGA.3C08836/ASSET/IMAGES/LARGE/AO3C08836_0009.JPEG.

[107] J. Griesser, G. Hetényi, and A. Bernkop-Schnürch, “Thiolated Hyaluronic Acid as Versatile Mucoadhesive Polymer: From the Chemistry Behind to Product Developments—What Are the Capabilities?,” *Polymers 2018, Vol. 10, Page 243*, vol. 10, no. 3, p. 243, Feb. 2018, doi: 10.3390/POLYM10030243.

[108] S. Hu *et al.*, “A mussel-inspired film for adhesion to wet buccal tissue and efficient buccal drug delivery,” *Nat. Commun.*, vol. 12, no. 1, Dec. 2021, doi: 10.1038/S41467-021-21989-5,.

[109] J. G. Edmans *et al.*, “Bioactive Protein and Peptide Release from a Mucoadhesive Electrospun Membrane,” *Biomedical Materials and Devices*, vol. 2, no. 1, pp. 444–453, Mar. 2024, doi: 10.1007/S44174-023-00098-5,.

[110] A. Vaidya and S. Mitragotri, “Ionic liquid-mediated delivery of insulin to buccal mucosa,” *Journal of Controlled Release*, vol. 327, pp. 26–34, Nov. 2020, doi: 10.1016/J.JCONREL.2020.07.037.

[111] A. A. Amer, L. Bingle, C. S. Chaw, and A. A. Elkordy, “Development of Vancomycin, a Glycopeptide Antibiotic, in a Suitable Nanoform for Oral Delivery,” *Molecules 2025, Vol. 30, Page 1624*, vol. 30, no. 7, p. 1624, Apr. 2025, doi: 10.3390/MOLECULES30071624.

[112] A. Wanasathop, P. B. Patel, H. A. Choi, and S. K. Li, “Permeability of Buccal Mucosa,” *Pharmaceutics*, vol. 13, no. 11, p. 1814, Nov. 2021, doi: 10.3390/PHARMACEUTICS13111814.

[113] A. S. Macedo *et al.*, “Novel and revisited approaches in nanoparticle systems for buccal drug delivery,” *Journal of Controlled Release*, vol. 320, pp. 125–141, Apr. 2020, doi: 10.1016/J.JCONREL.2020.01.006.

[114] M.-A. Shahbazi and H. A. Santos, “Improving Oral Absorption Via Drug-Loaded Nanocarriers: Absorption Mechanisms, Intestinal Models and Rational Fabrication,” *Curr. Drug Metab.*, vol. 14, no. 1, pp. 28–56, Dec. 2012, doi: 10.2174/138920013804545133.

[115] J. M. Rabanel, V. Aoun, I. Elkin, M. Mokhtar, and P. Hildgen, “Drug-loaded nanocarriers: passive targeting and crossing of biological barriers,” *Curr. Med. Chem.*, vol. 19, no. 19, pp. 3070–3102, Jun. 2012, doi: 10.2174/092986712800784702.

[116] A. des Rieux, V. Fievez, M. Garinot, Y. J. Schneider, and V. Préat, “Nanoparticles as potential oral delivery systems of proteins and vaccines: a mechanistic approach,” *J. Control. Release*, vol. 116, no. 1, pp. 1–27, Nov. 2006, doi: 10.1016/J.JCONREL.2006.08.013.

[117] C. Damgé, C. P. Reis, and P. Maincent, “Nanoparticle strategies for the oral delivery of insulin,” *Expert Opin. Drug Deliv.*, vol. 5, no. 1, pp. 45–68, Jan. 2008, doi: 10.1517/17425247.5.1.45.

[118] V. J. Mohanraj and Y. Chen, “Nanoparticles - A review,” *Tropical Journal of Pharmaceutical Research*, vol. 5, no. 1, pp. 561–573, Jul. 2006, doi: 10.4314/TJPR.V5I1.14634.

[119] S. Hua, “Advances in Nanoparticulate Drug Delivery Approaches for Sublingual and Buccal Administration,” *Front. Pharmacol.*, vol. 10, p. 1328, 2019, doi: 10.3389/FPHAR.2019.01328.

[120] B. J. Teubl, C. Meindl, A. Eitzlmayr, A. Zimmer, E. Fröhlich, and E. Roblegg, “In-vitro permeability of neutral polystyrene particles via buccal mucosa,” *Small*, vol. 9, no. 3, pp. 457–466, Feb. 2013, doi: 10.1002/SMLL.201201789.

[121] S. Hua, “Advances in nanoparticulate drug delivery approaches for sublingual and buccal administration,” *Front. Pharmacol.*, vol. 10, p. 491535, Nov. 2019, doi: 10.3389/FPHAR.2019.01328/BIBTEX.

[122] R. Pokrowiecki *et al.*, “Nanoparticles And Human Saliva: A Step Towards Drug Delivery Systems For Dental And Craniofacial Biomaterials,” *Int. J. Nanomedicine*, vol. 14, p. 9235, 2019, doi: 10.2147/IJN.S221608.

[123] G. Koller, E. Schürholz, T. Ziebart, A. Neff, R. Frankenberger, and J. W. Bartsch, “Clinical Evaluation of Pathognomonic Salivary Protease Fingerprinting for Oral Disease Diagnosis,” *J. Pers. Med.*, vol. 11, no. 9, p. 866, Sep. 2021, doi: 10.3390/JPM11090866.

[124] T. Mumtaz, N. Ahmed, N. ul Hassan, M. Badshah, S. Khan, and A. ur Rehman, “Voriconazole nanoparticles-based film forming spray: An efficient approach for potential treatment of topical fungal infections,” *J. Drug Deliv. Sci. Technol.*, vol. 70, p. 102973, Apr. 2022, doi: 10.1016/J.JDDST.2021.102973.

[125] B. J. Teubl, C. Meindl, A. Eitzlmayr, A. Zimmer, E. Fröhlich, and E. Roblegg, “In-vitro permeability of neutral polystyrene particles via buccal mucosa,” *Small*, vol. 9, no. 3, pp. 457–466, Feb. 2013, doi: 10.1002/SMLL.201201789.

[126] R. Jeitler *et al.*, “Investigation of Cellular Interactions of Lipid-Structured Nanoparticles With Oral Mucosal Epithelial Cells,” *Front. Mol. Biosci.*, vol. 9, p. 917921, May 2022, doi: 10.3389/FMOLB.2022.917921.

[127] B. J. Teubl, C. Meindl, A. Eitzlmayr, A. Zimmer, E. Fröhlich, and E. Roblegg, “In-vitro permeability of neutral polystyrene particles via buccal mucosa,” *Small*, vol. 9, no. 3, pp. 457–466, Feb. 2013, doi: 10.1002/SMLL.201201789,.

[128] A. Sharma, S. V. Madhunapantula, and G. P. Robertson, “Toxicological considerations when creating nanoparticle based drugs and drug delivery systems?,” *Expert Opin. Drug Metab. Toxicol.*, vol. 8, no. 1, p. 47, Jan. 2011, doi: 10.1517/17425255.2012.637916.

[129] L. Bierbaumer, U. Y. Schwarze, R. Gruber, and W. Neuhaus, “Cell culture models of oral mucosal barriers: A review with a focus on applications, culture conditions and barrier properties,” *Tissue Barriers*, vol. 6, no. 3, p. 1479568, Jul. 2018, doi: 10.1080/21688370.2018.1479568.

[130] A. K. Mahor *et al.*, “Nanostructured Lipid Carriers for Improved Delivery of Therapeutics via the Oral Route,” *J. Nanotechnol.*, vol. 2023, no. 1, p. 4687959, Jan. 2023, doi: 10.1155/2023/4687959.

[131] G. C. Lin *et al.*, “Optimization of an oral mucosa in vitro model based on cell line TR146,” *Tissue Barriers*, vol. 8, no. 2, p. 1748459, 2020, doi: 10.1080/21688370.2020.1748459.

[132] C. Twarog, S. Fattah, J. Heade, S. Maher, E. Fattal, and D. J. Brayden, “Intestinal Permeation Enhancers for Oral Delivery of Macromolecules: A Comparison between Salcaprozate Sodium (SNAC) and Sodium Caprate (C10),” *Pharmaceutics*, vol. 11, no. 2, p. 78, Feb. 2019, doi: 10.3390/PHARMACEUTICS11020078.

[133] T. Keum, G. Noh, J. E. Seo, S. Bashyal, D. H. Sohn, and S. Lee, “Examination of Effective Buccal Absorption of Salmon Calcitonin Using Cell-Penetrating Peptide-Conjugated Liposomal Drug Delivery System,” *Int. J. Nanomedicine*, vol. 17, pp. 697–710, 2022, doi: 10.2147/IJN.S335774.

[134] Y. Guo *et al.*, “Deformable Nanovesicle-Loaded Gel for Buccal Insulin Delivery,” *Pharmaceutics*, vol. 14, no. 11, p. 2262, Nov. 2022, doi: 10.3390/PHARMACEUTICS14112262/S1.

[135] T. Sangnim, D. Dheer, N. Jangra, K. Huanbutta, V. Puri, and A. Sharma, “Chitosan in Oral Drug Delivery Formulations: A Review,” *Pharmaceutics*, vol. 15, no. 9, p. 2361, Sep. 2023, doi: 10.3390/PHARMACEUTICS15092361.

[136] S. Maher, D. J. Brayden, L. Casettari, and L. Illum, “Application of Permeation Enhancers in Oral Delivery of Macromolecules: An Update,” *Pharmaceutics*, vol. 11, no. 1, p. 41, Jan. 2019, doi: 10.3390/PHARMACEUTICS11010041.

[137] Midaform® Insulin PharmFilm, “Phase 2a Trial for Oral Insulin Film | Aquestive.” Accessed: Oct. 10, 2025. [Online]. Available: https://aquestive.com/monosol-rx-announces-initiation-of-phase-2a-trial-for-oral-insulin-film

[138] B. Xiao *et al.*, “Effects of tripolyphosphate on cellular uptake and RNA interference efficiency of chitosan-based nanoparticles in Raw 264.7 macrophages,” *J. Colloid Interface Sci.*, vol. 490, pp. 520–528, Mar. 2017, doi: 10.1016/j.jcis.2016.11.088.

[139] M. Roldo, M. Hornof, P. Caliceti, and A. Bernkop-Schnürch, “Mucoadhesive thiolated chitosans as platforms for oral controlled drug delivery: Synthesis and in vitro

evaluation," *European Journal of Pharmaceutics and Biopharmaceutics*, vol. 57, no. 1, pp. 115–121, 2004, doi: 10.1016/S0939-6411(03)00157-7.

[140] C. Giovino, I. Ayensu, J. Tetteh, and J. S. Boateng, "An integrated buccal delivery system combining chitosan films impregnated with peptide loaded PEG-b-PLA nanoparticles," *Colloids Surf. B Biointerfaces*, vol. 112, pp. 9–15, Dec. 2013, doi: 10.1016/j.colsurfb.2013.07.019.

[141] M. G. Lancina, R. K. Shankar, and H. Yang, "Chitosan Nanofibers for Transbuccal Insulin Delivery," *J. Biomed. Mater. Res. A*, vol. 105, no. 5, p. 1252, May 2017, doi: 10.1002/JBM.A.35984.

[142] S. Zhou *et al.*, "Thiolated Nanoparticles Overcome the Mucus Barrier and Epithelial Barrier for Oral Delivery of Insulin," *Mol. Pharm.*, vol. 17, no. 1, pp. 239–250, Jan. 2020, doi: 10.1021/ACS.MOLPHARMACEUT.9B00971,.

[143] S. S. Hallan, P. Kaur, V. Kaur, N. Mishra, and B. Vaidya, "Lipid polymer hybrid as emerging tool in nanocarriers for oral drug delivery," *Artif. Cells Nanomed. Biotechnol.*, vol. 44, no. 1, pp. 334–349, Jan. 2016, doi: 10.3109/21691401.2014.951721.

[144] S. S. Hallan, P. Kaur, V. Kaur, N. Mishra, and B. Vaidya, "Lipid polymer hybrid as emerging tool in nanocarriers for oral drug delivery," *Artif. Cells Nanomed. Biotechnol.*, vol. 44, no. 1, pp. 334–349, Jan. 2016, doi: 10.3109/21691401.2014.951721.

[145] Y. Yang *et al.*, "Factors affecting the buccal delivery of deformable nanovesicles based on insulin–phospholipid complex: an in vivo investigation," *Drug Deliv.*, vol. 27, no. 1, pp. 900–908, Jan. 2020, doi: 10.1080/10717544.2020.1778814.

[146] A. S. Macedo *et al.*, "Novel and revisited approaches in nanoparticle systems for buccal drug delivery," *Journal of Controlled Release*, vol. 320, pp. 125–141, Apr. 2020, doi: 10.1016/j.jconrel.2020.01.006.

[147] M. Liu, D. Svirskis, T. Proft, J. Loh, Y. Huang, and J. Wen, "Cellular Uptake and Transport Mechanism Investigations of PEGylated Niosomes for Improving the Oral Delivery of Thymopentin," *Pharmaceutics*, vol. 16, no. 3, p. 397, Mar. 2024, doi: 10.3390/PHARMACEUTICS16030397.

[148] K. A. Farha and R. A. Farha, “NEURODEVELOPMENTAL DEFICITS IN 16P11.2 MICRODELETION SYNDROME. WOULD RISPERIDONE MAKE A DIFFERENCE? A 2-YEAR-OLD MALE TODDLER-CASE STUDY,” 2020, doi: 10.5455/IJMRCR.Microdeletion-Syndrome.

[149] P. Wichayapreechar, S. Anuchapreeda, R. Phongpradist, W. Rungseevijitprapa, and C. Ampasavate, “Dermal targeting of Centella asiatica extract using hyaluronic acid surface modified niosomes,” *J. Liposome Res.*, vol. 30, no. 2, pp. 197–207, Apr. 2020, doi: 10.1080/08982104.2019.1614952.

[150] N. A. Abtahi *et al.*, “Multifunctional stimuli-responsive niosomal nanoparticles for co-delivery and co-administration of gene and bioactive compound: In vitro and in vivo studies,” *Chemical Engineering Journal*, vol. 429, p. 132090, Feb. 2022, doi: 10.1016/J.CEJ.2021.132090.

[151] M. Haroun *et al.*, “Significant of injectable brucine PEGylated niosomes in treatment of MDA cancer cells,” *J. Drug Deliv. Sci. Technol.*, vol. 71, p. 103322, May 2022, doi: 10.1016/J.JDDST.2022.103322.

[152] X. Ge, M. Wei, S. He, and W.-E. Yuan, “Advances of Non-Ionic Surfactant Vesicles (Niosomes) and Their Application in Drug Delivery,” *Pharmaceutics 2019, Vol. 11, Page 55*, vol. 11, no. 2, p. 55, Jan. 2019, doi: 10.3390/PHARMACEUTICS11020055.

[153] I. Ali *et al.*, “Synthesis of long-tail nonionic surfactants and their investigation for vesicle formation, drug entrapment, and biocompatibility,” *J. Liposome Res.*, vol. 30, no. 3, pp. 255–262, Jul. 2020, doi: 10.1080/08982104.2019.1630645.

[154] S. Chen, S. Hanning, J. Falconer, M. Locke, and J. Wen, “Recent advances in non-ionic surfactant vesicles (niosomes): Fabrication, characterization, pharmaceutical and cosmetic applications,” *European Journal of Pharmaceutics and Biopharmaceutics*, vol. 144, pp. 18–39, Nov. 2019, doi: 10.1016/J.EJPB.2019.08.015.

[155] P. Bhardwaj, P. Tripathi, R. Gupta, and S. Pandey, “Niosomes: A review on niosomal research in the last decade,” *J. Drug Deliv. Sci. Technol.*, vol. 56, Apr. 2020, doi: 10.1016/J.JDDST.2020.101581.

[156] M. Yaghoobian, A. Haeri, N. Bolourchian, S. Shahhosseni, and S. Dadashzadeh, “The Impact of Surfactant Composition and Surface Charge of Niosomes on the Oral Absorption of Repaglinide as a BCS II Model Drug</p>,” *Int. J. Nanomedicine*, vol. 15, pp. 8767–8781, Nov. 2020, doi: 10.2147/IJN.S261932.

[157] R. Bartelds *et al.*, “Niosomes, an alternative for liposomal delivery,” *PLoS One*, vol. 13, no. 4, Apr. 2018, doi: 10.1371/JOURNAL.PONE.0194179.

[158] N. Ruwizhi and B. A. Aderibigbe, “The Efficacy of Cholesterol-Based Carriers in Drug Delivery,” *Molecules 2020, Vol. 25, Page 4330*, vol. 25, no. 18, p. 4330, Sep. 2020, doi: 10.3390/MOLECULES25184330.

[159] F. Nowroozi, A. Almasi, J. Javidi, A. Haeri, and S. Dadashzadeh, “Effect of Surfactant Type, Cholesterol Content and Various Downsizing Methods on the Particle Size of Niosomes,” *Iran. J. Pharm. Res.*, vol. 17, no. Suppl2, p. 1, Sep. 2018.

[160] E. Mazzotta, C. Orlando, and R. Muzzalupo, “New nanomaterials with intrinsic antioxidant activity by surface functionalization of niosomes with natural phenolic acids,” *Pharmaceutics*, vol. 13, no. 6, p. 766, Jun. 2021, doi: 10.3390/PHARMACEUTICS13060766/S1.

[161] D. B. Momekova, V. E. Gugleva, and P. D. Petrov, “Nanoarchitectonics of Multifunctional Niosomes for Advanced Drug Delivery,” *ACS Omega*, vol. 6, no. 49, pp. 33265–33273, Dec. 2021, doi: 10.1021/ACSOMEGA.1C05083/ASSET/IMAGES/LARGE/AO1C05083_0007.JPEG.

[162] E. Ojeda *et al.*, “The influence of the polar head-group of synthetic cationic lipids on the transfection efficiency mediated by niosomes in rat retina and brain,” *Biomaterials*, vol. 77, pp. 267–279, Jan. 2016, doi: 10.1016/J.BIOMATERIALS.2015.11.017.

[163] S. Grijalvo *et al.*, “Cationic Niosomes as Non-Viral Vehicles for Nucleic Acids: Challenges and Opportunities in Gene Delivery,” *Pharmaceutics 2019, Vol. 11, Page 50*, vol. 11, no. 2, p. 50, Jan. 2019, doi: 10.3390/PHARMACEUTICS11020050.

[164] N. Pippa *et al.*, “PEO-b-PCL grafted niosomes: The cooperativilty of amphiphilic components and their properties in vitro and in vivo,” *Colloids Surf. B Biointerfaces*, vol. 177, pp. 338–345, May 2019, doi: 10.1016/J.COLSURFB.2019.01.036.

[165] W. Rangsimawong, P. Opanasopit, T. Rojanarata, S. Duangjit, and T. Ngawhirunpat, “Skin Transport of Hydrophilic Compound-Loaded PEGylated Lipid Nanocarriers: Comparative Study of Liposomes, Niosomes, and Solid Lipid Nanoparticles,” *Biol. Pharm. Bull.*, vol. 39, no. 8, pp. 1254–1262, Aug. 2016, doi: 10.1248/BPB.B15-00981.

[166] L. You, X. Liu, Z. Fang, Q. Xu, and Q. Zhang, “Synthesis of multifunctional Fe3O4@PLGA-PEG nano-niosomes as a targeting carrier for treatment of cervical cancer,” *Materials Science and Engineering: C*, vol. 94, pp. 291–302, Jan. 2019, doi: 10.1016/J.MSEC.2018.09.044.

[167] B. L. Mui, P. R. Cullis, E. A. Evans, and T. D. Madden, “Osmotic properties of large unilamellar vesicles prepared by extrusion,” *Biophys. J.*, vol. 64, no. 2, pp. 443–453, Feb. 1993, doi: 10.1016/S0006-3495(93)81385-7.

[168] B. Banke and N. Thakre, “Design of Gatifloxacin Niosomes by film hydration method,” 2020, doi: 10.25215/2455/0502002.

[169] M. J. H. Barbara Mui, *Formation of Large Unilamellar Vesicles by Extrusion*. CRC Press, 2018. doi: 10.1201/9781420005875-8.

[170] G. V. R. Ganesh Sai Myneni, “NOVEL VESICULAR DRUG DELIVERY SYSTEMS: A REVIEW”, doi: 10.5281/ZENODO.4772544.

[171] C. Cerqueira-Coutinho, E. P. dos Santos, and C. R. E. Mansur, “Niosomes as Nano-Delivery Systems in the Pharmaceutical Field,” *Critical Reviews™ in Therapeutic Drug Carrier Systems*, vol. 33, no. 2, pp. 195–212, 2016, doi: 10.1615/CRITREVTHERDRUGCARRIERSYST.2016016167.

[172] G. P. Kumar and P. Rajeshwarrao, “Nonionic surfactant vesicular systems for effective drug delivery—an overview,” *Acta Pharm. Sin. B*, vol. 1, no. 4, pp. 208–219, 2011, doi: 10.1016/j.apsb.2011.09.002.

[173] L. Tavano, P. Alfano, R. Muzzalupo, and B. De Cindio, “Niosomes vs microemulsions: New carriers for topical delivery of Capsaicin,” *Colloids Surf. B Biointerfaces*, vol. 87, no. 2, pp. 333–339, Oct. 2011, doi: 10.1016/J.COLSURFB.2011.05.041.

[174] A. Girigoswami, S. Das, and S. De, “Fluorescence and dynamic light scattering studies of niosomes-membrane mimetic systems,” *Spectrochim. Acta A Mol. Biomol. Spectrosc.*, vol. 64, no. 4, pp. 859–866, Jul. 2006, doi: 10.1016/J.SAA.2005.08.015.

[175] S. Biswal, P. N. Murthy, J. Sahu, P. Sahoo, and A. F, “Vesicles of Non-ionic Surfactants (Niosomes) and Drug Delivery Potential,” *International Journal of Pharmaceutical Sciences and Nanotechnology(IJPSN)*, vol. 1, no. 1, pp. 1–8, May 2008, doi: 10.37285/IJPSN.2008.1.1.1.

[176] P. L. Yeo, S. M. Chye, A. Pick, K. Ling, and R. Y. Koh, “Niosome: A Mini Review on Its Structure, Properties, Methods of Preparation and Medical Applications,” *Available online www.jocpr.com Journal of Chemical and Pharmaceutical Research*, vol. 8, no. 10, 2016.

[177] P. Aparajay and A. Dev, “Functionalized niosomes as a smart delivery device in cancer and fungal infection,” *European Journal of Pharmaceutical Sciences*, vol. 168, p. 106052, Jan. 2022, doi: 10.1016/J.EJPS.2021.106052.

[178] L. K. Yeo, T. O. B. Olusanya, C. S. Chaw, and A. A. Elkordy, “Brief Effect of a Small Hydrophobic Drug (Cinnarizine) on the Physicochemical Characterisation of Niosomes Produced by Thin-Film Hydration and Microfluidic Methods,” *Pharmaceutics 2018, Vol. 10, Page 185*, vol. 10, no. 4, p. 185, Oct. 2018, doi: 10.3390/PHARMACEUTICS10040185.

[179] K. Owodeha-Ashaka, M. O. Ilomuanya, and A. Iyire, “Evaluation of sonication on stability-indicating properties of optimized pilocarpine hydrochloride-loaded niosomes in ocular drug delivery,” *Prog. Biomater.*, vol. 10, no. 3, pp. 207–220, Sep. 2021, doi: 10.1007/S40204-021-00164-5/TABLES/4.

[180] V. Gugleva, S. Titeva, S. Rangelov, and D. Momekova, “Design and in vitro evaluation of doxycycline hyclate niosomes as a potential ocular delivery system,” *Int. J. Pharm.*, vol. 567, p. 118431, Aug. 2019, doi: 10.1016/J.IJPHARM.2019.06.022.

[181] S. Mehraji and D. L. DeVoe, “Microfluidic synthesis of lipid-based nanoparticles for drug delivery: recent advances and opportunities,” *Lab Chip*, vol. 24, no. 5, pp. 1154–1174, Feb. 2024, doi: 10.1039/D3LC00821E.

[182] K. Asaithambi, J. Muthukumar, R. Chandrasekaran, N. Ekambaram, and M. Roopan, "Synthesis and characterization of turmeric oil loaded non-ionic surfactant vesicles (niosomes) and its enhanced larvicidal activity against mosquito vectors," *Biocatal. Agric. Biotechnol.*, vol. 29, p. 101737, Oct. 2020, doi: 10.1016/J.BCAB.2020.101737.

[183] A. Manosroi, R. Chutoprapat, M. Abe, and J. Manosroi, "Characteristics of niosomes prepared by supercritical carbon dioxide (scCO2) fluid," *Int. J. Pharm.*, vol. 352, no. 1–2, pp. 248–255, Mar. 2008, doi: 10.1016/J.IJPHARM.2007.10.013.

[184] P. García-Manrique, N. D. Machado, M. A. Fernández, M. C. Blanco-López, M. Matos, and G. Gutiérrez, "Effect of drug molecular weight on niosomes size and encapsulation efficiency," *Colloids Surf. B Biointerfaces*, vol. 186, p. 110711, Feb. 2020, doi: 10.1016/J.COLSURFB.2019.110711.

[185] A. Manosroi, P. Jantrawut, H. Akazawa, T. Akihisa, W. Manosroi, and J. Manosroi, "Transdermal absorption enhancement of gel containing elastic niosomes loaded with gallic acid from Terminalia chebula galls," *Pharm. Biol.*, vol. 49, no. 6, pp. 553–562, Jun. 2011, doi: 10.3109/13880209.2010.528432/ASSET/A7435801-2570-405F-AEFB-9BF2BE2E8550/ASSETS/IMAGES/IPHB_A_528432_ILG0006.GIF.

[186] C. Marianecci, F. Rinaldi, M. Carafa, L. Di Marzio, and S. Esposito, "Niosomes," *Fundamentals of Pharmaceutical Nanoscience*, pp. 65–90, Jan. 2013, doi: 10.1007/978-1-4614-9164-4_4.

[187] FDA, "Drug Products, Including Biological Products, that Contain Nanomaterials Guidance for Industry Contains Nonbinding Recommendations," 2022.

[188] N. Hoshyar, S. Gray, H. Han, and G. Bao, "The Effect of Nanoparticle Size on In Vivo Pharmacokinetics and Cellular Interaction," *Nanomedicine*, vol. 11, no. 6, pp. 673–692, Mar. 2016, doi: 10.2217/NNM.16.5.

[189] F. Oroojalian *et al.*, "Recent advances in nanotechnology-based drug delivery systems for the kidney," *Journal of Controlled Release*, vol. 321, pp. 442–462, May 2020, doi: 10.1016/J.JCONREL.2020.02.027.

[190] A. A. Halwani, “Development of Pharmaceutical Nanomedicines: From the Bench to the Market,” *Pharmaceutics 2022, Vol. 14, Page 106*, vol. 14, no. 1, p. 106, Jan. 2022, doi: 10.3390/PHARMACEUTICS14010106.

[191] E. Blanco, H. Shen, and M. Ferrari, “Principles of nanoparticle design for overcoming biological barriers to drug delivery,” *Nature Biotechnology 2015 33:9*, vol. 33, no. 9, pp. 941–951, Sep. 2015, doi: 10.1038/nbt.3330.

[192] S. Cao *et al.*, “Shape Matters: Comprehensive Analysis of Star-Shaped Lipid Nanoparticles,” *Front. Pharmacol.*, vol. 11, p. 541677, Apr. 2020, doi: 10.3389/FPHAR.2020.00539/BIBTEX.

[193] D. Lombardo and M. A. Kiselev, “Methods of Liposomes Preparation: Formation and Control Factors of Versatile Nanocarriers for Biomedical and Nanomedicine Application,” *Pharmaceutics 2022, Vol. 14, Page 543*, vol. 14, no. 3, p. 543, Feb. 2022, doi: 10.3390/PHARMACEUTICS14030543.

[194] Y. Eygeris, S. Patel, A. Jozic, G. Sahay, and G. Sahay, “Deconvoluting Lipid Nanoparticle Structure for Messenger RNA Delivery,” *Nano Lett.*, vol. 20, no. 6, pp. 4543–4549, Jun. 2020, doi: 10.1021/ACS.NANOLETT.0C01386/ASSET/IMAGES/LARGE/NL0C01386_0005.JPEG.

[195] P. Nakhaei *et al.*, “Liposomes: Structure, Biomedical Applications, and Stability Parameters With Emphasis on Cholesterol,” *Front. Bioeng. Biotechnol.*, vol. 9, p. 705886, Sep. 2021, doi: 10.3389/FBIOE.2021.705886/BIBTEX.

[196] I. K. Herrmann, M. J. A. Wood, and G. Fuhrmann, “Extracellular vesicles as a next-generation drug delivery platform,” *Nature Nanotechnology 2021 16:7*, vol. 16, no. 7, pp. 748–759, Jul. 2021, doi: 10.1038/s41565-021-00931-2.

[197] M. Mohamed *et al.*, “PEGylated liposomes: immunological responses,” *Sci. Technol. Adv. Mater.*, vol. 20, no. 1, pp. 710–724, Dec. 2019, doi: 10.1080/14686996.2019.1627174/ASSET/8F5E39F1-C3E7-4FFE-9F56-0676188BE413/ASSETS/IMAGES/TSTA_A_1627174_F0003_OC.JPG.

[198] G. Arias-Alpizar *et al.*, “Light-triggered switching of liposome surface charge directs delivery of membrane impermeable payloads in vivo,” *Nature Communications 2020 11:1*, vol. 11, no. 1, pp. 1–14, Jul. 2020, doi: 10.1038/s41467-020-17360-9.

[199] M. L. Immordino, F. Dosio, and L. Cattel, “Stealth liposomes: review of the basic science, rationale, and clinical applications, existing and potential,” *Int. J. Nanomedicine*, no. 3, pp. 297–315, 2006, doi: 10.2147/DIJN.1.S633.

[200] M. Alavi and M. Hamidi, “Passive and active targeting in cancer therapy by liposomes and lipid nanoparticles,” *Drug Metab. Pers. Ther.*, vol. 34, no. 1, Mar. 2019, doi: 10.1515/DMPT-2018-0032/ASSET/GRAPHIC/J_DMPT-2018-0032_FIG_005.JPG.

[201] A. A. Amer, Y. Karkar, L. Bingle, A. A. Elkordy, and C. S. Chaw, “Fast-Disintegrating Oral Films Containing Nisin-Loaded Niosomes,” *Molecules 2025, Vol. 30, Page 3715*, vol. 30, no. 18, p. 3715, Sep. 2025, doi: 10.3390/MOLECULES30183715.

[202] R. Sharma, U. Gupta, N. K. Garg, R. K. Tyagi, and N. K. Jain, “Surface engineered and ligand anchored nanobioconjugate: An effective therapeutic approach for oral insulin delivery in experimental diabetic rats,” *Colloids Surf. B Biointerfaces*, vol. 127, pp. 172–181, Mar. 2015, doi: 10.1016/J.COLSURFB.2015.01.035.

[203] ICH HARMONISED TRIPARTITE GUIDELINE, “VALIDATION OF ANALYTICAL PROCEDURES: TEXT AND METHODOLOGY Q2(R1).”

[204] F. Nowroozi, A. Almasi, J. Javidi, A. Haeri, and S. Dadashzadeh, “Effect of Surfactant Type, Cholesterol Content and Various Downsizing Methods on the Particle Size of Niosomes,” *Iran. J. Pharm. Res.*, vol. 17, no. Suppl2, p. 1, Sep. 2018, Accessed: Apr. 15, 2025. [Online]. Available: https://pmc.ncbi.nlm.nih.gov/articles/PMC6447874/

[205] M. Balouiri, M. Sadiki, and S. K. Ibnsouda, “Methods for in vitro evaluating antimicrobial activity: A review,” *J. Pharm. Anal.*, vol. 6, no. 2, p. 71, Apr. 2015, doi: 10.1016/J.JPHA.2015.11.005.

[206] S. Dash, P. Murthy, L. Nath, and P. Chowdhury, “Kinetic modeling on drug release from controlled drug delivery systems.,” *Acta Pol. Pharm.*, 2010.

[207] I. Andreana *et al.*, “Freeze Drying of Polymer Nanoparticles and Liposomes Exploiting Different Saccharide-Based Approaches,” *Materials*, vol. 16, no. 3, p. 1212, Feb. 2023, doi: 10.3390/MA16031212/S1.

[208] G. Degobert, D. Aydin, F. Mosqueira, and R. S. Araújo, “Lyophilization of Nanocapsules: Instability Sources, Formulation and Process Parameters,” *Pharmaceutics 2021, Vol. 13, Page 1112*, vol. 13, no. 8, p. 1112, Jul. 2021, doi: 10.3390/PHARMACEUTICS13081112.

[209] W. C. Luo *et al.*, “Impact of formulation on the quality and stability of freeze-dried nanoparticles,” *European Journal of Pharmaceutics and Biopharmaceutics*, vol. 169, pp. 256–267, Dec. 2021, doi: 10.1016/J.EJPB.2021.10.014.

[210] P. Zhao *et al.*, “Long-term storage of lipid-like nanoparticles for mRNA delivery,” *Bioact. Mater.*, vol. 5, no. 2, p. 358, Jun. 2020, doi: 10.1016/J.BIOACTMAT.2020.03.001.

[211] S. Gupta, R. Kesarla, and A. Omri, “Formulation strategies to improve the bioavailability of poorly absorbed drugs with special emphasis on self-emulsifying systems,” *ISRN Pharm.*, vol. 2013, pp. 1–16, Dec. 2013, doi: 10.1155/2013/848043.

[212] W. H. De Jong and P. J. A. Borm, “Drug delivery and nanoparticles:applications and hazards,” *Int. J. Nanomedicine*, vol. 3, no. 2, pp. 133–149, 2008, doi: 10.2147/IJN.S596.

[213] A. K. Dash and G. C. Cudworth, “Therapeutic applications of implantable drug delivery systems,” *J. Pharmacol. Toxicol. Methods*, vol. 40, no. 1, pp. 1–12, 1998, doi: 10.1016/S1056-8719(98)00027-6.

[214] J. E. Bennett, R. Dolin, and M. J. Blaser, *Mandell, Douglas, and Bennett’s Principles and Practice of Infectious Diseases*, vol. 1–2. Elsevier Inc., 2014. doi: 10.1016/s1473-3099(10)70089-x.

[215] M. L. Hans and A. M. Lowman, “Biodegradable nanoparticles for drug delivery and targeting,” *Curr. Opin. Solid State Mater. Sci.*, vol. 6, no. 4, pp. 319–327, Aug. 2002, doi: 10.1016/S1359-0286(02)00117-1.

[216] C. Zinutti, M. Barberi-Heyob, M. Hoffman, and P. Maincent, “In-vivo evaluation of sustained release microspheres of 5-FU in rabbits,” *Int. J. Pharm.*, vol. 166, no. 2, pp. 231–234, May 1998, doi: 10.1016/S0378-5173(98)00040-4.

[217] P. E. Reynolds, “Structure, biochemistry and mechanism of action of glycopeptide antibiotics,” *Eur. J. Clin. Microbiol. Infect. Dis.*, vol. 8, no. 11, pp. 943–950, Nov. 1989, doi: 10.1007/BF01967563.

[218] J. M. Swenson, R. R. Facklam, and C. Thornsberry, “Antimicrobial susceptibility of vancomycin-resistant Leuconostoc, Pediococcus, and Lactobacillus species,” *Antimicrob. Agents Chemother.*, vol. 34, no. 4, pp. 543–549, 1990, doi: 10.1128/AAC.34.4.543.

[219] M. ; K. J. KAMIENSKI, Ed., *PHARMACOLOGY DEMYSTIFIED*. New York : McGRAW-HILL.

[220] M. Mehrarya *et al.*, “Niosomal formulation for antibacterial applications,” *J. Drug Target.*, vol. 30, no. 5, pp. 476–493, 2022, doi: 10.1080/1061186X.2022.2032094.

[221] S. Yasamineh *et al.*, “A state-of-the-art review on the recent advances of niosomes as a targeted drug delivery system,” *Int. J. Pharm.*, vol. 624, Aug. 2022, doi: 10.1016/J.IJPHARM.2022.121878.

[222] M. Mansouri *et al.*, “Streptomycin Sulfate–Loaded Niosomes Enables Increased Antimicrobial and Anti-Biofilm Activities,” *Front. Bioeng. Biotechnol.*, vol. 9, p. 745099, Oct. 2021, doi: 10.3389/FBIOE.2021.745099/BIBTEX.

[223] P. Kraisit, S. Limmatvapirat, M. Luangtana-Anan, and P. Sriamornsak, “Buccal administration of mucoadhesive blend films saturated with propranolol loaded nanoparticles,” *Asian J. Pharm. Sci.*, vol. 13, no. 1, pp. 34–43, Jan. 2018, doi: 10.1016/J.AJPS.2017.07.006.

[224] P. García-Manrique *et al.*, “Continuous flow production of size-controllable niosomes using a thermostatic microreactor,” *Colloids Surf. B Biointerfaces*, vol. 182, p. 110378, Oct. 2019, doi: 10.1016/J.COLSURFB.2019.110378.

[225] S. Joshi *et al.*, “Microfluidics based manufacture of liposomes simultaneously entrapping hydrophilic and lipophilic drugs,” *Int. J. Pharm.*, vol. 514, no. 1, pp. 160–168, Nov. 2016, doi: 10.1016/J.IJPHARM.2016.09.027.

[226] D. A. Seleci, V. Maurer, F. Stahl, T. Scheper, and G. Garnweitner, “Rapid Microfluidic Preparation of Niosomes for Targeted Drug Delivery,” *Int. J. Mol. Sci.*, vol. 20, no. 19, p. 4696, Oct. 2019, doi: 10.3390/IJMS20194696.

[227] H. Aghaei and A. R. Solaimany Nazar, “Continuous Production of the Nanoscale Liposome in a Double Flow-Focusing Microfluidic Device,” *Ind. Eng. Chem. Res.*, vol. 58, no. 51, pp. 23032–23045, Dec. 2019, doi: 10.1021/ACS.IECR.9B04079.

[228] S. G. M. Ong, L. C. Ming, K. S. Lee, and K. H. Yuen, “Influence of the Encapsulation Efficiency and Size of Liposome on the Oral Bioavailability of Griseofulvin-Loaded Liposomes,” *Pharmaceutics*, vol. 8, no. 3, p. 25, Sep. 2016, doi: 10.3390/PHARMACEUTICS8030025.

[229] B. J. Teubl *et al.*, “The buccal mucosa as a route for TiO2 nanoparticle uptake,” *Nanotoxicology*, vol. 9, no. 2, pp. 253–261, Mar. 2015, doi: 10.3109/17435390.2014.921343.

[230] E. Roblegg, E. Fröhlich, C. Meindl, B. Teubl, M. Zaversky, and A. Zimmer, “Evaluation of a physiological in vitro system to study the transport of nanoparticles through the buccal mucosa,” *Nanotoxicology*, vol. 6, no. 4, pp. 399–413, Jun. 2012, doi: 10.3109/17435390.2011.580863.

[231] A. S. Holpuch *et al.*, “Nanoparticles for local drug delivery to the oral mucosa: proof of principle studies,” *Pharm. Res.*, vol. 27, no. 7, pp. 1224–1236, Jul. 2010, doi: 10.1007/S11095-010-0121-Y.

[232] J. Rathi, S. Tamizharasi, A. Dubey, and V. Rathi, “Development and characterization of niosomal drug delivery of gliclazide,” *Journal of Young Pharmacists*, vol. 1, no. 3, p. 205, 2009, doi: 10.4103/0975-1483.57065.

[233] Y. Chen *et al.*, “Nanomaterials against intracellular bacterial infection: from drug delivery to intrinsic biofunction,” *Front. Bioeng. Biotechnol.*, vol. 11, p. 1197974, Apr. 2023, doi: 10.3389/FBIOE.2023.1197974/PDF.

[234] M. Mehrarya *et al.*, “Niosomal formulation for antibacterial applications,” *J. Drug Target.*, vol. 30, no. 5, pp. 476–493, 2022, doi: 10.1080/1061186X.2022.2032094.

[235] A. M. Allahverdiyev, K. V. Kon, E. S. Abamor, M. Bagirova, and M. Rafailovich, "Coping with antibiotic resistance: combining nanoparticles with antibiotics and other antimicrobial agents," *Expert Rev. Anti. Infect. Ther.*, vol. 9, no. 11, pp. 1035–1052, Nov. 2011, doi: 10.1586/ERI.11.121.

[236] E. Gross and J. L. Morell, "The Structure of Nisin," *J. Am. Chem. Soc.*, vol. 93, no. 18, pp. 4634–4635, Sep. 1971, doi: 10.1021/JA00747A073/ASSET/JA00747A073.FP.PNG_V03.

[237] H. Fael and A. L. Demirel, "Nisin/polyanion layer-by-layer films exhibiting different mechanisms in antimicrobial efficacy," *RSC Adv.*, vol. 10, no. 17, pp. 10329–10337, Mar. 2020, doi: 10.1039/C9RA10135G.

[238] W. Liu and J. N. Hansen, "Some chemical and physical properties of nisin, a small-protein antibiotic produced by Lactococcus lactis," *Appl. Environ. Microbiol.*, vol. 56, no. 8, pp. 2551–2558, 1990, doi: 10.1128/AEM.56.8.2551-2558.1990.

[239] J. W. M. MULDERS, I. J. BOERRIGTER, H. S. ROLLEMA, R. J. SIEZEN, and W. M. de VOS, "Identification and characterization of the lantibiotic nisin Z, a natural nisin variant," *Eur. J. Biochem.*, vol. 201, no. 3, pp. 581–584, 1991, doi: 10.1111/J.1432-1033.1991.TB16317.X.

[240] S. T. D. Hsu *et al.*, "The nisin–lipid II complex reveals a pyrophosphate cage that provides a blueprint for novel antibiotics," *Nature Structural & Molecular Biology 2004 11:10*, vol. 11, no. 10, pp. 963–967, Sep. 2004, doi: 10.1038/nsmb830.

[241] S. Punyauppa-Path, P. Phumkhachorn, and P. Rattanachaikunsopon, "NISIN: PRODUCTION AND MECHANISM OF ANTIMICROBIAL ACTION," *Int J Cur Res Rev*, no. 2, 2015.

[242] Z. Benmechernene, I. Fernandez-No, M. Kihal, K. Böhme, P. Calo-Mata, and J. Barros-Velazquez, "Recent Patents on Bacteriocins: Food and Biomedical Applications," *Recent Pat. DNA Gene Seq.*, vol. 7, no. 1, pp. 66–73, 2013, doi: 10.2174/1872215611307010010.

[243] C. Piper, L. A. Draper, P. D. Cotter, R. P. Ross, and C. Hill, "A comparison of the activities of lacticin 3147 and nisin against drug-resistant Staphylococcus aureus and Enterococcus species," *Journal of Antimicrobial Chemotherapy*, vol. 64, no. 3, pp. 546–551, Sep. 2009, doi: 10.1093/JAC/DKP221.

[244] T. Haider, V. Pandey, C. Behera, P. Kumar, P. N. Gupta, and V. Soni, “Nisin and nisin-loaded nanoparticles: a cytotoxicity investigation,” *Drug Dev. Ind. Pharm.*, vol. 48, no. 7, pp. 310–321, 2022, doi: 10.1080/03639045.2022.2111438.

[245] J. C. Colas, W. Shi, V. S. N. M. Rao, A. Omri, M. R. Mozafari, and H. Singh, “Microscopical investigations of nisin-loaded nanoliposomes prepared by Mozafari method and their bacterial targeting,” *Micron*, vol. 38, no. 8, pp. 841–847, Dec. 2007, doi: 10.1016/J.MICRON.2007.06.013.

[246] J. M. Shin, J. W. Gwak, P. Kamarajan, J. C. Fenno, A. H. Rickard, and Y. L. Kapila, “Biomedical applications of nisin,” *J. Appl. Microbiol.*, vol. 120, no. 6, pp. 1449–1465, Jun. 2016, doi: 10.1111/JAM.13033.

[247] K. I. Okuda *et al.*, “Effects of Bacteriocins on Methicillin-Resistant Staphylococcus aureus Biofilm,” *Antimicrob. Agents Chemother.*, vol. 57, no. 11, p. 5572, Nov. 2013, doi: 10.1128/AAC.00888-13.

[248] I. H. JOHNSON, H. HAYDAY, and G. COLMAN, “The Effects of Nisin on the Microbial Flora of the Dental Plaque of Monkeys (Macaca fascicularis),” *Journal of Applied Bacteriology*, vol. 45, no. 1, pp. 99–109, Aug. 1978, doi: 10.1111/J.1365-2672.1978.TB04203.X.

[249] T. H. Howell, J. P. Fiorellini, P. Blackburn, S. J. Projan, J. de la Harpe, and R. C. Williams, “The effect of a mouthrinse based on nisin, a bacteriocin, on developing plaque and gingivitis in beagle dogs,” *J. Clin. Periodontol.*, vol. 20, no. 5, pp. 335–339, May 1993, doi: 10.1111/J.1600-051X.1993.TB00369.X.

[250] E. Kastner, V. Verma, D. Lowry, and Y. Perrie, “Microfluidic-controlled manufacture of liposomes for the solubilisation of a poorly water soluble drug,” *Int. J. Pharm.*, vol. 485, no. 1–2, pp. 122–130, May 2015, doi: 10.1016/j.ijpharm.2015.02.063.

[251] A. F. Borges, C. Silva, J. F. J. Coelho, and S. Simões, “Oral films: Current status and future perspectives: I — Galenical development and quality attributes,” *Journal of Controlled Release*, vol. 206, pp. 1–19, May 2015, doi: 10.1016/J.JCONREL.2015.03.006.

[252] D. Field, P. D. Cotter, C. Hill, and R. P. Ross, “Bioengineering lantibiotics for therapeutic success,” *Front. Microbiol.*, vol. 6, no. NOV, p. 170560, Nov. 2015, doi: 10.3389/FMICB.2015.01363/BIBTEX.

[253] C. A. dos Santos *et al.*, “Bacterial nanocellulose membranes combined with nisin: a strategy to prevent microbial growth,” *Cellulose*, vol. 25, no. 11, pp. 6681–6689, Nov. 2018, doi: 10.1007/S10570-018-2010-1/METRICS.

[254] H. S. Chung and M. Lee, “Different Antimicrobial Susceptibility Testing Methods to Determine Vancomycin Susceptibility and MIC for Staphylococcus aureus with Reduced Vancomycin Susceptibility,” *Diagnostics 2022, Vol. 12, Page 845*, vol. 12, no. 4, p. 845, Mar. 2022, doi: 10.3390/DIAGNOSTICS12040845.

[255] J. P. Jeong, I. Yoon, K. Kim, and S. Jung, “Structural and Physiochemical Properties of Polyvinyl Alcohol–Succinoglycan Biodegradable Films,” *Polymers 2024, Vol. 16, Page 1783*, vol. 16, no. 13, p. 1783, Jun. 2024, doi: 10.3390/POLYM16131783.

[256] J. Siepmann and N. A. Peppas, “Modeling of drug release from delivery systems based on hydroxypropyl methylcellulose (HPMC),” *Adv. Drug Deliv. Rev.*, vol. 64, no. SUPPL., pp. 163–174, Dec. 2012, doi: 10.1016/j.addr.2012.09.028.

[257] D. Borrmann, A. Danzer, and G. Sadowski, “Water Sorption in Glassy Polyvinylpyrrolidone-Based Polymers,” *Membranes (Basel).*, vol. 12, no. 4, p. 434, Apr. 2022, doi: 10.3390/MEMBRANES12040434/S1.

[258] M. A. Repka and J. W. McGinity, “Physical–mechanical, moisture absorption and bioadhesive properties of hydroxypropylcellulose hot-melt extruded films,” *Biomaterials*, vol. 21, no. 14, pp. 1509–1517, Jul. 2000, doi: 10.1016/S0142-9612(00)00046-6.

[259] P. Panraksa, P. Jantrawut, P. Tipduangta, and K. Jantanasakulwong, “Formulation of Orally Disintegrating Films as an Amorphous Solid Solution of a Poorly Water-Soluble Drug,” *Membranes 2020, Vol. 10, Page 376*, vol. 10, no. 12, p. 376, Nov. 2020, doi: 10.3390/MEMBRANES10120376.

[260] D. Kowalczuk and M. Pitucha, “Application of FTIR Method for the Assessment of Immobilization of Active Substances in the Matrix of Biomedical Materials,” *Materials 2019, Vol. 12, Page 2972*, vol. 12, no. 18, p. 2972, Sep. 2019, doi: 10.3390/ma12182972.

[261] G. Thamilselvan *et al.*, “Polymer based dual drug delivery system for targeted treatment of fluoroquinolone resistant Staphylococcus aureus mediated infections,” *Scientific Reports 2023 13:1*, vol. 13, no. 1, pp. 11373-, Jul. 2023, doi: 10.1038/s41598-023-38473-3.

[262] M. T. Khorasani, A. Joorabloo, H. Adeli, Z. Mansoori-Moghadam, and A. Moghaddam, “Design and optimization of process parameters of polyvinyl (alcohol)/chitosan/nano zinc oxide hydrogels as wound healing materials,” *Carbohydr. Polym.*, vol. 207, pp. 542–554, Mar. 2019, doi: 10.1016/J.CARBPOL.2018.12.021.

[263] H. R. Luthfianti *et al.*, “Physicochemical Characteristics and Antibacterial Activities of Freeze-Thawed Polyvinyl Alcohol/Andrographolide Hydrogels,” *ACS Omega*, vol. 8, no. 3, pp. 2915–2930, Jan. 2023, doi: 10.1021/ACSOMEGA.2C05110,.

[264] C. Tsioptsias, D. Fardis, X. Ntampou, I. Tsivintzelis, and C. Panayiotou, “Thermal Behavior of Poly(vinyl alcohol) in the Form of Physically Crosslinked Film,” *Polymers 2023, Vol. 15, Page 1843*, vol. 15, no. 8, p. 1843, Apr. 2023, doi: 10.3390/POLYM15081843.

[265] M. I. Mohammed and F. El-Sayed, “PEG’s impact as a plasticizer on the PVA polymer’s structural, thermal, mechanical, optical, and dielectric characteristics,” *Optical and Quantum Electronics 2023 55:13*, vol. 55, no. 13, pp. 1141-, Oct. 2023, doi: 10.1007/S11082-023-05420-5.

[266] T. Yang, J. Wu, Y. Yao, K. Wang, Q. Zhang, and Q. Fu, “Towards the toughness-strength balance of poly(vinyl alcohol) films via synergic plasticization,” *Polymer (Guildf).*, vol. 301, p. 127031, May 2024, doi: 10.1016/J.POLYMER.2024.127031.

[267] Y. Garavand, A. Taheri-garavand, F. Garavand, F. Shahbazi, D. Khodaei, and I. Cacciotti, “Starch-Polyvinyl Alcohol-Based Films Reinforced with Chitosan Nanoparticles: Physical, Mechanical, Structural, Thermal and Antimicrobial Properties,” *Applied Sciences 2022, Vol. 12, Page 1111*, vol. 12, no. 3, p. 1111, Jan. 2022, doi: 10.3390/APP12031111.

[268] Y. Karkar, T. Anis, A. A. Elkordy, and A. Faheem, “Flexipill: A novel 3D printed flexible dose combination for hypertension with a floating element,” *European Journal of Pharmaceutics and Biopharmaceutics*, vol. 212, p. 114736, Jul. 2025, doi: 10.1016/J.EJPB.2025.114736.

[269] P. V. Pedersen and J. W. Myrick, “Versatile kinetic approach to analysis of dissolution data,” *J. Pharm. Sci.*, vol. 67, no. 10, pp. 1450–1455, May 1978, doi: 10.1002/jps.2600671034.

[270] A. A. Amer, Y. Karkar, L. Bingle, A. A. Elkordy, and C. S. Chaw, “Fast-Disintegrating Oral Films Containing Nisin-Loaded Niosomes,” *Molecules 2025, Vol. 30, Page 3715*, vol. 30, no. 18, p. 3715, Sep. 2025, doi: 10.3390/MOLECULES30183715.

[271] B. A. Tegegne *et al.*, “A critical review on diabetes mellitus type 1 and type 2 management approaches: from lifestyle modification to current and novel targets and therapeutic agents,” *Front. Endocrinol. (Lausanne).*, vol. 15, p. 1440456, Oct. 2024, doi: 10.3389/FENDO.2024.1440456/FULL.

[272] “Diabetes.” Accessed: Oct. 30, 2025. [Online]. Available: https://www.who.int/news-room/fact-sheets/detail/diabetes?utm_source=chatgpt.com

[273] A. D. Association, “Diagnosis and Classification of Diabetes Mellitus,” *Diabetes Care*, vol. 37, no. Supplement_1, pp. S81–S90, Jan. 2014, doi: 10.2337/DC14-S081.

[274] P. D. Home, “An overview of insulin therapy for the non-specialist,” *Diabetes Obes. Metab.*, vol. 27 Suppl 5, no. Suppl 5, pp. 3–15, Jul. 2025, doi: 10.1111/DOM.16280.

[275] X. Guo and W. Wang, “Challenges and recent advances in the subcutaneous delivery of insulin,” *Expert Opin. Drug Deliv.*, vol. 14, no. 6, pp. 727–734, Jun. 2017, doi: 10.1080/17425247.2016.1232247.

[276] S. Gentile *et al.*, “Lipodystrophy in Insulin-Treated Subjects and Other Injection-Site Skin Reactions: Are We Sure Everything is Clear?,” *Diabetes Therapy*, vol. 7, no. 3, p. 401, Sep. 2016, doi: 10.1007/S13300-016-0187-6.

[277] L. W. Limenh, “A review on oral novel delivery systems of insulin through the novel delivery system formulations: A review,” *SAGE Open Med.*, vol. 12, p. 20503121231225320, Jan. 2024, doi: 10.1177/20503121231225319.

[278] C. : Baral, K. C. ; Choi, K. Chandra Baral, and K. Y. Choi, “Barriers and Strategies for Oral Peptide and Protein Therapeutics Delivery: Update on Clinical Advances,”

Pharmaceutics 2025, Vol. 17, Page 397, vol. 17, no. 4, p. 397, Mar. 2025, doi: 10.3390/PHARMACEUTICS17040397.

[279] S. Spoorthi Shetty, P. Halagali, A. P. Johnson, K. M. A. Spandana, and H. V. Gangadharappa, "Oral insulin delivery: Barriers, strategies, and formulation approaches: A comprehensive review," *Int. J. Biol. Macromol.*, vol. 242, no. Pt 3, Jul. 2023, doi: 10.1016/j.ijbiomac.2023.125114.

[280] S. Malhotra, T. Lijnse, E. O. Cearbhaill, and D. J. Brayden, "Devices to overcome the buccal mucosal barrier to administer therapeutic peptides," *Adv. Drug Deliv. Rev.*, vol. 220, p. 115572, May 2025, doi: 10.1016/J.ADDR.2025.115572.

[281] M. Razzaghi, "Polymeric 3D-Printed Microneedle Arrays for Non-Transdermal Drug Delivery and Diagnostics," *Polymers 2025, Vol. 17, Page 1982*, vol. 17, no. 14, p. 1982, Jul. 2025, doi: 10.3390/POLYM17141982.

[282] M. Prajapat *et al.*, "3D printing technology in microneedles: An emerging era in transdermal drug delivery," *Hybrid Advances*, vol. 10, p. 100447, Sep. 2025, doi: 10.1016/J.HYBADV.2025.100447.

[283] R. Haj-Ahmad, A. Elkordy, and C. Chaw, "In vitro characterisation of Span 65 niosomal formulations containing proteins," *Curr. Drug Deliv.*, vol. 12, no. 5, pp. 628–639, Nov. 2015, doi: 10.2174/1567201812666150511095432.

[284] S. A. Jaber, M. Saadh, Q. Abuhassan, and M. A. Obeid, "Curcumin-loaded Niosomes Prepared by Microfluidic Mixing; Characterization and Cytotoxicity Evaluation," *Journal of Pharmaceutical Innovation 2025 20:4*, vol. 20, no. 4, pp. 1–9, Jul. 2025, doi: 10.1007/S12247-025-10003-W.

[285] K. .J.rathod and R. A. B. Kuldeepsinh .J.rathod, "Evalution of mouth dissolving film by physico-chemical method," *BioMedSciDirect Publications*, vol. 16, no. 1, pp. 7991–7996, 2025, doi: 10.65048/IJBMR.

[286] K. Wasilewska and K. Winnicka, "How to assess orodispersible film quality? A review of applied methods and their modifications," *Acta Pharm.*, vol. 69, no. 2, pp. 155–176, Jun. 2019, doi: 10.2478/ACPH-2019-0018.

[287] I. S. Bayer, “Recent Advances in Mucoadhesive Interface Materials, Mucoadhesion Characterization, and Technologies,” *Adv. Mater. Interfaces*, vol. 9, no. 18, p. 2200211, Jun. 2022, doi: 10.1002/ADMI.202200211;WGROUP:STRING:PUBLICATION.

[288] K. N. Kumar, S. Mallik, and K. Sarkar, “Role of freeze-drying in the presence of mannitol on the echogenicity of echogenic liposomes,” *J. Acoust. Soc. Am.*, vol. 142, no. 6, p. 3670, Dec. 2017, doi: 10.1121/1.5017607.

[289] M. A. Mensink, H. W. Frijlink, K. van der Voort Maarschalk, and W. L. J. Hinrichs, “How sugars protect proteins in the solid state and during drying (review): Mechanisms of stabilization in relation to stress conditions,” *European Journal of Pharmaceutics and Biopharmaceutics*, vol. 114, no. 4, pp. 288–295, May 2017, doi: 10.1016/j.ejpb.2017.01.024.

[290] D. Rimmerman *et al.*, “Insulin Hexamer Dissociation Dynamics Revealed by Photoinduced T-jumps and Time-Resolved X-Ray Solution Scattering,” *Photochem. Photobiol. Sci.*, vol. 17, no. 7, p. 874, 2018, doi: 10.1039/C8PP00034D.

[291] M. V. Sefton and G. M. Antonacci, “Adsorption isotherms of insulin onto various materials,” *Diabetes*, vol. 33, no. 7, pp. 674–680, 1984, doi: 10.2337/DIAB.33.7.674.

[292] T. Ballet, L. Boulange, Y. Brechet, F. Bruckert, and M. Weidenhaupt, “Protein conformational changes induced by adsorption onto material surfaces: An important issue for biomedical applications of material science,” *Bulletin of the Polish Academy of Sciences: Technical Sciences*, vol. 58, no. 2, pp. 303–315, 2010, doi: 10.2478/V10175-010-0028-0.

[293] A. Beig, J. M. Miller, and A. Dahan, “Accounting for the solubility–permeability interplay in oral formulation development for poor water solubility drugs: The effect of PEG-400 on carbamazepine absorption,” *European Journal of Pharmaceutics and Biopharmaceutics*, vol. 81, no. 2, pp. 386–391, Jun. 2012, doi: 10.1016/J.EJPB.2012.02.012.